11-29-2012 12:00 AM

Characterization of novel ichnofossils in meteorite impact glass from the Ries impact structure, Germany

Haley M. Sapers
The University of Western Ontario

Supervisor
Dr. Gordon Osinski
The University of Western Ontario Joint Supervisor
Dr. Neil Banerjee
The University of Western Ontario

Graduate Program in Planetary Science
A thesis submitted in partial fulfillment of the requirements for the degree in Doctor of Philosophy

CHARACTERIZATION OF NOVEL ICHNOFOSSILS HOSTED IN METEORITE IMPACT GLASS FROM THE RIES IMPACT STRUCTURE, GERMANY

(Spine title: Novel Ichnofossils in Impact Glass)

(Thesis format: Integrated Article)

by

Haley M. Sapers

Graduate Program in Geology: Planetary Science

A thesis submitted in partial fulfillment
of the requirements for the degree of
Doctor of Philosophy

The School of Graduate and Postdoctoral Studies
The University of Western Ontario
London, Ontario, Canada

THE UNIVERSITY OF WESTERN ONTARIO
The School of Graduate and Postdoctoral Studies

CERTIFICATE OF EXAMINATION

Joint-Supervisor

Dr. Gordon R. Osinski

Joint-Supervisor

Dr. Neil R. Banerjee

Supervisory Committee

Dr. Gordon Southam

Examiners

Dr. Sean Shieh

Dr. Cam Tsujita

Dr. Amanda Moehring

Dr. Chris McKay

The thesis by

Haley Morgan Sapers

entitled:

Characterization of novel ichnofossils in meteorite impact glass from the Ries impact structure, Germany

is accepted in partial fulfillment of the
requirements for the degree of
Doctor of Philosophy

Date

Chair of the Thesis Examination Board

Abstract

The initial catastrophic biological effects of hypervelocity impacts are well established. However, a growing body of evidence suggests that meteorite impact events have beneficial effects for microbial life. This, in turn, has led many to suggest that impact craters may have been important habitats for life on early Earth. Any large meteorite impact into a water-rich target on a solid planetary body has the potential to generate hydrothermal systems. Impact-generated hydrothermal systems expand the potential environments for microbial colonization to environments without endogenous volcanic heat sources to drive hydrothermal activity. Examination of impact glass from the Ries impact structure, Germany, has revealed the presence of putative microbial alteration. Given the probable ubiquity of impact glasses in post-impact environments throughout the Solar System, it is important to understand the biological components and potential of such systems. A multi-analytical approach to assess the biogenicity of the tubular features in the Ries glasses has been used. Their complex morphology (spiralling, bifurcation, avoidance, lack of intersection) has been studied extensively using both optical and scanning electron microscopy. Using Energy Dispersive Spectroscopy we have shown the presence of a depletion zone indicative of biological processing surrounding the tubules. Fourier Transform Infrared Spectroscopy has identified the presence of organic compounds spatially associated with the tubules and absent in crystallite regions. Synchrotron near edge fine structure (NEXAFS) spectroscopy at the C K-edge also indicates the presence of organically bound carbon in the glassy matrix surrounding the tubules, but absent in the matrix hosting only crystallites. NEXAFS spectroscopy at the Fe L_2 and L_3 -edges indicates distinct patterns of Fe speciation in the tubules not present in the Fe-rich abiotic quench crystallites. Together, these results are strongly suggestive of a microbial alteration origin for the tubules in the Ries glasses. Impact cratering is a significant and ubiquitous geological process on terrestrial bodies in the Solar System as well as on the early Earth, as such the discovery of biogenic features in impact glass has profound implications for early life on Earth and the early evolution of life on Earth as well as for life on other terrestrial planets.

Keywords

Astrobiology, biosignatures, ichnofossils, biogenicity, impact cratering, planetary science, biogeochemistry, SEM, TEM, NEXAFS, FTIR

Co-Authorship Statement

The author was primarily responsible for sample collection and preparation, data collection, data interpretation, data analyses and synthesis of results and for writing of the manuscript with the following exceptions. Samples collected prior to 2008 were not collected by the author; although the author did subsequently visit the collection sites. Fourier transform infrared spectroscopy data was collected and analyzed by Dr. L. J. Preston. The author was actively involved in all stages of sample preparation and data collection as well as interpretation and synthesis of results within the context of this thesis. Micro X-ray diffraction data was collected and analyzed with under the guidance of Dr. R. L. Flemming. Transmission electron microscopy (TEM) including TEM based energy dispersive spectroscopy and electron diffraction were carried out by Dr. D. Schumann. The author was actively involved in all stages of sample preparation and data collection as well as interpretation and synthesis of results within the context of this thesis.

Epigraph

Stones of the Sky

To harden the earth
the rocks took charge;
instantly
they grew wings;
the rocks
that soared;
the survivors
flew up
the lightening bolt,
screamed in the night,
a watermark,
a violet sword,
a meteor.

The succulent
sky
had not only clouds,
not only space smelling of oxygen,
but an earthly stone
flashing here and there
changed into a dove,
changed into a bell,
into immensity, into a piercing
wind:
into a phosphorescent arrow,
into salt of the sky.

~Pablo Neruda
(translation by James Nolan)

Dedication

This thesis: this work and the time and the effort; the joy and the frustration; the pride and disappointment; and the pure curiosity that it represents is dedicated to my Mother: my confidant, my friend and the *other* scientist in the family. *For I will live your unlived years*

Acknowledgments

First and foremost I would like to acknowledge the unconditional support, encouragement and patience of my supervisors, Dr. Gordon Osinski and Dr. Neil Banerjee. Without their dedicated mentorship and guidance, both academic and personal, this thesis would not have come to be. The compassion and enthusiasm of my supervisors has been instrumental to my academic success and has allowed me to gain the confidence required to transition from a student into a scientist. I would like to thank everyone in the Earth Sciences department and Planetary Science and Exploration program at Western University. I have had the honour of working within a truly world-class research environment: a climate of contagious intellectual curiosity in which students thrive. I would also like to thank my many colleagues and collaborators for inspiration, technical assistance, discussion and discourse. I would like to reflect on the many wonderful friendships that have developed over the past four years: I would not have made it through the all-nighters, frantic proposal and abstract deadlines, first conference presentations and poster sessions without the kindness and reassurance of my friends and fellow students. It is the absolute support and endless love and encouragement of my family that has allowed me to truly excel as I journeyed through graduate school and as I embark on the next stage of my academic career.

Table of Contents

List of Tables

List of Figures

List of Appendices

List of Abbreviations, Symbols, Nomenclature

Å: angstrom

µm: micron; micrometre

µ-XRD: micro X-ray diffraction

AIT: ambient inclusion trail

ATR: attenuated total reflectance

BSE: back scatter electron mode

Bt: biotite

Chl: chlorite

CLS: Canadian Light Source

EDF: extended depth of focus

EDX: energy dispersive X-ray spectroscopy

FIB: focused ion beam

Fsp: feldspar

FTIR: Fourier transform infrared spectroscopy

GADDS: general area detector diffraction system

ICDD: International Center for Diffraction Data

IUGS: International Union of Geological Science

NEXAFS: near edge X-ray absorption fine structure

PDF: powder diffraction file

PDFs: planar deformation features

SCMR: Subcommission on the Systematics of Metamorphic Rocks

SE: secondary electron mode

SEM: scanning electron microscopy

SM: spectro-microscopy

STXM: scanning transmission X-ray microscopy

TEM: transmission electron microscopy

Qtz: quartz

XRD: X-ray diffraction

Chapter 1

1 Introduction

Initially, meteorite impact events are biologically catastrophic, as result of immediate sterilization of the target area (*e.g.,* Sleep *et al.* 1989). However, the ecological succession following such biological resetting may prove beneficial to microbial life, creating novel habitat and metabolic niches. This has led to the suggestion that impact craters may have been important habitats for primitive microbial life on early Earth (Cockell & Lee 2002). More speculatively, impacts may have acted as 'cradles' for prebiotic chemical reactions (*e.g.*, Cockell 2006). Impact-ejected rocks may have provided refuges for microbial life during the ~3.8 Ga late heavy bombardment and may even have allowed the transfer of life between planetary bodies (*e.g.*, Cockell 2006). Although impact craters are uncommon on present day Earth, (182 terrestrial impacts constituting ~50 000 km^2; Earth Impact Database, September 28, 2012), they are ubiquitous on rocky and icy bodies within the solar system, often comprising the dominant geological features.

Any hypervelocity impact into a water-rich target on a solid planetary body has the potential to generate hydrothermal systems (Naumov 2005), resulting in the 'thermal phase of biology' (Cockell & Lee 2002) following an impact. The hyperthermophilic root of the phylogenetic tree of life suggests an essential role for thermophilic environments in the origin or the early evolutionary history of life (Pace 1994; Schwartzman & Lineweaver 2004). Previous work has associated primitive life on Earth with submarine volcanic activity: filamentous microfossils as old as ca. 3.2 Ga have been found in volcanogenic massive sulphide deposits (Rasmussen 2000); bioalteration of volcanic glasses back to 3.5 Ga provide the earliest record of life on Earth (Banerjee *et al.* 2006; Staudigel *et al.* 2008a) suggesting that submarine hydrothermal settings may have played an essential role in the origin of life. Impact-induced hydrothermal systems share many characteristics with submarine volcanic hydrothermal systems including the presence of chemical and thermal energy for microbial metabolism and the precipitation of hydrothermal minerals such as clays and zeolites, which may have catalyzed important prebiotic chemical reactions. Thus, post-impact hydrothermal systems expand the potential environments for the origin of life and for later microbial colonization to environments without endogenous volcanic heat sources to drive hydrothermal activity. During the Late Heavy Bombardment period when life purportedly arose on Earth, impact generated habitats were likely much more common on Earth than submarine hydrothermal systems suggesting the former as a more statistically probable habitat for the origin of life. The Late Heavy Bombardment period affecting the planets of inner Solar System 3.8 – 4.2 Ga resulted from disruption of the main asteroid belt during possible orbital migration of the gas giants (Strom *et al.* 2005; Gomes *et al. 2005*).

The Ries crater is exceptionally preserved and well characterized (Pohl *et al.* 1977). In addition, a post-impact hydrothermal system at Ries has been documented (*e.g.*, Newsom *et al.* 1986; Osinski 2005). This structure possesses a variety of impactites including a well-preserved ejecta blanket including a glass-bearing breccia ('suevite'). The surficial suevite, comprising one of the preserved proximal ejecta deposits contains abundant glass clasts that have been studied in great detail (Osinski 2003). The rapid quenching of molten material following a hypervelocity impact often results in the formation of impact glasses. Impact glasses share many similarities with volcanic glasses, however, fundamental differences make impact glasses unique geochemical systems. The bulk compositions of impact melts are diverse, reflecting the target lithologies from which they were derived. Furthermore, impact glasses often display chemical and textural heterogeneity on multiple scales. In addition, the presence of lechatelierite (a pure silica glass phase) is indicative of high temperatures (>1713^{o}C; Stöffler 1984) reflecting formation conditions distinct from normal igneous processes. Meteoritic contamination may result in siderophile element anomalies or isotopic anomalies (Osinski 2003).

It is notable that microbial alteration of terrestrial sub-marine basaltic glasses produces characteristic tubular and granular aggregate textures (*e.g.*, Banerjee *et al.* 2004; Staudigel *et al.* 2006). Significant to the present study are distinctive tubular and granular aggregate textures observed in ancient to modern basaltic glasses; these are suspected to have been produced via microbially mediated dissolution of the glass (*e.g.*, Staudigel *et al.* 2006). Such bioalteration textures documented from Archean greenstone belts constitute one of the oldest forms of evidence suggesting life on Earth (Banerjee *et al.*

2006). Examination of glasses from the Ries crater in Germany has revealed tubular alteration textures with remarkably similar morphologies to the putative bioalteration of volcanic glasses. Given the probable ubiquity of impact glasses in post-impact environments throughout the Solar System, it is important to understand the biological components and potential of such systems.

This thesis examines the enigmatic tubular features in the Ries glasses establishing an argument for biogenicity. Chapter 3 uses a suite of impactites from the Rochechouart impact structure to illustrate the importance of consistent and unambiguous nomenclature in the literature. The descriptive nomenclature proposed in Chapter 3 for the transitional melt-bearing Rochechouart impactites allows for the classification of transitional lithologies without *a priori* knowledge of geological context. This study sets a precedent for scenarios such as sample returns, deeply eroded terrestrial structures and meteorite breccias where the geological context is unavailable or details of the original geologic context are obscured. Chapter 4, a detailed petrographic study of the glass-bearing breccias of the Ries impact structure, provides the geological context for the tubules ruling out a purely abiotic origin. In Chapter 5, a geochemical study of the tubules is presented establishing several lines of evidence for biological processing. High-resolution synchrotron and transmission electron microscopy analyses are presented in Chapter 6 providing an unprecedented high-resolution geochemical study of putative ichnofossils in impact glass. Chapter 7 summarizes the research to date on the tubular features in the Ries impact glasses following the arguments and criteria for biogenicity (McLoughlin *et al.* 2007; Banerjee *et al.* 2008; Staudigel *et al.* 2008b).

The tubules within the Ries glasses constitute the first putative bioalteration texture to be reported in an impact glass and have significant implications for the habitability of impact sites as well as the potential importance of terrestrial impacts in the evolution of life on early Earth. Impact derived endolithic habitats are being considered as possible locations for life on early Earth (Westall & Folk 2003) and on the surface of other planets such as Mars (Cockell *et al.* 2002; Cockell *et al.* 2005). Establishing the biogenicity of features in impact glasses has significant astrobiological implications. As bioalteration textures preserved in Archean greenstone belts constitute one of the oldest records of life on Earth (Furnes *et al.* 2004; Banerjee *et al.* 2006; Staudigel *et al.* 2008a), linking potential microbial activity in volcanic and impact glasses may yield insight into early life and the origin of life on Earth. Understanding the geomicrobiology of impact craters on Earth is critical in furthering the search for life on Mars. Studies constraining the biogeochemistry of impact craters may not only yield insight into early life on Earth, but, furthermore, may comprise a potential habitat for life and past life on other terrestrial planets such as Mars.

1.1 References cited

BANERJEE N. R., FURNES H., MUEHLENBACHS K. and STAUDIGEL H. (2004) Microbial alteration of volcanic glass in modern and ancient oceanic crust as a proxy for studies of extraterrestrial material. In *Lunar and Planetary Science XXXV*.

BANERJEE N. R., FURNES H., MUEHLENBACHS K., STAUDIGEL H. and DE WIT M. (2006) Preservation of ~3.4 – 3.5 Ga microbial biomarkers in pillow lavas and hyaloclastites from the Barberton Greenstone Belt, South Africa. *Earth and Planetary Science Letters* **241**(3 – 4), 707 – 722.

BANERJEE N. R., FURNES H., MUEHLENBACHS K., STAUDIGEL H., MCLOUGHLIN N. and BEBOUT G. (2008) Biogeochemical tracers of modern and ancient life in seafloor lavas. *Geochimica et Cosmochimica Acta* **72**(12), A51 – A51.

COCKELL C. S. (2006) The origin and emergence of life under impact bombardment. *Philos Trans R Soc Lond B Biol Sci* **361**(1474), 1845 –1856.

COCKELL C. S. and LEE P. (2002) The biology of impact craters — a review. *Biol Rev Camb Philos Soc* **77**(3), 279 – 310.

COCKELL C. S., LEE P., BROADY P., LIM D. S. S., OSINSKI G. R., PARNELL J., KOEBERL C., PESONEN L. and SALMINEN J. (2005) Effects of asteroid and comet impacts on habitats for lithophytic organisms — A synthesis. *Meteoritics & Planetary Science* **40**(12), 1901 – 1914.

COCKELL C. S., LEE P., OSINSKI G., HORNECK G. and BROADY P. (2002) Impact-induced microbial endolithic habitats. *Meteoritics & Planetary Science* **37**(10), 1287 – 1298.

FURNES H., BANERJEE N. R., MUEHLENBACHS K., STAUDIGEL H. and DE WIT M. (2004) Early Life Recorded in Archean Pillow Lavas. *Science* **304**(5670), 578 – 581.

GOMES, R. LEVISON, H. F., TSIGANIS, K., and MORBIDELLI, A. (2005) Origin of the cataclysmic Late Heavy Bombardment period of the terrestrial planets. *Nature* **435,** 466 – 469.

McLoughlin N., Brasier M., Wacey D., Green O. and Perry R. (2007) On biogenicity criteria for endolithic microborings on early Earth and beyond. *Astrobiology* **7**, 10 – 26.

Naumov M. V. (2005) Principal features of impact-generated hydrothermal circulation systems: mineralogical and geochemical evidence. *Geofluids* **5**(3), 165 – 184.

Newsom H. E., Graup G., Sewards T. and Keil K. (1986) Fluidization and Hydrothermal Alteration of the Suevite Deposit at the Ries Crater, West-Germany, and Implications for Mars. *Journal of Geophysical Research-Solid Earth and Planets* **91**(B13), E239 – E251.

Osinski G. R. (2003) Impact glasses in fallout suevites from the Ries impact structure, Germany: An analytical SEM study. *Meteoritics & Planetary Science* **38**(11), 1641 – 1667.

- (2005) Hydrothermal activity associated with the Ries impact event, Germany. *Geofluids* **5**(3), 202 – 220.

Pace, N. R. (1997) A Molecular View of Microbial Dirversity and the Biosphere. *Science* **276**, 634 – 740.

Pohl J., Stöffler D., Gall H. and Ernstson K. (1977) The Ries impact crater; Impact and explosion cratering; planetary and terrestrial implications; Proceedings of the Symposium on planetary cratering mechanics. In *Lunar Science Institute topical conference ; Symposium on planetary cratering mechanics, Flagstaff, Ariz* (eds. D. J. Roddy, R. O. Pepin and R. B. Merrill). Pergamon Press New York N.Y. United States (USA), United States (USA).

Rasmussen B. (2000) Filamentous microfossils in a 3,235-million-year-old volcanogenic massive sulphide deposit. *Nature* **405**, 676 – 679.

Schwartzman, D. W. and Lineweaver, C. H. (2004) The hyperthermophilic origin of life revisited. *Biochemical Society Transactions* **32**(2), 168 – 171.

Sleep, N. H., Zahnle, K. J., Kasting, J. F., and Morowitz, H. J. (1989) Annihilation of ecosystmes by large asteroid impacts on the early Earth. *Nature* **342**, 139 – 142.

Staudigel H., Furnes H., Banerjee N. R., Dilek Y. and Muehlenbachs K. (2006) Microbes and volcanoes: A tale from the oceans, ophiolites, and greenstone belts. *GSA Today* **16**(10), 4 – 10.

Staudigel H., Furnes H., McLoughlin N., Banerjee N. R., Connel L. B. and Templeton A. (2008a) 3.5 billion years of glass bioalteration: Volcanic rocks as a basis for microbial life? *Earth-Science Reviews* **89**(3 – 4), 156 – 176.

Staudigel H., Furnes H., McLoughlin N., Banerjee N. R., Connell L. B. and Templeton A. (2008b) Microbial glass bioalteration: Inferring mechanisnis of blocorrosion from trace fossil morphology. *Geochimica et Cosmochimica Acta* **72**(12), A893 – A893.

STÖFFLER D. (1984) Glasses formed by hypervelocity impact. *Journal of Non-Crystalline Solids* **67**, 465 – 502.

STROM, R. G., MALHOTRA, R., ITO, T., YOSHIDA, F. and KRING, D. A. (2005) The Origin of Planetary Impactors in the Inner Solar System. *Science* **309**, 1847 – 1850.

WESTALL F. and FOLK R. L. (2003) Exogenous carbonaceous microstructures in early Arcaean cherts and BIFs from the Isua greenstone belt; implications for the search for life in ancient rocks. *Precambrian Research* **126**(3 – 4), 313 – 330.

Chapter 2

2 Background Information

2.1 Impact-generated Hydrothermal Systems

Recent work has shown that hydrothermal activity is commonplace in the immediate aftermath of an impact event on any H_2O-rich solid planetary surface (Naumov 2005). In an impact crater, the heat source is provided by impact-melted or -heated materials providing a transient source of heat in an otherwise cold environment. The interaction of water with these hot materials forms a hot rock-water circulatory system that can dissolve, transport, and precipitate various mineral species (Osinski *et al.* 2001; Osinski *et al.* 2005). An exceptionally well-preserved example of impact-generated hydrothermal systems is located at the Ries impact structure (Fig. 2.1), southern Germany (Newsom *et al.* 1986; Osinski 2005; Fig. 2.2).

In addition to generating hydrothermal systems, impacts on Earth are capable of altering the pre-existing terrestrial environment that can, in turn, render them viable biotic habitats with evolutionary and adaptive advantages for lithophytic organisms (i.e., organisms that live on or within rocks; Cockell *et al.* 2002, 2005; Cockell 2004). Studies of shock-metamorphosed target rocks at the Haughton impact structure, Devon Island, Nunavut, have indicated that impact induced fracturing and shock metamorphism may increase both the porosity (by up to a factor of 25; Cockell 2004), and translucence (penetration of photosynthetically available radiation) of target rocks, including crystalline lithologies, thereby increasing the surface area for colonizing microbes (Cockell *et al.* 2005). These endolithic habitats offer relatively warm, moist, and UV-protected environments relative to the surroundings, which persist for much longer than the fundamentally transient post-impact hydrothermal systems. Previously, it was thought that endolithic habitats were restricted to sedimentary rocks, such as sandstone and carbonates. However, the discovery at Haughton that shock metamorphism can transform crystalline rock into to suitable endolithic habitats facilitating microbial colonization (Cockell *et al.*, 2002) has important implications for the search for life on Mars.

2.2 The Ries impact structure: Geologic Setting

The mid-Miocene Ries impact crater located in southern Germany is arguably one of the best-characterized and best-preserved terrestrial impact structures (see Pohl *et al.* 1977; Engelhardt 1990 for reviews). Shoemaker and Chao (1961) first recognized the impact origin of the Ries structure in 1961 by the identification of coesite, a high-pressure polymorph of SiO_2, and lechatelierite, a pure SiO_2 glass, within the glass-bearing impact breccia. $^{40}Ar/^{39}Ar$ laser-probe dating of tektites constrains the age of the Ries Crater to 14.6 $\pm$ 0.2 Ma (Buchner *et al.* 2010). Ries is a complex crater with a total diameter of ~24 km (Pohl *et al.*, 1977). The approximately circular inner basin has a diameter of 12 km representing the maximum extent of the transient cavity (Wunnemann *et al.* 2006). A crystalline inner ring of uplifted basement surrounds the inner basin. The megablock zone, a tectonic ridge comprised of a system of concentric normal faults, extends from the inner ring to the crater rim with a maximum extent of ~24 km (Pohl *et al.*, 1977; Fig. 2.1).

The two-layer target is comprised of dominantly Mesozoic flat lying sediments that unconformably overlie crystalline Hercynian basement (Pohl *et al.* 1977). At the time of impact the thickness of the sedimentary package varied from ~470 m in the north to ~820 m in the south. The lower sedimentary unit consists of sandstone, siltstone and marl overlain by an upper limestone unit (Schmidt-Kaler 1978). The Hercynian basement consists of steeply dipping gneisses, amphibolites, and ultrabasic rocks that are cut by later granitic intrusions (Graup, 1978).

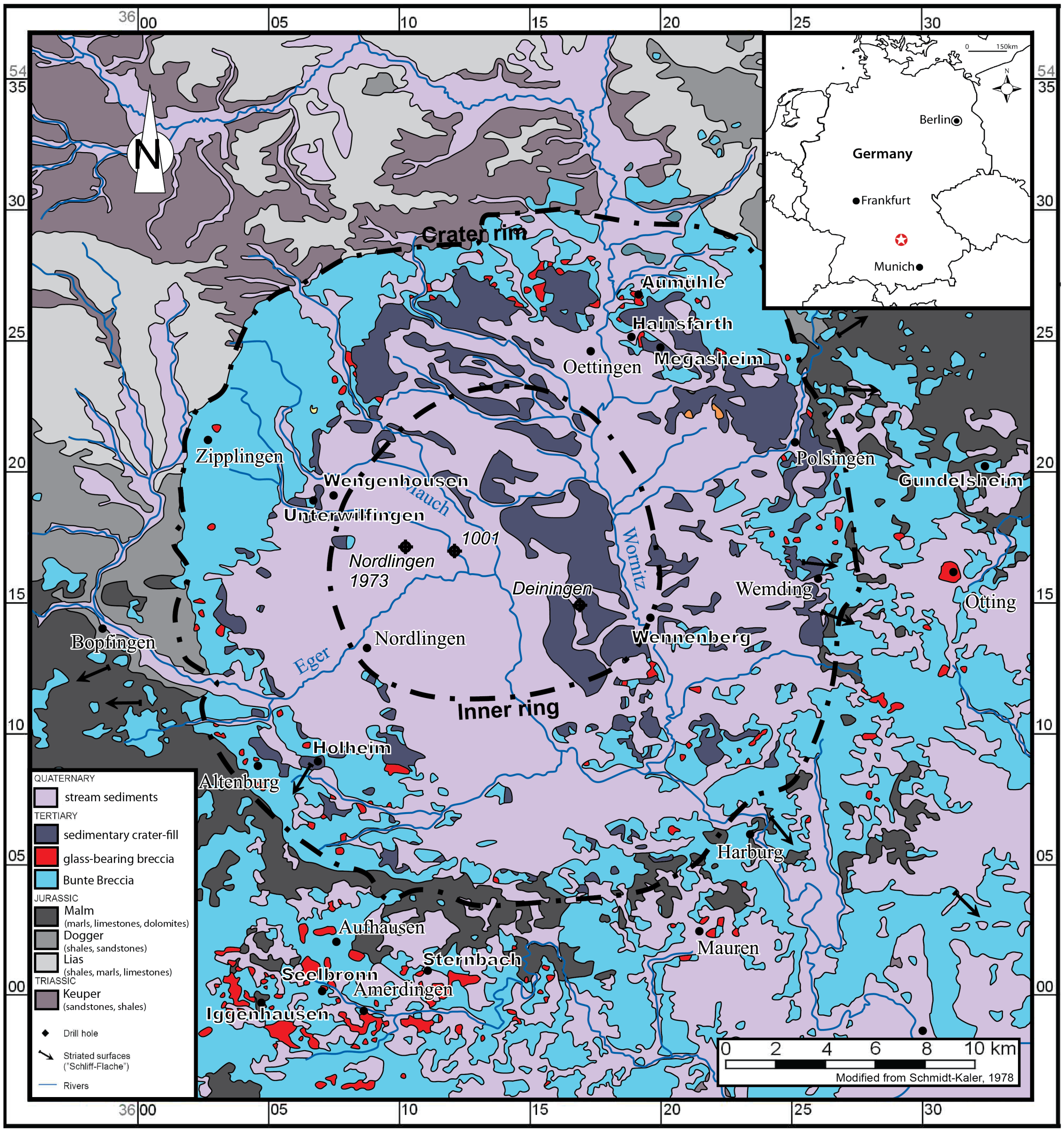

Figure 2.1: Simplified geologic map of the Ries impact structure, with sample locations.

Modified from Osinski (2003). The inner dotted line delineates the crystalline inner ring of uplifted basement that surrounds the ~12 km inner basin. The outer dotted line marks the ~24 km diameter crater rim. Samples were obtained (appendix A) from the indicated locations representing the spatial distribution of the impactite outcrops.

2.2.1 Impactites and ejecta

Impactites and ejecta deposits are exceptionally well preserved at the Ries crater. The sequence of impactites preserved at the Ries crater include: a) a thick series of crater-fill rocks ('crater suevite'); b) various proximal ejecta deposits preserved up to a radius of ~37 km from the crater centre (Fig. 2.1); and c) a tektite strewn field extending out to distances of 260 – 400 km east and northeast of Ries (Hörz 1982). The allochthonous crater-fill units occur within the inner basin and consist of 'crater suevite' overlain by ~400 m of post-impact lacustrine sedimentary rocks (Pohl *et al.*, 1977) reflecting the existence of a post-impact crater lake. There are four main types of proximal ejecta identified at the Ries impact crater which overlie the outer zone of the structure: 1) Bunte Breccia and megablocks; 2) polymict crystalline breccias; 3) 'surficial' suevites; and 4) coherent impact melt rocks (Engelhardt 1990; Osinski 2004; Fig. 2.1).

The Bunte Breccia is the most abundant proximal ejecta unit by volume. Outcrops of this poorly sorted, glass free, polymict breccia have been interpreted as remnants of a continuous ejecta blanket which was emplaced along ballistic trajectories (Oberbeck 1975; Morrison & Oberbeck 1978; Hörz 1982; Hörz *et al.* 1983), The Bunte Breccia is derived predominantly from the uppermost sedimentary target sequences (Hörz 1982; Hörz *et al.* 1983). The Bunte Breccia is comprised of two main components: a) primary ejecta excavated from the initial crater that is dominantly sedimentary rock with subordinate admixtures of crystalline material (predominantly granites); and b) local material or secondary ejecta. The secondary ejecta zone includes deposits of primary ejecta that have been re-mobilized and incorporated by the secondary cratering action of the primary ejecta (Hörz *et al.* 1983). Megablocks are defined as "displaced fragments of all stratigraphic units of the target rocks, which are larger than 25 m in size and can be mapped geologically" (Pohl *et al.* 1977, p. 354).

The Polymict crystalline breccias are mixtures of crystalline rock fragments of different lithologies and shock levels (Pohl *et al.* 1977). Rare irregular outcrops (a few tens of meters in size) of the polymict crystalline breccias occur overlying the Bunte Breccia in the inner ring and megablock zone (Engelhardt 1990). Stratigraphic relationships between the polymict crystalline breccias and the Bunte Breccia are not always clear (Pohl *et al.* 1977).

The surficial suevite (after Engelhardt *et al.* 1995) is distinct from the crater-fill suevite. Isolated outcrops of surficial suevite overlie the Bunte Breccia inside the morphological rim of the Ries Crater and up to radial distances of ~14 km beyond the rim to the south-southwest and east-northeast (Engelhardt 1990; Fig. 2.1). The surficial suevite was deposited on the uneven surface of the upper Bunte Breccia. Deposits of the surficial suevite range in thickness from a few meters to ~25 – 30 m (Engelhardt *et al.* 1990). The Wörnitzostheim drill hole within the megablock zone penetrated ~80 m of suevite. The surficial suevite contains lithic, mineral and glass clasts hosted within a dominantly montmorillonite (30 – 40 vol%) and glass (30 – 50 vol%) groundmass which constitutes ~ 80 vol% of the suevite units (Engelhardt 1990). The remainder of the groundmass is composed of fine-grained lithic and mineral clasts. The abundance of calcite within the groundmass is variable accounting for up to 40 – 50 vol% (Graup 1999), In contrast to the Bunte Breccia, crystalline material dominates the lithic clasts hosted within the suevite (*e.g.*, Pohl *et al.* 1977; von Engelhardt & Graup 1984; Engelhardt *et al.* 1995). However, a new road cut exposes suevites that conation ~8 vol% limestone clasts (Srebenschock *et al.* 1998). Glasses within the surficial suevite occur as either angular or amoeboid particles (Engelhardt 1990). Bringemeier (1994), divided the surficial suevite into two distinct lithologic units: 1) dominant main suevite that represents a clast-rich impact melt rock emplaced via impact melt flows (Osinski *et al.* 2004); and 2) subordinate basal suevite, a fall-out suevite, *sensu stricto*.

The well-consolidated main suevite forms the bulk of all surficial suevite outcrops. The main suevite contains abundant glass, mineral and lithic clasts. There are no indications of sorting or layering (Engelhardt *et al.* 1995) and the preferred horizontal orientation of flat glass clasts constitutes the only observed textural regularity (Engelhardt & Hörz 1965; Bringemeier 1994). Glasses within the main suevite occur both as groundmass phases and as discrete glass clasts (Osinski 2004). Glass clasts are typically vesiculated, schlieren-rich mixtures containing abundant mineral and lithic fragments (Engelhardt & Hörz 1965; Engelhardt 1972; Stähle 1972; Pohl *et al.* 1977; von Engelhardt & Graup 1984;

Engelhardt *et al.* 1995; Vennemann *et al.* 2001; Osinski 2003, 2004), identified four main glass types present within the main suevites.

The groundmass of the main suevites is defined after Osinski (2004) as the fine-grained material that encloses fragments of shocked/unshocked target material exclusive of any identifiable mineral and lithic clasts (>10 – 20 µm across). In a recent study Osinski *et al.* (2004) characterized the groundmass, *sensu stricto*, of the main suevites and has interpreted the groundmass phases as a series of impact melts on the basis of observable textures in SEM BSE. The discrete groundmass components include: silicate mineral and lithic fragments (8.9 – 50.1 vol%), carbonate mineral and lithic fragments (0 – 12.0 vol%), angular impact glass clasts (0 – 18.3 vol%), crystalline calcite (0 – 42.6 vol%), fine-grained clay minerals (1.6 – 70.6 vol%), impact glass comingled with calcite and clay (0 – 16.6 vol%), Fe-Mg-rich plagioclase (0 – 7.5 vol%), rare garnet and pyroxene crystallites (<0.5 vol%), francolite (carbonate-hydroxy-fluor-apatite; 0 – 5.3 vol%), Ba-rich phillipsite (Ca-K-Ba zeolite; 0 – 34.2 vol%). Vesicles can comprise up to several vol% of a sample. The main surficial suevites are typically groundmass supported, however the proportions of the various groundmass phases and clasts vary from thin-section scale to outcrop scale (Osinski *et al.* 2004).

Osinski *et al.* (2004) presents textural evidence that the groundmass phases of the main suevite were in a liquid state at the time of deposition. Furthermore, the observation that the clays are the host phases for the vesicles suggests the generation of volatile-rich melt with vesicles forming following deposition (Osinski *et al.* 2004). The main mass of surficial suevite was emplaced as a high temperature ($580^{o}C$ – $>900^{o}C$; Engelhardt *et al.* 1995; Harker & Tuttle 1955) melt-rich flow containing entrained glass and lithic clasts that emanated from different regions of the evolving crater during the formation of the central uplift during the modification stage of crater formation (Osinski *et al.* 2004).

2.2.2 Ries impact glasses

The glasses hosted in the Ries suevites have been classified on the basis of composition and microstructural characteristics (Osinski 2003). The type I glasses, which host the tubular alteration textures, are most abundant in the Ries suevites, contain Al-rich pyroxene quench crystallites and have SiO_2 contents ~63%. Of all 4 glass types, type I glasses have the highest concentrations of FeO and MgO. The type II glasses have a similar SiO_2 content as type I however contain only plagioclase crystallites. Type III glasses have low SiO_2 contents, are hydrated relative to the other glasses and contain relatively little FeO and MgO while having high Al, Ca, and Na contents. Type IV glasses have very high SiO_2 contents commonly >90% (Osinski 2003).

Silica content and crystallinity affect the dissolution (weathering) and cation release rates of natural materials (*e.g.*, Wolff-Boenisch *et al.* 2004; Wolff-Boenisch *et al.* 2006). The rate-limiting step determining dissolution rates in silicates is the breaking of strong Si-O bonds (Oelkers 2001). The weathering rates (low temperature dissolution) of natural silicates increase systematically with increasing Si content and polymerization. The effect of crystallinity on polymerization consequently affecting dissolution rates is a function of Si content (Wolff-Boenisch *et al.* 2006). Silica-rich glasses have weathering rates ~ 1.6X the weathering rates of their crystalline counterparts (Wolff-Boenisch *et al.* 2006). However, in silica-poor material (once crystalline minerals no longer contain bridging Si-O-Si bonds), crystallinity has little effect on Si polymerization. As a result, the weathering rates of silica-poor glass and crystalline material are approximately equal (Wolff-Boenisch *et al.* 2006). In silica rich material, such as impact glasses, the degree of polymerization is critical to stability. The rapid quenching of natural glasses precludes Si polymerization such that, Si-rich crystalline material will persist 2 orders of magnitude longer than Si-rich glass while the lifetime of Si-poor crystalline material approximates that of Si-poor glass (Wolff-Boenisch *et al.* 2006). Based on theoretical calculations at far from equilibrium conditions, the lifetime of a 1mm natural glass sphere increases exponentially with increasing Si content (Wolff-Boenisch *et al.* 2004). Cation release rates (as non-framework metal ions are leached from the glass) decrease exponentially with increasing Si content (Wolff-Boenisch *et al.* 2004).

The stability (or dissolution rate) and corresponding cation release rates (metal availability) of natural glasses has implications for potential microbial colonization (*e.g.*, (Cockell *et al.* 2009). It has been noted that bioalteration textures are more abundant in basaltic (Si-poor) glasses relative to obsidian (Si-rich glass; *e.g.*, Cockell 2009). The preferential microbial colonization of basaltic glass has been hypothesized to result from greater availability of bio-essential cations as well as easier dissolution of the glass. Impact glasses are characteristically silica rich. In the absence of less-stable basaltic glass, cation content may become more important to potential microbial colonization than cation availability as related to Si content. Despite their high silica content relative to the Ries type II glasses, tubular alteration textures are hosted within type I glass. The significantly higher Fe and Mg contents of the type I glasses relative to the type II glass may explain the presence of the tubular alteration hosted exclusively within type I glass.

The basal suevite is a fine-grained, poorly consolidated, moderately- to well-sorted suevitic impactite unit deficient in glass clasts relative to the main suevite (Chao *et al.* 1978; Osinski 2004). The basal suevite is stratigraphically located between the Bunte Breccia and the main suevite at an outcrop in the Aumühle quarry, Osinski (2004), studied the relationship between the Bunte Breccia and the basal suevite in detail. There is a transitional layer containing clasts of Bunte Breccia material up to ~55 cm thick locally developed between the basal suevite and the Bunte Breccia (Osinski *et al.* 2004; Chao *et al.* 1978). The basal suevite may represent "lateral extensions of the sorted fallback layer from the crater interior" (Newsom *et al.* 1990; Osinski *et al.* 2004).

Isolated bodies of coherent melt rock overlie the Bunte Breccia or megablocks (Graup 1999). Outcrops have a lateral extent of 10 – 50 m (Pohl *et al.* 1977). The microscopic groundmass hosts variably shocked lithic (dominantly granite) and mineral (dominantly quartz) clasts (Engelhardt *et al.* 1969; Pohl 1977). The microcrystalline groundmass consists of alkali feldspar, plagioclase, quartz and illite. Interstices are filled with fresh or devitrified glassy mesostasis (Osinski *et al.* 2004). The impact melt rock has been interpreted by Osinski (2004) as a coherent and discrete impact melt flow that emanated from the evolving crater during the modification stage of crater formation.

2.2.3 Ries impact-generated hydrothermal system

The Ries crater is one of the first impact sites where an impact-generated hydrothermal system has been proposed (Engelhardt 1972; Salger 1977; Stähle & Ottemann 1977; Osinski 2005). The occurrence of secondary mineralization and hydrothermal alteration of the impact suites has been noted and described (*e.g.*, Förstner 1967; Engelhardt 1972; Stähle 1972; Jankowski 1977; Stöffler *et al.* 1977; von Engelhardt & Graup 1984; Newsom *et al.* 1986; Engelhardt *et al.* 1995; Graup 1999; Osinski 2003, 2004; Osinski *et al.* 2004; see Osinski, 2005 for a detailed study of hydrothermal alteration of the Ries impactites).

Using a combination of petrographic and analytical SEM techniques, Osinski (2005) has identified a number of hydrothermal alteration phases within the surficial suevites including clays (dominantly montmorillonite), zeolites, quartz, calcite, hematite and goethite. Alteration phases of the crater suevite include: potassium-feldspar, albite, clays, chlorite, zeolites, calcite, and minor phases including pyrite, goethite, barite and siderite. Alteration assemblages occur in three main settings: 1) open-space cavity and fracture fillings within the groundmass; 2) vesicle linings/fillings within impact glass clasts; and 3) pervasive alteration of groundmass phases and glass clasts (Osinski 2005). Overall the glass clasts are well preserved in the surficial suevites (Engelhardt & Graup, 1984; Engelhardt *et al.* 1995; Graup 1999; Osinski 2003, 2005). The hydrothermal fluids of the Ries impact-generated hydrothermal system were likely derived from a combination of meteoric water from the overlying crater lake and ground waters from nearby country rocks. There is no evidence of a magmatic or metamorphic source (Osinski 2005).

Due to the focused hydrothermal alteration of the suevite units, these impactites were likely the main heat source driving hydrothermal circulation (Osinski 2005; Fig. 2.2). Emplacement temperatures >750^{o}C – 900^{o}C have been suggested for the suevites based on evidence of ductile deformation in glasses following deposition (Osinski *et al.* 2004). Intense pervasive hydrothermal alteration is limited to the crater suevites indicating that early, high temperature (200^{o}C – 300^{o}C) hydrothermal activity was restricted to the crater fill units (Osinski 2005). The surficial suevites were affected by the main and late stages of hydrothermal activity that are characterized by lower peak temperatures (<100^{o}C – 130^{o}C constrained by the lack of illite) and intermediate argillic alteration and zeolitization (Osinski 2005). With the exception of rare instances of pervasive alteration noted in glasses at some localities, the dominant alteration of the surficial suevites is montmorillonite and Ba-phillipsite within cavities, fractures and vesicles. It is significant to note that neither clasts of pre-impact target rocks nor impactite phases were enriched in Ba. Therefore the Ba must have been dissolved by the hydrothermal fluids, transported and precipitated during zeolitization of the surficial suevites (Osinski 2005).

Recent work by Muttik *et al.* (2008) suggests that the Ries impact-generated hydrothermal system was limited to the intensely altered crater suevites and that the alteration of the surficial suevites can be entirely attributed to ambient weathering processes. It is argued that the main alteration phase of the surficial suevites identified as montmorillonite by whole rock powder XRD is chemically homogenous throughout the surficial suevites consistent with low temperature hydrous devitrification of impact glasses. However, Osinski (2005) noted that hydrothermal alteration in the surficial suevites was limited to localized zones including fractures and vugs. Bulk XRD alone is not a suitable technique to identify trace assemblages in spatially restricted zones. It is likely that alteration assemblages formed by post-impact weathering processes are the predominant assemblages of the surficial suevites considering the limited extent of hydrothermal activity in these units. Furthermore no explanation is offered regarding the Ba-phillipsite phase within the surficial suevites.

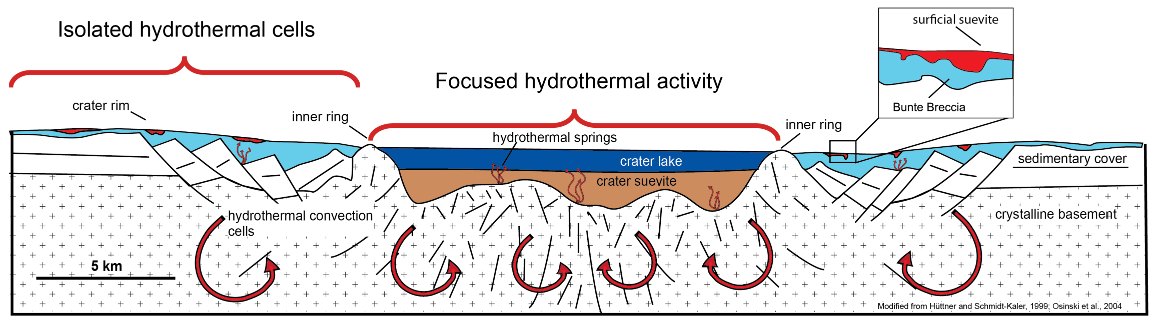

Figure 2.2: Idealized cross section of the Ries crater schematically illustrating the post-impact hydrothermal system.

Schematic cross section showing the heterogeneous distribution of hydrothermal cells relative to the crater centre. The main, high temperature hydrothermal activity is concentrated in the crater fill material beneath a transient crater lake with isolated, patchy systems distal to the crater rim. The primary heat source driving hydrothermal circulation is from impact-heated materials. Note the discontinuous nature of isolated outcrops of glass-bearing breccia (suevite) overlying the Bunte breccia outside the crater rim. Modified from Osinski (2004).

2.2.3.1 Alteration of Crater Suevite

Alteration phases of the crater suevite include: K-feldspar, albite, clays, chlorite, zeolites, calcite, and minor phases including pyrite, goethite, barite and siderite. The alteration assemblages as recorded in the Nördlingen core, are consistent with an early, high-temperature (200 – 300^{o}C) phase of K-metasomatism coinciding with albitization and chloritization followed by pervasive intermediate argillic alteration and zeolitization (Osinski 2005).

2.2.3.2 Alteration of Surficial Suevite

A number of hydrothermal alteration phases consistent with low-temperature (<100 – 200^{o}C) hydrothermal activity including clays, zeolites, quartz, calcite, hematite and goethite have been identified in glass bearing breccia located beyond the crater rim (Newsom *et al.* 1986). The main alteration phase is montmorillonite and Ba-phillipsite. It is significant to note that neither clasts of pre-impact target rocks nor impactite phases were enriched in Ba. Therefore the Ba was likely dissolved by the hydrothermal fluids, transported and precipitated during zeolitization of the surficial suevites (Osinski 2005).

2.2.3.3 Alteration of Surficial Suevite at Depth

Study of the Wörnitzostheim core has shown alteration assemblages consistent with the surficial suevites described above defined by vesicle filling montmorillonite, Ba-rich phillipsite forming within vesicles, and groundmass montmorillonite. At depth (>78 m) montmorillonite and illite become major components and zeolitization occurs. Mineralogical and petrographic evidence of the hydrothermal alteration assemblages present in glass-bearing breccias at the Ries impact structure are presented blow.

2.2.3.4 Evidence for Hydrothermal Activity Outside the Crater Rim

Alteration textures are spatially restricted at the metre scale and include coliform/rhythmic banding, vesicle infilling, pervasive alteration to complete replacement of glass clasts by clay minerals and the occurrence of platy clays. If a limited extent of hydrothermal activity is assumed in these units, then alteration assemblages within the ejected glass-bearing breccia are predominantly formed by post-impact weathering processes. However, an extremely spatially limited hydrothermal system outside the crater rim does not offer an explanation for the Ba-phillipsite phase within the glass-bearing breccias. Furthermore, the similarity of the alteration assemblages between the surficial suevite and the suevite in the Wörnitzostheim core(s) suggests these phases are not due to weathering processes as the Wörnitzostheim core suevite was protected by ~20 m of overburden.

2.2.3.5 Hydrothermal Alteration Summary

Studies of the alteration textures of glassy and formerly glassy clasts within both the ejected and crater-fill glass-bearing breccias has shown a consistent progression from fresh glass through various states of alteration. The phases of alteration inferred from such textures include incipient, low temperature alteration (perlitic fracturing, devitrification and decomposition textures) to evidence of fluid circulation (alteration zones surrounding perlitic fractures and vesicles, banding and zonation) resulting in progressive alteration (globular replacement textures, platy clays) and finally pervasive alteration and complete replacement including the formation of Ba-phillipsite (harmatone) and montmorillonite in both the crater-fill and ejected glass-bearing breccias. Alteration of the surficial suevite followed a progression from high- to low-temperature with textures consistent with hydrothermal alteration, *sensu stricto* over a wide temperature spectrum. Hydrothermal systems were likely spatially extensive in the surficial suevites with localized, higher intensity systems sporadically distributed (Fig. 2.2). Hydrothermal alteration was likely preceded by high-temperature devitrification or autometamorphism and followed by low-temperature weathering.

Similar textural and mineralogical evidence of hydrothermal alteration in both the crater-fill and ejected glass-bearing breccias suggests a similar progression of alteration processes in both units consistent with hydrothermal alteration. It is suggested that the impact-generated hydrothermal system at the Ries impact structure was much more extensive and pervasive outside the crater rim area than previously reported.

2.3 Bioalteration of Natural Glasses

Bioalteration of natural glasses is a well-documented phenomenon. Conspicuous tubular and granular morphologies, with no known parsimonious abiotic formation mechanism, hosted within oceanic basaltic glasses are widely accepted to represent microbially mediated alteration textures (Thorseth *et al.* 1995, 2003; Fisk *et al.* 1998; Torsvik *et al.* 1998; Furnes *et al.* 2001a,b, 2004; Banerjee & Muehlenbachs 2003; Furnes & Muehlenbachs 2003; Banerjee *et al.* 2004, 2006a,b, 2008; Staudigel *et al.* 2006, 2008a,b; Benzerara *et al.* 2007; Peckmann *et al.* 2008; Izawa *et al.* 2010a,b). Tubular and granular alteration of submarine volcanic glasses are recognized in modern oceanic crust, Phanerozoic ophiolites and Archaean greenstone belt constituting both temporally and spatially distributed ichnofossils (McLoughlin *et al.*, 2008; Thorseth *et al.*, 1991; Banerjee 2006, 2007; Banerjee & Muehlenbachs, 2003; Furnes 2004; Furnes *et al.*, 2008; Staudigel *et al.*, 2008a).

Microbial alteration textures in basaltic glass formed through endolithic microboring are characterized by microstructures of two distinct morphologic types: agglomerations of micron-scale pits forming a granular texture emanating from a single point; and vermicular tubular features. The latter have large length to width ratios that may spiral, bifurcate and/or display regular segmentation (*e.g.*, Banerjee & Muehlenbachs 2003; Furnes *et al.* 2008; McLoughlin *et al.* 2008a; Staudigel *et al.* 2008a,b). These characteristic hollow etch features are commonly filled with authigenic mineral phases such as phyllosilicates, zeolites, Fe-oxyhydroxides and titanite (Banerjee & Muehlenbachs 2003; Benzerara *et al.* 2007; Staudigel *et al.* 2006).

In addition, it has been shown that endolithic microbial communities thrive in terrestrial and submarine volcanic glasses with a range of SiO_2 contents (Richardson *et al.* 2007; Santelli *et al.* 2008; Cockell *et al.* 2009; Herrera *et al.* 2009). Pitted and elongated alteration features have been described in subaerial volcanic glass (*e.g.*, Furnes 1984; Thorseth *et al.* 1992; Herrera *et al.* 2008; Cockell *et al.* 2009). However, elongate features have only been observed in glasses of basaltic composition while microbial alteration is confined to rounded (convex hemispherical) etch pits in more siliceous glasses (Cockell 2009). In the case of terrestrial biologically mediated glass alteration, biomorphic features have only been observed on the exposed surfaces suggesting a role for phototrophic communities (Thorseth *et al.* 1992; Herrera *et al.* 2008).

Secondary ion mass spectrometry (SIMS) analyses of basaltic glass samples with abundant tubular bioalteration from the Ontong Java Plateau revealed significant chemical variations in areas with tubular microbial etch structures including: alkalis, which show depletion in Na with enrichment in K and Rb; enrichments in the alkaline elements (Ca, Sr, Ba) and the high field strength elements (Ti, Y, Zr); the first row transition metals V, Cr, and Mn are slightly enriched, while Fe, Co, Ni, Cu, and Zn are depleted; Mo and W and the lanthanides are enriched in tubule-bearing regions; slight enrichments in U and P are also observed. Overall findings indicate a correlation between element variation and the presence or absence of tubular alteration in the OJP glasses. This is consistent with microbial dissolution of the glass but no direct link between a particular element and a microbial metabolic pathway has been established. Enrichment of elements like titanium and calcium are consistent with the identification of titanite by micro-XRD within the tubules (Izawa *et al.* 2010a). Titanite mineralization is coeval with glass dissolution and tubule formation. An interesting and unexpected outcome of the SIMS analyses is the discovery of delicate, spongy textures within the tubules revealed by ion sputtering. These textures have been interpreted to be the direct result of incongruent dissolution of the glass in proximity to the tubules.

Additional evidence for biogenicity is focused on chemical evidence for biological processing and includes; elemental distribution patterns, stable isotope signatures, and evidence of organic matter (Giovannoni *et al.* 1996; Torsvik *et al.* 1998; Furnes *et al.* 2001b; Banerjee & Muehlenbachs 2003; Walton & Schiffman 2003). X-ray element mapping of basaltic glass hosting microborings is often enriched in carbon, nitrogen and phosphorous (*e.g.*, Furnes *et al.* 2001a; Banerjee & Muehlenbachs 2003; Banerjee *et al.* 2006, 2007; Staudigel *et al.* 2008a). In addition, Mg, Fe, Ca, and Na depletion zones surrounding tubule alteration have been identified as a biological processing signature as microbes extract essential elements from glass resulting in leached zones (McLoughlin *et al.* 2007). Stable isotope studies have been conducted on several modern oceanic glasses (*e.g.*, Furnes *et al.* 2001a,b; Banerjee & Muehlenbachs 2003; Furnes *et al.* 2007, 2008;

Staudigel *et al.* 2008a, 2008b), obducted Phanerozoic ophiolites (Furnes & Muehlenbachs 2003; Furnes *et al.*, 2001a,b, 2007, 2008; Staudigel *et al.* 2008a,b), as well as Archean greenstone belts (Furnes *et al.* 2004; Banerjee *et al.* 2006, 2007; Furnes *et al.* 2007, 2008; McLoughlin *et al.* 2008a) all documenting negative $\delta^{13}C_{carb}$ isotopic signatures interpreted as evidence for biologically processed carbon. Fluorescence (DAPI: 4,6 diamino-phenyl-indole) staining of tubular features in modern basaltic glass samples has identified nucleic acids within the terminal end of the tubules (*e.g.*, Banerjee & Muehlenbachs 2003). Organic carbon coating the micro-burrows has also been identified through carbon X-ray mapping (Torsvik *et al.* 1998; Banerjee & Muehlenbachs 2003) and near-edge fine-structure X-ray spectroscopy (Benzerara *et al.* 2007).

2.4 Biogenicity Criteria

It is notoriously difficult to assign biogenicity to a putative ichnofossil (*e.g.*, Brasier *et al.* 2002; Cady *et al.* 2003; Garcia-Ruiz *et al.* 2003). Systematic criteria for determining the biogenic morphology of tubular glass alteration has been reviewed in detail elsewhere (*e.g.*, Morrison & Oberbeck 1978; Staudigel *et al.* 2006; McLoughlin *et al.* 2008). McLoughlin *et al.* (2007) developed a three-pronged approach to assessing the biogenicity of putative ichnofossils. Tentative bioalteration features must satisfy the following three criteria before a biogenic origin can be determined: "(1) a geological context that demonstrates the syngenicity and antiquity of the putative biological remains; (2) evidence of biogenic morphology and behaviour; and (3) geochemical evidence for biological processing" (McLoughlin 2007).

Staudigel *et al.* (2007) introduces a series of textual arguments further expanding on morphological evidence for biogenicity. These arguments are summarized below in the context of the Ries tubules:

- Tubules do not line up on opposite sides of fracture and therefore do not represent planes of weakness.

- Tubule diameters are on the order of a micron, consistent with the size of microbial cells and microbial borings in terrestrial volcanic glass (Staudigel *et al.* 2008a).

- The tubule diameter remains constant, i.e. there is no narrowing or flaring at the entrance or terminus of the tubule as would be expected from abiotic dissolution or vesicle generation.

- A population of tubules in the Ries glasses display regular segmentation consistent with segmented biotic filaments suggestive of multiple cells within a sheath.

- A sub-population of segmented tubules shows clear bifurcation suggestive of cell division.

- The spiral morphology of some tubules in the Ries glasses is extremely hard to reconcile abiotically, but closely resembles bacterial spirochete morphology (McLoughlin *et al.* 2009).

Recently this biogenicity criteria has been applied to a series of tubular alteration textures observed in a Palaeozoic ophiolite and Precambrian greenstone belts: Titanite mineralized tubular textures were observed in ~442 Ma pillow lavas from a Caledonian west Norwegian ophiolite (Fliegel *et al.* 2011); Annulated tubular textures in Proterozoic pillow lavas from the Pechanga greenstone belt (Fliegel *et al.* 2010); and tubular alteration features in Archean pillow lavas from the Wutai greenstone belt (McLoughlin *et al.* 2010). In all three cases, titanite dating and the overprinting of later metamorphic events demonstrated the syngenicity and antiquity of the features.

The Caledonian tubules (Fliegel *et al.* 2011) lacked the morphological complexity and large length to width ratios typically associated with tubule bioalteration features (*e.g.*, Furnes *et al.* 2004; Banerjee *et al.* 2006a; McLoughlin *et al.* 2009). In contrast, the Pechanga (Fliegel *et al.* 2010) and Wutai (McLoughlin *et al.* 2010) features do display a complexity suggestive of biogenic morphology and behaviour. The Caledonian features did not meet the biogenicity criteria as they did not display complex morphologies suggestive of a biotic origin and geochemical evidence could neither support nor refute biological processing. The origin of these features remains ambiguous although the authors suggest they may represent the initial stages of microbial etching (Fliegel *et al.* 2011).

The complex morphology together with geochemical evidence of biological processes allowed the Pechanga tubular features to be classified as ichnofossils preserving microbial tunnelling (Fliegel *et al.* 2010). Geochemical evidence is not discussed with respect to the Wutai features, however their morphological similarity to both *in situ* bioalteration of modern ocean crust and ichnofossils in other Precambrian greenstone belts led the authors to conclude that the Wutai tubular features are biogenic in origin (McLoughlin *et al.* 2010).

2.5 Mechanisms of Microbially Mediated Glass Alteration

Various mechanisms of glass tunnelling by microorganisms have been hypothesized (*e.g.*, McLoughlin *et al.* 2010b). Community structures are likely complex and difficult to elucidate as there is likely not a one-to-one correlation between an organism and the tubular structure preserving behaviour. One species may preserve multiple tunnel morphologies depending on life cycle stage or environmental conditions; conversely, multiple organisms may create similar tunnel morphologies. In addition, taphonomical change, such as that caused by mineralization, and diagenesis may distort tubule morphologies and the resulting preserved structure likely represents a combination of biological behaviour and preservation history.

McLoughlin *et al.* (2010b) provides detailed reasoning concluding that chemical dissolution is the only feasible mechanism of tubule formation in natural glass. Microbes are able to selectively dissolve various substrates to gain essential nutrients resulting in the generation of protective endolithic habitats (*e.g.*, Cockell & Herrera 2008). Experimental studies show that congruent and incongruent dissolution of rock substrates occurs via localized pH changes. Microbes are able to locally alter pH through bioalkalization (*e.g.*, Büdel *et al.* 2004) or production of organic acids (*e.g.*, Callot *et al.*

1987). Microbes may initially colonize fractures and grain boundaries, as the microbe continues to dissolve the substrate extracting essential metabolites, a cavity forms. Initially, fluid circulation removes waste products as well as preventing authigenic mineral precipitation from sealing off the tunnel. As the tunnel extends, however, circulating fluid would become minimal and alteration and metabolic waste products would begin to build up. Cellular extensions, such as fungal hyphae, have been suggested as a mechanism to continue localized dissolution and tunnel formation (Staudigel *et al.* 2008). Many prokaryotes (*e.g.*, the actinomyces) are also capable of forming hypha-like extensions (McLoughlin *et al.* 2010b). Eventually, it can be speculated that tunnel formation would no longer be advantageous as waste products and low-permeability mineral alteration products continue to increase. Once no longer sustained by fluid circulation, or cellular extensions are withdrawn, the tubular cavities become preserved by authigenic minerals and their diagenetic products.

Molecular profiling of endolithic microbial communities in submarine volcanic glasses suggest autotrophs as initial colonizers employing Fe and Mg cycling as potential metabolic strategies (*e.g.*, Edwards *et al.* 2005 and references therein; Thorseth *et al.* 2001). Chemoautolithotrophs may actively oxidize reduced species such as Fe^{2+}, Mn^{4+}, and $(SO^4)_2$, in the glasses with the oxidized fluids acting as the electron acceptor (McLoughlin *et al.* 2010). Such dependence on reduced species may explain the chemical control on tubule distribution and the experimental finding that endoliths prefer Fe rich substrates (Roberts-Rogers & Bennett 2004). Tubules in the Ries glasses are enriched in Mg, Ca, and Fe and depleted in Na, K, Al, and Si relative to the glassy matrix. Ca-clinopyroxene quench crystallites present in the type I glass clast display similar enrichment and depletion patterns. Pyroxene crystallites are rich in bio-essential elements such as Fe and Ca that are lacking in the glassy matrix. It is conceivable that microbes are preferentially extracting these bio-essential elements from crystallites. These elements would therefore become concentrated within the tubules and preserved following decay of organic matter. A similar preservation mechanism has been suggested for tubules preserved by titanite mineralization in Archaean greenstone belts (Izawa et al 2010a). In the case of Archaean tubules, Ti is passively accumulated by microbes and concentrated within bioalteration features.

2.6 Biology of Impact Craters

2.6.1 Impact craters as microbial habitats

The intense heat generated by hypervelocity impacts results in local sterilization of the target area. Meteorite impacts can therefore be viewed as biological resetting events resulting in the generation of a primary succession environment. The earliest phase of ecological recovery following an impact event, the phase of thermal biology 'during which the thermal anomaly associated with a recently formed crater sustains biological activity of a nature or at a level requiring warmed environmental conditions' is of astrobiological interest (Cockell & Lee 2002). The impact flux on the Archean Earth was more than twice the present level (Cockell 2004). As a result, endolithic habitats are being considered as possible locations for life on early Earth (Westall & Folk 2003) and on the surface of other planets such as Mars (Wierzchos *et al.* 2003). Understanding the geomicrobiology of impact craters on Earth is critical in furthering the search for life on Mars. The hydrothermal systems associated with impact events may therefore provide an additional setting to study evidence of early life on Earth. Further studies considering the potential hydrothermal habitats of impact craters may not only yield insight into early life and the origin of life on Earth, but furthermore, may comprise a potential habitat for life and past life on other terrestrial planets such as Mars.

2.6.2 Early Earth

The environment created by an impact crater has several characteristics that make it conducive to prebiotic chemistry (Cockell 2006). Theories of prebiotic synthesis must consider the following: an energy source for growth and metabolism, a localized area in which reactants can concentrate suitable mechanisms of catalysis and an appropriate geochemical environment which is stable over a time scale over which life can evolve. Environments created by impact events are driven by diverse energies, ranging from latent heat to the redox potential of novel juxtapositions of chemical species. The fracturing of target rocks and hydrothermally driven fluid migration act as mechanisms that may act to concentrate the possible precursors of prebiotic chemistry within the hydrothermal system. The secondary hydrothermal minerals such as clays and zeolites have been suggested as prebiotic templates (Cockell 2006). Hydrothermal activity at Haughton (~23 Km diameter) is estimated to have lasted for tens of thousands of years (Osinski *et al.* 2005). Studies of larger structures such as of the ~250 km diameter Sudbury impact structure suggest that the impact-generated hydrothermal system may have been sustained for up to 2 Ma based purely on conductive cooling (Ames *et al.* 1998).

Tubular bioalteration of volcanic glasses back to ~3.5 Ga provide one of the earliest records of life on Earth (Banerjee *et al.* 2006a; Staudigel et al 2008a) suggesting that submarine hydrothermal settings may have played an essential role in the origin of life. Periodic global heating may account for the thermophilic root of life preserved in 16s rRNA sequences (Pace 1997; Schwartzman & Lineweaver 2004). In this sense meteorite impacts could not only have generated the putative bottleneck resulting in a perceived thermophilic last universal common ancestor, but would also select for thermo-tolerant life surviving previous impacts (Cockell & Lee 2002). Therefore, the endolithic habitats produced by increasing the porosity of crystalline targets during shock metamorphism would provide a refuge from frequent meteorite bombardment and intense UV radiation. The high flux rate of meteorite impacts on the early Earth would favour life in endolithic environments suggesting that meteorite impacts played a pivotal role in the early evolution, if not origin of, life on Earth and possibly life on other planets.

2.6.3 Beyond Earth

On Earth, endolithic microbes are often present in extreme conditions such as vast temperature changes, high UV intensity and desiccation, suggesting that endolithic microbes can tolerate and thrive in environmental extremes. The extreme conditions present on Mars, such as intense UV flux, low temperature, and absence of liquid water may also encourage the exploitation of endolithic strategies. McLaughlin *et al.* (2007, 2010) suggest microborings into volcanic glasses as a potential planetary biosignature and lists natural glasses as one of the most promising preservation environments for ichnofossils on early Earth and Mars. By extending this to impact glasses we greatly increase the number of candidate environments. Although impact craters are uncommon on present day Earth, (~50,000 km^2 globally), impact events are the only ubiquitous geological processes in the Solar System and impact structures represent the dominant geological landform amongst the terrestrial planets (Grieve 1987; Melosh 1989; French 1998; Melosh & Ivanov 1999; French & Koeberl 2010; Osinski 2012).

2.6.4 Impact craters as sites of biological preservation

Impact systems are understudied from the perspective of biological preservation. To the best of the authors' knowledge there are only four studies reporting fossil evidence of biological activity in impact systems: microbial etching of hydrothermal minerals at the Ries impact structure (Glamoclija *et al.* 1989); the presence of rod-shaped biomorphs in post-impact hydrothermally altered sediments from the Chesapeake Bay impact structure (Glamoclija 2007); evidence of extracellular polymeric substances in a hydrothermally precipitated calcite vein from the Siljan impact structure (Hode *et al.* 200); and most recently, a report of filamentous 'fossils' hosted in hydrothermally precipitated mineral assemblages within fractured impact breccia from the Dellen impact structure (Lindgren *et al.* 2010). In all the above studies there is a systemic failure to recognize biogenicity criteria and all evidence rests on tenuous morphological evidence.

Glamoclija (1989) describes titanium oxide 'biomineralized' rod-shaped features and associated etch pits on hydrothermal clinoptilolite. The biogenicity of the rod-shaped features is based solely on their morphology. The images presented depict a mass of ovoid particles, whose morphology is not necessarily biogenic. Furthermore, syngenicity and antiquity of the biological remains is not demonstrated, nor is a uniquely biogenic morphology.

Glamoclija (2007) recognized the importance of establishing biogenicity based on multiple lines of evidence stating: "further work is needed in order to verify biogenicity of observed communities by multiple datasets, and to confirm their syngenicity with the hydrothermal overprint." Further work has not been as of yet completed. The textures described, if biological, may represent microbial communities taking advantage of the chemical disequilibria created by the precipitation of hydrothermal minerals at any point post the ~35.3 Ma impact.

The most recent work by Lindgren *et al.* (2010) at the Dellen impact structure, Sweden, fails to address all previously proposed criteria for biogenicity. Furthermore, the samples and hydrothermal alteration in which the putatively biological structures occur, cannot unambiguously be tied to the impact event. The samples were collected from 'large blocks and boulders' apparently lacking field context. The granite samples do not show impact shock effects other than fracturing suggestive of a very low shock level. The unidentified hydrothermal clays and zeolites may be from any post-impact aqueous alteration and do not unequivocally represent impact-generated hydrothermal activity. Impact-generated hydrothermal activity is heterogeneously distributed and occurs only as isolated, limited patches distal to the crater centre. The impactites collected likely represent distal ejecta indicated by their low shock level and occurrence in monomict breccias. Even though no evidence of syngenicity is presented, the authors cite formation of the feature coeval with impact-generated hydrothermal activity as the only line of evidence for biogenicity. Further to the lack of geological context, the authors fail to address biological behaviour as indicated by distribution or a uniquely biogenic morphology. The photomicrographs presented are obscure and the features cannot be unambiguously differentiated from ambient inclusion trails (AITs). In addition, no geochemical evidence of biogenicity is offered. The features lack evidence of organic matter and are not associated with alteration of the hosting material. In summary Lindgren *et al.*, (2010) present an unconvincing argument for both biogenicity as well as association with an impact-generated hydrothermal system.

Although the Glamoclija and Hode studies do present convincing cases for association with a post-impact hydrothermal system, biological activity at hydrothermal systems is not novel, and microbes exploiting this well-studied niche in post-impact hydrothermal systems are not unexpected. In contrast, the subject of this thesis presents evidence of microbial activity in a previously unstudied substrate unequivocally tied to an impact event and an impact-generated hydrothermal system.

2.7 Characterization of the Ries Tubules

2.7.1 Fieldwork

Fieldwork was conducted July 2009 and 2010 at the Ries impact structure. A list of samples and sampling locations is presented in Appendix A. See appendix 2 for a collection of representative field photograph. In 2009 sites of interest identified during previous field seasons by Osinski were visited and a sample suite was collected. Sampling was focused on A: obtaining a variety (both in location and morphology) of suevitic glass clasts to constrain the distribution of the tubular alteration; and B: collecting samples with a focus on identifying various alteration assemblages. Understanding and identifying the many different and complex alteration assemblages at the Ries impact structure may help to better constrain the impact-generated hydrothermal system with implication for microbial colonization.

In addition to sample collection, as putative bioalteration at the Ries crater has not previously been documented and previous field sampling plans were not executed as to address the question of bioalteration and putative microbial colonization of suevitic glasses, a list of sites of interest was assembled with a focus on constraining the distribution of putative bioalteration textures and understanding the complex alteration history at the Ries. Additional fieldwork in 2010 at the Ries crater was focused on determining fine scale distribution of the tubular alteration in association to hydrothermal alteration. Sampling and transect sites were be chosen based on the distribution of tubular alteration observed in thin sections cut from 2009 field samples. Depth profiles and transects were constructed across surficial suevite outcrops and samples obtained at regular intervals to assess the distribution of putative bioalteration within suevite outcrops. The distribution of alteration is significant and may have biological and ecological implications. In addition, sites of interest with respect to hydrothermal alteration were revisited.

2.7.2 Establishing geologic context

It is imperative to document and thoroughly describe the geological context of a putative ichnofossil. A representative suite of impact-melt bearing breccias from the Ries impact structure were examined in hand sample and polished thin section. Approximately 100 thin sections derived from five field campaigns (2000, 2001, 2005, 2009, 2010), were chosen for petrographic study, see appendix 3 for representative petrographic light photomicrographs. In Chapter 3, an impact suite from the Rochechouart impact structure is used as a case study to identify and classify impact lithologies based on their intrinsic characteristics.

Classical impactite classification schemes do not account for intermediate lithologies and as a result, transitional lithologies are inadequately described by end-member nomenclature. Further to the issue of transitional lithologies, the currently accepted IUGS impactite classification scheme is based on the location of the impactite with respect to the transient cavity. Such classification requires interpretation of field context and absolute knowledge of the location of the crater rim. Both of these perquisites are currently debated in the literature leading to ambiguous and inconsistent use of nomenclature in the literature. Interpretive bias aside, the majority of terrestrial impact structures are not preserved well enough to consistently and accurately delineate the extent of the transient cavity. Furthermore, in cases where there is no field context, such as deeply eroded structures, meteorite breccias, and future sample returns, classification based on provenance is purely speculative. The petrographic evaluation of the Rochechouart impactites presented in Chapter 3 allows for a systematic classification integrating the most recent recommendations of the IUGS Subcommission on the Systematics of Metamorphic Rocks (SCMR; Stöffler and Grieve, 2007) with descriptive nomenclature allowing for indeterminate and transitional units.

Chapter 4 presents the results of a detailed petrographic and electron microscope study defining the geological context of the Ries tubules, see appendix 4 for additional electron microscopy images. Reflected and transmitted plane polarized and crossed polarized light was used for imaging using a Nikon Eclipse LV100POL petrographic light microscope equipped with a Nikon DS-Ri1 12 Megapixel camera. Extended-depth of focus images (EDF) were obtained using plane-polarized transmission microscopy by aligning multiple images in the z plane using Nikon Elements software. On average 25 – 35 images were collected at ~0.4μm *z*-spacing and merged to created a single EDF image. Reflected light was used to target areas for SEM analysis by identifying regions where tubules intersected the thin section surface. Two glass clasts one from the Amerdingen and Seelbronn localities that contained representative tubular textures were chosen from the optical images for further analysis.

Three glass clasts were chosen for micro-X-ray diffraction (μ-XRD) analysis from a polished thin section of the Amerdingen. Glass clasts were chosen based on size (>50μm) and absence of large vesicles and lithic inclusions. X-ray diffraction data were collected in coupled geometry with θ1=5º and θ2= 17º with a frame width of 30.5º and scanning speed of 1.22º/min using the Bruker D8 Discover micro X-ray diffractometer (μXRD) at the University of Western Ontario (Flemming 2007), operated using Cu Kα radiation generated at 40 kV and 40 mA with a beam diameter of 50 μm. Diffracted X-rays were detected by a General Area Detector Diffraction System (GADDS). Diffractograms were analyzed using the BrukerAXS EVA software package and the International Center for Diffraction Data (ICDD) PDF-4 database.

High-resolution backscatter electron (BSE) imaging and energy dispersive X-ray (EDX) spectroscopy spot analyses were carried out with a Leo 1540 FIB/SEM CrossBeam field emission SEM equipped with an Oxford Instruments INCA EDX system allowing for elemental analysis, sensitive to ~0.5 wt.% or less for all elements from C – U in the Nanofabrication Laboratory, University of Western Ontario. Samples were Pt sputter coated using the Denton Vacuum Desk 2 for 200 seconds at 15 mA. The sections were analyzed under high vacuum with an accelerating voltage of 15 – 20 kV and a working distance ~10 mm. Energy dispersive X-ray (EDX) spectroscopy mapping and spot analyses of selected samples allowed for the identification of elemental distribution on a micron scale.

Further SEM imaging and EDX mapping was carried out on a Hitachi SU6600 variable pressure field emission SEM (Schottky emitter) equipped with an Oxford Instruments 80mm^2 silicon drift detector at the University of Western Ontario Zircon and Accessory Phase analysis facility. The spectral resolution of the EDX detector was 129 eV at an accelerating voltage of 5.9 keV. Samples were analyzed under vacuum at a working distance between ~10 – 15 μm and an accelerating voltage of 10 – 15 kV with a probe current of 1 – 2 nA. BSE images were captured with a five segment solid-state detector. Samples were coated as above and all data was analyzed with Oxford Instruments INCA software.

Additional quantitative electron probe analyses were analyzed by energy dispersive X-ray spectroscopy (EDX) conducted on a Cameca SX100 electron microprobe at the Electron Microprobe Laboratory at the University of Alberta. A defocused 10μm beam was used to collect EDX spectra of the matrix glass while a 5μm focused beam was used to collect spectra from the tubular features and crystallites. EDX mapping was collected for areas of interest. See appendix 5 for EDX spectra and elemental maps.

A carbon tab was prepared for BSE imaging. Pieces of a large glass clast from the Seelbronn sample were crumbled then crushed with a mortar and pestle to sub-millimeter sized angular fragments. The fragments were then stuck to a 1 cm double-backed conductive adhesive carbon tab, which was then stuck to a titanium stub mount. The full assembly was then Pt coated using the Denton Vacuum Desk 2 for 200 seconds at 15 mA.

2.7.3 Establishing biogenicity

Characterizing the tubules will involve several laboratory-based techniques. Micro X-ray diffraction (μXRD) allows for *in situ* mineralogical analysis at scales of tens to hundreds of microns. Establishing the mineralogy of the alteration structures and the host glasses will provide a basis for further characterization. An understanding of the mineral phases hosted within the tubular structures is significant to establishing their biogenicity. Electron beam based techniques such as scanning electron microscopy (SEM) will be paramount in substantiating the chemical composition of the host glass. Establishing the composition of the host glass may demonstrate the presence of chemical species relevant to potential microbial metabolism. Microprobe mapping may establish enrichment of biologically significant elements (P, C, N, K) that can be correlated with the structural information provided by μXRD. Detailed mapping with higher resolution techniques may demonstrate the presence of biomarkers such as a carbon anomaly or remnant organic matter. Combining μXRD with SEM and TEM will allow for *in situ* correlation of compositional and structural analyses providing preliminary characterization of the putative bioalteration textures hosted within the Ries glasses.

To further elucidate potential chemical variations on a sub-micron scale focused ion beam (FIB) milled foils containing the tubules and relevant tubule cross-sections will be cut from petrographic thin sections which have previously been characterized via optical and electron microscopy and laboratory micro X-ray diffraction techniques as described above. Transmission electron microscopy (TEM), energy dispersive X-ray spectrometry (EDXS) and electron energy loss spectroscopy (EELS) of these FIB foils will allow for preliminary high-resolution (nano-meter scale) mineralogical and chemical characterization of the tubules followed by scanning transmission X-ray microscopy (STXM) coupled with near edge X-ray absorption fine structure spectroscopy (NEXAFS). STXM will provide three-dimensional tomographic imaging of the tubules. NEXAFS allows for high-resolution chemical analyses including an assessment of valence states. Therefore NEXAFS will assess the valence states of transition elements with significant implications to potential microbial metabolism. Coupling NEXAFS with STXM will produce high-resolution three-dimensional chemical maps of the tubules as well as potential 'redox' maps. Previous TEM and STXM studies on putative bioalteration textures in basaltic glasses from the Ontong Java Plateau have provided a wealth of mineralogical and chemical information pertinent to constraining the physical and chemical conditions of formation with the potential of establishing a biogenic origin (Benzerara *et al.* 2007). Detailed sub-micron scale chemical studies may yield the presence of remnant organic matter or enrichment of biologically relevant elements within the tubules not observed at larger scales. Furthermore, elemental gradients or subtle chemical difference between unaltered glass, altered glass, and glass in close proximity to alteration (visually unaltered glass) may be significant and allow for speculation with regard to possible microbial metabolic reactions.

2.8 References cited

AMES D. E., WATKINSON D. H. and PARRISH R. R. (1998) Dating of a regional hydrothermal system induced by the 1850 Ma Sudbury impact event. *Geology* **26**(5), 447 – 450.

BANERJEE N. R., FURNES H., MUEHLENBACHS K. and STAUDIGEL H. (2004) Microbial alteration of volcanic glass in modern and ancient oceanic crust as a proxy for studies of extraterrestrial material. In *Lunar and Planetary Science XXXV*.

BANERJEE N. R., FURNES H., MUEHLENBACHS K., STAUDIGEL H. and DE WIT M. (2006a) Preservation of ~3.4 – 3.5 Ga microbial biomarkers in pillow lavas and hyaloclastites from the Barberton Greenstone Belt, South Africa. *Earth and Planetary Science Letters* **241**(3 – 4), 707 – 722.

BANERJEE N. R., FURNES H., MUEHLENBACHS K., STAUDIGEL H., MCLOUGHLIN N. and BEBOUT G. (2008) Biogeochemical tracers of modern and ancient life in seafloor lavas. *Geochimica et Cosmochimica Acta* **72**(12), A51 – A51.

BANERJEE N. R., FURNES H., SIMONETTI A., MUEHLENBACHS K., STAUDIGEL H., DE WIT M. and VAN KRANENDONK M. J. (2006b) Ancient Microbial Alteration of Oceanic Crust on Two Early Archean Cratons and the Search for Extraterrestrial Life. In *37th Annual Lunar and Planetary Science Conference*, League City, TX.

BANERJEE N. R. and MUEHLENBACHS K. (2003) Tuff life: Bioalteration in volcaniclastic rocks from the Ontong Java Plateau. *Geochemistry, Geophysics, Geosystems* **4**(4), 1037 – 1059.

BENZERARA K., MENGUY N., BANERJEE N. R., TYLISZCZAK T., BROWN G. E. and GUYOT F. (2007) Alteration of submarine basaltic glass from the Ontong Java Plateau: A STXM and TEM study. *Earth and Planetary Science Letters* **260**(1 – 2), 187 – 200.

BRASIER M. D., GREEN O. R., JEPHCOAT A. P., KLEPPE M. J., VAN KRANENDONK M. J., LINDSAY J. F., STEELE A. and GRASSINEAU N. V. (2002) Questioning the evidence of Earth's oldest fossils. *Nature* **416**, 76 – 81.

BRINGEMEIER D. (1994) Petrofabric examination of the main suevite of the Otting Quarry, Nordlinger Ries, Germany. *Meteoritics & Planetary Science* **29**(3), 417 – 422.

BUCHNER E., SCHWARZ W. H., SCHMIEDER M. and TRIELOFF M. (2010) Establishing a 14.6 ± 0.2 Ma age for the Nördlinger Ries impact (Germany) — A prime example for concordant isotopic ages from various dating materials. *Meteoritics & Planetary Science* **45**(4), 662 – 674.

Cady S. L., Farmer J. D., Grotzinger J. P., Schopf J. W. and Steele A. (2003) Morphological Biosignatures and the Search for Life on Mars. *Astrobiology* **3**(2), 351 – 368.

Chao E. C. T., H TTNER R. and Schmidt-Kaler H. (1978) *Principal Exposures of the Ries Meteorite Crater in Southern Germany*. Bayerisches Geologisches Landesamt, Munich. pp. 1.

Cockell C. S. (2004) Impact-shocked rocks - insights into Archean and extraterrestrial microbial habitats (and sites for prebiotic chemistry?). *Advances in Space Research* **33**, 1231 – 1235.

— (2006) The origin and emergence of life under impact bombardment. *Philosophical Transactions of the Royal Society B* **361**, 1845 – 1856.

Cockell C. S. and Lee P. (2002) The biology of impact craters — a review. *Biological Reviews* **77**, 279 – 310.

Cockell C. S., Lee P., Broady P., Lim D. S. S., Osinski G. R., Parnell J., Koeberl C., Pesonen L. and Salminen J. (2005) Effects of asteroid and comet impacts on habitats for lithophytic organisms — A synthesis. *Meteoritics & Planetary Science* **40**(12), 1901 – 1914.

Cockell C. S., Lee P., Osinski G., Horneck G. and Broady P. (2002) Impact-induced microbial endolithic habitats. *Meteoritics & Planetary Science* **37**(10), 1287 – 1298.

Cockell C. S., Olsson-Francis K., Herrera A. and Meunier A. (2009) Alteration textures in terrestrial volcanic glass and the associated bacterial community. *Geobiology* **7**(1), 50 – 65.

Edwards K. J., Wolfgang B., McCollom T. M. (2005) Geomicrobiology in oceanography: microbe-mineral interactions at and below the seafloor. *Trends in Microbiology* **13**(9), 449 – 456.

Engelhardt W. V. (1972) Shock produced rock glasses from the Ries Crater. *Contributions to Mineralogy and Petrology* **36**, 265 – 292.

— (1990) Distribution, petrography and shock metamorphism of the ejecta of the Ries crater in Germany — a review. *Tectonophysics* **171**, 259 – 273.

Engelhardt W. V., Arndt J., Fecker B. and Pankau H. G. (1995) Suevite breccia from the Ries crater, Germany: Origin, cooling history, and devirtrification of impact glass. *Meteoritics* **30**, 279 – 293.

Engelhardt W. V. and Hörz F. (1965) Ries glasses and moldavite. *geochimica et Cosmochimica Acta* **29**, 609 – 620.

FISK M. R., GIOVANNONI S. J. and THORSETH I. H. (1998) Alteration of oceanic volcanic glass: textural evidence of microbial activity. *Science* **281**, 978 – 980.

FLEMMING R. L. (2007) Micro X-ray diffraction (mXRD): A versatile technique for characterization of Earth and planetary materials. *Canadian Journal of Earth Sciences* **44**, 1333 – 1346.

FLIEGEL D., WIRTH R., SIMONETTI A., FURNES H., STAUDIGEL H., HANSKI E. and MUEHLENBACHS K. (2010) Septate-tubular textures in 2.0-Ga pillow lavas from the Pechenga Greenstone Belt: a nano-spectroscopic approach to investigate their biogenicity. *Geobiology* **8**(5), 372 – 390.

FLIEGEL D., WIRTH R., SIMONETTI A., SCHREIBER A., FURNES H. and MUECHLENBACHS K. (2011) Tubular textures in pillow lavas from a Caledonian west Norwegian ophiolite: A combined TEM, LA–ICP–MS, and STXM study. *Geochemistry, Geophysics, Geosystems* **12**(2) Q02010.

FÖRSTNER U. (1967) Petrographische Untersuchungen des Suevit aus den Bohrungen Deiningen und Wörnitzostheim im Ries von Nördlingen. *Contributions to Mineralogy and Petrology* **15**, 281 – 307.

FRENCH B. F. (1998) *Traces of Catastrophe: A Handbook of Shock-Metamorphic Effects in Terrestrial Meteorite Impact Structures*. Lunar and Planetary Institute, Houston. pp. 120.

FRENCH B. F. and KOEBERL C. (2010) The convincing identification of terrestrial meteorite impact structures: What works, what doesn't, and why. *Earth-Science Reviews* **98**, 123 – 170.

FURNES H., BANERJEE N. R., MUEHLENBACHS K., STAUDIGEL H. and DE WIT M. (2004) Early Life Recorded in Archean Pillow Lavas. *Science* **304**(5670), 578 – 581.

FURNES H. and MUEHLENBACHS K. (2003) Bioalteration recorded in ophiolitic pillow lavas. In *Ophiolites in Earth's History, Geological Society of London, Special Publication* (eds. Y. Dilek and P. T. Robinson), pp. 415 – 426. Geological Society of London.

FURNES H., MUEHLENBACHS K., TORSVIK V., THORSETH I. H. and TUMYR O. (2001a) Microbial fractionation of carbon isotopes in altered basaltic glass from the Atlantic Ocean, Lau Basin and Costa Rica Rift. *Chemical Geology* **173**(4), 313 – 330.

FURNES H., STAUDIGEL H., THORSETH I. H., TORSVIK T., MUEHLENBACHS K. and TUMYR O. (2001b) Bioalteration of basaltic glass in the oceanic crust. *Geochemistry, Geophysics, Geosystems* **2**(8), 1049 – 1069.

GARCIA-RUIZ J. M., HYDE S. T., CARNERUP A. M., CHRISTY A. G., VAN KRANENDONK M. J. and WELHAM N. J. (2003) Self-assembled silica-carbonate structures and detection of ancient microfossils. *Science* **302**, 1194 – 1197.

GRAUP G. (1999) Carbonate-silicate liquid immiscibility upon impact melting: Ries crater, Germany. *Meteoritics & Planetary Science* **34**, 425 – 438.

GRIEVE R. A. F. (1987) Terrestrial impact structures. *Annual Reviews in Earth and Planetary Science* **15**, 245 – 270.

HERRERA A., COCKELL C. S., SELF S., BLAXTER M., REITNER J., THORSTEINSSON T., ARP G., DRÖSE W. and TINDLE A. G. (2009) A Cryptoendolithic Community in Volcanic Glass. *Astrobiology* **9**(4), 369 – 381.

HÖRZ F. (1982) Ejecta of the Ries Crater, Germany. In *Geological implications of impacts of large asteroids and comets on the Earth* (eds. L. T. Silver and P. H. Schultz), pp. 39 – 56. Geolgical Society of America Special Paper.

HÖRZ F., OSTERTAG R. and RAINEY D. A. (1983) Bunte Breccia of the Ries: Continuous deposits of large impact craters. *Reviews of Geophysics* **21**(8), 1667 – 1725.

IZAWA M. R. M., BANERJEE N. R., FLEMMING R. L. and BRIDGE N. J. (2010a) Preservation of microbial ichnofossils in basalitc glass by titanite mineralization. *Canadian Mineralogist* **48**, 1233 – 1265.

IZAWA M. R. M., BANERJEE N. R., FLEMMING R. L., BRIDGE N. J. and SCHULTZ C. (2010b) Basaltic glass as a habitat for microbial life: Implications for astrobiology and planetary exploration. *Planetary and Space Science* **58**(4), 583 – 591.

JANKOWSKI B. (1977) Die gradiertr Einheit oberhalb des Suevits der Forschungsbohrung Nördllingen 1973. *Geologica Bavarica* **75**, 155 – 162.

MELOSH H. J. (1989) *Impact Cratering: A Geologic Process*. Oxford: Clarendon Press, Oxford. pp. 126.

MELOSH H. J. and IVANOV B. A. (1999) Impact crater collapse. *Annual Reviews in Earth and Planetary Science* **27**, 385 – 415.

MCLOUGHLIN N., FLIEGEL D. J., FURNES H., STAUDIGEL H., SIMONETTI A., ZHAO G. and ROBINSON P. T. (2010a) Assessing the biogenicity and syngenicity of candidate bioalteration textures in pillow lavas of the ~2.52 Ga Wutai greenstone terrane of China. *Chin. Sci. Bull.* **55**(2), 188 – 199.

MCLOUGHLIN N., FURNES H., BANERJEE N., MUEHLENBACHS K. and STAUDIGEL H. (2009) Ichnotaxonomy of microbial trace fossils in volcanic glass. *Journal of the Geological Society* **166**(1), 159 – 169.

McLoughlin N., Furnes H., Banerjee N., Staudigel H., Muechlenbachs K., de Wit M. and Van Kranendonk M. (2008) Micro-bioerosion in volcanic glass: extending the ichnofossil record to Archaean basaltic crust. In *Current Developments in Bioerosion* (eds. M. Wisshak and L. Tapanila). Springer-Verlag, Berlin Heidelberg.

McLoughlin N., Staudigel H., Furnes H., Eickmann B. and Ivarsson M. (2010b) Mechanisms of microtunneling in rock substrates: distinguishing endolithic biosignatures from abiotic microtunnels. *Geobiology* **8**(4), 245 – 255.

Morrison R. H. and Oberbeck V. R. (1978) A composition and thickness model for lunar impact crater and basin deposits. *Proccedings of 9th Lunar and Planetary Sciences Conference*, 3763 – 3785.

Muttik N., Kirsimae K., Somelar P. and Osinski G. R. (2008) Post-impact alteration of surficial suevites in Ries Crater, Germany; hydrothermal modification of weathering processes? *Meteoritics & Planetary Science* **43**(11), 1827 – 1840.

Naumov M. V. (2005) Principal features of impact-generated hydrothermal circulation systems: mineralogical and geochemical evidence. *Geofluids* **5**(3), 165 – 184.

Newsom H. E., Graup G., Iseri D., Geissman J. W. and Keil K. (1990) The formation of the Ries crater, West Germany; Evidence of atmosphereic interactions during a large cratering event. *Geological Society of America Special Paper* **247**, 195 – 206.

Newsom H. E., Graup G., Sewards T. and Keil K. (1986) Fluidization and Hydrothermal Alteration of the Suevite Deposit at the Ries Crater, West-Germany, and Implications for Mars. *Journal of Geophysical Research-Solid Earth and Planets* **91**(B13), E239 – E251.

Oberbeck V. R. (1975) The role of ballistic erosion and sedimentation in lunar statigraphy. *Reviews of Geophysics and Space Physics* **13**, 337 – 362.

Oelkers E. H. (2001) A general kinetic description of multi-oxide silicate mineral and glass dissolution. *geochimica et Cosmochimica Acta* **65**, 3703 – 3719.

Osinski G. R. (2003) Impact glasses in fallout suevites from the Ries impact structure, Germany: An analytical SEM study. *Meteoritics & Planetary Science* **38**(11), 1641 – 1667.

— (2004) Impact melt rocks from the Ries structure, Germany: an origin as impact melt flows? *Earth and Planetary Science Letters* **226**(3 – 4), 529 – 543.

— (2005) Hydrothermal activity associated with the Ries impact event, Germany. *Geofluids* **5**(3), 202 – 220.

OSINSKI G. R., GRIEVE R. A. F. and SPRAY J. G. (2004) The nature of the groundmass of surficial suevite from the Ries impact structure, Germany, and constraints on its origin. *Meteoritics & Planetary Science* **39**(10), 1655 – 1683.

OSINSKI G. R., LEE P., PARNELL J., SPRAY J. G. and BARON M. (2005) A case study of impact-induced hydrothermal activity: The Haughton impact structure, Devon Island, Canadian High Arctic. *Meteoritics & Planetary Science* **40**(12), 1859 – 1878.

OSINSKI G. R. and PIERAZZO E. (2012) *Impact Cratering: Processes and Products*. Wiley-Blackwell, USA. pp. 336.

OSINSKI G. R., SPRAY J. G. and LEE P. (2001) Impact-induced hydrothermal activity within the Haughton impact structure, arctic Canada: Generation of a transient, warm, wet oasis. *Meteoritics & Planetary Science* **36**, 731 – 745.

PACE, N. R. (1997) A Molecular View of Microbial Dirversity and the Biosphere. *Science* **276**, 634 – 740.

PECKMANN J., BACH W., BEHRENS K. and REITNER J. (2008) Putative cryptoendolithic life in Devonian pillow basalt, Rheinisches Schiefergebirge, Germany. *Geobiology* **6**(125 – 135).

POHL J., STÖFFLER D., GALL H. and ERNSTSON K. (1977) The Ries impact crater; Impact and explosion cratering; planetary and terrestrial implications; Proceedings of the Symposium on planetary cratering mechanics. In *Lunar Science Institute topical conference ; Symposium on planetary cratering mechanics, Flagstaff, Ariz* (eds. D. J. Roddy, R. O. Pepin and R. B. Merrill). Pergamon Press New York N.Y. United States (USA), United States (USA).

RICHARDSON L. J., DEMING D., HORNING K., SEAGER S. and HARRINGTON J. (2007) A spectrum of an extrasolar planet. *Nature* **445**, 892 – 895.

SALGER M. V. (1977) Die Tonminerale der Forschungsbohrung Nördlingen 1973. *Geologica Bavarica* **75**, 67 – 73.

SANTELLI C. M., ORCUTT B. N., BANNING E., BACH W., MOYER C. L., SOGIN M. L., STAUDIGEL H. and EDWARDS K. J. (2008) Abundance and diversity of microbial life in ocean crust. *Nature* **453**, 653 – 657.

SAPERS H. M., OSINSKI G. R. and BANERJEE N. R. (2009) Differential alteration of glass clasts in the surficial suevites of the Ries crater, Germnay. *Meteoritics & Planetary Science Supplement* **44**, 5175.

SCHMIDT-KALER H. (1978) Geological setting and history. In *Principle exposures of the Ries meteorite crater in southern Germany* (eds. E. C. T. Chao, R. Hüttner and H. Schmidt-Kaler), pp. 8 – 11. Verlag Bayerisches Geologisches Landesamt, München, Germany.

SCHWARTZMAN, D. W. and LINEWEAVER, C. H. (2004) The hyperthermophilic origin of life revisited. *Biochemical Society Transactions* **32**(2), 168 – 171.

SHOEMAKER E. M. and CHAO E. C. T. (1961) New evidence for the impact origin of the Ries Basin, Bavaria, Germany. *Journal of Geophysical Research* **66**(10), 3371 – 3378.

STÄHLE V. (1972) Impact glasses from the suevite of the Nördlinger Ries. *Earth and Planetary Science Letters* **17**(1), 275 – 293.

STÄHLE V. and OTTEMANN J. (1977) Ries-Forschungsbohrung 1973: Zeolithisierung der Gläser im Suevit und Petrographie der Beckensuevite und Gangbreccien. *Geologica Bavarica* **73**, 191 – 217.

STAUDIGEL H., FURNES H., BANERJEE N. R., DILEK Y. and MUEHLENBACHS K. (2006) Microbes and volcanoes: A tale from the oceans, ophiolites, and greenstone belts. *GSA Today* **16**(10), 4 – 10.

STAUDIGEL H., FURNES H., MCLOUGHLIN N., BANERJEE N. R., CONNEL L. B. and TEMPLETON A. (2008a) 3.5 billion years of glass bioalteration: Volcanic rocks as a basis for microbial life? *Earth-Science Reviews* **89**(3 – 4), 156 – 176.

STAUDIGEL H., FURNES H., MCLOUGHLIN N., BANERJEE N. R., CONNELL L. B. and TEMPLETON A. (2008b) Microbial glass bioalteration: Inferring mechanisnis of blocorrosion from trace fossil morphology. *Geochimica et Cosmochimica Acta* **72**(12), A893 – A893.

STÖFFLER D., EWALD U., OSTERTAG R. and REIMOLD W. U. (1977) Research drilling Nördlingen 1973 (Ries): Composition and texture of polymict impact breccias. *Geologica Bavarica* **75**, 163 – 189.

THORSETH I. H., PEDERSEN R. and CHRISTIE D. (2003) Microbial alteration of 0 – 30 Ma seafloor and sub-seafloor basaltic glasses frm the Australian Antartctic discordance. *Earth and Planetary Science Letters* **215**, 237 – 247.

THORSETH I. H., TORSVIK T., FURNES H. and MUEHLENBACHS K. (1995) Microbes play an important role in the alteration of oceanic crust. *Chemical Geology* **126**, 137 – 146.

THORSETH I. H., TORSVIK T., TORSVIK V., DAAE F. L., PEDERSEN R. B., KELDYSH-98 SCIENTIFIC PARTY. (2001) Diversity of life in ocean floor basalt. *Earth and Planetary Science Letters* **194**, 31 – 37.

TORSVIK T., FURNES H., MUEHLENBACHS K., THORSETH I. H. and TUMYR O. (1998) Evidence for microbial activity at the glass-alteration interface in oceanic basalts. *Earth and Planetary Science Letters* **162**, 165 – 176.

VENNEMANN T., MORLOK A., ENGELHARDT W. V. and KYSER K. (2001) Stable isotope composition of impact glasses from the Nördlinger Ries impact crater, Germany. *geochimica et Cosmochimica Acta* **65**(8), 1325 – 1336.

VON ENGELHARDT W. and GRAUP G. (1984) Suevite of the Ries Crater, Germany; source rocks and implications for cratering mechanics. *Geologische Rundschau* **73**(2), 447.

WESTALL F. and FOLK R. L. (2003) Exogenous carbonaceous microstructures in Early Archaean cherts and BIFs from the Isua Greenstone Belt: implications for the search for life in ancient rocks. *Precambrian Research* **126,** 313 – 330.

WIERZCHOS J., ASCASO C., SANCHO L. G. and GREEN A. (2003) Iron-rich diagenetic minerals are biomarkers of microbial activity in antarctic rocks. *Geomicrobiology Journal* **20**, 15 – 24.

WOLFF-BOENISCH D., GISLASON S. R. and OELKERS E. H. (2006) The effect of crystallinity on dissolution rates and CO_2 consumption capacity of silicates. *geochimica et Cosmochimica Acta* **70**, 858 – 870.

WOLFF-BOENISCH D., GISLASON S. R., OELKERS E. H. and PUTNIS C. V. (2004) The dissolution rates of natural glasses as a function of their composition at pH 4 and 10.6 and temperatures from 25 to 74 ∘C. *geochimica et Cosmochimica Acta* **68**(23), 4843 – 4858.

WUNNEMANN K., COLLINS G. S. and MELOSH H. J. (2006) A strain-based porosity model for use in hydrocode simulations of impacts and implications for transient crater growth in porous targets. *Icarus* **180**(2), 514 – 527.

Chapter 3

3 Re-evaluating the Rochechouart impact structure: setting a precedent for classification with limited geologic context

Sapers, H. M., Osinski, G. R., Banerjee, N. R., Ferrière, L. Lambert, P., Izawa, M. R. M.

3.1 Introduction

Impact cratering is one of the most important geological processes on the terrestrial planets and rocky and icy moons of the Solar System. Once thought to be relatively unimportant for Earth history, it has become increasingly apparent over the past two decades that impact cratering has played a major role in shaping the origin and evolution of Earth, and possibly of life itself. The importance of the link between meteorite impacts and Earth evolution finally entered the geological mainstream in the 1980s, with evidence for a major impact as the cause of the mass extinction event at the Cretaceous – Palaeogene (K – Pg) boundary 65 Myr ago (Alvarez *et al.* 1980). The actual impact site, the ~180 km diameter Chicxulub crater, was subsequently identified in 1991, buried beneath ~1 km of sediments in the Yucatan peninsula, Mexico (Hildebrand *et al.* 1991). Despite some controversy, it is apparent that the Chicxulub impact event and its aftermath account for the sudden extinctions at the K – Pg boundary (Schulte *et al.* 2010). This remains, to date, the only unambiguous association of an impact crater with a mass extinction event in the geological record. First suspected following the discovery of an iridium anomaly (Olsen *et al.* 2002), a recent *Nature* News Feature noted the correspondence between the age of the Triassic – Jurassic boundary and a new reported age for the Rochechouart impact structure in France (Smith 2011).

The Rochechouart impact structure is an eroded, late Triassic impact site, located in south-central France (45°50’N and 0°46’E; Kraut *et al.* 1969; Kraut & French 1971). Despite erosion, a wide variety of “impactites” are preserved. Impactites comprise all rocks affected by impact processes and range from fracture, displaced, and/or shocked rocks (including shatter cones) and lithic (melt-free) breccias, to impact melt-bearing breccias and melt rocks. While detailed petrographic studies at the thin-section to hand sample scale have been conducted on Rochechouart impactites (*e.g.*, Kraut & French 1971; Lambert 1974, 1977), the complex relationships between clasts and matrix as well as the nature of the matrix itself can only be fully observed at the micrometer to nanometer scale using scanning electron microscopy (SEM) imaging techniques (*e.g.*, Osinski & Spray 2001; Osinski *et al.* 2004; Nelson & Newsom 2006). We have carried out such a study for the first time on Rochechouart impactites. Our SEM-based observations demonstrate the transitional nature of impact melt-bearing impactites. We show that they form a continuum between impact melt-poor and melt-rich breccias and melt rocks, *sensu stricto*. In describing a suite of impactites from the Rochechouart structure we hope to illustrate the highly variable usage of impactite nomenclature in the literature. We then apply new nomenclature based on the matrix/groundmass textures (Osinski *et al.* 2008) to this suite of investigated impactites avoiding previous tautological classifications (Stöffler & Grieve 2007). The Rochechouart impact structure provides an opportunity to study a suite of impactites with extremely limited field exposures (*e.g.*, as in the case of lunar exploration missions). As such, the majority of samples were examined without *a priori* knowledge of detailed geological context due to lack of exposure and poor quality of outcrops available on site. Subsequent classification is largely based on observable characteristics intrinsic to the samples at the micrometer scale. When taken together with new information on impact-generated hydrothermal activity, a more complete picture of the Rochechouart impact structure emerges. The eroded nature of this site complicates reconstruction of the original impact crater. One possible reconstruction suggests that the structure is much larger than originally thought, with implications for a possible impact cause of the Triassic – Jurassic extinction as proposed by Olsen *et al.* (2002).

3.2 Geologic setting of the Rochechouart impact structure

The late Triassic Rochechouart impact structure was formed in Hercynian age (300 – 400 Ma) granitic intrusive and metamorphic rocks at the northwestern edge of the French Massif Central near the margin of a Mesozoic sea (*e.g.*, Turpin *et al.* 1990). The currently accepted age of the Rochechouart structure, 214 ± 8 Ma, is based on $^{40}Ar/^{39}Ar$ laser spot fusion dating of pseudotachylite generated during transient crater collapse providing the most robust age estimate to date (Kelley & Spray 1997). However, recent age determinations of hydrothermal K-feldspar in shocked gneisses suggest an age of 201 ± 2 Ma, coincident within error of the Triassic – Jurassic boundary (Schmieder *et al.* 2010). The crystalline target rocks are comprised of granite, gneiss, and metamorphosed, intercalated, fine-grained quartzofeldspathic and metabasic rocks (leptynites) of the French Massif Central (Turpin *et al.* 1990). The crystalline basement is unconformably overlain to the west by the Triassic – Cretaceous limestones and sediments of the Aquitaine Basin (Lambert 1977b).

As a result of erosion, the Rochechouart impact structure is not delimited by any specific topographic expression, as previously described by Kraut and French (1971; Fig. 3.1). Originally interpreted as a volcanic feature (Manes 1833), the identification of shock metamorphic features such as planar deformation features (PDFs) in quartz (Kraut 1967) and shatter cones (Kraut 1969; Kraut *et al.* 1969) led to the recognition of an impact origin. Rochechouart contains scattered outcrops of monomict and polymict impact breccias, impact melt-bearing rocks, shatter cones and other shocked target rocks (see *e.g.*, Lambert 2010 and references therein). Allochthonous impactites (impact breccias and impact melt-bearing materials) occur as remnant outcrops distributed in a centrosymmetric, discontinuous sheet, over an area of ~150 km^2 (Fig. 3.1). These outcrops delineate a somewhat circular area with a diameter of approximately 15 km that was considered by Kraut and French (1971) to be "the minimum original diameter of the crater". Estimating the original crater size is an area of active debate (*e.g.*, Lambert 1974, 1977c, 2010). Pohl *et al.* (1978) cite a diameter related to the 18 – 25 km diameter disturbed zone, which represents the minimum diameter of the structure. This estimate is consistent with a negative gravity anomaly centered on the structure (Pohl *et al.* 1978). A shock zoning study conducted by Lambert (1977b) estimated the size of the structure to be 20 – 25 km. recently, a 40 – 50 km diameter for the Rochechouart structure has been proposed (Lambert 2010). The conservative estimates (18 – 25 km) are based on the extent of damage to the basement and do not take into account the extensive removal of material by erosion.

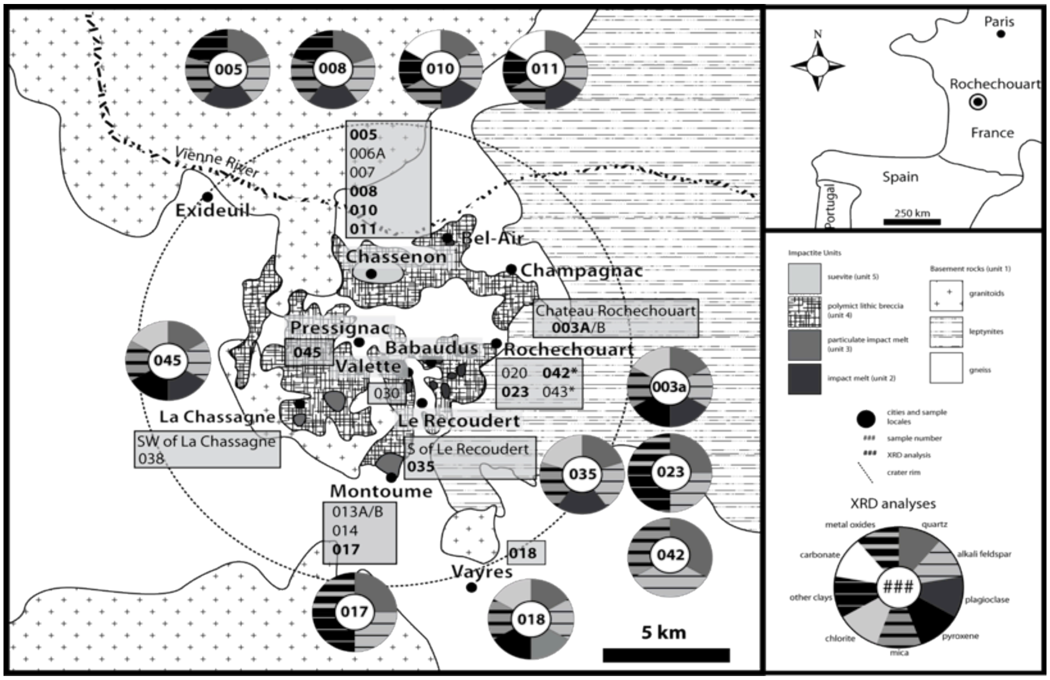

Figure 3.1: Simplified geologic map of the Rochechouart impact structure, with sample locations.

Modified from Kelley and Spray (1997), and Lambert (1974, 1977c). The dotted line delineates the 23 km impact structure. Mineralogy for selected samples based on bulk XRD analysis is illustrated by the pie charts (see text for details). Note that the wedge size is not indicative of relative mineral amounts, but rather the presence of a particular mineral phase. Basement samples: 010, 018, 038, 045; unit 1, lithic breccia (Rochechouart breccia): 003, 020, 023, 035; unit 2, impact melt-bearing breccia (Chassenon suevite): 005, 006, 011; unit 4, particulate, clast-rich impact melt rock (Montoume breccia): 008, 013, 014, 017, 029, 030; unit 5, impact melt rock (Babaudus melt): 042, 043.

The impact structure has been affected by later regional tectonic activity (Kraut & French 1971). A north – south cross sectional profile indicates that regional deformation has tilted the crater floor about 0.6^o to the north such that the southern part of the structure is raised relative to the northern region (Lambert 1977, 2008, 2010). It is notable that the crater floor beneath the allochthonous impactites is extremely flat, ± 50 m over 300 km^2 (Lambert 1977a 1982, 2010).

The Rochechouart allochthonous impactites are complex and heterogeneous at all scales. Five main impactite units overlying the impact-damaged parautochthonous basement rock have been described as follows with many of the units named with respect to their location of discovery and/or main occurrence (Fig. 3.2; Table 3.1): unit 1) lithic breccia ("Rochechouart breccia"); unit 2) suevitic breccia ("Chassenon suevite"); unit 3) "basal suevite", a recently-discovered transitional impact melt-bearing breccia (see Lambert, 2010); unit 4) red "welded" breccia or suevite ("Montoume breccia"); unit 5) finely crystalline melt rock ("Babaudus melt"; Kraut & French 1971). Lambert (1974, 1977b,c) described and named the Rochechouart impactites based on shock level, in contrast with the stratigraphic ordering of Kraut and French (1971). In the present study, we have followed and expanded Lambert's classification. It should be noted that it has recently been suggested that some of the crater fill units (units 1 – 5) are also capped by a graded, impactoclastic, ash-like deposit of very fine-grained, glass-poor lithic debris compositionally consistent with the basement (Lambert 2010). This unit is not studied here. For clarity and consistency, in this paper we will refer to the different impactites as unit 1, 2, etc., in the results section. We then reclassify and reinterpret these impactites in the discussion section.

Table 3-1: Summary of nomenclature used to depict the Rochechouart impactites.

Correlation of various classification and nomenclature used to define the Rochechouart impacts in the literatures.

	Lambert 1977	Lambert 2010	Kraut 1969	This Study*
	A (fractured basement rock)	shocked basement	n.a.	shocked/fractured basement
	B (monomict breccia)	monomict lithic breccia	Rochechouart breccia	monomict lithic breccia
unit 1	C (polymict breccia, no glass)	polymict lithic breccia		[melt-free] lithic breccia
unit 2	D (polymict breccia, with glass)	melt poor (upper)suevite	Chassenon Suevite	[clastic] melt-bearing breccia
unit 3	n.a.	melt rich (basal) suevite	n.a.	Melt-rich impactite
unit 4	E (melt)	impact melt	Montoume breccia	[particulate clast-rich] impact melt rock
unit 5			Babaudus melt	[clast-poor] impact melt rock

*Square brackets are used to delineate descriptive terms applicable to specific Rochechouart samples

n.a. not applicable to the referenced study

3.3 Methodology

Twelve samples representing each of the five main impactite lithologies described above were prepared for powder X-ray diffraction (XRD) analysis. Nineteen representative polished thin sections from sixteen samples representing each of the main impact lithologies were chosen for petrographic study in transmitted light. Six of those thin sections representing each impactite unit exclusive of the basement material were selected for further investigations using scanning electron microscopy (SEM). Powdered samples for XRD analysis were prepared by grinding with an agate mortar and pestle for approximately 30 minutes. Representative matrix material was chosen from each sample avoiding large (> 3 mm) clasts; ~400 mg of each powdered sample was used for analysis. Back-packed mounts were used to reduce the effects of preferred orientation and surface roughness. X-ray diffraction data were collected from 2º to 82º 2θ with a step size of 0.02º and scanning speed of 10º per minute using the Rigaku Rotaflex diffractometer at the Laboratory for Stable Isotope Studies, University of Western Ontario (London, Canada), operating at 45 kV accelerating voltage and 160 mA tube current with a Co rotating anode source (Co Kα, λ = 1.7902 Å). Diffractograms were analyzed using the BrukerAXS 2005 EVA software package using the International Center for Diffraction Data Powder Diffraction File (ICDD PDF-4) database.

Polished, carbon-coated thin sections were analyzed using a Hitachi S-4300S/E field emission variable pressure scanning electron microscope with EDAX Pegasus 4040 integrated EDX/EBSD X-ray spectrometer at the Imaging Center, Texas Tech University (Lubbock, U.S.A); with 15 kV accelerating voltage, and a working distance ~12 – 15 mm. Additional backscattered electron (BSE) and secondary electron (SE) imaging was carried out using a tungsten-filament Hitachi S-2500C SEM at the Zircon and Accessory Phase Laboratory, University of Western Ontario, using a Robinson Backscatter detector. Additional high-resolution BSE imaging and EDX spot analysis was carried out with a Leo 1540 FIB/SEM CrossBeam field emission SEM equipped with an Oxford Instruments INCA EDX system allowing for semi-quantitative elemental analysis, sensitive to ~0.5 wt. % or less for all elements from C – U in the Nanofabrication laboratory, University of Western Ontario. The sections were analyzed under high vacuum with an accelerating voltage of 15 – 20 kV and a working distance ~10 mm. Energy dispersive X-ray (EDX) spectroscopy mapping and spot analyses of selected samples allowed for the identification of elemental phases representing mineral phases that may be present in low concentrations beneath the bulk XRD threshold.

3.4 Results

3.4.1 Petrographic shock indicators

All impactites examined contain petrographic indicators of shock-metamorphism, including planar fractures (PF) and planar deformation features (PDFs) in quartz, mosaicism of quartz, diaplectic quartz glass and feldspar glass. Kink banding in mica was also observed in many of the investigated samples; even it is not considered to be an indicator of shock-metamorphism, it is clear that in the present case, kink banding is related to the impact event. The presence of "toasted quartz" (*e.g.*, Whitehead *et al.* 2002, Ferrière *et al.* 2009b) was also noted in all of the melt-bearing impactites lithologies. Ballen silica was observed in "Babaudus melt" and in "Montoume breccia" samples, in agreement with previous reports by Ferrière *et al.* (2009a, 2010). The petrographic shock indicators observed in this study are consistent with previous studies (*e.g.*, Lambert 1977c) indicating that clasts within both the autochthonous and the allochthonous impactites have been subjected to a certain range of pressures and temperatures.

3.4.2 Bulk mineralogy

Bulk powder XRD was used to determine the main mineral assemblages present in each of the impactite units, as well as in the unshocked basement rocks (Fig. 3.1). As expected, the mineralogy is somewhat limited and consistent with the Hercynian target rocks. Diffractograms containing peaks corresponding to clay minerals, calcite, and Fe-Ti-oxides are suggestive of various alteration phases. Phyllosilicates including muscovite, glauconite, illite, chlorite, and montmorillonite/smectite group clays, were identified by XRD in all units, including the unshocked basement rocks. Analyses from the units 1 and 4 have XRD patterns corresponding to Fe-Ti-oxides (hematite, ilmenite, and lepidocrocite). Bulk XRD analysis of an altered glass clast from unit 2 indicated quartzofeldspathic mineralogy consistent with the bulk suevite. However, alteration mineralization (calcite and mica-clay minerals) is more prevalent in the glass clast compared to the bulk impactite.

3.4.3 Groundmass textures and clasts

3.4.3.1 Unit 1: lithic breccia (*'Rochechouart breccia'*)

Transmitted light microscopy observations indicate that the groundmass is composed of angular to sub angular lithic and mineral fragments of quartzofeldspathic composition set in a matrix of fine-grained material, forming a cataclastic texture (Fig. 3.2). The fine-grained matrix is a minor component compared to the lithic and mineral clasts (Fig. 3.2B). Mineral and lithic fragments range in size from ~2 – 15μm to larger clasts of up to a centimeter in size. Mineral clasts are dominantly feldspars, mica, and quartz. Mineral grains display various shock induced features including fracturing, PDFs in quartz, and partial melting. Chloritization is present (Fig. 3.2B) and is pervasive in some areas giving the matrix a "crystalline appearance". No impact glass clasts were observed in the investigated samples.

Backscattered electron images highlight the angular clastic matrix of the polymict lithic breccia (Fig. 3.2D). Mineral grains have discrete margins, are fragmented, and fractured, and range in size from >1 μm to >500 μm. Most mineral grains have angular to subangular boundaries. Rare rounded apatite grains were also observed. Evidence of variable shock levels in mineral clasts was observed, including kink banding in mica, fracturing, and displacement of mineral grains. Some quartz grains show evidence of partial melting. Spaces between large mineral and lithic clasts are infilled by fine-grained clastic material (Figs. 3.2 C – D). Uncommon, sub-micron Fe-Ti oxide grains disseminated in the matrix were observed (Fig. 3.2D).

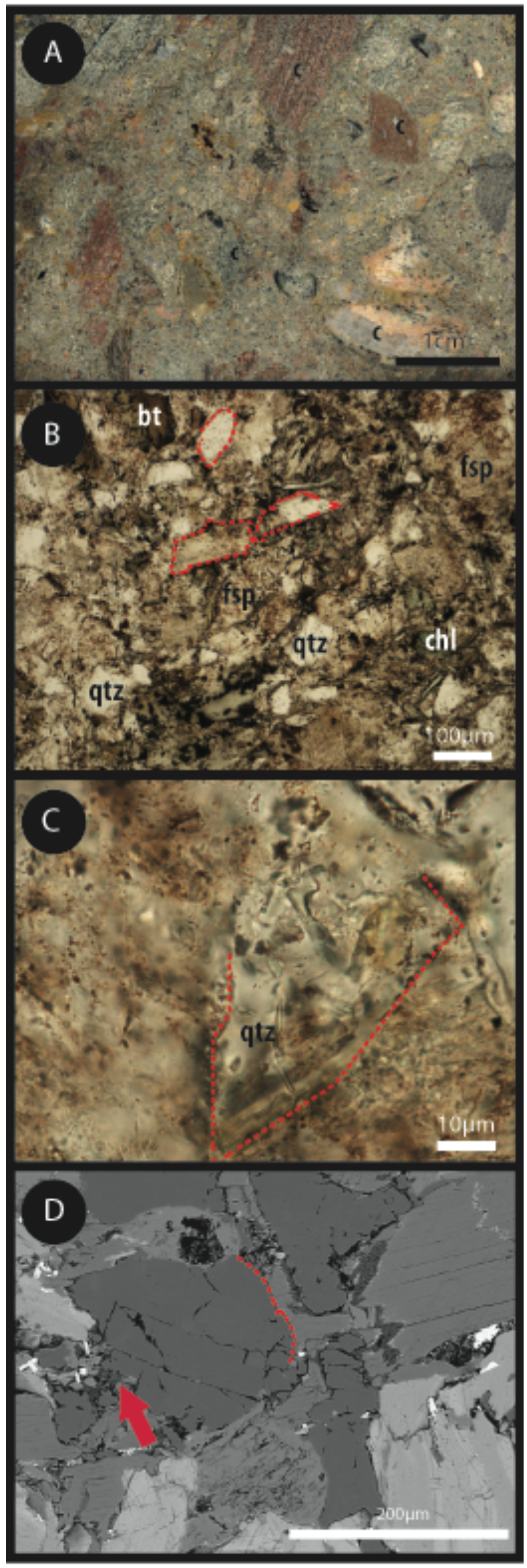

Figure 3.2: Unit 1: melt-free lithic impact breccia.

Figure 3.2: Unit 1: melt-free lithic impact breccia. A: Hand sample. Note the clastic nature of the sample composed of various fragmented lithic clasts (c) ranging in size. There is a notable absence of melt/ glassy inclusions. B – C: Transmitted light micrographs: Note the clastic nature of the groundmass composed of various lithic and mineral clasts (bt: biotite; qtz: quartz; fsp: feldspar). Sharp, irregular grain boundaries are outlined in red. Chloritization (chl) is also observed. D: Backscattered electron (BSE) image. Note the fragmental, cataclastic nature of the groundmass and the similarity of the jagged, sharp grain boundaries (red line) to those in the melt bearing impact breccia. Also note the fine-grained clastic matrix material between larger clasts (red arrow).

3.4.3.2 Unit 2: Clastic melt-bearing impact breccia (*'Chassenon Suevite'*)

Transmitted light microscopy suggests that the groundmass is composed of angular to subangular lithic and mineral fragments in a matrix of fine-grained material forming a cataclastic texture (Fig. 3.3). Mineral fragments are generally smaller than those observed in unit 1, ranging in size from ~2 – 5 µm (Fig. 3.3C). In contrast to the unit 1, the matrix material of unit 2 is a major component forming ~50% of the bulk rock (Fig. 3.3B). Mineral clasts are dominantly feldspar, mica, and quartz. Shock induced features are observed including irregular fracturing, PDFs in quartz, and partial melting. Impact glass clasts are present and are irregular in shape with amoeboid margins and vary in size from micrometers to centimeters. There is a diversity of glass clasts observed. Color ranges from black through pale green. In some samples the glass has been altered to a deep-red brown material. All glassy clasts have intricate relationships with the matrix.

SEM-based observations of the matrix are very similar to unit 1, comprising fragmental, angular mineral grains (Fig. 3.3D) displaying various shock induced features, including fractures and annealed PDFs in quartz. Areas of formerly glassy melt inclusions are now replaced with an Fe-Ti oxide similar in EDX composition to the Fe-Ti oxide grains present in unit 1 (Fig. 3.3D). Occasionally, flow banding is preserved in the oxide grains. Euhedral Fe-Ti oxide crystals have replaced the primary margin between fine-grained matrix breccia and former melt (Fig. 3.3D). The fine-grained infilling breccia contains euhedral to subhedral feldspar crystals at the interface between former melt and matrix that may represent a silica rich phase crystallizing out of the melt.

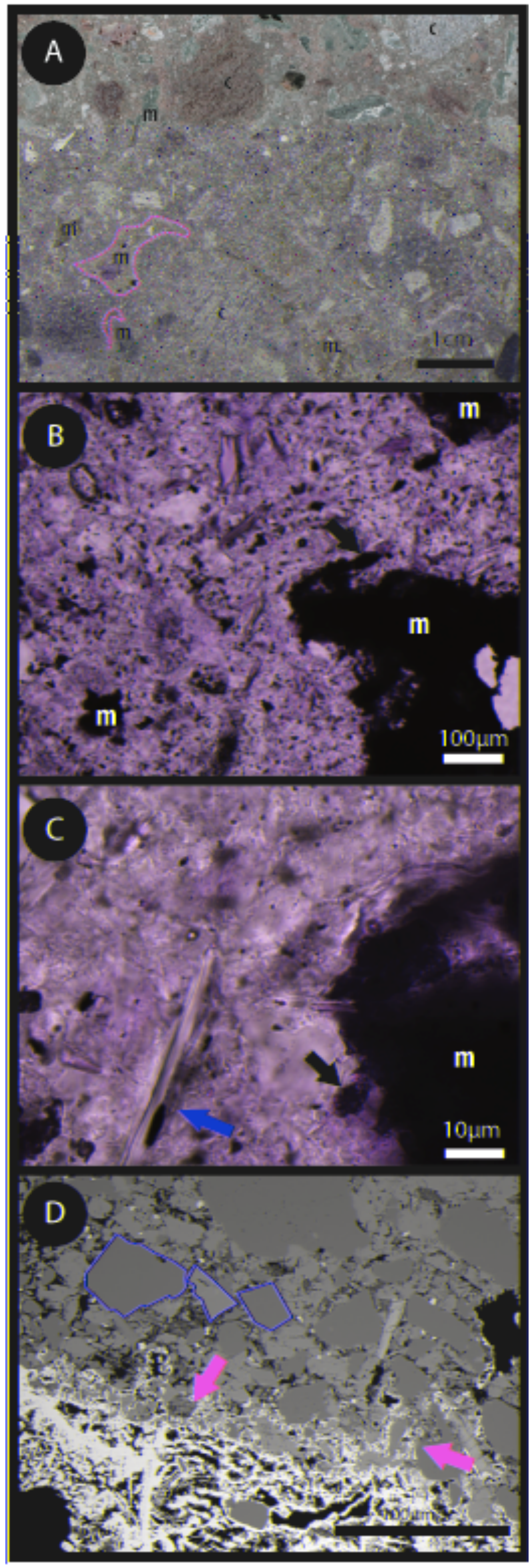

Figure 3.3: Unit 2: clastic melt-bearing impact breccia.

Figure 3: Unit 2: clastic melt-bearing impact breccia. A: Hand sample. Note the numerous lithic clasts (c) and melt inclusions (m). Melt inclusions have complex, delicate, amoeboid morphologies (yellow dashed line) unlikely to survive aerial transport. B – C: Transmitted light photomicrographs. Note the clastic nature of the matrix (red arrow). Former melt clasts (m) have irregular borders and have recrystallized to a red-brown mineral phase. Note the irregular amoeboid protrusions of the former melt inundating the clastic matrix (black arrows). D: Backscattered electron (BSE) image. Note the fragmental, cataclastic nature of the groundmass (example grains outlined in red). The melt phase has recrystallized to a Fe-Ti oxide (white phase at bottom of image). Notice the former melt inundating the grains of the matrix forming becoming an interstitial phase (yellow arrows).

3.4.3.3 Unit 3: Melt-rich impactite (*'basal suevite')*

The impact glass content of this unit visible in hand specimen varies from <10% to >60%. Numerous lithic clasts, angular to rounded, and of varying shock level recorded are present. Some of these clasts are enclosed by glass (Fig. 3.4A). The matrix is purple in color while the glass fragments varies from deep red to yellow in color. The glass and matrix boundaries are irregular in shape and convoluted. Under plane-polarized light the intricate textures between the matrix and melt are easily observed (Fig. 3.4B). At high magnification under scanning electron microscopy the nature of the matrix is somewhat ambiguous. Clast margins are poorly defined and irregular. Interstitial material is poorly resolved. Red-brown, ~1 μm across irregularly-shaped grains are disseminated throughout the matrix (Fig. 3.4C).

Numerous sub-angular lithic and mineral clasts are visible in a quartzofeldspathic matrix with BSE imaging (Fig. 3.4D). Up to ~30% of the matrix is composed of irregular pits filled with fine-grained clay minerals. Glassy, former melt regions have irregular, amoeboid margins and intricate relationships with the matrix. An Fe-Ti oxide phase is disseminated as patchy grains with feathery margins throughout the matrix and within voids in clasts.

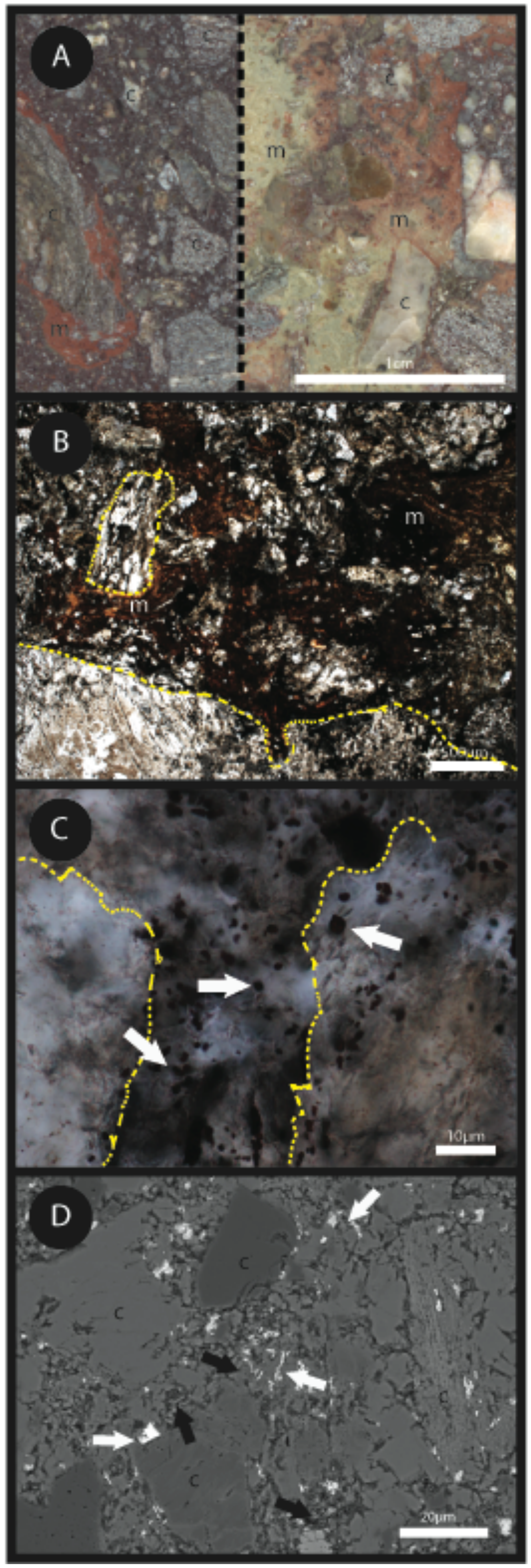

Figure 3.4: Unit 3: melt-rich impactite.

Figure 4: Unit 3: melt-rich impactite. A: hand sample. Left: low melt content, note the large, highly shocked and partially melted clast (c) wrapped in reddish melt (m). Right: high melt content. The matrix has a purple hue in contrast to the extensively altered and discoloured melt phase. The melt region hosts several subrounded lithic clasts (c). Note also the intricate margins between the melt and the breccia matrix. B – C: Microphotographs. Note the intermingling of the glassy melt phase (m) with the matrix. The melt phase has been altered and appears black and opaque to a translucent yellow-orange. Two large, shocked lithic clasts with irregular, obscure boundaries are outlined in yellow. The nature of the interstitial space is ambiguous. Also note the presence of disseminated Ti-Fe oxide grains (white arrows) within the matrix and the similarity of the matrix texture to that of the particulate melt rock (unit 4). D: Backscattered electron (BSE) image. Numerous lithic and mineral clasts (c) are visible in a quartzofeldspathic matrix. Irregular pits (black arrows) are filled with fine-grained clay minerals. It is not clear if these pits represent a preferentially altered phase within a crystalline matrix or altered clasts in a clastic matrix. A secondary Fe-Ti oxide phase (white arrows) is disseminated throughout the matrix and within voids of clasts.

3.4.3.4 Unit 4: Clast-rich impact melt rock (*'Montoume breccia'*)

Under transmitted light the unit 4 has a crystalline matrix that varies in color from grey-brown to red (Fig. 3.5). The matrix often displays flow banding that is cross-cut by fractures associated with red-brown discoloration (Figs. 3.5A – B). Flow banding around centimeter sized lithic clasts is also observed in hand specimens (Fig. 3.5A). This network of fractures and associated discoloration gives the matrix a mesh-like appearance (Fig. 3.5B). The matrix forms between 10 and 80% of the bulk rock; the remaining material is composed of angular to sub-angular mineral, lithic, and amoeboid glassy clasts (Fig. 3.5B). Lithic and mineral clasts are dominantly quartz and feldspar, most of them displaying various shock-induced features including fractures, PDFs (Fig. 3.5C), and partial melting. The matrix surrounding the clasts also displays the red-brown discoloration (Fig. 3.5C). Under high magnification, sub-micron, red-brown, subhedral crystallites disseminated throughout the crystalline matrix, are visible (Fig. 3.5C). These mineral grains give the matrix a granular texture (Figs. 3.5B – C). Former glassy melt "pockets"/clasts have highly irregular boundaries and often fill interstitial spaces within the groundmass.

SEM based observations indicate that the matrix has an igneous texture, including interlocking grains of feldspar (Fig. 3.5D). Lath-shaped pits filled with clay range in size from 25 nm × 1 µm to 2 µm × 25 µm suggesting that one phase of the matrix has been pervasively altered. These pits may make up to 50 % of any given area (Fig. 3.5D). Larger pits have irregular borders, while smaller pits have a more defined lath shape. Other areas are very silica-rich. In these areas the pits make up only ~3 – 5 % (area). The margins between the feldspathic and silica-rich areas are highly irregular. The quartz-rich areas may represent a different initial melt phase or large, partially assimilated, quartz grains. There are distinct lithic and mineral grains of millimeter scale throughout the sample. Quartz clasts have complex, undulating margins suggestive of partial assimilation (Fig. 3.5D). Thread-like strings of Fe-Ti oxide crystals decorate the boundaries between immiscible phases. The distribution of this oxide is heterogeneous; disseminated grains (~10%) appear as isolated rounded grains in the melt ranging from 500 nm to cluster up to ~20 µm in size (Ti >>Fe) and as lath shaped (Ti > Fe) ~25 nm × 1 μm to clusters up to 5 μm × 15 μm; there are also occasional larger (>100 μm) clusters (Fig. 3.5D).

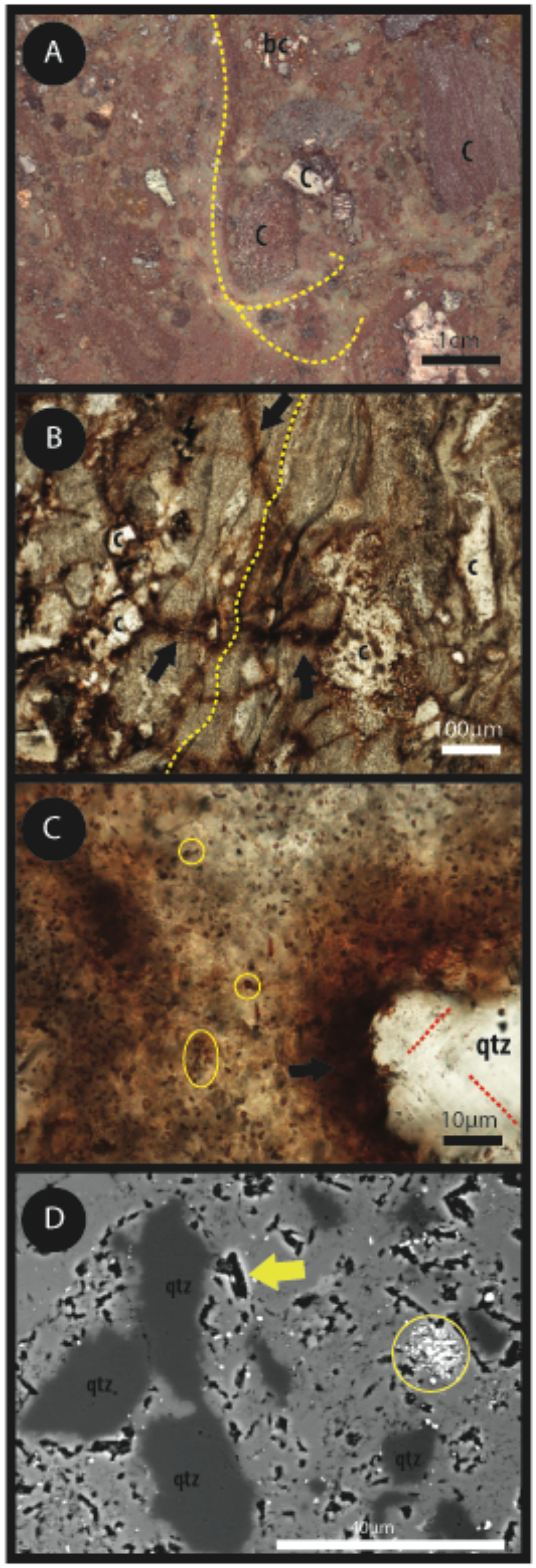

Figure 3.5: Unit 4: particulate clast-rich impact melt rock.

Figure 3.5: Unit 4 particulate clast-rich impact melt. A: Hand sample. Note the presence of multiple lithic clasts (c) and one breccia clast (bc). Yellow dashed lines highlight matrix flow features around lithic clasts. B – C: Transmitted light microphotographs. Note the presence of multiple lithic and mineral clasts (c) and a quartz clast (qtz) displaying planar deformation features (red dashed lines). Also note the flow banding in the melt matrix (yellow dashed line) and the multiple sets of fractures cross cutting the flow banding (black arrows). The fractures and clasts are associated with rusty discoloration. The discoloration of the fractures formed a mesh-like texture. Also note the red-brown disseminated Fe-Ti oxide grains in the melt matrix circled in yellow. D: Backscattered electron (BSE) image: Note the interlocking crystalline nature of the feldspathic matrix. Lath-shaped voids (yellow arrow) are interpreted to represent areas where a mineral phase was completely weathered out. There are many partially resorbed quartz clasts (qtz). The yellow circle encloses a cluster of Fe-Ti oxide grains that are also disseminated throughout the melt.

3.4.3.5 Unit 5: Clast-poor impact melt rock (*'Babaudus melt'*)

In transmitted light, the quartzofeldspathic groundmass of unit 5 appears buff coloured and has a larger overall grain size (average size of 25 μm) compared to the other impactite units (Fig. 3.6). The crystalline, vesicular nature of unit 5 is illustrated in Figures 3.6B and 3.6D. Sub-micron scale dark crystallites are disseminated in the interlocking, semi-polygonal grains, giving the matrix a surgery texture (Fig. 3.6C). The matrix is remarkably homogenous and is mottled with patches of oxide or oxyhydroxide staining (Fig. 3.6B). The groundmass hosts few clasts in comparison to the other impactite units (Fig. 3.6A). Lithic clasts are quartzofeldspathic in composition and are generally uniformly small and rounded. Clasts and vesicles are commonly surrounded by alteration halos of iron oxyhydroxide staining. Vesicles are either empty or infilled with fine-grained mineral assemblages. Scanning electron microscopy highlights the presence of interlocking, sutured grain boundaries indicative of recrystallization (Fig. 3.6D). Micron-scale vesicles are semi-elliptical in contrast to the centimeter-scale elongated vesicles visible in hand specimen. Sub-micron iron-titanium oxide grains are disseminated throughout the melt (Fig. 3.6D).

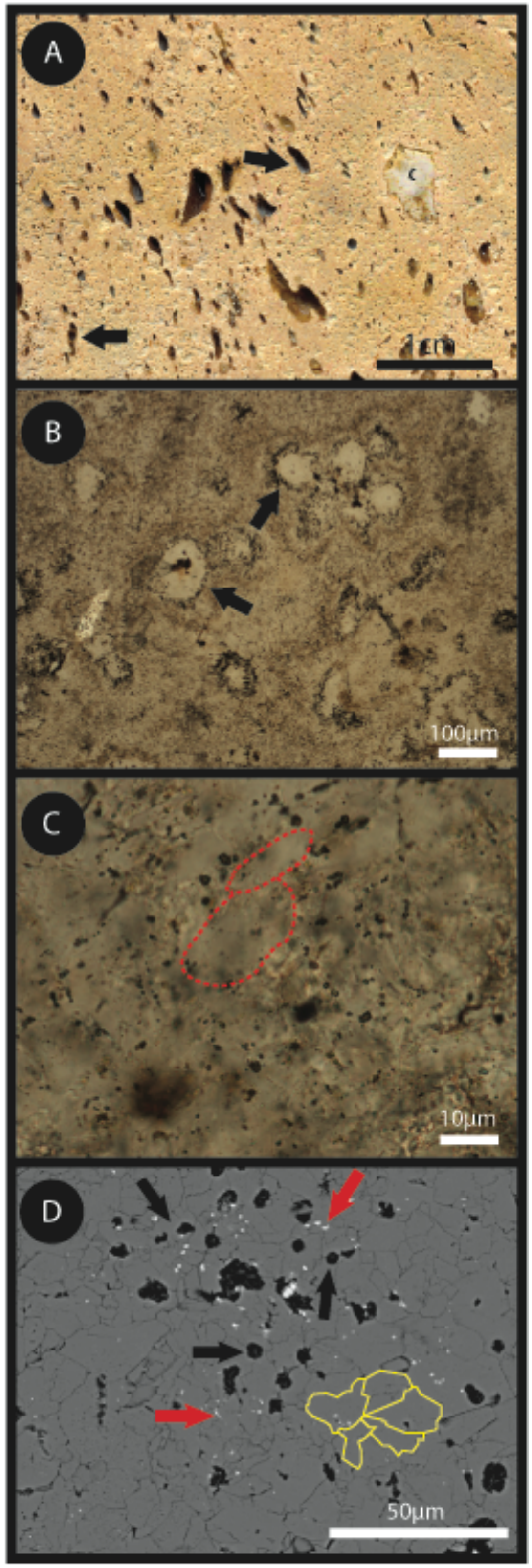

Figure 3.6: Unit 5: clast-poor impact melt rock.

Figure 3.6. Unit 5: Clast-poor impact melt rock. A: Hand sample. Note the homogenous nature of the groundmass and numerous slightly elongated vesicles (black arrows). Elongation may be a flow feature. A rare lithic clast (c) with irregular grain boundaries. B – C: Transmitted light photomicrographs: Note the vesicular nature of the melt (B, black arrows) and the igneous texture of interlocking, semi-polygonal grains (C, red dashed lines). Disseminated Fe-Ti oxide grains give the matrix a speckled texture. D: Backscattered electron (BSE) image: Notice the interlocking sutured grain boundaries indicative of recrystallization (outlined in yellow). Black arrows highlight the vesicular nature of the sample. Red arrows point to disseminated Fe-Ti oxide grains.

3.5 Interpretation and Discussion

3.5.1 Impactites

3.5.1.1 Nomenclature

Impactite nomenclature and classification has been burdened by ambiguity in the literature (*e.g.*, Reimold 2008). In 1994, the first recommendations for the systematic naming and classification of impactites were proposed (Stöffler & Grieve 1994). Stöffler and Grieve (2007), on the behalf of the IUGS SCMR, published a revised proposal on impactite nomenclature and classification based on texture, degree of shock metamorphism, and lithological components. Reimold *et al.* (2008) highlighted a number of recent studies that give rise to problems and potential issues with the revised impactite classification scheme. Five specific areas of ambiguity have been identified: (1) suevites; (2) scale of classification; (3) marine impactites; (4) transitional lithologies; and (5) pseudotachylitic breccias. With the exception of marine impactites and pseudotachylitic breccias, this paper presents the Rochechouart impactite suite as a case study to address these problematic areas of classification.

One of the most notable discussion points is the application of the term "suevite", which was first used in 1920 to describe a breccia (at that time, interpreted as being volcanic) thought to be unique to the Roman "Provincia Suevia" in Germany (Sauer, 1920) at what is now recognized as the Ries impact structure (Pohl *et al.* 1977). Based on the most recent recommendations of the IUGS SCMR, a "suevite" is an impact breccia with a fine-grained lithic (clastic or particulate) matrix hosting both lithic and glass clasts. This represents a revision to the original definition of "suevite" by Stöffler *et al.* (1977), which was defined as a polymict impact breccia with a clastic matrix/groundmass containing fragments and shards of impact glass and shocked mineral and lithic clasts. Unfortunately, the term "suevite" is used loosely in the literature to refer to any impact glass-containing impactite, regardless of groundmass texture (*e.g.*, Kelley & Spray, 1997; Masaitis, 1999). Indeed, at least three of the impactites studied here, units 2, 3, and 4, have been termed "suevites" in the past based on the IUGS classification scheme, despite the vast differences in appearance, even at the hand specimen scale (Figs. 3.3 – 3.5). As demonstrated in the subsequent section, these impactites also differ in terms of the nature of their groundmass.

The groundmass texture of an impactite is significant with respect to the mode of emplacement. For example, suevite *sensu stricto* has been classically interpreted to be emplaced through the atmosphere (*e.g.*, Stöffler 1977, Masaitis 1999). Recent studies of the Ries "suevite", however, suggest that the type locality outcrops have a melt-rich matrix (Osinski *et al.* 2004). A melt-rich matrix is not consistent with an airborne mode of origin and suggests that these impactites may have been emplaced via surface flow (Osinski *et al.*, 2004). So-called "suevites" have also been documented to underlie coherent impact melt rocks at a variety of structures (Osinski *et al.* 2011), which is not consistent with an airborne mode of origin for the former. Furthermore, drill cores from the Bosumtwi impact structure, Ghana, suggest a continuum of fine-scale intercalations between melt-bearing and melt-free clastic breccias (Coney *et al.* 2007, Ferrière *et al.* 2007), which require more complex, multi-stage emplacement models.

3.5.1.2 Classification of the Rochechouart impactites

High-resolution imaging of the Rochechouart impactites using scanning electron microscopy allowed for detailed observations of textual relationships within, and between, the groundmass and clasts. The Rochechouart impactites have historically been classified based on observable characteristics at the hand sample to thin section (i.e., optical microscopy) scale and contextual relationships in the field (*e.g.*, Kraut and French 1971, Lambert 1977a). These macro- to intermediate-scale observations are excellent 'first principle' classifications and field divisions. However, recommendations proposed by the IUGS SCMR involve a classification scheme for impactites based on the degree of shock metamorphism and lithological components (Stöffler & Grieve 2007). To take into account gradational boundaries and transitional lithologies, a recent sub-classification of melt-bearing impactites has been proposed, based on textural analysis of the groundmass or matrix and its relationship with the melt phase(s) and clasts (Osinski *et al.* 2008). Such clast-matrix relationships require microscopic-scale observations as presented in our study for the different types of impactites from Rochechouart. Importantly, the proposed micro-scale analysis and subsequent classification of impactites is by no means meant to diminish the importance of field observation and classification; rather, it augments detailed field studies and enables the classification of impact lithologies based on observable intrinsic properties rather than interpretations of field context. For example, as noted above, at the Rochechouart impact structure, several different “suevite” units have previously been classified, including “basal suevite”, “welded suevite”, and “upper suevite”; the upper suevite has also been referred to as “Chassenon suevite” and suevite “*sensu stricto”.* The non-uniform use of nomenclature makes it difficult to correlate and compare different studies at this impact structure, let alone between multiple impact craters. Furthermore, the terms “basal” and “upper” are dependent on field relationships between different units. Due to partial erosion at the Rochechouart structure, determining these field relationships are somewhat difficult and in some cases even impossible. Thus, a “suevite” sample with no relative context would not be able to be classified using the current IUGS impactite classification scheme.

A recent study by Lambert (2010) uses the terminology “suevite *sensu stricto” and* “melt-rich suevite” to refer to unit 2 and unit 3 respectively. We suggest that this nomenclature be modified and the units classified based on their observable characteristics independent of the connotation of terms such as “suevite”, which have been historically misrepresented in the literature. In accord with the proposed classification schemes of Stöffler and Grieve (2007) and Osinski *et al.* (2008), the following nomenclature is proposed for the Rochechouart impactites (Fig. 3.7). Square brackets are used to delineate descriptive terms applicable to specific Rochechouart samples. We suggest descriptive terminology be used for transitional lithologies where end-member (IUGS) classification cannot be used to distinguish between units such as Rochechouart units 3 through 5

Unit 1: [Melt-free] lithic impact breccia.

Unit 2: [clastic] melt-bearing impact breccia (formerly the “Chassenon" or “green” suevite).

Unit 3: Melt-rich impactite. As the primary nature of the groundmass cannot unambiguously be determined, unit 3 cannot be classified as either a lithic breccia or impact melt. This unit is a transitional lithology resulting from a continuum between melt and melt-free impactites.

Unit 4: [Particulate clast-rich] impact-melt rock; this unit, previously known as a "Montoume breccia", "red welded breccia/suevite" has a crystalline, rather than clastic, matrix. As such, this unit is here classified as an impact melt rock.

Unit 5: [Clast-poor to clast-free aphanitic vesicular] impact-melt rock.

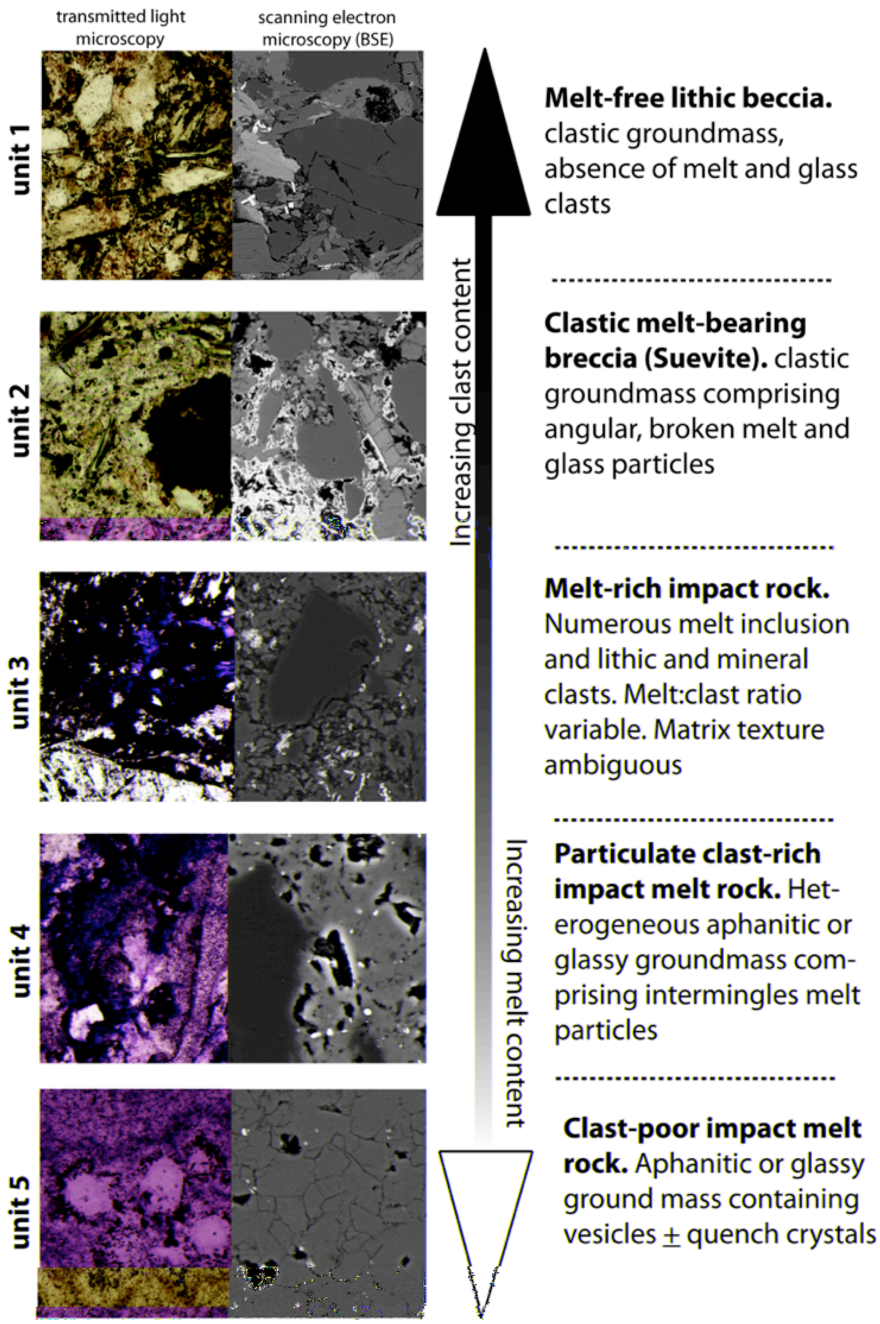

Figure 3.7: Descriptive classification of the Rochechouart impactites based on groundmass textures.

Descriptive classification of the Rochechouart impactites based on groundmass textures. Note the defining characteristics of each impactite highlighted in the right column text. The images on the left side are representative transmitted light microphotographs and scanning electron images of each units. The full images with scale bars are depicted in Figures 3.2 – 3.5.

While the distinction between a lithic breccia and an impact melt-bearing impactite is easily defined by the presence or absence of melt phases (either as clastic or matrix material), the textural and genetic relationships between the impact melt-bearing units (units 2, 3, and 4) are complex. It is only with careful microscopic imagery that characteristic relationships between the matrix and melt phases can be elucidated. As noted by Osinski *et al.* (2004) and exemplified here by units 3 and 4, care should be exercised when interpreting seemingly "clastic" textures based on hand specimen and optical studies alone. Unit 2, corresponding to the classic "Chassenon suevite" or "upper suevite" of Lambert (2010) likely represents a lithology in the continuum between impact melt-free and melt-rich impactites. The recently discovered impact melt-rich impactite (unit 3; previously basal suevite) is highly variable in composition and texture. This impact melt-rich unit is located in direct contact with the basement rocks and always in close proximity to the particulate impact melt rocks (Lambert 2010). The matrix, formerly reported as clastic, incorporates up to 50 vol% melt clasts (Lambert 2010). We cannot definitively classify the matrix as either clastic or crystalline as extensive post-impact hydrothermal alteration obscures the primary texture (Figs. 3.4 C – D). The matrix is very similar in texture and composition, as assessed by EDX analyzes, to that of unit 4 (the particulate clast-rich impact melt rock). The characteristics of this melt-rich impactite do not conform to the definition of suevite *sensu stricto* and should not be termed as such. The unit 3 is both texturally and genetically transitional between the polymict lithic breccia and particulate melt rock, as proposed and discussed by Lambert (2010).

3.5.1.3 Complications due to weathering and alteration

Impactite lithologies were subject to complex alteration processes as noted above and as exemplified by unit 3. Weathering and alteration lead to the formation of secondary and even tertiary mineral phases that overprint primary textures and mineralogy. For example, argillic clay alteration and chloritization (Fig. 3.2B) often completely replace feldspar grains in the Rochechouart impact breccias. The matrix of the impact melt-rich impactite (unit 3) contains numerous 'pits' filled with fine-grained clay minerals. It is not clear if these patches of clay represent a mineral phase within a crystalline matrix that has been preferentially altered (as in the crystalline impact melt rock), or altered fine-grained material interstitial to larger clasts within a cataclastic matrix. Such an extensive alteration, as with the examples presented above, leads to difficulties assigning primary mineralogy and even in some cases primary textures. Impact glasses may be completely devitrified to clay minerals, recrystallized to an Fe-Ti oxide, or weathered out completely, leaving a vesicular-like texture to glass-bearing impact breccias. The alteration of the fractures and surrounding clasts in the particulate clast-rich impact melt rock is suggestive of hydrous alteration. SEM imaging can elucidate complex relationships between clasts and the matrix and potentially deconvolve complex overprinting relationships resulting from weathering, post-impact hydrothermal activity, and regional metamorphism. The extensive alteration resulting from devitrification, post-impact hydrothermal activity, and terrestrial weathering processes underscores the importance of detailed micro-scale observations.

3.5.2 Impact-generated hydrothermal activity at Rochechouart

Alteration of the Rochechouart impactites has been previously noted by several researchers (Kraut & French 1971, Lambert 1977b, c, Reimold *et al.* 1987); however, the post-impact hydrothermal system has not been described in any detail in previous studies. Three main alteration assemblages are recognized (Table 2): (1) argillic-like (commonly dominated by phyllosilicates); (2) carbonate; and (3) oxide, possibly reflecting differing alteration conditions and heterogeneous primary material. The dominant K-rich clay mineralization alteration assemblage at Rochechouart is consistent with the general patterns of post-impact hydrothermal systems discussed by Naumov (2002, 2005). The alteration assemblages are present in both allochthonous and autothchonous impactites, but are most prevalent in units 3 and 5.

The intense evidence of K-metasomatism in all impactite units is indicative of pervasive, deep-circulation of hydrothermal fluids (Lambert 1977b, 2009). All impactite units have positive K_2O/Na_2O ratios (Lambert 1977b). Interestingly, this K enrichment systematically increases with melt content. The K_2O/Na_2O ratios of the lithic polymict breccia is approximately five times that of the unshocked basement rocks; approximately six times higher in suevite; approximately ten times higher in lithic clasts within melt rocks, and approximately fifteen times higher in melt (Lambert 1977b, 2009). The pervasive argillic-like alteration assemblages, together with fine-grained quartz and carbonate mineralization, are consistent with the development of a post-impact hydrothermal system (*e.g.*, Naumov 2005, Osinski *et al.* 2012), as previously suggested by Reimold *et al.* (1984). Staining by alteration products is most prevalent in oxide rich units, such as in the hematite-rich particulate melt rock (Unit 3). However, it is still unclear why the melt in the particulate melt rock is richer in oxides than the crystalline melt.

It is notable that the accessory phases present in the impactite units vary with the melt content. Both the lithic breccia and suevite contain rounded, embayed apatite grains. Apatite was not seen in the particulate clast-rich melt or crystalline melt units. It is interesting to note that apatite is unstable in the presence of Cl-rich fluids (Boudreau *et al.* 1986). The increasing K_2O/Na_2O ratios with the presence of melt suggest that hydrothermal alteration was more intense in these units, possibly resulting in apatite recrystallization. In contrast, oxides and oxyhydroxides are more prevalent in the melt-rich units. This may be a consequence of homogenization and immiscibility between phases at a local scale. Oxides also often form skeletal quench textures within the silicate melt, thus, there is likely three generations of oxides: (1) primary relict accessory mineral oxides from the target rock occurring in the melt-free impactites; (2) impact-generated oxides forming quench crystallites within the melt; and (3) oxide mineralization as a result of post-impact hydrothermal alteration.

3.5.3 Implications for the Rochechouart impact structure

3.5.3.1 Comparison with other craters in crystalline targets

A major question for the Rochechouart structure is why does there not appear to be a "simple" relatively clast-free impact melt sheet? Studies of other mid-sized complex impact structures developed in crystalline targets — such as the 24-km-diameter Boltysh (Grieve *et al.* 1987), the 24-km-diameter and 36-km-diameter East and West Clearwater Lakes (Simonds *et al.* 1978b), and the 28-km-diameter Mistastin (Grieve 1975) impact structures — and considerations of the origin and emplacement of impact melts (Grieve *et al.* 1977, Osinski *et al.* 2008) would suggest that this should be the case. The reclassification of impactites proposed herein goes part way to answering this question, but uncertainty remains. As an example, the well-preserved 24 km Boltysh impact crater, Ukraine, (Grieve *et al.* 1987), which formed in the crystalline Precambrian basement of the Ukrainian shield, shares a similar stratigraphic sequence of impactites to that proposed here for Rochechouart. The ~200 m thick Boltysh impact melt sheet lies directly over polymict lithic breccias of the crater floor and is overlain by ~25 m of "suevitic breccia" (Grieve *et al.* 1987). This melt sheet contains ~10% granitic clasts displaying varying degrees of assimilation (Grieve *et al.* 1987). It is also of note that the top ~60 m of the Boltysh melt unit is described as a clast-poor microcrystalline impact melt (Grieve *et al.* 1987), which is similar to the aphanitic vesicular impact melt at Rochechouart (unit 5). Thus, we suggest that the clast-poor aphanitic vesicular impact melt rock (unit 5) may have occurred as scattered, isolated lenses within and/or near the top of the impact melt "sheet" that did not interact with underlying, unconsolidated breccia or that these outcrops represent melt near the crater centre that presumably lined the transient cavity crater immediately after its formation.

We suggest that the textural and chemical properties, together with the stratigraphic relations, of the Rochechouart impactites, are consistent with the particulate clast-rich impact melt rock being the main allochthonous crater-fill unit, equivalent to the coherent impact melt sheets observed in impact structures such as Mistastin (Grieve 1975). This is supported by the presence of columnar joints that are clearly visible in the Montoume quarry. Similar columnar jointing in impactites has only been observed in impact melt sheets, such as at the Mistastin (Grieve 1975) and Manicouagan (Simonds *et al.* 1978a) impact structures (both in Canada). However, it is unclear as to why the clast content of the main Rochechouart melt sheet (interpreted here to be the clast-rich melt rock) is so high; although the partial erosion of Rochechouart may be a factor in that we may only be viewing the basal sequence of the original melt sheet.

3.5.3.2 Location of the crater center and size of the Rochechouart structure

The above discussions have potential implications for determining the center of the Rochechouart impact structure and, correspondingly, its size. Previous workers (Kraut & French 1971, Lambert 1974, 1977c) estimate the crater center to be in the Valette area (Fig. 3.1), based on the distribution of the impact breccias/impact melt rocks and on the distribution and orientation of shatter cones. It has since been shown that the distribution and orientation of shatter cones is an inherently unreliable method to determine the center of an impact structure (Osinski & Spray 2006, Wieland *et al.* 2006). In addition, if unit 3 (i.e., melt-rich impactite) represents the main crater-fill material, then, the center of crater may be further to the south, near the village of Montoume (Fig. 3.1). The Montoume quarry hosts a 900 m long, 600 m wide, and 25 m high outcrop of the particulate impact melt lithology (unit 4) and is the thickest known sequence of crater-fill material at the scale of the whole structure. Moving the crater center to the south would place the main outcropping area of the unit 5 (i.e., at Chassenon; Fig. 3.10, in the crater rim area — if the crater diameter remains the same (i.e., 24 km). However, a few shatter cones occurrences are known in the Chassenon area (*e.g.*, Lambert 1977a, 2010) and were recently confirmed during a recent mapping campaign of the distribution of shatter cones at the scale of the Rochechouart structure by (L.F.). If these occurrences of shatter cones are truly in situ, then this would be inconsistent with placing Chassenon in the crater rim area. Invoking a larger crater diameter is one possible solution. Thus, if the crater diameter is increased and the crater center placed further south, near the village of Montoume, then the Chassenon area would be well inside the crater rim, consistent with the recent mapping of shatter cone distribution. A crater diameter in the 40 – 50 km range has been suggested by studying topographic comparisons using crater profile data of Rochechouart with other structures, including the Ries and the El’gygytgyn impact structures (Lambert 2010). More conclusive data is required to support this suggestion but a diameter in this range certainly seems possible from the results of our study, in particular, if the particulate clast-rich impact melt rock is a small remnant of the basal parts of a once much more extensive and thicker crater-fill impact melt sheet.

Finally, we note that the distribution of impactites and shock indicators may be biased in the northern part of the structure as the crater floor is inclined 0.6^{o} to the north (Lambert 1977a, 2008, 2010). Such an inclination of 0.6^{o} over a 24 km lateral distance corresponds to an approximate vertical difference of 250 m between the northern and southern extents of the structure. This inclination may have lead to preferential erosion of impactite outcrops south of the structure, as the present-day erosional level is approximately equal to the crater floor. Such asymmetrical erosion could have led to the preservation of stratigraphically higher impactite units to the northern part such as impact melt-bearing breccias and an impactoclastic unit and resulted in the erosion of ejecta deposits.

3.6 Closing Remarks

High-resolution imaging of the Rochechouart impactites using scanning electron microscopy combined with optical microscope observations, has enabled elucidation of textual relationships within, and between, the groundmass and clasts. In summary, groundmass textures form a continuum largely based on the proportion of impact melt (glass and crystallites) between the aphanitic crystalline matrix of the clast-poor to clast-free impact melt rock (unit 5) and the fragmental, clastic matrix of the melt-free lithic breccia (unit 1). This study of the Rochechouart impactites underscores the importance of establishing consistent use of nomenclature in the literature.

The classification system applied to the Rochechouart impactites in this study allows for gradational lithologies in addition to being highly beneficial for samples/sites with limited exposure and little to no field context. Developing such a system and applying it to all impact structures will allow correlation between sites and studies as well as set a precedent for limited sample environments. It is hoped that this type of "multi-scale" classification of impactites will allow correlations between impact structures in very different target lithologies, as the impactite nomenclature is independent of relationships between impactite lithologies and relationships between lithologies and the impact structure itself.

It is hoped that these new observations will stimulate renewed interest in the study of the Rochechouart impact structure. Despite its location in western Europe, the Rochechouart impact structure has been relatively little studied, especially compared to its close neighbour, the Ries impact structure in Germany. As we have shown here, erosion hampers our understanding of this structure, but important new observations and interpretations can still be made. The potential larger diameter of the Rochechouart structure, in the range of 40 to 50 km, which is supported by our study, would definitely have affected a much larger area than previously thought and likely induced regional or even continental environmental perturbations (*e.g.*, Pierazzo & Artemieva, 2011).

3.7 Acknowledgements

This research was funded by Natural Sciences and Engineering Council of Canada (NSERC) Discovery Grants to GRO and NB the Canadian Space Agency's (CSA) Canadian Analogue Research Network (CARN). GRO is supported by an NSERC/MDA/CSA Industrial Research Chair in Planetary Geology. Ivan Barker (UWO ZAPLab), Callum Hetherington and Mark Grimson (Texas Tech), and Todd Simpson (UWO Nanofabrication laboratory) are thanked for technical assistance with the SEM measurements. We thank the Rochechouart museum for providing us the samples 42 and 43. This paper is dedicated to the memory of François Kraut (1907 – 1983), who first described the Rochechouart breccias as impactites.

3.8 References Cited

ALVAREZ, L.W., ALVAREZ, W., ASARO, F. AND MICHEL, H.V. (1980) Extraterrestrial cause for the Cretaceous/Tertiary extinction. *Science* **208**, 1095 – 1108.

BARTOSOVA K., FERRIÈRE L., KOEBERL C., REIMOLD W. U., AND GIER S. (2009) Petrographic and shock metamorphic studies of the impact breccia section (1397 – 1551 m depth) of the Eyreville drill core, Chesapeake Bay impact structure, USA. *The ICDP-USGS deep drilling project in the Chesapeake Bay impact structure: Results from the Eyreville core holes* edited by Gohn G. S., Koeberl C., Miller K. G., and Reimold W. U. Boulder: *Geological Society of America, Special Paper* 458. pp. 317 – 348.

BOUDREAU A. E., MATHEZ E. A., AND MCCALLUM I. S. (1986) Halogen geochemistry of the Stillwater and Bushveld complexes; evidence for transport of the platinum-group elements by Cl-rich fluids. *Journal of Petrology* **27**, 967 – 986.

CHÈVREMONT P. AND FLOC'H J. P. (1996) Carte Géologique de la France (1:50,000), feuille Rochechouart (687). Orléans: Bureau de Recherches Géologiques et

Minières, France. Notice explicative par P. Chèvremont *et al.* (1996) 172 p.

CONEY L., GIBSON R. L., REIMOLD W. U., AND KOEBERL C. (2007) Lithostratigraphic and petrographic analysis of ICDP drill core LB-07A, Bosumtwi impact structure, Ghana. *Meteoritics & Planetary Science* **42**, 569 – 589.

FERRIÈRE L., KOEBERL C., AND REIMOLD W. U. (2007) Drill core LB-08A, Bosumtwi impact structure, Ghana: Petrographic and shock metamorphic studies of material from the central uplift. *Meteoritics & Planetary Science* **42,** 611 – 633.

FERRIÈRE L., KOEBERL C., AND REIMOLD W. U. (2009a) Characterization of ballen quartz and cristobalite in impact breccias: New observations and constraints on ballen formation. *European Journal of Mineralogy* **21**, 203 – 217.

FERRIÈRE L., KOEBERL C., REIMOLD W. U., HECHT L., AND BARTOSOVA K. (2009b) The origin of "toasted" quartz in impactites revisited (abstract #1751). 40th Lunar and Planetary Science Conference. CD-ROM.

FERRIÈRE L., KOEBERL C., LIBOWITZKY E., REIMOLD W. U., GRESHAKE A., AND BRANDSTÄTTER F. (2010) Ballen quartz and cristobalite in impactites: new investigations. In *Large Meteorite Impacts and Planetary Evolution IV*, edited by Gibson R. L. and Reimold W. U. Geological Society of America, Special Paper 465, pp. 609 – 618.

GOHN G. S., KOEBERL C., MILLER K. G., REIMOLD W. U., COCKELL C. S., HORTON J. W., JR., SANFORD W. E., AND VOYTEK M. A. (2006) Chesapeake Bay impact structure drilled. *EOS, Transactions, American Geophysical Union* **87**, 349 – 355.

GRIEVE R. A. F. (1975) Petrology and chemistry of impact melt at Mistastin Lake crater, Labrador. *Geological Society of America Bulletin* **86**, 1617 – 1629.

GRIEVE R. A. F., DENCE, M. R., ROBERTSON, P. B. (1977) Cratering processes — As interpreted from the occurrence of impact melts. In *Impact and explosion cratering; planetary and terrestrial implications; Proceedings of the Symposium on planetary cratering mechanics,* editied by Roddy D. J., Pepin R. O., and Merrill R. B. New York: Pergamon Press. pp. 791 – 814.

GRIEVE R. A. F., RENY G., GUROV E. P., AND RYABENKO V. A. (1987) The melt rocks of the Boltysh impact crater, Ukraine, USSR. *Contributions to Mineralogy and Petrology* **96**, 56 – 62.

HILDEBRAND, A.R., PENFIELD, G.T., KRING, D.A., PILKINGTON, M., CAMARGO, A.Z., JACOBSEN, S.B. AND BOYNTON, W.V. (1991) Chicxulub Crater: A possible Cretaceous/Tertiary boundary impact crater on the Yucatan Peninsula, Mexico. *Geology* **19**, 867 – 871.

KELLEY S. P. AND SPRAY J. G. (1997) A Late Triassic age for the Rochechouart impact structure, France. *Meteoritics & Planetary Science* **32**, 629 – 636.

KENKMANN T., IVANOV B. A., AND STÖFFLER D. (2000) Identification of ancient impact structures: Low-angle normal faults and related geological features of crater basements. In *Impacts and the Early Earth* edited by Gilmour I. and Koeberl C., Lecture Notes in Earth Sciences, Springer-Verlag, **91**, 279 – 307.

KOEBERL C., SHUKOLYUKOV A., AND LUGMAIR G. W. (2007) Chromium isotopic studies of terrestrial impact craters: identification of meteoritic components at Bosumtwi, Clearwater East, Lappajarvi, and Rochechouart. *Earth and Planetary Science Letters* **256**, 534 – 546.

KRAUT F. (1967) Sur l'origine des clivages du quartz dans les brèches "volcaniques" de la région de Rochechouart. *Comptes-Rendus de l'Académie des Sciences de Paris* **264**(série D), 2609 – 2612.

KRAUT F. (1969) Über ein neues Impaktit-Vorkommen im Gebiete von Rochechouart-Chassenon (Départements Haute Vienne und Charente, Frankreich). *Geologica Bavarica* **61**, 428 – 450.

KRAUT F. AND FRENCH B. M. (1971) The Rochechouart meteorite impact structure, France: preliminary geological results. *Journal of Geophysical Research* **76**, 5407 – 5413.

KRAUT F., SHORT N. M., AND FRENCH B. M. (1969) Preliminary report on a probable meteorite impact structure near Chassenon, France. *Meteoritics* **4**(3):190 – 191.

LAMBERT P. (1974) Etude géologique de la structure impactitique de Rochechouart (Limousin, France) et son contexte. *Bulletin du Bureau de Recherches Géologiques et Minières. Section 1: Géologie de la France* **3**, 153 – 164.

LAMBERT P. (1977a) Les effets des ondes de choc naturelles et artificielles, et le cratère d'impact de Rochechouart (Limousin, France). Habilitation thesis, Université de Paris-Sud, Orsay, France. 515 p.

LAMBERT P. (1977b) Rochechouart impact crater: statistical geochemical investigations and meteoritic contamination. In *Impact and explosion cratering; planetary and terrestrial implications; Proceedings of the Symposium on planetary cratering mechanics*, edited by Roddy D. J., Pepin R. O., and Merrill R. B. New York: Pergamon Press. pp. 449 – 460.

LAMBERT P. 1977c. The Rochechouart crater: shock zoning study. *Earth and Planetary Science Letters* **35**, 258 – 268.

LAMBERT P. (1982) Rochechouart: a flat crater from a clustered impact, *Meteoritics* **17**(4), 240 – 241.

LAMBERT P. (2010) Target and impact deposits at Rochechouart impact structure, France. In *Large Meteorite Impacts and Planetary Evolution IV*, edited by Gibson R. L. and Reimold W. U., Geological Society of America, Special Paper 465, pp.509 –

541.

MANES G. (1833) *Description géologique et industrielle du département de la Haute-Vienne.* Ducourtieux, Limoges. 140 p.

MASAITIS V. L. (1999) Impact structures of northeastern Eurasia: the territories of Russia and adjacent countries. *Meteoritics & Planetary Science* **34**, 691 – 711.

NAUMOV M. V. (2005) Principal features of impact-generated hydrothermal circulation systems: mineralogical and geochemical evidence. *Geofluids* **5**, 165 – 184.

NAUMOV M. V., PLADO J., AND PESONEN L. J. (2002) Impact-generated hydrothermal systems; data from Popigai, Kara, and Puchezh-Katunki impact structures; Impacts in Precambrian shields. In *Impacts in Precambrian shields,* edited by Koeberl C. Berlin: Springer. pp. 117 – 171.

NELSON M. J. AND NEWSOM H. E. (2006) Yaxcopoil-1 impact melt breccias: Silicate melt clasts among dolomite melt and implications for deposition: 37th Lunar and Planetary Science Conference.

OSINSKI G. R., GRIEVE R. A. F., AND SPRAY J. G. (2004) The nature of the groundmass of surficial suevite from the Ries impact structure, Germany, and constraints on its origin. *Meteoritics & Planetary Science* **39**, 1655 – 1683.

OSINSKI G. R. AND SPRAY J. G. (2005) Tectonics of complex crater formation as revealed by the Haughton impact structure, Devon Island, Canadian High Arctic. *Meteoritics & Planetary Science* **40**, 1813 – 1834.

OSINSKI G. R. AND SPRAY J. G. (2006) Shatter cones of the Haughton impact structure, Canada. *Proceedings of the 1st International Conference on Impact Cratering in the Solar System, European Space Agency Special Publication SP-612* (CD-ROM).

OSINSKI G. R., SPRAY J. G., AND GRIEVE R. A. F. (2008) Impact melting in sedimentary target rocks: An assessment. In *The sedimentary record of meteorite impacts*, edited by Evans K, R., Hoeton W., King D. K. Jr., Morrow J. R., and Warme J. E. GSA Special Paper 437. Boulder, Colorado: Geological Society of America.

PIERAZZO, E. AND ARTEMIEVA, N. (2012) Local and Global Environmental Effects of Impacts on Earth. *Elements* **8**, 55 – 60.

POHL J. (1994) Magnetic investigations in the Rochechouart impact structure (abstract). In *European Science Foundation, Third International Workshop, Shock Wave Behaviour of Solids in Nature and Experiments*, Limoges/Rochechouart, France, p 52.

POHL J., ERNSTSON K., AND LAMBERT P. (1978) Gravity measurements in the Rochechouart impact structure (France). *Meteoritics* **13**, 601 – 604.

POHL J., POSCHLOD K., REIMOLD W. U., AND CRASSELT C. (2008) Ries crater, Germany: the Enkingen magnetic anomaly and associated drill core SUBO 18. *Large Meteorite Impacts and Planetary Evolution IV* (abstract # 3030). August 17 – 21, 2008. Vredefort Dome, South Africa.

POHL J., STÖFFLER D., GALL H., AND ERNSTSON K. (1977) The Ries impact crater. In *Impact and explosion cratering; planetary and terrestrial implications; Proceedings of the Symposium on planetary cratering mechanics,* editied by Roddy D. J., Pepin R. O., and Merrill R. B. New York: Pergamon Press. pp. 343 – 404.

REIMOLD W. U., HORTON, J. W. JR., SCHMITT R. T. (2008) Debate about impactite nomenclature — recent problems. *Large Meteorite Impacts and Planetary Evolution IV* (abstract # 3033). August 17 – 21, 2008. Vredefort Dome, South Africa.

REIMOLD W. U., OSKIERSKI W., AND HUTH J. (1987) The pseudotachylite from Champagnac in the Rochechouart meteorite crater, France. *Journal of Geophysical Research* **92**(B4), E737 – E748.

REIMOLD W. U., OSKIERSKI W., AND SCHAEFER H. (1984) The Rochechouart impact melt: geochemical implications and Rb-Sr chronology. Proceedings, XV^{th} Lunar and Planetary Science Conference. pp. 685 – 686.

SAUER A. (1920) Erlauterungen zur geologischen. Blatt 20 Bopfingen, Karte Wurttemberg.

SCHMIEDER M., BUCHNER E., SCHWARZ W. H., TRIELOFF M., AND LAMBERT P. (2010) A Rhaetian $^{40}Ar/^{39}Ar$ age for the Rochechouart impact structure (France) and implications for the latest Triassic sedimentary record. *Meteoritics & Planetary Science* **45**(8), 1225 – 1242.

SCHULTE, P., ALEGRET, L., ARENILLAS, I., ARZ, J.A., BARTON, P.J., BOWN, P.R., BRALOWER, T.J., CHRISTESON, G.L., CLAEYS, P., COCKELL, C.S., COLLINS, G.S., DEUTSCH, A., GOLDIN, T.J., GOTO, K., GRAJALES-NISHIMURA, J.M., GRIEVE, R.A.F., GULICK, S.P.S., JOHNSON, K.R., KIESSLING, W., KOEBERL, C., KRING, D.A., MACLEOD, K.G., MATSUI, T., MELOSH, J., MONTANARI, A., MORGAN, J.V., NEAL, C.R., NICHOLS, D.J., NORRIS, R.D., PIERAZZO, E., RAVIZZA, G., REBOLLEDO-VIEYRA, M., REIMOLD, W.U., ROBIN, E., SALGE, T., SPEIJER, R.P., SWEET, A.R., URRUTIA-FUCUGAUCHI, J., VAJDA, V., WHALEN, M.T. AND WILLUMSEN, P.S. (2010) The Chicxulub asteroid impact and mass extinction at the Cretaceous-Paleogene boundary. *Science* **327**, 1214 – 1218.

SIMONDS C. H., FLORAN R. J., MCGEE P. E., PHINNEY W. C. AND WARNER J. L. (1978a) Petrogenesis of melt rocks, Manicouagan impact structure, Quebec. *Journal of Geophysical Research* **83**, 2773 – 2778.

SIMONDS C. H., PHINNEY W. C., MCGEE P. E., AND COCHRAN A. (1978b) West Clearwater, Quebec impact structure, Part I: Field geology, structure and bulk chemistry. *Proceedings of the 9th Lunar and Planetary Science Conference.* pp. 2633 – 2658.

SMITH R. (2011) Dark days of the Triassic: Lost world. Nature **479**, 287 – 289.

STÖFFLER D. (1977) Research drilling Nördlingen 1973: polymict breccias, crater basement, and cratering model of the Ries impact structure. *Geologica Bavarica* **75**, 443 – 458.

STÖFFLER D. AND GRIEVE R. (2007) Classification and nomenclature scheme; impactites [modified]. In *Metamorphic rocks, a classification and glossary of terms; recommendations of the International Union of Geological Sciences Subcommission on the Systematics of Metamorphic Rocks* edited by Fettes D. and Desmons J. Cambridge: University Press Cambridge. pp. 82 – 92.

STÖFFLER D., RYDER G., IVANOV B. A., ARTEMIEVA N., CINTALA M. J. AND GRIEVE R. A. F. (2006) Cratering history and lunar chronology. *Reviews in Mineralogy and Geochemistry* **60**, 519 – 596.

TURPIN L., CUNEY M., FRIEDRICH M., BOUCHEZ J. L., AND AUBERTIN M. (1990) Meta-igneous origin of Hercynian peraluminous granites in N. W. French Massif Central; implications for crustal history reconstructions. *Contributions to Mineralogy and Petrology* **104**, 163 – 172.

WHITEHEAD J., SPRAY J. G., AND GRIEVE R. A. F. (2002) Origin of "toasted" quartz in terrestrial impact structures. Geology **30**(5), 431 – 434.

WIELAND F., REIMOLD W. U., AND GIBSON R. L. (2006) New observations on shatter cones in the Vredefort impact structure, South Africa, and evaluation of current hypotheses for shatter cone formation. *Meteoritics & Planetary Science* **41**, 1737 – 1759.

Chapter 4

4 Enigmatic tubular features in impact glass from the Ries impact structure, Germany

Sapers, H. M., Osinski, G. R., Flemming, R. L., Banerjee, N. R.

4.1 Introduction

The rapid quenching of a silicate melt results in the formation of natural glass. While glasses produced through volcanism are well known, they are also a ubiquitous product of meteorite impact events in craters as small as ~45 m (Folco *et al.* 2010) and as large as ~250 km (Dressler *et al.* 1996) in diameter. Impact glasses form during decompression from the shocked (compressed) state during shock metamorphism. They may be derived from individual minerals or whole rocks (Stöffler 1984) and can be found as individual particles (*e.g.*, tektites) or may be incorporated into impact melt-bearing breccia deposits. They can also form glassy regions in cohesive impact melt sheets as well as dikes and veins in the crater floor.

The rapid undercooling required to produce a purely amorphous, homogeneous glass is rarely achieved in a natural setting and as a result the majority of natural glasses contain an abundance of microcrystallites (*e.g.*, Iddings 1899; Lofgren 1977). Primary crystallites or quench crystallites that form during rapid solidification are usually flow oriented, have well-developed skeletal morphologies, and the majority are too small to allow for unequivocal petrographic identification (*e.g.*, Marshall 1961). Previous studies of the crystallites in the glass clasts from the impact melt-bearing breccias of the Ries impact structure identified unusual tubular features with complexly curved morphologies (*e.g.*, Osinski 2003; Engelhardt 1995). These features were tentatively described as non-canonical pyroxene crystallites (Osinski 2003). Here, we present the results of a detailed petrological, geochemical and mineralogical investigation of these enigmatic tubules and demonstrably abiotic crystallites suggesting that the former may not be purely mineralogical in origin. The purpose of this study is to provide a well-constrained geological context to the tubules in the Ries glass effectively ruling out a purely mineralogical formation mechanism.

4.2 Ries impact structure

The 24 km diameter mid-Miocene (14.6 $\pm$ 0.2 Ma; Buchner *et al.*, 2010) Ries impact structure located in southern Germany is arguably one of the best-characterized and best-preserved terrestrial impact structures (see Pohl *et al.*, 1977 and Engelhardt, 1990, for reviews). A wide variety of impactites are present at the Ries structure. So-called "crater suevites" fill the interior cavity, bounded by the inner ring to a thickness of ~400 m (Pohl *et al.* 1977). They are buried by post-impact lacustrine sediments and are only known in drill cores. Outside of this inner ring, there are 4 main proximal impact ejecta lithologies: 1) polymict, melt-free sedimentary-rich breccia (Bunte Breccia) and megablocks; 2) polymict crystalline breccias; 3) impact glass-bearing breccias or "suevites"; and 4) coherent impact melt rocks (refer to Osinski, 2004 for a detailed overview of the melt-bearing impactite lithologies). It is the glass clasts within the impact glass-bearing breccias or "suevites" that host the enigmatic tubular structures described in this study.

Four main glass types occur within the impact melt-bearing ejecta deposits both as groundmass phases and as discrete glass clasts (Osinski 2003). Type I glasses are the most abundant and are the only glasses in which tubular features have been observed. These glasses contain Al-rich pyroxene quench crystallites and have SiO_2 contents ~63%. Type I glasses have the highest concentrations of FeO and MgO of all 4 glass types. Type II glasses contain only plagioclase crystallites, have a similar SiO_2 content as type I, and also host micrometer-scale vesicles. Type III glasses have low SiO_2 contents, are hydrated relative to the other glasses, and contain relatively little FeO, MgO, and K_2O, while having high Al_2O_3, CaO, and Na_2O contents. Type IV glasses have very high SiO_2 contents, commonly >90%. An extensive review of the geochemistry and quench crystallites of the Ries glasses is presented elsewhere (Osinski 2003, 2004).

4.3 Observations

4.3.1 Matrix Glass

The glass clasts hosting the tubular textures in this study correspond to the type 1 glasses as defined by Osinski (2003). These glasses represent >90% of all glassy material at the Ries impact structure. Approximately 100 polished thin sections made from samples representing the spatial distribution of melt-bearing breccia outcrops were chosen for study. In hand specimen the glasses are black and may appear vesicular. Vesicles occur on multiple scales (centimetre - micron). In transmitted light the glasses are dominantly yellow-brown in color, but vary from colourless to brown, yellow, pink or green. The glass typically has a cloudy or dusty appearance, which increases with tubule density, alteration, and hydration. Of the glass clasts studied, all contain quench crystallites and ~70% contain tubular features affecting 50 – 80% of the clast as observed by optical petrography. Highly altered glass clasts may appear dark brown to black (*cf.* Osinski 2003). Glass clasts are schlieren-rich and are characterized by complex flow textures commonly defined by dense assemblages of crystallites (Fig. 4.1A, B).

Electron microprobe energy dispersive X-ray (EDX) spectroscopy allowed for bulk elemental characterization of the larger (>300 μm) glass clasts. Detailed analytical techniques are available in supplemental information. Previous work indicated that the type I glasses, on average, have SiO_2 contents of ~63% (Osinski 2003). However, the glass composition is heterogeneous on a micrometer scale as a result of randomly distributed, locally partially resorbed quartz grains with SiO_2 contents range from ~50% in regions devoid of partially resorbed grains to >80% in relict quartz grains (Table 4S1). Areas dominated by tubular features have a remarkably consistent SiO_2 composition of ~53 wt%. The average total for these regions is <90%, consistent with a relatively high volatile content due to hydrous alteration as seen previously by Osinski (2003, 2005). Minor elements such as Ti, P, and Cl were not analyzed for in this study, previous work (Osinski 2005) has shown that these elements may contribute up to ~1 wt. % and their absence in the present analyses may contribute to the lower totals. The heterogeneity of the glass is such that within a 50μm area, replicate analysis with a 10μm defocused beam vary by as much as 20 wt% SiO_2. In general, areas dominated by crystallites had higher

SiO_2 contents (ranging from 57 to 59 wt% similar to the average composition reported by Osinski 2003) and generally slightly higher totals (>90%). The areas devoid of both tubules and crystallites have the highest average SiO_2 content ranging from 64 – 83 wt%. In general tubule features tend to be associated with lower SiO_2 contents and lower totals reflecting areas subjected to hydrous alteration. This is consistent with micro-XRD conducted on nine spots within glassy clasts suggesting the presence of a complex suite of secondary mineral phases (Fig. 4S1). Alteration assemblages were dominated by clay minerals including montmorillonite, illite and saponite with subordinate chlorite, zeolites, carbonate, and goethite (Fig. 4S1).

4.3.2 Crystallites and tubules

Transmitted light optical microscopy allows the tubular structures to be viewed in a three-dimensional context (Fig. 4.1 C). Tubules are concentrated along fractures or clast margins (Fig. 4.2 A), form radiating aggregates, and have complex morphologies including spirals, and other convoluted morphologies (Figs. 4.1D, E). Smooth-walled tubules, without segmentation, typically display complex curvatures forming a morphological continuum between loose undulating curves and tightly coiled morphologies. Curvature appears random, non-oriented and specific to individual tubules, however, tubules are not observed to crosscut each other, even display evidence of avoidance (Fig. 4.2 B) and dextrally versus sinistrally coiled tubules appear to cluster respectively. Spiral morphologies typically have one complete revolution but may display up to five coils with loops of a fixed size (Fig. 4.1D). Non-segmented tubules have diameters ~1 μm. Tubule length is difficult to estimate as tubules continue in three dimensions. The observable length of tubules commonly exceeds 100 μm. Approximately one-third of these tubules display annulation reminiscent of distinct segmentation (Fig. 4.1C). Segmented tubules typically display less curvature than non-segmented tubules. Individual segments have length to width ratios of approximately 1:2 (Fig. 4.1C). Segmented tubules vary in diameter from ~1 μm to approaching 3 μm. Tubules appear to display bifurcation or branching (Fig. 4.1C). Branching is asymmetric, however, branches are nearly identical in diameter and segmentation to the parent tubule (Fig. 4.1C, F). Rare segmented tubules with large (~3 μm) diameters have segments with length to width ratios approaching 1:6. There is a positive relationship between the extent of glass alteration and tubule density.

Scanning electron microscopy (SEM) was used to image the surface expression of the tubules. They appear as irregular, sub-linear to tightly curled, high-brightness regions in the darker grey glassy matrix under back-scattered electron operating conditions (Figs. 4.1D, E). The margins of the features are sharp and range from highly irregular to smooth. The tubules either appear solid and infilled with an unidentified mineral phase(s) (the extremely fine-grained (<<1 μm) nature of this material precludes definitive mineral identification; Fig. 4.1D) or hollow (Fig. 4.1E) Filled tubules may have either an ovoid or rhomboid cross-section and hollow tubules are approximately circular in cross-section. Hollow tubules have smooth margins, may display annulations, are approximately 0.4 – 1μm in diameter, and up to hundreds of micrometers in length. Filled tubules may have either smooth margins or highly irregular ornamentation perpendicular to the long axis. Filled tubules tend to be shorter compared to the hollow tubules and vary in diameter from 1 – 3 μm.

Three types of crystallites are identified with SEM and EDX, distinguished by morphology and elemental chemistry. Most abundant are skeletal dendrites enriched in K, Mg, Ca, and Fe and depleted in Na relative to the matrix (possibly pyroxene; Fig. 4.3). Tabular crystalline laths enriched in Al, Ca, and Na and depleted in K, Mg, and Fe relative to the matrix are also present (possibly plagioclase; Fig. 4.2). There are rare, rounded Ti, Mg, and Fe oxides. Partially absorbed quartz grains are scattered throughout the matrix. The dendrites are commonly clustered together (Fig. 4.1A) and may form a fine-grained phase complexly intergrown with the lath shaped crystals at the matrix-crystal lath boundary (Fig. 4.1B).

The sub-micron size of both the tubules and crystallites preclude quantitative elemental analyses. The tubular features are enriched in Mg, Fe, and Ca and depleted in Na, K, and Al relative to the matrix (Fig. 4.3). Amoeboid zones enriched in K and depleted in Mg, Fe, Na, and Ca surround the tubular features (Fig. 4.3). In contrast to the crystalline intergrowths surrounding the lath-shaped crystallites, no recognizable crystal morphology can be discerned in the zones surrounding the tubules. The tubular features are generally spatially associated with areas containing the dendritic crystallites. Areas dominated by relict quartz, have low tubule density if tubules are present at all.

Secondary electron imaging of angular fragments adhered to the stub-mount provided a three-dimensional perspective of the tubular structures not possible when imaging thin sections. Angular fragments were prepared by manual crushing with a mortar and pestle and required no further mechanical preparation. The tubules are present as dense masses within fracture systems that provide a window into the interior of the glass grain (Fig. 4.1F). The tubules are curved to sub-linear with diameters ranging from 0.2 μm to 1μm. The full extent of the tubule length could not be determined, but visible sections extend >10 μm. Two distinct morphologies are recognized: tubules with an ovoid cross section and tubules with a rhomboid cross section. The former are either hollow or solid while all tubules with a rhomboid cross-section are solid.

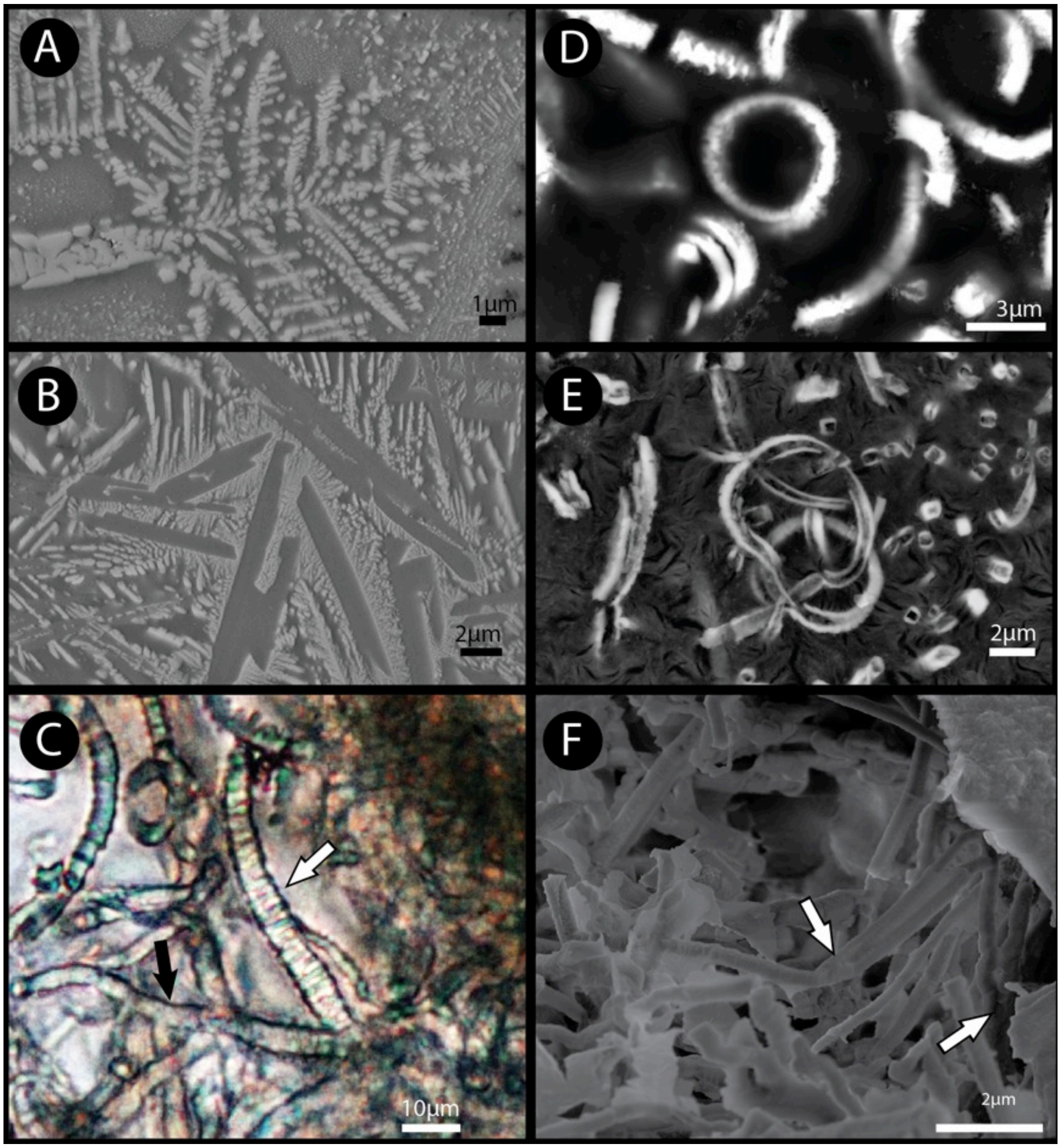

Figure 4.1: Quench crystallites and tubule morphologies.

Characteristic dendritic and skeletal morphologies of pyroxene (A: RI_09_006) and plagioclase laths (B: RI_09_006) imaged in back scatter electron scanning electron microscopy (BSE SEM). (C: RI_00_056) Extended depth of focus photomicrograph illustrating dense masses of non-intersecting tubular features. Notice branching, smooth-walled tubules indicated by black arrow; tubules displaying annulations suggestive of segmentation (white arrow). (D: RI_10_009A1) BSE SEM image showing smooth-walled, solid (filled) tubules display spirals. (E: RI_10_009A1) BSE SEM image illustrating the complex curvatures typical of the hollow tubules. (F: RI_09_006) Secondary electron SEM images of a dense mass of mineralized tubules in an altered void of impact-glass. Bifurcating tubules are indicated by white arrows, notice the parent tubule is approximately the same diameter as the daughter tubules.

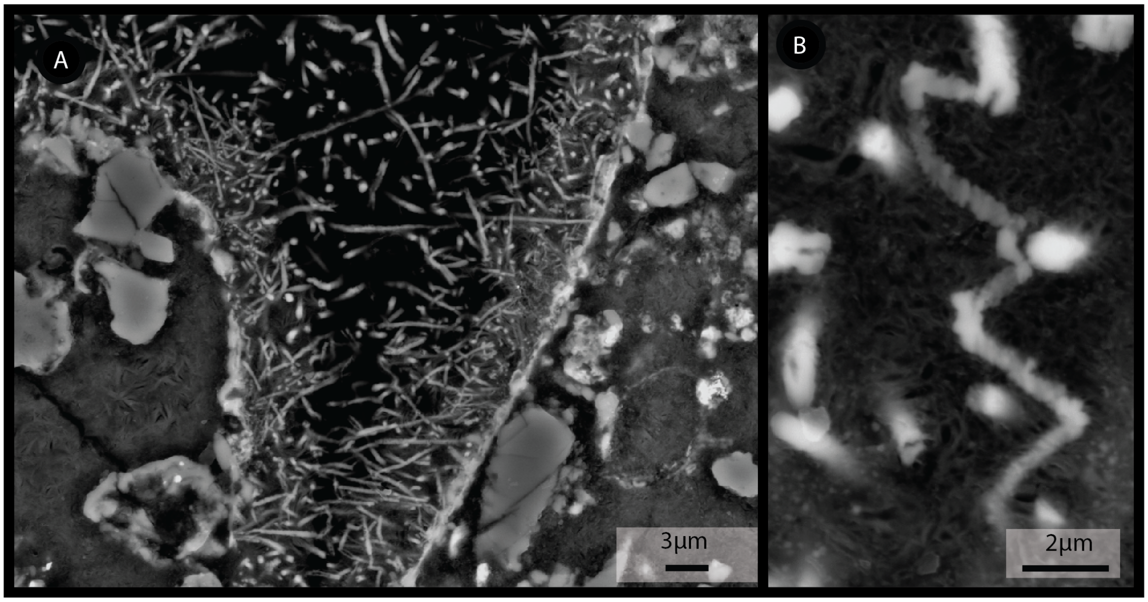

Figure 4.2: Distribution of tubular features.

Back scatter scanning electron microscopy images depicting the distribution of the tubular features relative to other features in the glass clasts. Sample RI_10_009A1. A: Note the association of the tubules with the clast margin radiating into the centre of the glass. B: Notice the convoluted morphology of the tubule and the apparent avoidance of other tubules in the glass.

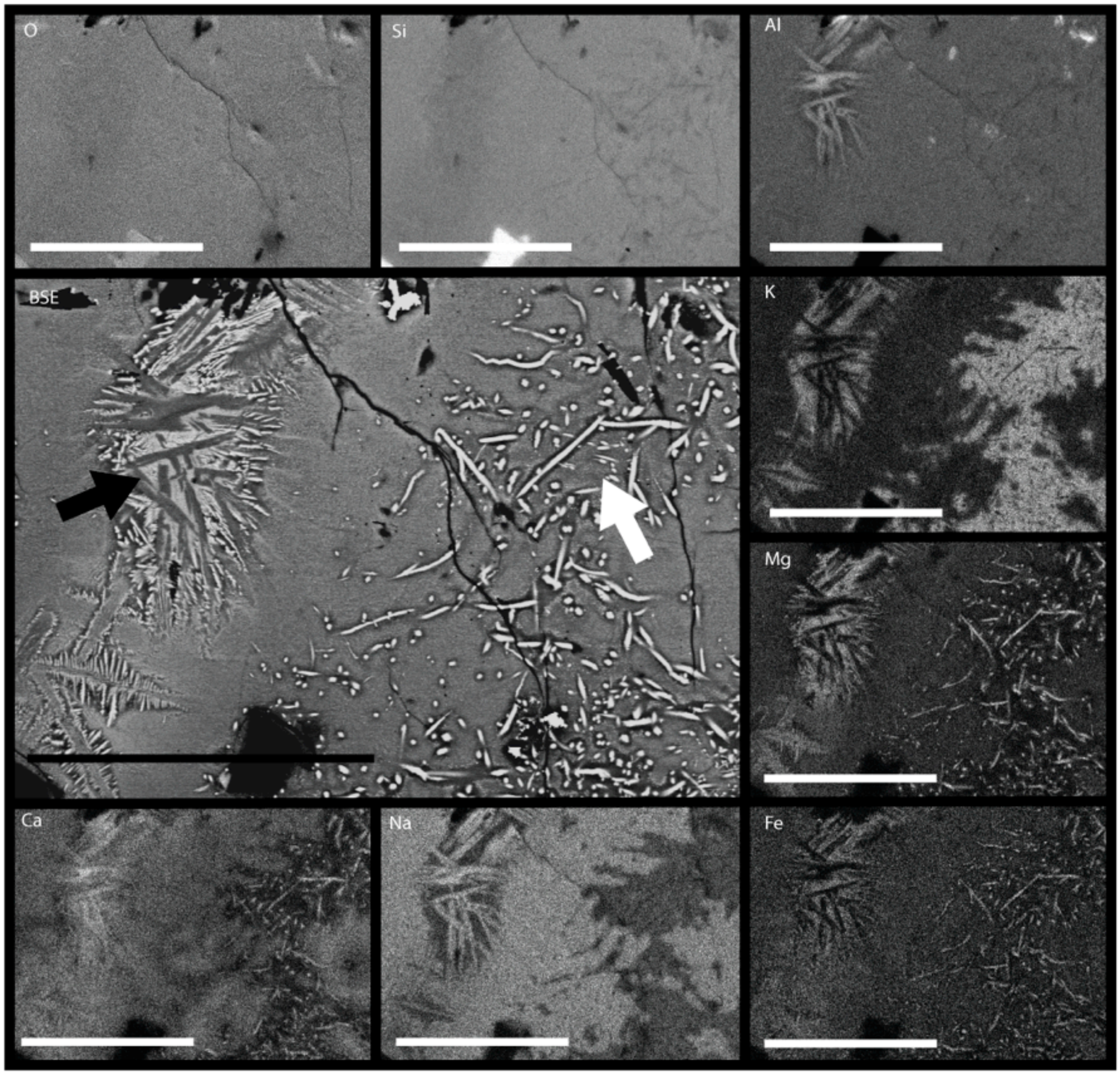

Figure 4.3: Elemental composition of tubular features, crystallites and matrix by EDX mapping.

Quench crystallites (black arrow) pyroxene (white) and plagioclase (grey) and tubules (white arrow) are mapped by EDX spectroscopy. The tubules are enriched in Fe, Mg and Ca while depleted in Al, Si, K, and Na. The pyroxene crystallites are enriched in Fe, Ca, Mg and K while the plagioclase crystallites are enriched in Al, Na, and Ca. Note the Si-Al-rich composition of the glassy matrix. The tubules are concentrated in areas of high K and lower Na and Ca compositions and surrounded by pronounced zones depleted in Ca, Na, Fe and Mg. Sample RI_00_006.

4.4 Discussion

The Ries glasses host a dense assemblage of quench crystallites with two main morphologies. The dominant crystallites are of calcic pyroxene composition and display dendritic to skeletal morphologies (Fig. 4.1A; Osinski 2003; this study). Lath-shaped crystallites with plagioclase composition surrounded by a complex intergrowth of fine-grained pyroxene (Fig. 4.1B) comprise the second morphological group of quench crystallites. These morphologies correspond to well-understood quench crystal morphologies indicative of rapid crystallization from a melt (Bryan 1972; Lofgren 1974, Marshall 1961). Such mineralogical distributions are expected as the Ca-rich plagioclase crystallization leaves a residual melt enriched in Mg, and Fe from which the pyroxene crystallizes. In areas with lower concentrations of Al, Ca and Na, plagioclase does not form large lath-shaped crystallites, and large pyroxene dendrites form.

In contrast to the well-established quench-crystallites, the enigmatic tubules have distinct morphologies that clearly distinguish them (Fig. 4.1, 4.2). Previous studies also describe tubular and complexly curved, non-canonical pyroxene crystallites (Pankau 1989; Engelhardt *et al.* 1995; Osinski 2003). The distinct forms of the tubular features, as revealed by high-resolution imaging techniques for the first time in this study, suggest that they are not purely mineralogical in origin, as they do not conform to any known quench crystal morphology.

Tubular ichnofossils have been attributed to ambient inclusion trails (AIT), hollow trails with convoluted morphologies formed by pressure solution, as discussed by Banerjee *et al.* (2006) and McLoughlin *et al.* (2010). We discount AITs as an explanation for the formation of the Ries tubules as tubules do not display longitudinal vertical striations, nor are the Ries tubules associated with mineral grains at their tips. The presence of striae and terminal inclusions are associated with and diagnostic of ambient inclusion trails (Tyler & Barghoorn 1963). The material constituting the terminal inclusion acts a bore carving out the trail, leaving longitudinal striations, driven by locally elevated fluid pressures. See McLoughlin *et al.* (2010) for a discussion of the primary difference between tubular ichnofossils and ambient inclusion trails.

Such tubular morphologies, with no known parsimonious abiotic formation mechanism, are consistent with numerous studies that have shown similar tubular features to exist within oceanic basaltic glasses that are widely accepted to represent microbial alteration textures (Banerjee *et al.* 2006, 2007, 2008; Banerjee & Muehlenbachs 2003; Benzerara *et al.* 2007; Fisk *et al.* 1998; Furnes *et al.* 2001a, 2001b, 2004, 2008; Furnes & Muehlenbachs 2003; Izawa *et al.* 2010a, 2010b; Peckmann *et al.* 2008; Staudigel *et al.* 2006, 2008a, 2008b; Thorseth *et al.* 1995, 2003; Torsvik *et al.* 1998.) Microbial alteration of natural volcanic glasses is a well-documented phenomenon in modern oceanic crust, Phanerozoic to Proterozoic ophiolites and Precambrian greenstone belts (McLoughin *et al.* 2008; Thorseth *et al.* 1991; Banerjee 2006, 2007; Banerjee & Muehlenbachs 2003; Furnes 2004; Furnes *et al.* 2008; Staudigel *et al.* 2008a). It is unclear if the transition from hollow, smooth-walled, circular tubules to solid, decorated, rhomboid features represents a continuum of preservation, or if the solid, rhomboid, linear features represent discrete, genetically unrelated features. Both the hollow and solid tubules have morphologies distinct from the characteristic skeletal and dendritic forms of the quench crystallites (Fig. 4.1).

Endolithic microbial communities occur in terrestrial and submarine volcanic glasses with a range of SiO_2 contents (*e.g.*, Cockell *et al.* 2009). It is notable that tubules are not present in Si-rich regions of the glass nor are they concentrated in areas dominated by partially resorbed quartz grains (Fig. 4.3). Interestingly, Mg, Fe, Ca, and Na depletion zones surrounding tubule alteration (Fig. 4.3) have been identified as a biological processing signature (McLoughlin *et al.* 2007). The tubule features themselves are preserved by a mineral phase enriched in Mg, Ca and Fe and depleted in Na, K, Al and Si relative to the glassy matrix (Fig. 4.3). Ca-clinopyroxene quench crystallites present in the type I glass clast display similar enrichment and depletion patterns. However, their distinct morphologies imply different origins (Fig. 4.1). The tubule features are associated with hydrothermal alteration fronts in the glass and are cross-cut by late brittle fractures that do not display evidence of hydrothermal alteration constraining the period of tubule formation to that of the post-impact hydrothermal system.

Micro-habitats created by meteorite impacts have been shown to be conducive to microbial colonization (Cockell & Lee 2002). In particular, impact-induced hydrothermal systems as documented to have occurred at Ries (Osinski 2005; Muttik *et al.* 2008) have been postulated to facilitate microbial colonization following an impact event (Osinski *et al.* 2001). Impact induced hydrothermal systems provide a heat source driving hydrothermal activity facilitating water rock interactions. In addition to the thermal and chemical disequilibria characterizing such systems that are able to support a variety of autotrophic microbial metabolisms, impact craters host metastable glass and shocked rock with interconnected pore space that constitute endolithic habitats. Previous literature has shown that microbes colonize glasses while extracting metabolically relevant elements leaving traces, such as tubular features, (*e.g.*, Banerjee & Muehlenbachs 2003; McLoughlin *et al.* 2008) of this activity. Based on the available data, we conclude that the tubules in the Ries glasses are not mineralogical in origin and likely constitute a novel microbial ichnofossil. In order to unequivocally demonstrate the biogenicity of these features, further high-resolution studies such as scanning transmission X-ray and electron microscopy coupled with near edge X-ray absorption spectroscopy aimed at identifying organic signatures is required.

4.5 Concluding Remarks

Through a detailed, multi-scaled microscopy study we have illustrated a unique class of tubular features morphologically distinct from quench crystallites hosted within impact glass from the Ries impact structure in south central Germany. The complex morphologies and convoluted structures characterizing these features suggest that these features are not mineralogical in origin. The similarity of these features to bioalteration textures in submarine basaltic glasses warrants further investigation into a possible biogenic origin of the Ries tubules. If the tubules are biotic in origin, impact glass would thus represent a previously unknown microbial habitat on Earth, with implications for the early evolution of life on Earth as well as for life on other terrestrial planets such as Mars.

4.6 Acknowledgements

We thank Sergei Matveev of the University of Alberta for his assistance with microprobe analyses and Jason Kanhai from the University of Western Ontario for his assistance with XRD. Funding for this project was provided by the Canadian Space Agency Canadian Analogue Research Network (CARN), NSERC, ADF (microscopes), CFI (μXRD). This research was also supported by a Barringer family grant to H.M.S.

4.7 Supplementary Information

4.7.1 Samples and Methods

A representative suite of more than 50 samples of impact-melt bearing breccias collected over five field campaigns from the Ries impact structure were examined in hand sample, polished thin section and analyzed with micro-X-ray diffraction and a variety of electron-beam based techniques. Samples were collected from samples were obtained from the Otting, Aumühle, Altenburg, Sternbach, Seelbron, Zipplingen, and Amerdingen quarries. Approximately 100 polished thin sections were chosen for petrographic study; 5 grain mounts prepared for secondary electron scanning electron microscopy; 7 polished thin-sections coated for backscatter scanning electron microscopy, 3 polished thin sections selected for micro-X-ray diffraction and 2 polished thin sections chosen for microprobe analyses.

Reflected and transmitted plane polarized and crossed polarized light was used for imaging using a Nikon Eclipse LV100POL petrographic light microscope equipped with a Nikon DS-Ri1 12 megapixel camera. Extended-depth of focus images (EDF) were obtained using plane-polarized transmission microscopy by aligning multiple images in the z plane using the Nikon NIS Elements software suite. Clay minerals characteristically have peaks at low angles, therefore micro X-ray diffraction data were collected in coupled scan mode with $\theta 1=8^{\circ}$ and $\theta 2= 12^{\circ}$ with a frame width of 32.5°. Each frame was collected for 45 minutes (while remaining stationary) using the Bruker D8 Discover micro X-ray diffractometer (μXRD) at the University of Western Ontario (Flemming 2007).

Polished thin sections selected for electron-beam based analyses and imaging were coated with amorphous Os prior to analyses with the exception of SE SEM imaging. S stubs were prepared by dipping C-tape coated Ti SEM stubs into crushed (~1mm grain size) glass clasts. The Tubules and matrix were analyzed with high-resolution backscatter electron (BSE) and secondary electron (SE) imaging and energy dispersive X-ray (EDX) spectroscopy carried out with a Leo 1540 FIB/SEM CrossBeam field emission SEM equipped with an Oxford Instruments INCA EDX system allowing for elemental analysis, sensitive to ~0.5 wt. % or less for all elements from C – U at the Nanofabrication Laboratory, University of Western Ontario EDX spectroscopy. Fourteen spots were analyzed by energy dispersive X-ray spectroscopy (EDX) conducted on a Cameca SX100 electron microprobe at the Electron Microprobe Laboratory at the University of Alberta. A defocused 10μm beam was used to collect EDX spectra of the matrix glass; nine spots in the vicinity of tubule features; 2 regions in areas dominated by pyroxene quench crystallites; and 3 areas without visible tubules or quench crystallites.

4.7.2 Supplementary References

FLEMMING, R.L., (2007) Micro X-ray Diffraction (μXRD): A versatile technique for characterization of Earth and planetary materials. *Canadian Journal of Earth Sciences* **44**, 1333 – 1346.

4.7.3 Supplementary Tables

Table S4-1: Microprobe analyses of glass clasts within glass-bearing impact breccia.

Analyses were conducted using a 10 μm defocused beam and reported in oxide wt%. SiO_2 contents of the glass range from 53 oxide wt% in glasses containing tubules to 83 oxide wt% in areas dominated by partially resorbed quartz grains. In general, the tubules are hosted in glasses containing the lowest wt% SiO_2

Sample #	SiO_2	Na_2O	MgO	K_2O	CaO	FeO	Al_2O_3	Total
glass containing tubules								
RI_00_056 036	53.0	4.82	2.75	0.709	5.40	5.57	16.3	89.5
RI_00_056 032	53.1	5.05	2.68	0.665	5.11	5.38	16.2	89.2
RI_00_056 035	53.7	4.82	2.47	0.996	4.78	4.88	15.8	88.4
RI_00_056 031	53.7	5.14	2.45	0.751	4.79	5.26	16.1	88.8
glass containing only crystallites								
RI_09_6 011 001	58.7	3.69	2.15	2.07	4.62	4.25	14.4	90.6
RI_09_6 011 002	58.7	3.77	2.42	2.66	3.41	4.68	14.5	91.0
RI_09_6 011 003	59.0	3.85	2.30	2.19	4.25	4.68	14.5	91.7
RI_09_6 009 011	58.1	3.93	2.44	2.08	4.08	4.83	14.6	91.0
RI_09_6 009 012	57.2	3.99	2.54	1.94	4.28	4.76	14.6	90.2
SiO_2-rich glasses								
RI_00_056 033	63.9	3.98	0.890	2.16	2.71	2.42	12.5	89.1
RI_00_056 034	67.5	1.45	0.956	4.32	0.893	3.02	9.04	88.1
RI_00_056 037	79.8	0.841	0.253	2.20	0.278	0.814	4.33	88.5
RI_00_056 038	82.2	0.881	0.117	1.51	0.273	0.926	3.68	89.6
RI_00_056 039	82.7	0.639	0.237	1.11	1.09	1.96	2.88	90.8

4.7.4 Supplementary Figures

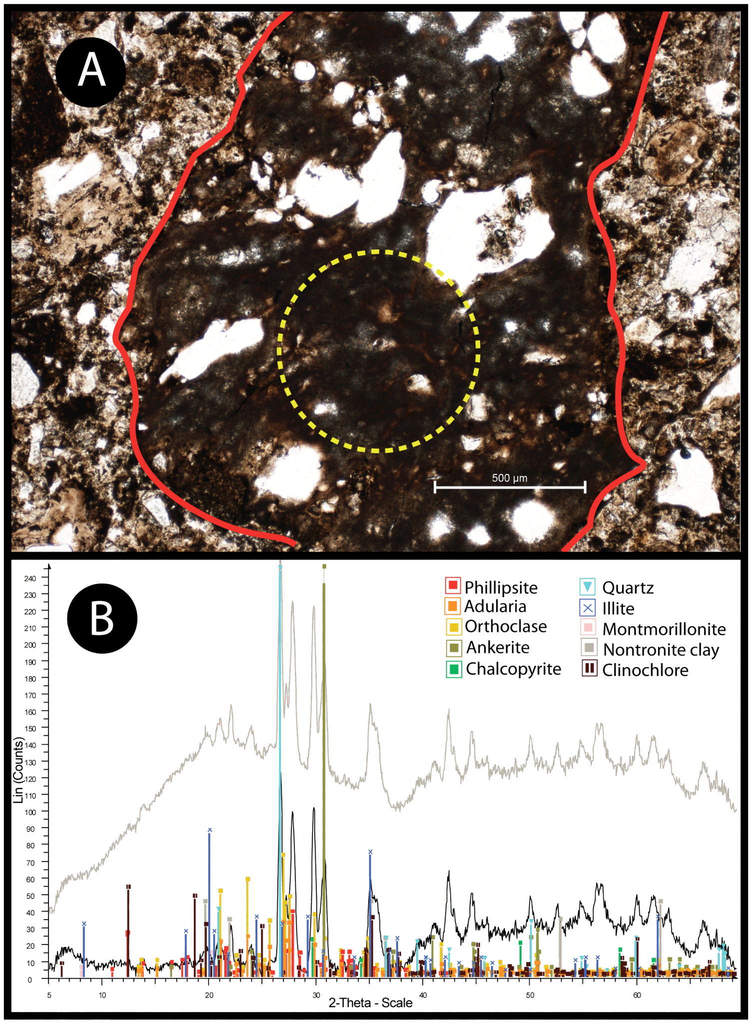

Figure S4.4: Mineralogy of glass clast as determined by µ-XRD.

An example analysis area and corresponding XRD patterns and their respective mineralogical assignments are shown. The 500 µm resolution of the micro-XRD precludes analyzing individual mineral or lithic fragments within the glassy clasts. The presented mineralogy is representative of the bulk material comprising the glassy clast and may represent secondary alteration phases as well as pre-impact material included, but not assimilated, into the glass. A broad hump around 20^{o} 2θ-scale indicates the presence of amorphous glass A: photomicrograph of a glass clast. The margins of the clast are shown in red and the approximate µ-XRD footprint is shown by the dashed yellow ellipse. B: µ-XRD patterns indicating the presence of a complex assemblage of micro-crystalline material. The original spectra is shown in grey; note the large glass hump. Effects of background and glass are subtracted out to produce the black spectra. Sample RI_00_056.

4.8 References Cited

BANERJEE, N.R., FURNES, H., MUEHLENBACHS, K., STAUDIGEL, H., DE WIT, M. (2006) Preservation of ~3.4 – 3.5 Ga microbial biomarkers in pillow lavas and hyaloclastites from the Barberton Greenstone Belt, South Africa. *Earth and Planetary Science Letters* **241**(3 – 4), 707 – 722.

BANERJEE, N.R., FURNES, H., MUEHLENBACHS, K., STAUDIGEL, H., MCLOUGHLIN, N., BEBOUT, G. (2008) Biogeochemical tracers of modern and ancient life in seafloor lavas. *Geochimica et Cosmochimica Acta* **72**(12), A51.

BANERJEE, N.R., MUEHLENBACHS, K. (2003) Tuff life: bioalteration in volcaniclastic rocks from the Ontong Java Plateau. *Geochemistry, Geophysics, Geosystems* **4**(4), 1037 – 1059.

BANERJEE, N.R., SIMONETTI, A., FURNES, H., MUEHLENBACHS, K., STAUDIGEL, H., HEAMAN, L., VAN KRANENDONK, M.J. (2007) Direct dating of Archean microbial ichnofossils. *Geology* **35**(6), 487 – 490.

BENZERARA, K., MENGUY, N., BANERJEE, N., TYLISZCZAK, T., BROWN JR, G. E., AND GUYOT, F. (2007) Alteration of submarine basaltic glass from the Ontong Java Plateau: A STXM and TEM study. *Earth and Planetary Science Letters* **260**, 187 – 200.

BRYAN, W. B. (1972) Morphology of quench crystals in submarine basalts. *Journal of Geophysical Research* **77**(29), 5812 – 5819.

BUCHNER, E., SCHWARZ, W., SCHMIEDER, M., AND TRIELOFF, M. (2010) Establishing a 14.6 ± 0.2 Ma age for the Nördlinger Ries impact (Germany) — A prime example for concordant isotopic ages from various dating materials. *Meteoritics and Planetary Science* **45**(4), 662 – 674.

COCKELL, C. S., AND LEE, P. (2002) The biology of impact crater — a review. *Biological Reviews* **77**, 279 – 310.

COCKELL, C. S., OLSSON-FRANCIS, K., HERRERA, A., AND MEUNIER, A. (2009) Alteration textures in terrestrial volcanic glass and the associated bacterial community. *Geobiology* **7**(1), 50 – 65.

DRESSLER, B. O., WEISER, T., AND BROCKMEYER, P. (1996) Recrystallized impact glasses of the Onaping Formation and the Sudbury Igneous Complex, Sudbury Structure, Ontario, Canada. *Geochimica et Cosmochimica Acta* **60**(11), 2019 – 2036.

ENGELHARDT, W. (1990) Distribution, petrography and shock metamorphism of the ejecta of the Ries Crater in Germany; a review. *Tectonophysics*, **171**(1 – 4), 259 – 273.

ENGELHARDT, W., ARNDT, J., FECKER, B., PANKAU, H. G. (1995) Suevite breccia from the Ries crater, Germany: Origin, cooling history and devitrification of impact glasses. *Meteoritics* **30**, 279 – 293.

FOLCO, L., MARTINO, M. D., EL BARKOOKY, A., D'ORAZIO, M., LETHY, A., URBINI, S., NICOLOSI, L., HAFEZ, M., CORDIER, C., VAN GINNEKEN, M., ZEOLI, A., RADWAN, A. M., EL KHREPY, S., EL GABRY, M., GOMAA, M., BARAKAT, A. A., SERRA, R., AND EL SHARKAWI, M. (2010) The Kamil Crater in Egypt. *Science* **329**(5993), 804.

FISK, M.R., GIOVANNONI, S.J., THORSETH, I.H. (1998) Alteration of oceanic volcanic glass: textural evidence of microbial activity. *Science* **281**(5379), 978 – 980.

FURNES, H., MUEHLENBACHS, K., TORSVIK, T., THORSETH, I.H., TUMYR, O., (2001b) Microbial fractionation of carbon isotopes in altered basaltic glass from the Atlantic Ocean, Lau Basin, and Costa Rica Rift. *Chemical Geology* **173**, 313 – 330.

FURNES, H., STAUDIGEL, H., THORSETH, I.H., TORSVIK, T., MUEHLENBACHS, K., TUMYR, O., (2001a) Bioalteration of basaltic glass in the oceanic crust. *Geochemistry, Geophysics, Geosystems* **2**(8), 1049 – 1079.

FURNES, H., BANERJEE, N.R., MUEHLENBACHS, K., STAUDIGEL, H., DE WIT, M., (2004) Early life recorded in Archean Pillow Lavas. *Science* **304**(5670), 578 – 581.

FURNES, H., BANERJEE, N., MUECHLENBACHS, K., STAUDIGEL, H., AND DE WIT, M., (2008) Early Life Recorded in Archean Pillow Lavas. *Science* **304**(5670), 578 – 581.

FURNES, H., BANERJEE, N., STAUDIGEL, H., MUECHLENBACHS, K., MCLOUGHLIN, N., DE WIT, M., AND VAN KRANENDONK, M., (2007) Comparing petrographic signatures of bioalteration in recent to Mesoarchean pillow lavas: Tracing subsurface life in oceanic igneous rocks. *Precambrian Research* **158**, 156 – 176.

FURNES, H., MUEHLENBACHS, K., (2003) Bioalteration recorded in ophiolitic pillow lavas. In: Dilek, Y., Robinson, P.T. (Eds.), Ophiolites in Earth's History, Geological Society of London, Special Publication. Geological Society of London, pp. 415 – 426.

HECHT, L., WITTMANN, A., SCHMITT, R–T., STÖFFLER, D., (2004) Composition of impact melt particles and the effects of post-impact alteration in suevitic rocks at the Yaxcopoil-1 drill core, Chicxulub crater, Mexico. *Meteoritics & Planetary Science* **39**(7), 1169 – 1186.

HERRERA, A., COCKELL, C. S., SELF, S., BLAXTER, M., REITNER, J., ARP, G., DRÖSE, W., THORSTEINSSON, T., AND TINDLE, A. G., (2008) Bacterial Colonization and Weathering of Terrestrial Obsidian in Iceland. *Geomicrobiology Journal* **25**, 25 – 37.

HERRERA, A., COCKELL, C. S., SELF, S., BLAXTER, M., REITNER, J., THORSTEINSSON, T., ARP, G., DRÖSE, W., AND TINDLE, A. G., (2009) A Cryptoendolithic Community in Volcanic Glass. *Astrobiology* **9**(4), 369 – 381.

IDDINGS, J., (1899) Geology of Yellowstone National Park. *U.S. Geological Survey Monograph* **32**(2), 893 p.

IZAWA, M.R.M., BANERJEE, N.R., FLEMMING, R.L. AND BRIDGE, N.J., (2010a) Preservation of microbial ichnofossils in basaltic glass by titanite mineralization, *Canadian Mineralogist* **48**, 1255 – 1265.

IZAWA, M.R.M., BANERJEE N.R., FLEMMING, R.L., BRIDGE, N.J. AND SCHULTZ, C., (2010b) Basaltic glass as a habitat for microbial life: Implications for astrobiology and planetary exploration. *Planetary and Space Science* **58**, 583 – 591.

LOFGREN, G., (1974) An experimental study of plagioclase crystal morphology: Isothermal crystallization. *American Journal of Science* **274**, 243 – 273.

MARSHALL, R. R., (1961) Devitrification of Natural Glass. *Geological Society of America Bulletin* **72**, 1493 – 1520.

MCLOUGHLIN, N., BRASIER, M., WACEY, D., GREEN, O., AND PERRY, R., (2007) On Biogenicity Criteria for Endolithic Microborings on Early Earth And Beyond. *Astrobiology* **7**(1), 10 – 26.

MCLOUGHLIN, N., FURNES, H., BANERJEE, N., STAUDIGEL, H., MUECHLENBACHS, K., DE WIT, M., AND VAN KRANENDONK, M., (2008) Micro-bioerosion in volcanic glass: extending the ichnofossil record to Archaean basaltic crust, *in* Wisshak, M., and Tapanila, L., eds., Current Developments in Bioerosion: Berlin Heidelberg, Springer-Verlag, p. 371 – 396.

MCLOUGHLIN, N., STAUDIGEL, H., FURNES, H., EICKMANN, B., IVARSSON, M., (2010) Mechanisms of microtunneling in rock substrates: distinguishing endolithic biosignatures from abiotic microtunnels. *Geobiology* **8**, 245 – 255.

MUTTIK, N., KIRSIMÄE, K., SOMELAR, P., AND OSINSKI, G. R., (2008) Post-impact alteration of surficial suevites in Ries crater, Germany: Hydrothermal modification or weathering processes? *Meteoritics & Planetary Science* **43**(11), 1827 – 1840.

OSINSKI, G. R., SPRAY, J. G., AND LEE, P., (2001) Impact-induced hydrothermal activity within the Haughton impact structure, arctic Canada: Generation of a transient, warm, wet oasis. *Meteoritics and Planetary Science* **36**, 731 – 745.

OSINSKI, G. R., (2003) Impact glasses in fallout suevites from the Ries impact structure, Germany: An analytical SEM study. *Meteoritics & Planetary Science* **38**(11), 1641 – 1667.

— 2005, Hydrothermal activity associated with the Ries impact event, Germany. *Geofluids* **5**(3), 202 – 220.

PECKMANN, J., BACH, W., BEHRENS, K., REITNER, J., (2008) Putative cryptoendolithic life in Devonian pillow basalt, Rheinisches Schiefergebirge, Germany. *Geobiology* **6**, 125 – 135.

POHL, J., STÖFFLER, D., GALL, H., AND ERNSTSON, K., The Ries impact crater, *in* Impact and Explosion Cratering, (1977) D.J. Roddy, R.O. Pepin, and R.B. Merrill, Editors. Pergamon Press: New York. p. 343 – 404.

SANTELLI, C. M., ORCUTT, B. N., BANNING, E., BACH, W., MOYER, C. L., SOGIN, M. L., STAUDIGEL, H., AND EDWARDS, K. J., (2008) Abundance and diversity of microbial life in ocean crust. *Nature* **453**, 653 – 657.

STAUDIGEL, H., FURNES, H., BANERJEE, N.R., DILEK, Y., MUEHLENBACHS, K., (2006) Microbes and volcanoes: a tale from the oceans, ophiolites, and greenstone belts. *GSA Today* **16**(10), 4 – 10.

STAUDIGEL, H., FURNES, H., MCLOUGHLIN, N., BANERJEE, N. R., CONNEL, L. B., AND TEMPLETON, A., (2008a) 3.5 billion years of glass bioalteration: Volcanic rocks as a basis for microbial life? *Earth-Science Reviews* **89**(3 – 4), 156 – 176.

STAUDIGEL, H., FURNES, H., MCLOUGHLIN, N., BANERJEE, N. R., CONNELL, L. B., AND TEMPLETON, A., (2008b) Microbial glass bioalteration: Inferring mechanisnis of blocorrosion from trace fossil morphology: *Geochimica et Cosmochimica Acta*, **72**(12), A893 – A893.

STÖFFLER, D., (1984) Glasses Formed by Hypervelocity Impact. *Journal of Non-Crystalline Solids* **67**, 465 – 502.

TEMPLETON, A., AND KNOWLES, E., (2009) Microbial Transformations of Minerals and Metals: Recent Advances in Geomicrobiology Derived from Synchrotron-Based X-Ray Spectroscopy and X-Ray Microscopy. *Annual Review of Earth and Planetary Sciences* **37**(1), 367 – 391.

THORSETH, I. H., FURNES, H., AND TUMYR, O., (1991) A textural and chemical study of Icelandic palagonite of varied composition and its bearing on the mechanism of the glass-palagonite transformation. *Geochimica et Cosmochimica Acta* **55**(3), 731 – 749.

THORSETH, I.H., TORSVIK, T., FURNES, H., MUEHLENBACHS, K., (1995) Microbes play an important role in the alteration of oceanic crust. *Chemical Geology* **126**, 137 – 146.

Thorseth, I.H., Pedersen, R.B., Christie, D.M., (2003) Microbial alteration of 0 – 30 Ma seafloor and sub-seafloor basaltic glasses from the Australian Antarctic discordance. *Earth and Planetary Science Letters* **215**, 237 – 247.

TYLER, S. A., BARGHOON, E. S., (1963) Ambient pyrite grains in Precambrian cherts. *American Journal of Science* **261**, 424 – 432.

TORSVIK, T., FURNES, H., MUEHLENBACHS, K., THORSETH, I.H., TUMYR, O., (1998) Evidence for microbial activity at the glass-alteration interface in oceanic basalts. *Earth and Planetary Science Letters* **162**, 165 – 176.

Chapter 5

5 Microbial ichnofossils preserved in impact glass

Sapers, H. M., Banerjee, N. R., Preston, L. J., Osinski, G. R.

5.1 Introduction

Tubular microbial alteration features are commonly recognized in modern oceanic crust, Phanerozoic ophiolites, and Archaean greenstone belts. Over the last two decades systematic criteria for establishing the biogenicity of these putative microbial alteration textures has been established to aid in the recognition and classification of such trace ichnofossils. Here we describe the first known occurrence of microbial ichnofossils in impact glass from the Ries structure in south central Germany. These tubular ichnofossils have a remarkable morphological similarity to the microbial alteration textures observed in submarine basaltic glass, including complex morphologies suggestive of biological behaviour. In addition, Fourier transform infrared spectroscopy analyses indicate the presence of a variety of organic compounds spatially associated with the tubules. Any hypervelocity impact into a water-rich target, such as Mars, has the potential to generate a post-impact hydrothermal system creating a novel ecological niche. Establishing the biogenicity of the Ries microbial alteration textures has significant astrobiological implications for the search for life on other planets such as Mars.

The catastrophic effects of hypervelocity impacts are well established (Schulte *et al.* 2010). However, a growing body of evidence suggests that meteorite impact events also have beneficial effects, particularly for microbial life (Osinski *et al.* 2001; Cockell *et al.* 2005b). For example, post-impact hydrothermal systems provide heat, water and chemical disequilibria creating a potentially suitable microbial habitat (Kring 2000; Osinski *et al.* 2001; Naumov *et al.* 2002; Naumov 2005).

Any hypervelocity impact into a water-rich target on a solid planetary body has the potential to generate a hydrothermal system (Naumov *et al.* 2002; Naumov 2005). In volcanic hydrothermal environments, microbial alteration of basaltic glasses produces characteristic tubular and granular textures (Fisk *et al.* 1998; Furnes *et al.* 2001, 2004, 2007; Banerjee *et al.* 2007; McLoughlin *et al.* 2008) that are now recognized as ichnofossils (McLoughlin *et al.* 2009). Such ichnofossils preserved in Archaean greenstone belts constitute the oldest directly dated microbial traces of life on Earth (Fliegel *et al.* 2010; Nisbet 2000; Furnes *et al.* 2004; Banerjee *et al.* 2006a; Staudigel *et al.* 2006; Banerjee *et al.* 2007). Impact-induced hydrothermal systems share many characteristics with submarine volcanic hydrothermal systems including the presence of chemical and thermal energy for microbial metabolism and the precipitation of hydrothermal minerals. Despite the similarities, post-impact hydrothermal systems and impact craters in general represent an understudied microbial habitat.

In this study, we investigate impact glasses from the Ries impact structure, Germany, that preserve tubular alteration textures that share a remarkable morphological similarity to tubular microbial ichnofossils found in volcanic basaltic glass (Fig. 5.1). Systematic criteria for determining the biogenicity of microbial alteration textures has been reviewed in detail elsewhere (*e.g.*, Banerjee & Muehlenbachs 2003; Staudigel *et al.* 2006; McLoughlin *et al.* 2007; McLoughlin *et al.* 2008). Here we follow the three-pronged approach to assessing the biogenicity of putative ichnofossils developed by McLoughlin *et al.* (2007). Tentative bioalteration features must satisfy the following three criteria before a biogenic origin can be determined: "(1) a geological context that demonstrates the syngenicity and antiquity of the putative biological remains; (2) evidence of biogenic morphology and behaviour; and (3) geochemical evidence for biological processing (McLoughlin *et al.* 2007)." Impact glasses are ubiquitous products of meteorite impact events on Earth and likely on other planets such as Mars (Melosh 1989); thus, this discovery may have implications for the prospect of finding life on Mars and other planetary bodies that may have hosted liquid water. Furthermore, our work may inform our understanding of potential ancient habitats on Earth and perhaps even the evolution of early life on Earth.

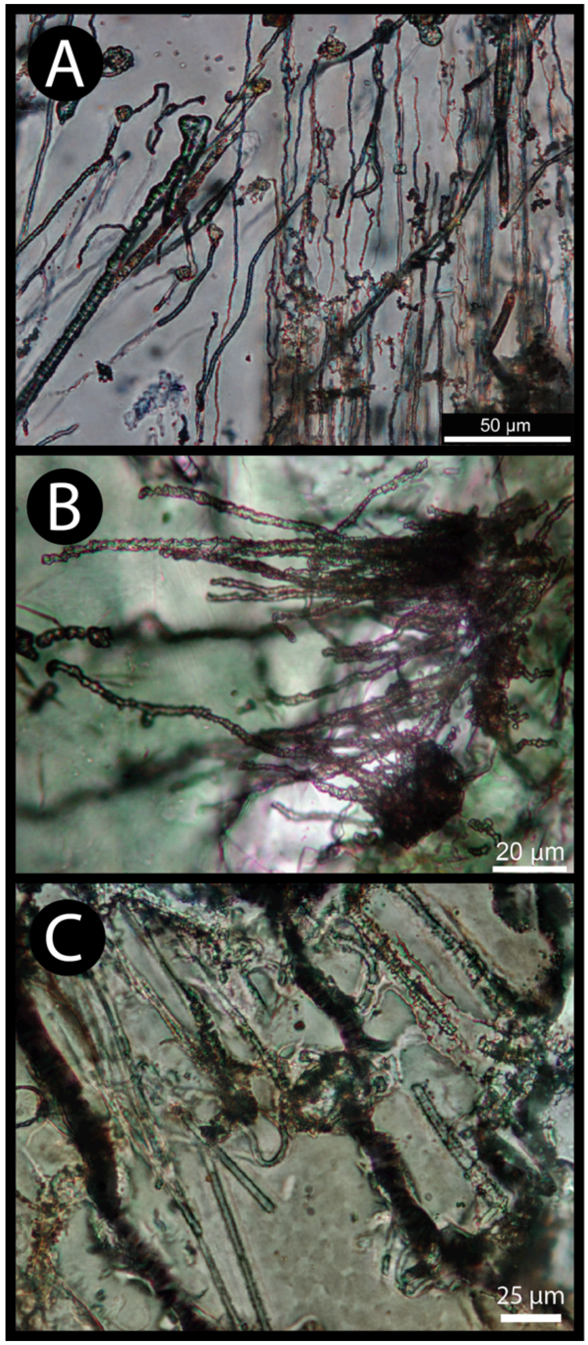

Figure 5.1: Tubular alteration textures in natural glasses.

A – C transmitted light micrographs of tubular alteration features in natural glasses. A: Segmented tubular bioalteration features in modern submarine basaltic glass from the Ontong Java Plateau. B: Elongate titanite mineralized tubular bioalteration features in Archean interpillow hyaloclastite samples from the Euro Basalt, Pilbara Craton. C: Tubular features in ~15 Ma impact glass from the Ries impact structure, Germany, sample RI_10_009A1.

5.2 Geologic Context

The mid-Miocene (14.6 ± 0.2 Ma; Buchner *et al.* 2010) Ries impact structure located in southern Germany is arguably one of the best-characterized and best-preserved terrestrial impact structures (see Pohl *et al.* 1977; von Engelhardt 1990 for reviews). Ries is a complex crater with a diameter of ~24 km (Pohl *et al.* 1977). The two-layer target is comprised of dominantly Mesozoic flat lying sediments that unconformably overlie crystalline Hercynian basement (Pohl *et al.* 1977; Graup 1978). Impactite units are well preserved (*e.g.*, Chao *et al.* 1978); the glass-bearing impact breccia or surficial "suevite" comprises one of four main proximal ejecta deposits (von Engelhardt 1990). Glass clasts are typically vesiculated, schlieren-rich mixtures containing abundant mineral and lithic fragments (von Engelhardt 1990). A detailed geochemical and petrological study of the Ries glasses is presented elsewhere (Osinski 2003). Post-impact hydrothermal alteration has been well documented at the Ries impact structure (Naumov 2005; Osinski 2005). A recent study suggests that alteration of glass clasts within the surficial suevite followed a progression from high- to low-temperature alteration with textures consistent with hydrothermal alteration, *sensu stricto*, between the two temperature end members (Sapers *et al.* 2009).

The impact glass itself is a theoretically suitable microbial substrate. Microorganisms are known to inhabit subaerial (Herrera *et al.* 2009) and submarine natural glasses (Mason *et al.* 2007 and references therein) with a variety of Si contents. The Ries glasses and the quench crystallites within it contain many bio-essential elements necessary for microbial metabolism such as K, Mn, Mg, Ca, Na, and Fe (Cady *et al.* 2003a). In addition, most microbes use transition metals as co-factors in enzymatic reactions. Many lithotrophic (rock-eating) microbes exploit redox disequilibria by oxidizing or reducing the transition metals depending on the environmental conditions providing metabolic energy along redox gradients.

5.3 Morphological Evidence

Staudigel *et al.* (2006) published a set of characteristic criteria regarding the distribution and morphology of putative microbial alteration features in volcanic glass. We summarize these criteria in the context of the Ries glasses. The tubule features in the Ries glasses are associated with clast margins, fractures, and vesicles displaying alteration fronts consistent with post-impact hydrothermal alteration (Sapers *et al.* in prep-a; Fig. 5.2A). This is consistent with tubule formation only where the impact glass was in contact with circulating fluids. As discussed below, tubules are crosscut by later fractures (Fig. 5.2 B, C), which do not exhibit hydration alteration fronts, or associated tubules. This distribution of tubules correlated with glass-fluid interfaces is consistent with reports of bioalteration in submarine basaltic glasses (*e.g.*, Furnes *et al.* 2007) and is fundamental to the proposed process of tubule formation discussed in detail elsewhere (Dole 1964 and references therein).

The integral nature of the tubules within the glass establishes their syngenicity and antiquity. The tubules must have formed following quenching, and deposition of the glass. The tubules are not flow aligned and in some cases crosscut flow features within the glass. The complex and delicate morphologies such as spirals (Fig. 5.2B) would not survive transport and deposition: none of the tubular features observed show elongation, distortion or other evidence of modification as would be expected if the features were incorporated into the glass as it formed rather than forming within the glass following emplacement (Fig. 5.2). A set of fractures in the glass not associated with hydrothermal alteration crosscuts the tubular features (Fig. 5.2B,C) restricting their time of formation between 15.9 Ma (time of impact) and a later event following the cessation of post-impact hydrothermal activity causing brittle fracture.

The tubules themselves are villiform forming straight to complex and highly convoluted vermicular features in the glass (*e.g.*, Figs. 5.2, 5.3). They may or may not bifurcate, branch (Fig. 5.3A) and/or exhibit annulations suggestive of segmentation (Sapers *et al.* in prep-b; *e.g.*, Fig. 5.2D). There is no parsimonious abiotic explanation of these morphologies. Ambient inclusion trails (AITs) are discounted as the hollow tubules lack the longitudinal striations diagnostic of AITs (Fig. 5.1G). Furthermore, none of the tubular features observed contain terminal inclusions. Biogenic behaviour is suggested by the distribution of the tubular features. Similar textural morphologies are commonly clustered together, suggestive of discrete populations. Segmented tubules are observed to cluster together in one region while non-segmented or spiral-shaped tubules cluster in other regions. Consistent with reports of bioalteration in submarine basaltic glasses (*e.g.*, Banerjee & Muehlenbachs 2003; Furnes *et al.* 2004; Furnes *et al.* 2007), the tubules in the Ries glasses do not intersect, in contrast to quench crystallites, and appear to avoid each other as indicated by changes in direction as two tubules approach each other (Fig. 5.2D). This is an expected behaviour in microbial populations sharing a substrate to avoid waste material.

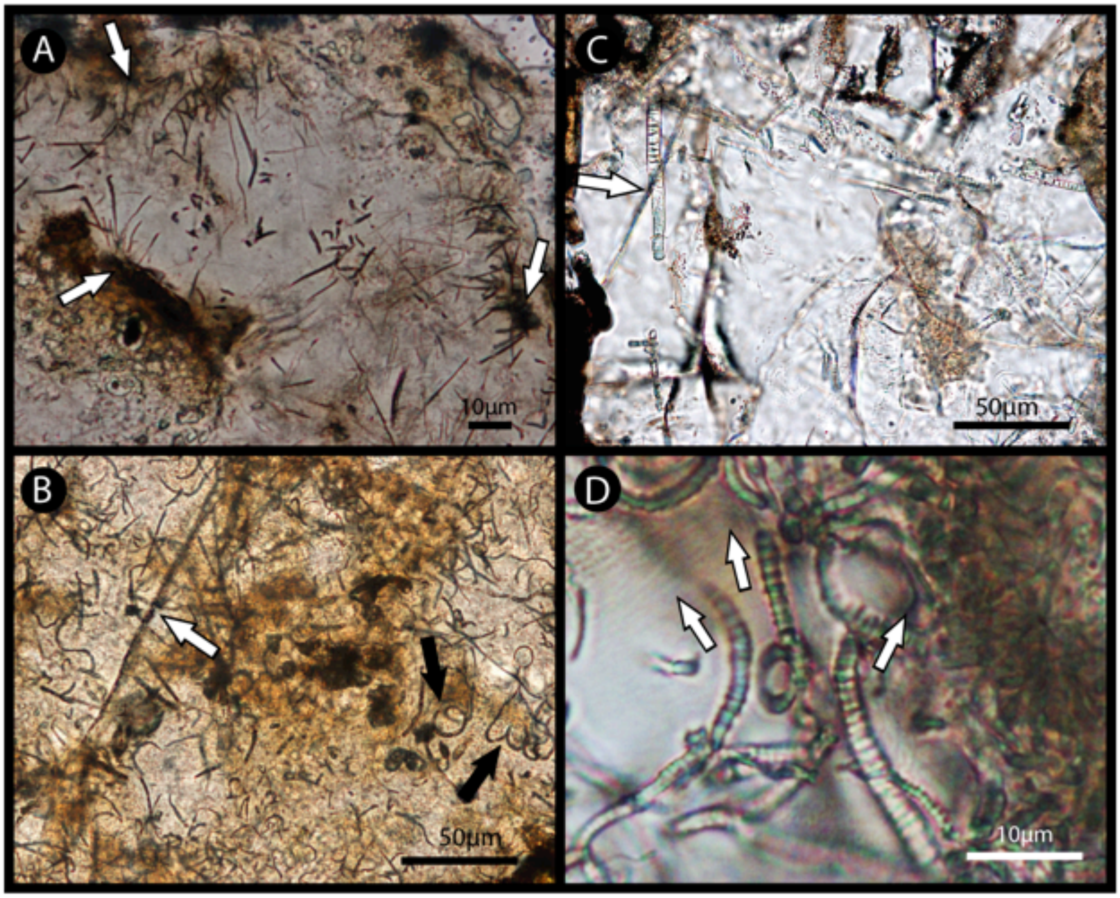

Figure 5.2: Transmitted light photomicrographs of the Ries tubules.

A (RI_10_013 5 m): extended depth of field images illustrating the association of tubular features with fractures displaying evidence of hydrous alteration (white arrows). B (RI_10_013 0 m): hydrated glass densely populated with non-intersecting tubular features. Black arrows indicate spirals; a late fracture (white arrow) cross-cuts the tubular features. C (RI_05_040): a segmented tubule is cross-cut by a fracture (white arrow); D (RI_00_056): segmented tubules diverge into different focal fields rather than intersecting, direction indicated by white arrows.

Scanning electron microscopy in secondary electron (SE) (Fig. 5.3 A, B) and back scattered electron (BSE) (Fig. 5.3 C, D) modes allows for three-dimensional and surface imaging, respectively. In SE mode, the tubules appear as dense clusters in natural voids within the glass. Examples of branching where daughter tubules are of approximately equal diameter to the parent tube are evident (Fig. 5.3A). The tubular features appear to be associated with a thin, film-like material (Fig. 5.3A) reminiscent of extra polymeric substance, a biologically produced 'biofilm' that adheres microbes to an abiotic substrate (*cf.* Banerjee & Muehlenbachs 2003). Furthermore, this material forms 'sheath-like' structures around individual tubules (Fig. 5.3B) strongly suggestive of sheaths. In BSE mode hollow (Fig. 5.3C) and solid (Fig 5.3D) tubules can be easily discerned. Some solid features have a rhomboid cross-section. It is unclear if the transition from hollow, smooth-walled, circular tubules to solid, decorated, rhomboid features represents a continuum of preservation and taphonomical change, or if the solid, rhomboid, linear features represent a discrete abiotic phenomena such as micro-crystallites. Both the hollow and solid tubules have morphologies distinct from the characteristic skeletal and dendritic forms of quench crystallites (Sapers *et al.* in prep-b).

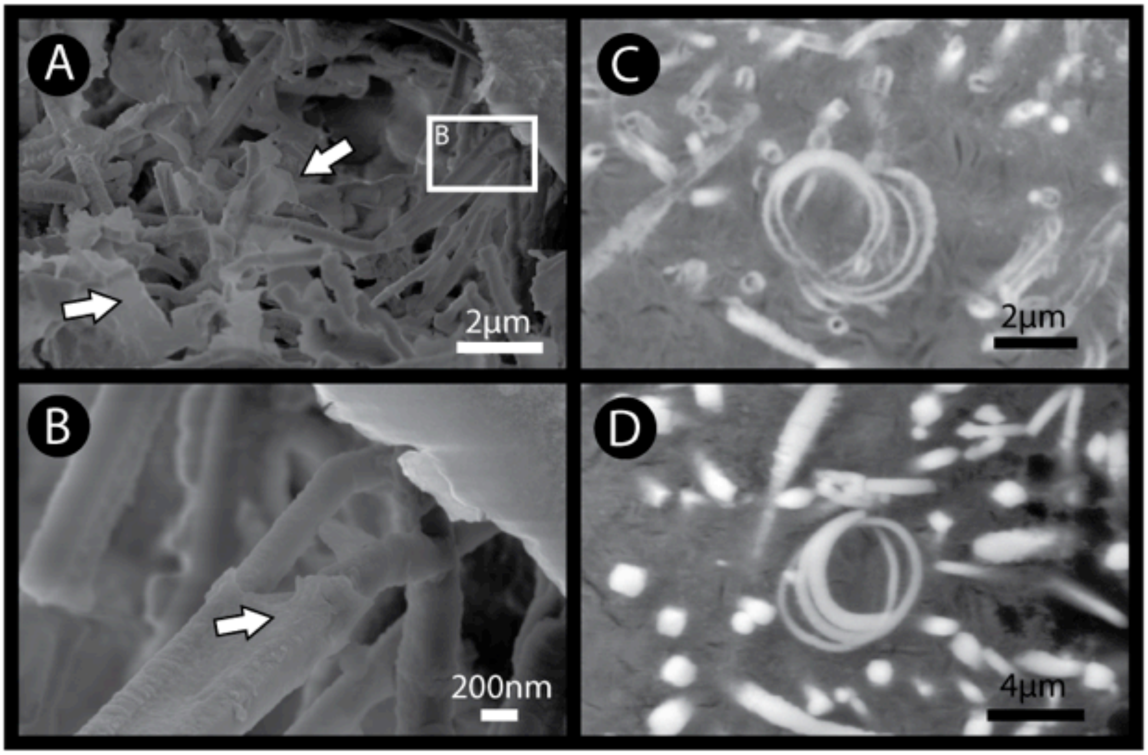

Figure 5.3: Scanning electron micrographs of the Ries tubules.

A – B: secondary electron mode. A (RI_10_006): Dense mass of mineralized tubules in altered void of impact-glass, note the thin EPS-like material associated with the tubular features (white arrows). Black arrows indicate examples of bifurcating tubules. B (RI_10_006): enlargement of boxed area in A. Note the sheath-like material (white arrow) coating the tubules not unlike cyanobacterial sheathed filaments. C – D (RI_10_009A1): back scatter electron mode. C: tubules are hollow in cross-section. Note the approximately ovoid cross-sections. D: tubules are solid in cross-section. Rhomboid features may crystallographically controlled due to preservation or may represent small crystallites.

5.4 Geochemical Evidence

Morphology alone is a notoriously controversial indicator of biogenicity (Brasier *et al.* 2002; Cady *et al.* 2003b; Garcia-Ruiz *et al.* 2003 and others), therefore, we also present geochemical evidence of biological processing including the presence of organic compounds associated with morphological evidence. As previously reported (Sapers *et al.* in prep-b) the tubules occur in zones enriched with respect the transition metals and alkali elements (Sapers *et al.* in prep-b). The Mg, Fe, Ca and Na depletion zone surrounding the tubules has been identified as a biological processing signature (McLoughlin *et al.* 2007). The elemental similarity between the mineral phase preserving the tubular features and the pyroxene quench crystallites may be explained by sequestering the available bioessential elements. Pyroxene crystallites are rich in bio-essential elements such as Fe and Ca that are lacking in the glassy matrix. It is conceivable that microbes could preferentially extract these bio-essential elements from crystallites. These elements would therefore become concentrated within the tubules and likely be preserved following decay of organic matter. Therefore, this enrichment would be expected if microbes are accumulating these metabolically relevant elements followed by passive accumulation of authigenic mineral phases and subsequent sealing of the channel and decay of organic matter. A similar preservation mechanism has been suggested for tubules preserved by titanite mineralization in Archaean greenstone belts (Banerjee *et al.* 2006a; Vogt *et al.* 2010). In the case of Archaean tubules, Ti is passively accumulated by microbes and concentrated within microbial alteration features.

Scanning transmission X-ray microscopy (STXM) at the Canadian Light Source spectromicroscopy beamline was used to measure near-edge X-ray absorbance spectra (NEXAFS) at the C K-edge. Spectra were collected between 200 – 310 eV to obtain high-resolution data in the 280 – 300 eV range in order to identify and differentiate organic carbon species based on C π bond energies calibrated to atmospheric CO_2. NEXAFS stacks were aligned using the Jacobsen model (Jacobsen *et al.* 2000) and spectra analysed with aXis2000 (Hitchcock 2000). Several spectral features indicative of organic carbon were found in association with the tubular features and notably absent in regions containing only crystallites (Fig. 5.4). In the matrix of regions hosting tubules, a

~285.2 eV peak consistent with the aromatic groups of protein (Myneni 2002); albumin used as a reference model for protein as per (Benzerara *et al.* 2004; H. Bluhm 2006) was evident. In spectra of the tubular features the well-resolved 285.2 eV peak is present in addition to two additional features: a ~288.5 eV feature interpreted to represent the carboxylic group in polysaccharides (Myneni *et al.* 2002; alginate used as a reference model for polysaccharides as per Bluhm *et al.* 2006; Benzarara *et al.* 2004); and a 283.6 eV feature tentatively interpreted to represent quinone structures (Solomon *et al.* 2005). Spectra of the areas containing only crystallites have a ~290 peak indicative of inorganic carbonate (Benzerara *et al.* 2004) and lack spectral features indicative of organic carbon species. The spectral features assigned to organic carbon species spatially associated with the tubules are consistent with C k-edge spectra of bacteria, and various biological compounds including proteins and polysaccharides. The spatial association of the organic carbon signatures with the tubules and absence of these spectral features in crystallite regions is consistent with the FTIR data discussed below and supports a biogenic origin of the tubules (Fig. 5.4).

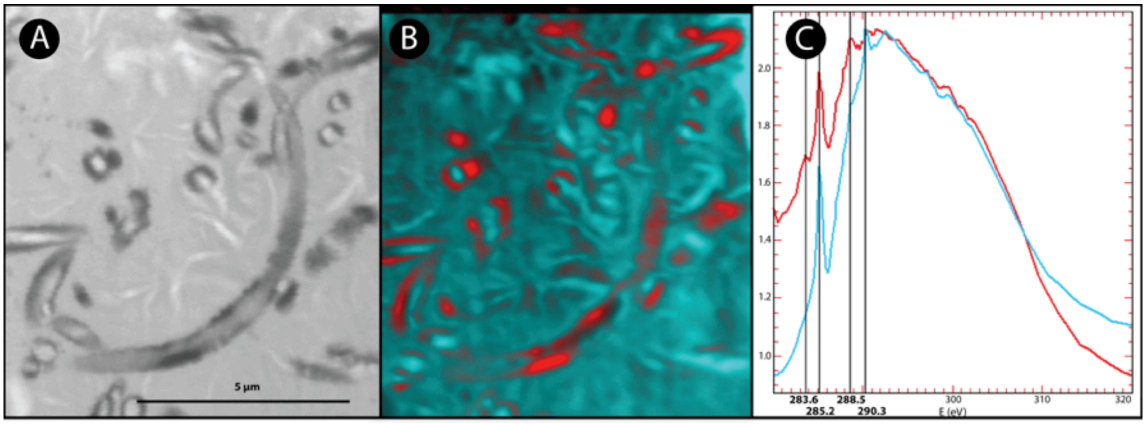

Figure 5.4: STXM observations of hollow tubules at the C 1S edge.

Spectra were collected between 200 – 310 eV to obtain high-resolution data in the 280 – 300 eV range in order to identify and differentiate organic carbon species based on C π bond energies calibrated to atmospheric CO_2. NEXAFS stacks were aligned using the Jacobsen model(Jacobsen *et al.* 2000) and spectra analysed with aXis2000(Hitchcock 2000) A: Scanning transmission X-ray photomicrograph of the area analyzed by NEXAFS spectroscopy. B: Composite image map illustrating the location of spectral features unique to the tubules (red) and matrix (cyan). C: Overplot of NEXAFS spectra obtained from the tubule walls (red) and matrix (blue) as imaged in A. Note the multiple peaks indicative of organic carbon species: 283.6 eV, 285.2 eV, and 288.5 eV representing the 1s-π* transition in quinones, aromatics and carboxylic acid groups respectively. Also resolved in the matrix spectra is a peak at 290.3 eV characteristic of inorganic carbonate groups. Sample RI_10_009.

Fourier Transform Infra-Red (FTIR) spectroscopy was carried out on both tubule-rich (Fig. 5.5A) and tubule-free (Fig. 5.5B) areas using a Bruker IFS55 FTIR with a Baseline TM Horizontal Attenuated Total Reflection (ATR) attachment equipped with a germanium crystal, under an IRScope II microscope. Within the Ries glasses, the dominant spectral features observed are those associated with silicate minerals and glasses due to Si-O-Si, Si-O-Al and/or Al-O-Al fundamental vibrational modes (Fig. 5.5) (*e.g.*, McMillan 1984; McMillan & Hofmeister 1988). These spectral features are centred on 977 cm^{-1} in the tubule-rich areas, and 985 cm^{-1} in the tubule-free glasses. The OH absorption bands observed around 3250 and 3400 cm^{-1} are common to all spectra obtained, indicating the samples are hydrated; likely representing water molecules bound within the glass matrix. Interestingly, in the tubular-rich areas a symmetric OH stretching vibrational mode of partially hydrogen bonded water molecules is identified at ~3590 cm^{-1}. In a study of microbially altered submarine volcanic glass from the Ontong Java Plateau using the same techniques this absorption band is interpreted to imply that the partially hydrogen bonded water molecules are bound to an organic matrix (Preston *et al.* 2011). In the tubule-rich areas of the Ries glasses a variety of organic bands are observed (Fig. 5.5A). Aliphatic C-H_x stretching absorption bands between 3000 and 2800 cm^{-1} are observed and may be derived from groups usually present in fatty acid components of cell membranes (Helm *et al.* 1991). Additionally, many of the important vibrational modes associated with lipids (Tamm & Tatulian 1997) are identified including the amide I C=O stretching vibrational mode of esters found within fatty acids (*e.g.*, Byler and Susi 1986; Arrondo *et al.* 1993; Goormaghtigh *et al.* 1994; Jackson & Mantsch 1995) and the amide II absorption band of secondary protein structure at 1731 cm^{-1} and 1562 cm^{-1} respectively. The identification of distinct functional group frequencies belonging to aliphatic hydrocarbons, amides and carbonyl group molecules, which may be assigned to various functional groups in lipids, proteins and carboxylic acids, and are found to be spatially associated with the tubules and notably absent from the tubular-free areas (Fig. 5.5B), strongly suggests the presence of biomolecules preserved within the tubules.

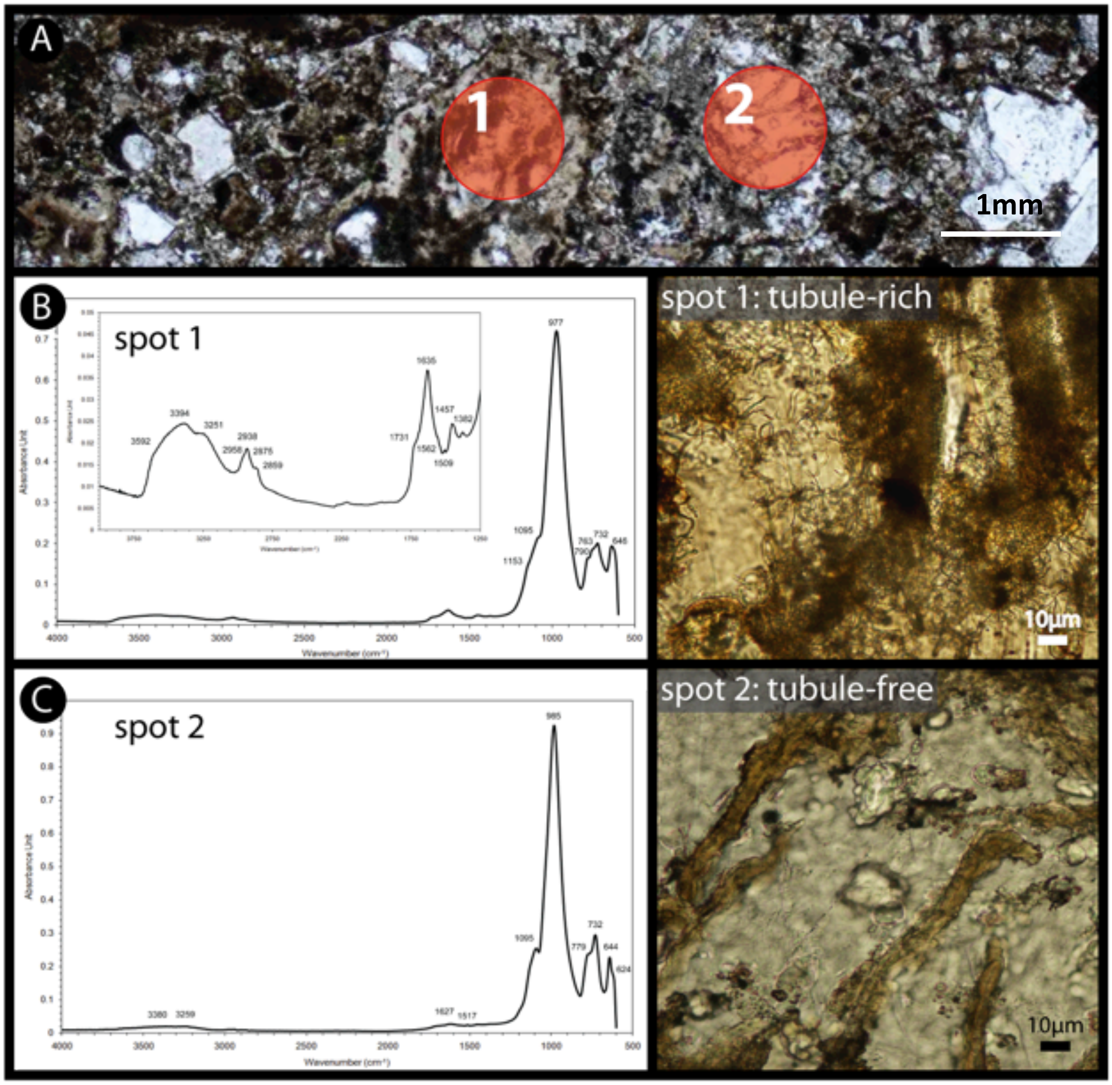

Figure 5.5: Transmitted light images and FTIR absorbance spectra.

Transmitted light images and FTIR absorbance spectra from a tubule-rich area (spot 1) and tubule-free area (spot 2). A: photomicrograph of a glass-bearing breccia indicating the approximate locations of FTIR analyses (red circles). B: FTIR absorbance spectra from spot 1, a tubule-rich area. Si-O, Ti-O and OH stretching absorption bands are observed. The main organic vibrational mode frequencies are identified on the inset expanded absorbance spectrum. Peak numbers match those described within the text. The photomicrograph to the right shows the dense clots of tubular features hosted within the glass. C: FTIR absorbance spectra from spot 2, a tubule-free area. Si-O, Ti-O and OH stretching absorption bands are again observed. No organic bands are observed. The photomicrograph to the right shows the absence of tubular features. Sample RI_00_056.

5.5 A New Astrobiology Target

Impact events are the only ubiquitous geological process in the Solar System and impact structures represent the dominant geological landform amongst the majority of the terrestrial planets. The habitability of subaerial (Herrera *et al.* 2009) and submarine natural glasses (Mason *et al.* 2007 and references therein) suggests that impact glasses, such as those found at the Ries impact structure, are potential habitats for microorganisms. Given the probable ubiquity of impact glasses in post-impact environments throughout the Solar System, it is important to understand the biological components and potential of such systems. Establishing the biogenicity of the tubular structures observed in the Ries impact glasses has significant astrobiological implications. The high flux rate of meteorite impacts on the early Earth would favour life in endolithic (within rock) environments such as glassy substrates, furthermore, impact events would provide transient energy to terrestrial bodies without endogenous volcanic heat sources to drive hydrothermal activity, such as Mars. The endolithic environments resulting from impact events are important targets for astrobiological investigations of the early Earth and of other terrestrial planets. The extreme conditions present on Mars, such as intense UV flux, low temperature, and absence of liquid water may encourage the exploitation of endolithic strategies. (Dole 1964; Banerjee *et al.* 2006b; McLoughlin *et al.* 2007a; Izawa *et al.* 2010), suggest microborings into volcanic glasses as a potential planetary biosignature and lists natural glasses as one of the most promising preservation environments for ichnofossils on early Earth and Mars. By extending this to impact glasses we greatly increase the number of candidate environments.

A recent paper by Ivarsson and Lindgren (2010) highlights the significance of impact ejecta as a target for an astrobiology focused Mars sample return mission. Impact events have the potential to excavate deep into the crust of the target body making the subsurface available for study precluding the need for drilling. The subsurface of Mars has been targeted as one of the most promising environments preserving past or present traces of life (Ivarsson & Lindgren 2010a and references therein). Impact structures have been heralded as prime astrobiology targets in the literature (Cockell *et al.* 2003; Cady and Noffke 2009; Ivarsson & Lindgren 2010b): post-impact hydrothermal systems provide an exogenous source of heat to an otherwise energetically 'dead' planets as well as source of metabolic energy in the form of chemical disequilibria resulting from water-rock interactions (Cockell *et al.* 2003) in addition, impact-shocked crystalline rock provides protective endolithic microbial habitats (Cockell *et al.* 2005a). The identification of ichnofossils in impact glass has tremendous implications for impact structures as astrobiology targets. Due to the ubiquity of impact events on terrestrial planets and the adaptive advantages of the post-impact environment to microbial colonization, impact glass may well represent one of the best targets in which to search for evidence of extra-terrestrial life. This discovery of biogenic tubules in the Ries impact glasses represents a novel habitat for life on Earth within impact ejecta. Such an environment can be extrapolated to a potential habitat within impact ejecta on other planets such as Mars.

5.6 The Case for Biogenicity

We have illustrated the presence of enigmatic tubular features hosted within glass clasts from impact melt-bearing breccias from the Ries impact structure, Germany. The host glasses at the Ries contain crystallites dominated by Ca- and Al-rich pyroxene (Osinski 2003; this study). These pyroxene crystallites are typically skeletal to dendritic, which are well-understood quench crystal morphologies (*e.g.*, Marshall 1961). The complex morphologies and convoluted structures characterizing these features (*e.g.*, Figs. 5.2, 5.3) combined with organic functional group identification indicate these features likely were not formed by purely mineralogical processes.

Here we have established the morphological similarity of the tubular textures in the Ries glasses to both *in situ* microbial alteration of modern oceanic crust and Palaeozoic and Precambrian ichnofossils preserving evidence of microbial glass tunnelling (Fig. 5.1) by satisfying the criteria put forward by (Staudigel *et al.* 2006). The morphological complexity and distribution of the Ries tubules (Figs. 5.2, 5.3) indicate biological morphology and behaviour. We have illustrated the syngenicity and antiquity of the Ries tubular features as the features are integral to the glass substrate and are crosscut by later fracture systems (Fig. 5.2B, C). In addition we present evidence of organic compounds spatially associated with the features and absent in the host impact glass. Taken together these data and observations satisfy the biogenicity criteria developed by McLoughlin *et* *al.* (2007) and we conclude a biogenic origin of the Ries tubules. Our study indicates that microbes colonized impact-generated glass of the Ries impact structure much in the same way they do modern submarine volcanic glass. Well-preserved impact glasses, a major component of craters on Earth and other rocky bodies in the solar system, represent a new niche in the search for microbial ichnofossils and may represent one of the best places to search for evidence of life beyond Earth.

5.7 References Cited

ARRONDO J. L. R., MUGA A., CASTRESANA J. and GOÑI F. M. (1993) Quantitative studies of the structure of proteins in solution by Fourier transform infrared spectroscopy. *Progress in Biophysics and Molecular Biology* **59**, 23 – 56.

BANERJEE N. R., FURNES H., MUEHLENBACHS K., STAUDIGEL H. and DE WIT M. (2006a) Preservation of ~3.4 – 3.5 Ga microbial biomarkers in pillow lavas and hyaloclastites from the Barberton Greenstone Belt, South Africa. *Earth and Planetary Science Letters* **241**(3 – 4), 707 – 722.

BANERJEE N. R., FURNES H., SIMONETTI A., MUEHLENBACHS K., STAUDIGEL H., DE WIT M. and VAN KRANENDONK M. J. (2006b) Ancient Microbial Alteration of Oceanic Crust on Two Early Archean Cratons and the Search for Extraterrestrial Life. In *37th Annual Lunar and Planetary Science Conference*, League City, TX.

BANERJEE N. R. and MUEHLENBACHS K. (2003) Tuff life: Bioalteration in volcaniclastic rocks from the Ontong Java Plateau. *Geochemistry, Geophysics, Geosystems* **4**(4), 1037 – 1059.

BANERJEE N. R., SIMONETTI A., FURNES H., MUEHLENBACHS K., STAUDIGEL H., HEAMAN L. and VAN KRANENDONK M. J. (2007) Direct dating of Archean microbial ichnofossils. *Geology* **35**(6), 487 – 490.

BENZERARA K., YOON T. H., TYLISZCAZAK T., CONSTANTZ B., SPORMANN A. M. and BROWN G. E. J. (2004) Scanning transmission X–ray microscopy study of microbial calcification. *Geobiology* **2**, 249 – 259.

BLUHM, H., ARAKI, K. A. T., BENZERARA, K., BROWN, G. E., DYNES, J. J., GHOSAL, S., GILLES, M. K., HANSEN, H.-CH., HEMMINGER, J. C., HITCHCOCK, A. P., KETTELER, G., KILCOYNE, A. L. D., KNEEDLER, E., LAWRENCE, J. R., LEPPARD, G. G., MAJZLAM, J., MUN, B. S., MYNENI, S. C. B., NILSSON, A., OGASAWARA, H. OGLETREE, D. F., PECHER, K., SALMERON, M., SHUH, D. K., TONNER, B., TYLISZCZAK, T., WARWICK, T., AND YOON, T. H. (2006) Soft X-ray microscopy and spectroscopy at the molecular environmental science beamline at the Advanced Light Source. *Journal of Electron Spectroscopy and Related Phenomena* **150**, 86 – 104.

BRASIER M. D., GREEN O. R., JEPHCOAT A. P., KLEPPE M. J., VAN KRANENDONK M. J., LINDSAY J. F., STEELE A. and GRASSINEAU N. V. (2002) Questioning the evidence of Earth's oldest fossils. *Nature* **416**, 76 – 81.

BUCHNER E., SCHWARZ W., SCHMIEDER M. and TRIELOFF M. (2010) Establishing a 14.6 ± 0.2 Ma age for the Nördlinger Ries impact (Germany) — A prime example for concordant isotopic ages from various dating materials. *Meteoritics and Planetary Science* **45**(4), 662 – 674.

BYLER D. M. and SUSI H. (1986) Examination of the secondary structure of proteins by deconvolved FTIR spectra. *Biopolymers* **25**, 469 – 487.

CADY S., FARMER J. D., GROTZINGER J. P., SCHOPF J. W. and STEELE A. (2003a) Biosignatures and the Search for Life on Mars. *Astrobiology* **3**, 351 – 368.

CADY S. and NOFFKE N. (2009) Geobiology: Evidence for early life on Earth and the search for life on other planets. *GSA Today* **19**(11), 4 – 10.

CADY S. L., FARMER J. D., GROTZINGER J. P., SCHOPF J. W. and STEELE A. (2003b) Morphological Biosignatures and the Search for Life on Mars. *Astrobiology* **3**(2), 351 – 368.

CHAO E. C. T., HüTTNER R. and SCHMIDT-KALER H. (1978) *Principal Exposures of the Ries Meteorite Crater in Southern Germany*. Bayerisches Geologisches Landesamt, Munich. pp. 1.

COCKELL C. S., LEE P., BROADY P., LIM D. S. S., OSINSKI G. R., PARNELL J., KOEBERL C., PESONEN L. and SALMINEN J. (2005a) Effects of asteroid and comet impacts on habitats for lithophytic organisms — A synthesis. *Meteoritics & Planetary Science* **40**(12), 1901 – 1914.

COCKELL C. S., OSINSKI G. R. and LEE P. (2003) The impact crater as a habitat: Effects of impact processing of target materials. *Astrobiology* **3**(1), 181 – 191.

DOLE S. H. (1964) *Habitable Planets for Man*. Blaisell, New York.

FISK M. R., GIOVANNONI S. J. and THORSETH I. H. (1998) Alteration of oceanic volcanic glass; textural evidence of microbial activity. *Science* **281**(5379), 978 – 980.

FLIEGEL D., KOSLER J., MCLOUGHLIN N., SIMONETTI A., DE WIT M. J., WIRTH R. and FURNES H. (2010) In-situ dating of the Earth's oldest trace fossil at 3.34Ga. *Earth and Planetary Science Letters* **299**(3 – 4), 290 – 298.

FURNES H., BANERJEE N. R., MUEHLENBACHS K., STAUDIGEL H. and DE WIT M. (2004) Early Life Recorded in Archean Pillow Lavas. *Science* **304**(5670), 578 – 581.

FURNES H., BANERJEE N. R., STAUDIGEL H., MUEHLENBACHS K., MCLOUGHLIN N., DE WIT M. and VAN KRANENDONK M. J. (2007) Comparing petrographic signatures of bioalteration in recent to Mesoarchean pillow lavas; tracing subsurface life in oceanic igneous rocks; Earliest evidence of life on Earth. *Precambrian Research* **158**(3 – 4), 156.

FURNES H., STAUDIGEL H., THORSETH I. H., TORSVIK T., MUEHLENBACHS K. and TUMYR O. (2001) Bioalteration of basaltic glass in the oceanic crust. *Geochemistry, Geophysics, Geosystems* **2**(8), 1049 – 1079.

GARCIA-RUIZ J. M., HYDE S. T., CARNERUP A. M., CHRISTY A. G., VAN KRANENDONK M. J. and WELHAM N. J. (2003) Self-assembled silica-carbonate structures and detection of ancient microfossils. *Science* **302**, 1194 – 1197.

GOORMAGHTIGH E., CABIAUX V. and RUYSSCHAERT J.-M. (1994) Determination of soluble and membrane protein structure by Fourier transform infrared spectroscopy. I. Assignments and model compounds. II. Experimental aspects, side chain structure, and H/D exchange. III. Secondary structures. In *Subcellular Biochemistry* (eds. H. J. Hilderson and G. B. Ralston), pp. 329 – 450. Plenum Press, New York.

GRAUP G. (1978) *Das Kristallin im Noerdlinger Ries; petrographische Zusammensetzung und Auswurfmechanismus der kristallinen Truemmermassen, Struktur des kristallinen Untergrundes und Beziehungen zum Moldanubikum. The crystallines of the Nordlinger Ries; petrographic composition and ejection mechanisms of crystalline debris, structure of crystalline basement and relationship to the Moldanubicum*. Ferdinand Enke Verlag, Stuttgart, Federal Republic of Germany (DEU), Federal Republic of Germany (DEU).

HELM D., LABISCHINSKI H., SCHALLEHN G. and NAUMANN D. (1991) Classification and identification of bacteria by Fourier-transform infrared spectroscopy. *Journal of General Microbiology* **137**, 69 – 79.

HERRERA A., COCKELL C. S., SELF S., BLAXTER M., REITNER J., THORSTEINSSON T., ARP G., DRÖSE W. and TINDLE A. G. (2009) A Cryptoendolithic Community in Volcanic Glass. *Astrobiology* **9**(4), 369 – 381.

HITCHCOCK A. P. H. (2006) aXis2000. aXis2000. Analysis of X-ray Images and Spectra. McMaster University, Hamilton, Ontario, Canada. Available from: http://unicorn.mcmaster.ca/aXis2000.html.

IVARSSON M. and LINDGREN P. (2010) The Search for Sustainable Subsurface Habitats on Mars, and the Sampling of Impact Ejecta. *Sustainability* **2**(7), 1969 – 1990.

IZAWA M. R. M., BANERJEE N. R., FLEMMING R. L., BRIDGE N. J. and SCHULTZ C. (2010) Basaltic glass as a habitat for microbial life: Implications for astrobiology and planetary exploration. *Planetary and Space Science* **58**(4), 583 – 591.

JACKSON M. and MANTSCH H. H. (1995) The use and misuse of FTIR spectroscopy in the determination of protein structure. *Critical Reviews in Biochemistry and Molecular Biology* **30**, 95 – 120.

JACOBSEN C., FLYNN G., WIRICK S. and ZIMBA C. (2000) Soft X-ray spectromicroscopy from image sequences with sub-100nm spatial resolution. *Journal of Microscopy* **197**(2), 173 – 184.

KRING D. A. (2000) Imapct events and their effect on the origin, evolution, and distribution of life. *GSA Today* **10**(8), 1 – 7.

MARSHALL R. R. (1961) Devitrification of Natural Glass. *Geological Society of America Bulletin* **72**, 1493 – 1520.

MASON O. U., STINGL U., WILHELM L. J., MOESENEDER M. M., DI MEO-SAVOIE C. A., FISK M. R. and GIOVANNONI S. J. (2007) The phylogeny of endolithic microbes associated with marine basalts. *Environmental Microbiology* **9**(10), 2539 – 2550.

MCLOUGHLIN N., BRASIER M., WACEY D., GREEN O. and PERRY R. (2007) On biogenicity criteria for endolithic microborings on early Earth and beyond. *Astrobiology* **7**, 10 – 26.

MCLOUGHLIN N., FURNES H., BANERJEE N., MUEHLENBACHS K. and STAUDIGEL H. (2009) Ichnotaxonomy of microbial trace fossils in volcanic glass. *Journal of the Geological Society* **166**(1), 159 – 169.

MCLOUGHLIN N., FURNES H., BANERJEE N., STAUDIGEL H., MUECHLENBACHS K., DE WIT M. and VAN KRANENDONK M. (2008) Micro-bioerosion in volcanic glass: extending the ichnofossil record to Archaean basaltic crust. In *Current Developments in Bioerosion* (eds. M. Wisshak and L. Tapanila). Springer-Verlag, Berlin Heidelberg.

MCMILLAN P. (1984) Structural studies of silicate glasses and melts — applications and limitations of Raman spectroscopy. *American Mineralogist* **69**, 622 – 644.

MCMILLAN P. F. and HOFMEISTER A. M. (1988) Infrared and Raman Spectroscopy. In *Spectroscopic Methods in Mineralogy and Geology* (ed. F. C. Hawthorne), pp. 99 – 150. Mineralogical Society of America.

MELOSH H. J. (1989) Impact cratering; a geologic process. *Oxford Monographs on Geology and Geophysics* **11**, 245.

MYNENI S. C. (2002) Soft X-ray spectroscopy and spectromicroscopy studies of organic molecules in the environment. In *Applications of Synchrotron Radiation in Low Temperature Geochemistry and Environmental Science: Reviews in Mineralogy and Geochemistry* (ed. P. A. Fenter, Rivers, M. L., Sturchio, N. C., Sutton, S. R.), pp. 485 – 579.

NAUMOV M. V. (2005) Principal features of impact-generated hydrothermal circulation systems: mineralogical and geochemical evidence. *Geofluids* **5**(3), 165 – 184.

NAUMOV M. V., PLADO J. and PESONEN L. J. (2002) Impact-generated hydrothermal systems; data from Popigai, Kara, and Puchezh-Katunki impact structures; Impacts in Precambrian shields. In *4th IMPACT programme workshop on Meteorite impacts in Precambrian shields, Lappajarvi* (ed. C. Koeberl). Springer Berlin Federal Republic of Germany (DEU)

NISBET E. (2000) Palaeobiology: The realms of Archaean life. *Nature* **405**(6787), 625 – 626.

OSINSKI G. R. (2003) Impact glasses in fallout suevites from the Ries impact structure, Germany: An analytical SEM study. *Meteoritics & Planetary Science* **38**(11), 1641 – 1667.

— (2005) Hydrothermal activity associated with the Ries impact event, Germany. *Geofluids* **5**(3), 202 – 220.

OSINSKI G. R., SPRAY J. G. and LEE P. (2001) Impact-induced hydrothermal activity within the Haughton impact structure, arctic Canada: Generation of a transient, warm, wet oasis. *Meteoritics and Planetary Science* **36**, 731 – 745.

POHL J., STÖFFLER D., GALL H. and ERNSTSON K. (1977) The Ries impact crater; Impact and explosion cratering; planetary and terrestrial implications; Proceedings of the Symposium on planetary cratering mechanics. In *Lunar Science Institute topical conference ; Symposium on planetary cratering mechanics, Flagstaff, Ariz* (eds. D. J. Roddy, R. O. Pepin and R. B. Merrill). Pergamon Press New York N.Y. United States (USA), United States (USA).

PRESTON L. J., BANERJEE N. R., AND IZAWA M. R. M. (2011) Infrared spectroscopic characterization of organic matter associated with microbial bioalteration textures in basaltic glass. *Astrobiology Special Edition* **11**, 585 – 599.

SAPERS H. M., BANERJEE N. R., PRESTON L. J. and OSINSKI G. R. (in prep-a) Microbial ichnofossils preserved in meteorite impact glass. *Nature*.

SAPERS H. M., OSINSKI G. R. and BANERJEE N. (2009) Differential alteration of glass clasts in the surficial suevites of the Ries Crater, Germany. In *72nd Annual Meteoritical Society Meeting*.

SAPERS H. M., OSINSKI G. R., FLEMMING R. L. and BANERJEE N. R. (in prep-b) Enigmatic tubular features in impact glass from the Ries impact structure, Germany. *Geology*.

SCHULTE P., ALEGRET L., ARENILLAS I., ARZ J. A., BARTON P. J., BOWN P. R., BRALOWER T. J., CHRISTESON G. L., CLAEYS P., COCKELL C. S., COLLINS G. S., DEUTSCH A., GOLDIN T. J., GOTO K., GRAJALES-NISHIMURA J. M., GRIEVE R. A.

F., GULICK S. P. S., JOHNSON K. R., KIESSLING W., KOEBERL C., KRING D. A., MACLEOD K. G., MATSUI T., MELOSH J., MONTANARI A., MORGAN J. V., NEAL C. R., NICHOLS D. J., NORRIS R. D., PIERAZZO E., RAVIZZA G., REBOLLEDO-VIEYRA M., REIMOLD W. U., ROBIN E., SALGE T., SPEIJER R. P., SWEET A. R., URRUTIA-FUCUGAUCHI J., VAJDA V., WHALEN M. T. and WILLUMSEN P. S. (2010) The Chicxulub asteroid impact and mass extinction at the Cretaceous – Paleogene boundary. *Science* **327**, 1214 – 1218.

SOLOMON D., LEHMANN J., KINYANGI J., LIANG B. and SCHÄFER T. (2005) Carbon K-Edge NEXAFS and FTIR-ATR Spectroscopic Investigation of Organic Carbon Speciation in Soils. *Soil Science Society of America Journal* **69**, 107 – 119.

STAUDIGEL H., FURNES H., BANERJEE N. R., DILEK Y. and MUEHLENBACHS K. (2006) Microbes and volcanoes: A tale from the oceans, ophiolites, and greenstone belts. *GSA Today* **16**(10), 4 – 10.

TAMM L. K. and TATULIAN S. A. (1997) Infrared spectroscopy of proteins and peptides in lipid bilayers. *Quarterly Reviews of Biopysics* **30**, 365 – 429.

VOGT S. S., BUTLER R. P., RIVERA E. J., HAGHIGHIPOUR N., HENRY G. W. and WILLIAMSON M. H. (2010) The Lick-Carnegie exoplanet survey: A 3.1M planet in the habitable zone of the nearby M3V star Gliese 581. *The Astrophysical Journal* **723**, 954 – 998.

VON ENGELHARDT W. (1990) Distribution, petrography and shock metamorphism of the ejecta of the Ries Crater in Germany; a review; Cryptoexplosions and catastrophes in the geological record, with a special focus on the Vredefort Structure. *Tectonophysics* **171**(1 – 4), 259

Chapter 6

6 Microbially Mediated Alteration of Impact Glass: a STXM and TEM Study

Sapers, H. M., Schumann, D., Banerjee, N. R., Osinski, G. R., Vali, H.

6.1 Introduction

Text Studies of impact glasses hosted within glass-bearing breccias of the Ries impact structure have revealed the presence of conspicuous tubular structures with complex morphologies and chemical signatures suggestive of a biogenic origin (Chapters 4 & 5). The previous studies the tubule features in the Ries glasses suggest a biogenic origin for the tubules. However, establishing the biogenicity of a trace fossil is notoriously difficult (Brasier *et al.* 2002; Cady *et al.* 2003; Garcia-Ruiz *et al.* 2003) and requires multiple lines of evidence and complementary data sets consistent with a biological origin while discounting abiotic formation mechanisms (*e.g.*, McLoughlin *et al.* 2007). Such investigations commonly produce equivocal evidence and ambiguous conclusions (*e.g.*, Brasier *et al.* 2002). This is especially problematic when dealing with ancient systems, or systems with very little to no organic matter, such as the Ries tubules. Without abundant organic matter such as nucleic acids and proteins, *in situ* detection of biological material is not possible and the biogenicity of such features is often questioned. This study is unique as not only do we merge complimentary analytical techniques to assess the biogenicity of the Ries tubules, but also incorporate an intrinsic negative control. We compare the results from analyses of abiotic quench crystallites with putatively biogenic tubular features. Using scanning transmission X-ray microscopy (STXM) near edge X-ray absorption fine structure spectroscopy (NEXAFS) at the Fe L2,3 and C 1s edges combined with transmission electron microscopy (TEM) we are able to identify and map chemical changes consistent with biological processing and organic carbon species spatially associated with putative microbial alteration features in the glassy substrate. The results of this study interpret the Ries tubules as ichnofossils providing the first evidence of microbially mediated alteration of impact materials.

Microbial alteration of natural glasses is a widespread natural phenomenon (Thorseth *et al.* 1995; Fisk *et al.* 1998; Torsvik *et al.* 1998; Furnes *et al.* 2001a,b, 2004, 2007; Banerjee & Muehlenbachs 2003; Banerjee *et al.* 2004a,b, 2006a,b, 2007, 2008; Staudigel *et al.* 2006, 2008a,b; Benzerara *et al.* 2007; Fliegel *et al.* 2008; Peckmann *et al.* 2008; Cockell *et al.* 2009; Izawa *et al.* 2010a,b). Biological weathering of subaerial volcanic glasses is also a well-documented process (Cockell & Herrera 2008; Cockell *et al.* 2009; Herrera *et al.* 2009) with significant impact on the persistence of natural glasses and their resistance to weathering and erosion. Here we present geochemical evidence through STXM and TEM of biologically mediated alteration of impact glass from the Ries impact structure, Germany. Impact glass represents a novel terrestrial microbial substrate and the discovery of microbial alteration features within the impact glass has significant implications for the earliest colonization of habitable niches on early Earth as well on other planets such as Mars.

Impact events are a relatively rare occurrence on modern Earth. With only 182 terrestrial impact structures identified they constitute a minor geographical feature on modern day Earth (Earth Impact Database, 2012). However, impact cratering is the only ubiquitous geological process in the Solar System and impact structures account for the dominant landform on many terrestrial planets including the early Earth. During the Late Heavy Bombardment (4.2 – 3.8 Ga) impact flux was an estimated 2X higher than it is today (Kring and Cohen 2002). The destructive effects of impact events are well studied; however, impact events may have beneficial effects particularly for microbial life (*e.g.*, Osinski *et al.* 2001; Cockell *et al.* 2002, 2003; Osinski 2003a). Impact event results in local sterilization and may be viewed as biological resetting events followed by distinct ecological successional stages (Cockell & Lee 2002b). The earliest phase of ecological recovery following an impact is the phase of thermal biology 'during which the thermal anomaly associated with a recently formed crater sustains biological activity of a nature or at a level requiring warmed environmental conditions' (Cockell & Lee 2002a). Impact events create novel microbial niches and substrates such as chemically and energetically diverse impact glass providing not only a novel microbial habitat on present day Earth, but furthermore, a potential preservation environment for microbial trace fossils of early Earth and possibly other planets such as Mars.

6.2 The Ries Impact Structure

The mid – Miocene Ries impact structure located in southern Germany is arguably one of the best-characterized and best-preserved terrestrial impact structures (see Pohl *et al.* 1977; von Engelhardt 1990 for reviews). $^{40}Ar/^{39}Ar$ laser-probe dating of tektites constrains the age of the Ries impact structure to 14.6 $\pm$ 0.2 Ma (Buchner *et al.* 2010). Ries is a complex crater with a diameter of ~24 km (Pohl *et al.*, 1977; Fig. 6.1).

Impactite units are well preserved (*e.g.*, Chao *et al.* 1978); surficial "suevite" comprises one of four main proximal ejecta deposits (von Engelhardt 1990). Four main glass types occur within the main suevite both as groundmass phases and as discrete glass clasts (Osinski 2003b). Glass clasts are typically vesiculated, schlieren-rich mixtures containing abundant mineral and lithic fragments (von Engelhardt 1990). The glass clasts hosted within the suevite have been classified based on composition and microtextures (Osinski 2003b).

Type I glasses are the most abundant in the Ries suevites. These glasses contain Al-rich pyroxene quench crystallites and have SiO_2 contents ~63%. Type II glasses have a similar SiO_2 content as type I; however, they contain only plagioclase crystallites as well as a generation of dense, micron-scale vesicles. Type III glasses have low SiO_2 contents, are hydrated relative to the other glasses, and contain relatively little FeO, MgO, and K_2O, while having high Al_2O_3, CaO, and Na_2O contents. Type IV glasses have very high SiO_2 contents commonly >90%. Type I glasses have the highest concentrations of FeO and MgO of all 4 glass types (Osinski 2003). Type I glasses are the focus of this study as they comprise >90% of the glass clasts hosted within the Ries surficial suevite (Osinski 2003).

The Ries crater in southern Germany is one of the best-characterized terrestrial impact structures (*e.g.*, Pohl *et al.* 1977). Furthermore, detailed studies have characterized the impact-generated hydrothermal system of the Ries crater. In addition, the Ries crater has exceptionally well preserved proximal impact ejecta deposits including an impact glass-bearing breccia unit. The rapid quenching of molten material following a hypervelocity impact results in the formation of impact glasses. Impact glasses share many similarities with volcanic glasses but the bulk compositions of impact melts are commonly more diverse, reflecting heterogeneities in the target lithologies. Furthermore, impact melts commonly display heterogeneity on multiple scales. In addition, the presence of lechatelierite (a silica glass phase) is indicative of high temperatures (>1713^{o}C; Stöffler 1984) reflecting formation conditions distinct from normal igneous processes.

6.3 Experimental Methods

6.3.1 Samples

Samples of glass-bearing impact breccia (suevite) for this study were obtained from the Seelbronn and Aumühle quarries at the Ries impact structure over two field seasons. Samples were previously characterized in Chapters 4, 5. Petrographic thin sections were sputter coated with Pt (sample A) or Os (sample B) to mitigate charge build-up during SEM observation. The tubular features within the impact glass clasts hosted in the glass bearing impact breccia from the Ries impact structure have been previously characterized with optical petrography and scanning electron microscopy. Previous work has documented the biogenicity of the features establishing their syngenicity to the impact glass, homologous morphology lacking a parsimonious abiotic formation mechanism, and chemical evidence of biological processing. These studies described tubular features ~ 1um in diameter extending hundreds of microns in length with complex morphologies including spirals and regular annulation.

Two of the previously studied glass clasts differentiated by size, both hosting dense assemblages of these tubular features were chosen for this study. Sample A (RI_10_006) represents a decimeter-sized glass clast with little visible surface alteration. A petrographic thin section was cut from the interior of sample A to minimize surface contamination. Two focused ion beam (FIB) samples were milled from this thin section: A1 contains dendritic pyroxene crystallite and A2 contains solid, coiled tubular features. Sample B (RI_10_009) is a petrographic section cut from the matrix of surficial glass-bearing breccia. Within the matrix are numerous micron-scale glassy clasts partially to completely replaced by clay minerals. One of these highly altered glass clasts was chosen for further study. Two FIB sections were milled from the chosen glass clast in sample B: B1 contains solid, coiled tubules and B2 contains hollow, coiled tubules.

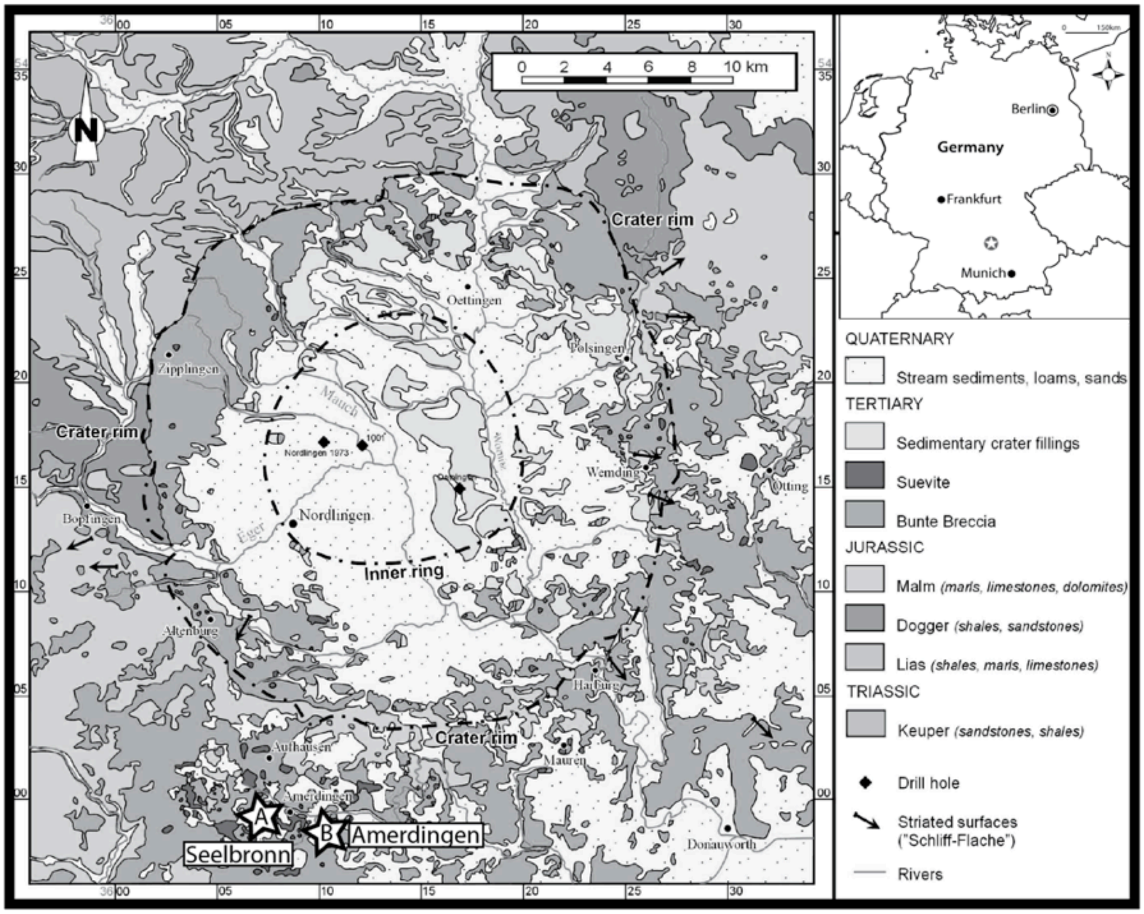

Figure 6.1: Geological map of the Ries impact structure.

Samples of glass-bearing breccia (suevite) A1 and A2 were obtained from Seelbronn and samples B1 and B2 from Amerdingen. Modified from Osinski (2003).

6.3.2 Focused Ion Beam Milling

Focused ion beam (FIB) milling was conducted at Fibics Inc. Ottawa, ON Canada using a Micrion 2500 Focused Ion Beam (FIB) microscope system and modified in-house FIB lift-out techniques (Patternson *et al.* 2002). Prior to milling, samples were cleaned with compressed air and remaining contaminates removed by 'high ion beam current milling' under visual guidance in ion mode on a FEI Vectra "FlipChip" 8" Wafer FIB system. A thin (~1 µm) protective strip (dimensions) of tungsten was deposited over the area to be milled. A Ga+ ion beam was used for milling at 50 kV operating conditions. Rough excavation troughs were milled into the sample using a FEI Vectra "FlipChip" 8" Wafer FIB surrounding the area of interest to the final dimensions of 30 µm X 1.5 µm and then thinned to ~800 nm via progressive trenching. The sample was then moved to the Micrion 2500 for final thinning to 80 – 100 nm and trimming to ~25 µm X ~1.5 µm followed by lift-out. FIB foil A1 was transferred at room pressure with a micromanipulator to the membrane of a Formvar-coated 300 mesh copper TEM grid (SPI supplies, West Chester, PA, USA #3330C). Similar preparation of FIB foils of ichnofossils in natural glass have been studied successfully using synchrotron radiation (Benzerara *et al.* 2007). FIB foils A2, B1, and B2 were fused to modified Cu TEM mounts as per an in-house method developed by Fibics Inc. (Patternson *et al.* 2002). Following milling and lift out, SEM and optical microscopy were conducted to confirm the areas of interest were correctly targeted during FIB milling.

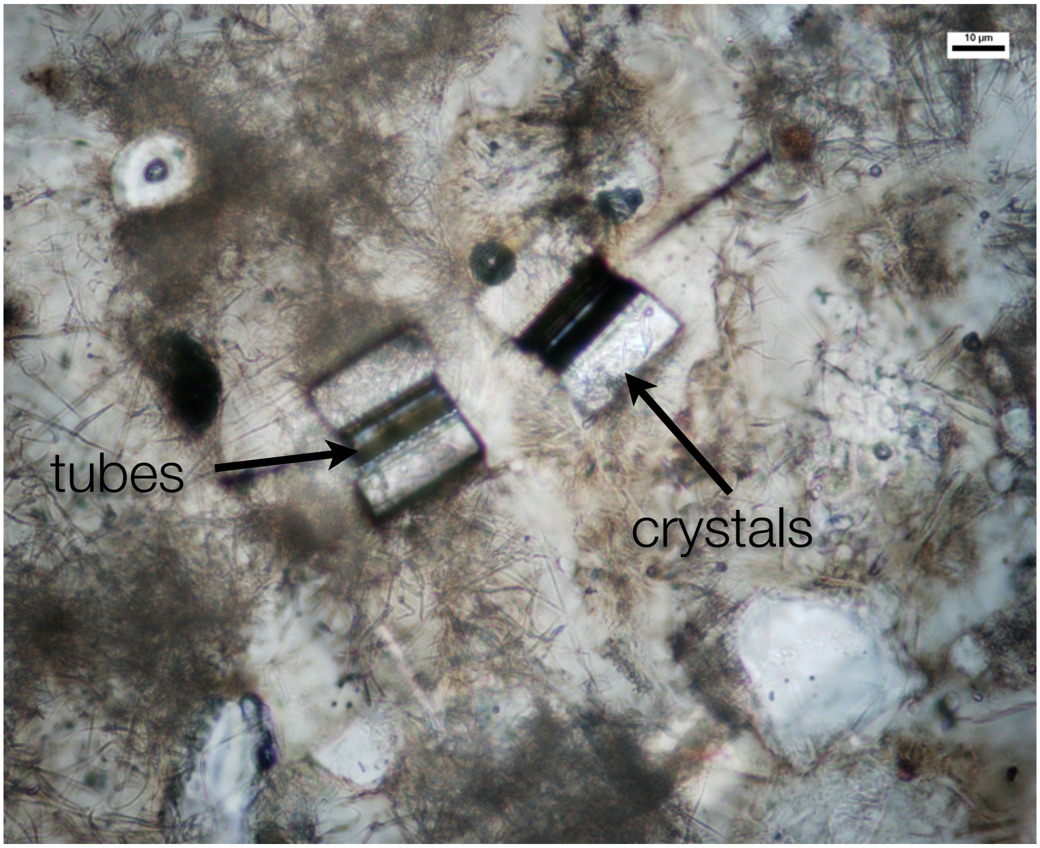

Figure 6.2: Proximity of crystallites and tubule features.

Plane polarized light micrograph indication the location of FIB foils in sample A. Note the proximity of sample A1 (crystallites) and sample A2 (tubes). Sample RI_10_006).

6.3.3 Scanning Transmission X-ray Microscopy (STXM)

STXM observations and near-edge X-ray absorption fine structure (NEXAFS) spectroscopy were preformed at the Canadian Light Source on the Soft X-ray Spectromicroscopy (SM) beamline (10ID-1) under the guidance of the beamline scientists following the methods reviewed by Leung et al, 2010. The synchrotron storage ring operates at 2.9 GeV with a maximum stored electron current of 300 mA. The 10ID-1 beamline uses a 75 mm generalized Apple II Elliptically Polarizing Undulator (EPU) source and STXM observations were conducted at a flux of $\sim 10^8$ ph/s in 30 nm spot normalized at 100 mA. A 250 l/mm grating and 35 μm vertical and horizontal exit slits were used for carbon imaging and spectroscopy. A 500 l/mm grating and 9 μm vertical and horizontal exit slits were used for iron imaging and spectroscopy. Energy calibration was accomplished using the 3p Rydberg peak at 294.96 eV of gaseous CO_2 for the C K-edge (Ma *et al.* 1991) and reference $FeCl_2$ and $FeCl_3$ spectra (Hitchcock, A. P., Per. Comm.) for the Fe $L_{2,3}$ -edges. NEXAFS data was collected over an energy range of 280 – 320 eV for the C K-edge and 700 – 730 eV for the Fe $L_{2,3}$ -edges. NEXAFS stacks were aligned using the Jacobson algorithm (Jacobsen *et al.* 2000) and data was analyzed using the aXis2000 software package (Hitchcock 2000).

6.3.4 Transmission Electron Microscopy (TEM)

The FIB foils were characterized in bright field mode and in selected area diffraction mode with a Philips CM200 TEM equipped with an AMT XR41B CCD camera system and an EDAX Genesis energy dispersive X-ray spectroscopy system (EDS) at an accelerating voltage of 200 kV. Transmission electron microscopy, energy dispersive X-ray spectroscopy and electron diffraction analyses were conducted at McGill University.

6.4 Results

6.4.1 Transmission electron microscopy

Transmission electron microscopy and EDXS analyses showed that the matrix impact glass is extremely heterogeneous both texturally and chemically on a micron to sub-micron scale. The character of the matrix glass is distinct between all four samples.

Matrix glass in sample A showed the least variability and largest degree of amorphous character. All EDXS spectra show the presence of the Cu Kα peak from the Cu TEM mount. The Ga L and K emission lines are also present in some EDX spectra revealing the presence of Ga^{+} ions implanted during FIB milling.

6.4.1.1 Sample A1: crystallites

Five glassy areas were selected for electron diffraction in sample A1 and four of these areas were also analyzed by EDXS (Fig. 6.3). The crystallites are hosted in amorphous glass as indicated by the presence of diffuse diffraction rings and general lack of spots on electron diffraction patterns (Fig. 6.3B). The glass is composed of primarily Si, O, Fe and Al as determined by EDXS. There are minor amounts of Ca, K, Na and Mg (Fig. 6.3C).

The crystallites themselves have skeletal morphologies, are mottled to streaky in appearance, and have sharp margins at the crystal/glass boundary (Fig. 6.3A, D, G, J). Crystals are elongate varying from ~500 nm to >5 µm in length and <100 nm to ~700 nm in width. Crystal faces are straight and are geometrically controlled (Fig. 6.3D, G). They are composed of numerous smaller crystal segments that are stacked along the long axis of the crystallite (Fig. 6.3D, G) .Individual crystals commonly intersect. Four separate crystals were selected for EDXS analyses and electron diffraction (Fig. 6.3D – L). Chemical composition is remarkably homogeneous between the crystals, dominantly Si, O, Mg, Al, Fe and subordinate K (Fig. 6.3E, H, K).

Electron diffraction analyses and EDXS analyses suggest that the crystallites are similar in composition and structure to the clinopyroxene augite. Electron diffraction analysis of the elongated crystallite in Figure 6.3D clearly shows the families of the {010} planes and also what seems to be the {001} planes (Fig. 6.3F). The *d*-value of 4.11 Å for the {001} plane is smaller than the value of the reference augite (*d*= 5.06 Å; PDF#41-1483; Table 6.1).

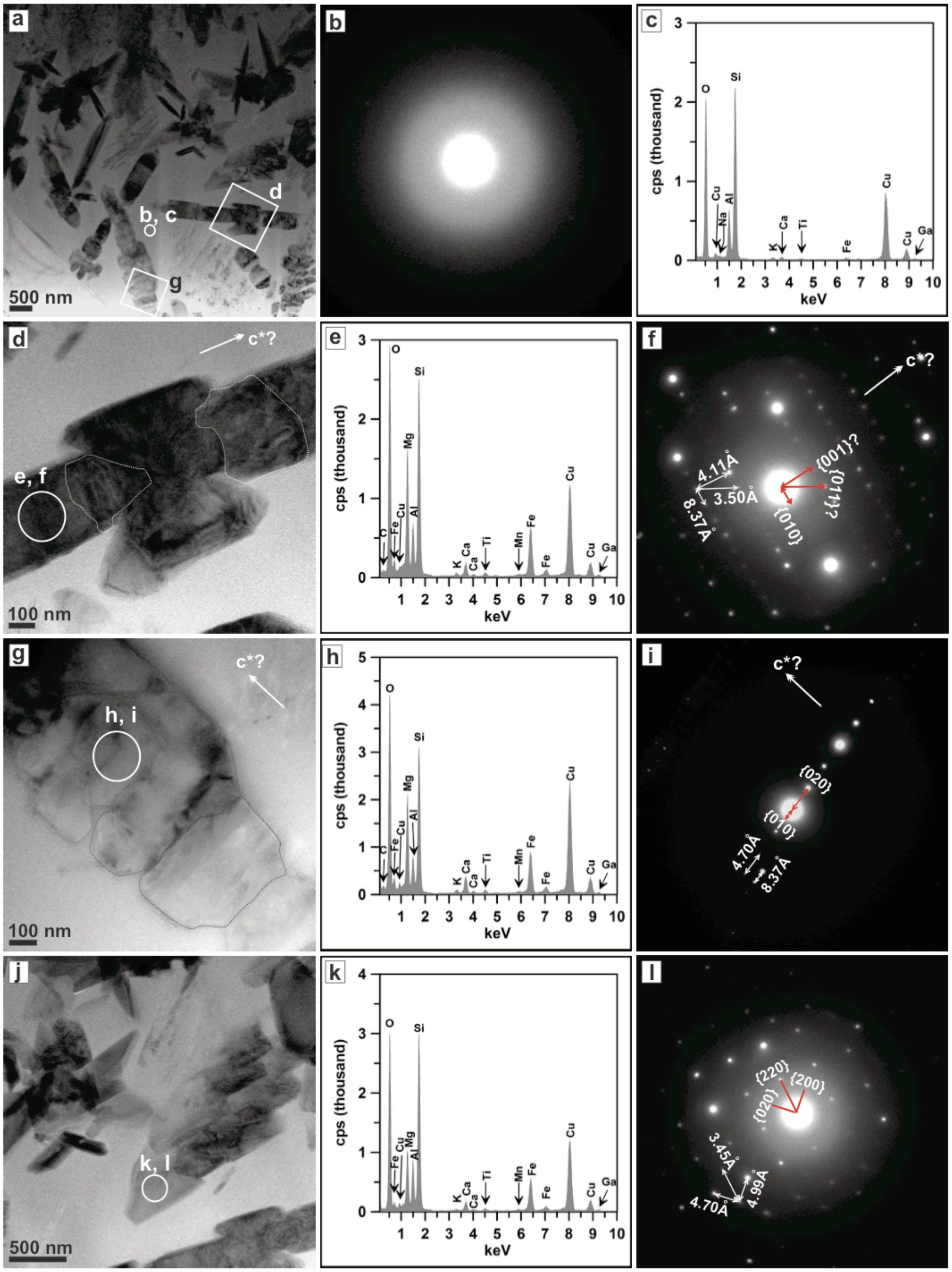

Figure 6.3: Sample A1: crystallites.

Transmission electron microscopy images (a, d, g, j); EDX analyses (c, e, h, k,) and electron diffraction analyses (b, f, i, l) of selected quench crystallites from sample A1.

6.4.1.2 Sample A2: solid tubule features

The glassy matrix of sample A2 displays two distinct textures (Fig. 6.4, 6.7). The matrix surrounding the crystallites and tubules is amorphous as indicated by the presence of diffuse diffraction rings in the electron diffraction patterns and complete lack of spots (Fig. 6.4B). The matrix distal to crystallites and tubules is densely populated with sub rounded, elongate octahedral, micro-crystallites ranging from ~1 nm to ~100 nm in diameter (Fig. 6.4A, D). The electron diffraction pattern is indicative of poorly crystalline material (Fig. 6.4E). EDXS analyses of the matrix glass indicate a predominance of Si, O, and Al as well as minor amounts Ca, K, Ti, and Fe (Fig. 6.4F). This composition is similar to the glass that surrounds the quenched crystallites in sample *A1* (Fig. 6.3C). There are two morphologically distinct types of larger (> 500 nm) features: several irregular, sub rounded, subhedral crystallites composed of multiple crystal domains (black arrows in Fig. 6.7 A, B, and C) and one tubule visible as an elongate (~ 2 μm X 200 nm) structure (Fig. 6.7 A, B, C).

The elongate feature has smooth, straight edges and sharp contacts with the amorphous matrix (Fig. 6.7 A, C). These features appear to be composed of multiple stacked 50 to 80 nm wide plates aligned along the long axis of the elongated feature (Fig. 6.7C). There is a poorly resolved, poorly crystalline, interstitial phase visible between the stacked platelets, becoming densest in the centre of the elongate feature (Fig. 6.7B, C)

There is a large (~ 1μm x 1.5μm) crystallite visible to the right of the elongated feature in Figure 6.7A. The EDX spectrum of the larger crystallites is dominated by Si and O with Mg, Al, Fe, Ca, and minor Ti and Mn (Fig. 6.4H, I).

Crystallographic axes of the visible crystal domains were determined by electron diffraction structure analyses of both the large crystallite and the elongate feature. Axes {020} (a-axis) and {300} (b-axis) form the crystallographic plane of the large crystallite shown in Fig. 6.7B and have *d*-spacing of 4.4Å and 2.8Å respectively (Fig. 6.7B inset). Axes {001} and {110} were determined for the elongate feature with *d*-spacing of 4.9Å and 6.1Å, respectively (Fig. 6.7C inset). The platelets are aligned along the *c*-axis corresponding to the long axis of the tubule.

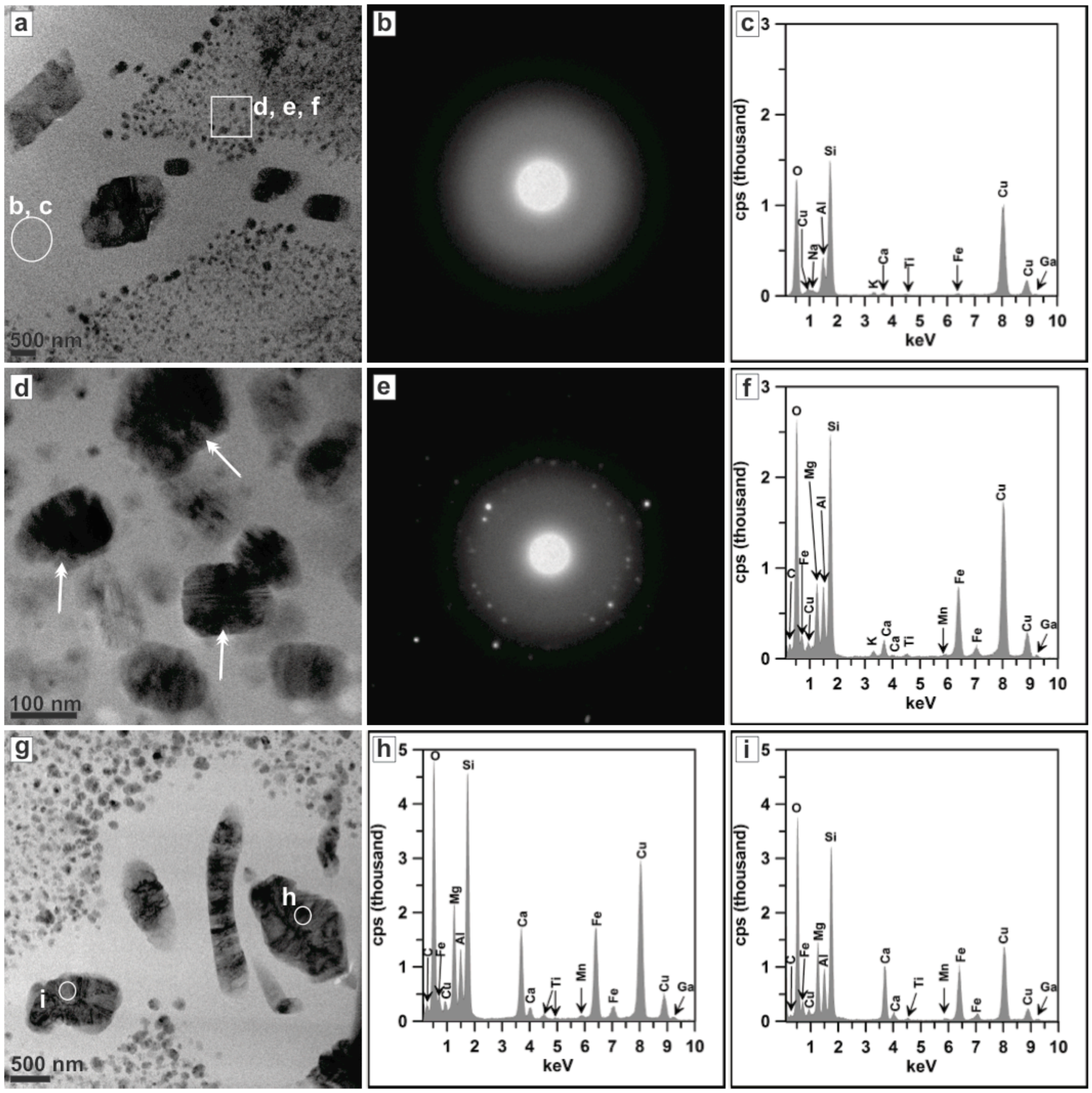

Figure 6.4: Sample A2: solid tubules.

Transmission electron microscopy images, diffraction patterns and energy dispersive spectroscopy of sample A2. A: overview. B: diffraction pattern of matrix area 'c' in panel a. C: EDX spectrum of matrix spot c in a. D: crystallites in matrix. E: diffraction pattern for matrix area 'e' in panel a F: EDX spectrum of matrix spot 'f' in panel a. G: elongate features and large crystals. H: EDX spectrum for crystal 'h' in panel g. I: EDX spectrum for crystal 'i' in panel g.

6.4.1.3 Sample B1: solid tubules

The matrix of sample B1 has been completely replaced by clay minerals and has a fibrous appearance with abundant void spaces giving a porous texture (Fig. 6.5). Clay mineral packets and void spaces are on the order of several hundreds of nanometers with nanometer scale crystallites diffusely scattered throughout the matrix. Sample B1 displays the most heterogeneity in matrix composition and texture. Nanometre scale microcrystallites are finely disseminated throughout the FIB foil (Fig. 6.5A, B, D, G). Microcrystallites may be blocky, elongate or skeletal in shape (Fig. 6.5G, H). A linear ~700nm wide grey strip of glassy material is amorphous and also contains blocky microcrystallites (Fig. 6.5A, B). Electron diffraction patterns of the clay matrix are suggestive of poorly crystalline material (Fig. 6.5E). EDXS analysis of both the amorphous glass and clay indicate they are very similar in composition composed dominantly of Si and O with minor Fe, Al and Ca (Fig. 6.5C, F).

The tubular features in sample B2 are solid, approximately 500nm in diameter and are visible in both horizontal and vertical cross-section. The tubules have irregular 'saw-tooth' like margins and are composed of multiple crystallographic domains (Fig. 6.7D, E, F). In longitudinal cross section the edges of the tubules are composed of subhedral, triangle shaped crystals pointed inwards roughly 100 nm at the widest point (Fig. 6.5A, 7E, F). The central portion of the tubules is composed of a poorly crystalline, fine grained material that cannot be fully resolved but seems to be of similar chemical composition to the triangle shaped crystals along the outer margin (Fig. 6.7E; white arrow). EDS spectra of the tubules are dominated by Si and O with Mg, Al, Ca, Fe and minor Ti (Fig. 6.5I).

X-ray diffraction structure analysis identified the {001}, {011}, and {010} families with *d*-values of 5.06 Å, 4.22 Å, and 7.9 Å respectively. Similarly to the elongate features in samples A2 and B1, the features in sample B2 are elongated along the c-axis. Despite the appearance of multiple crystal domains, electron diffraction patterns are suggestive of a single crystal that is due to the almost perfect alignment of the crystal platelets along the *c*-axis (Fig. 6.7D; insert).

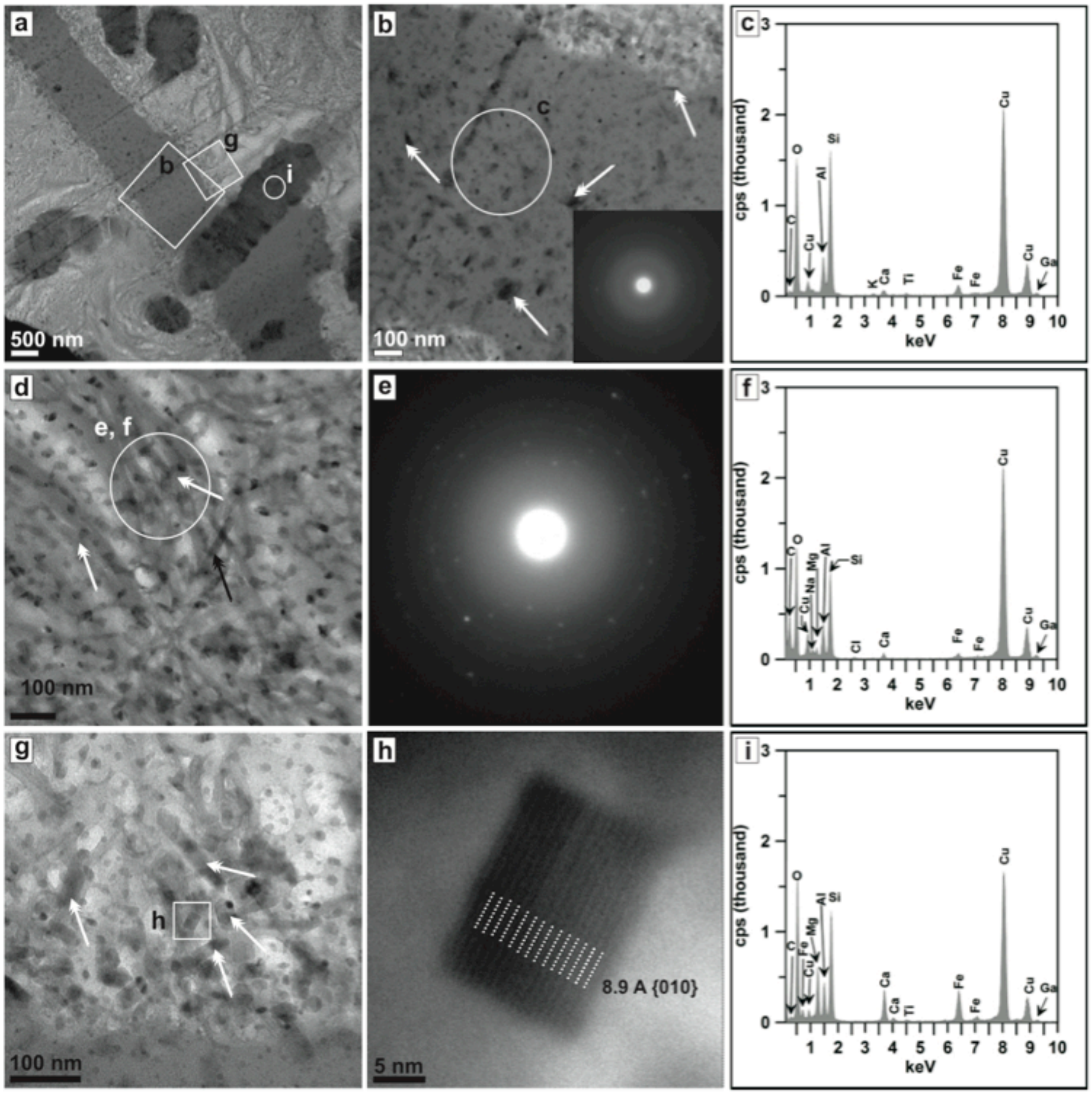

Figure 6.5: Sample B1: solid tubules.

Transmission electron microscopy images, diffraction patterns and energy dispersive spectroscopy of sample B1. A: overview. B: amorphous glass strip and corresponding diffraction pattern. C: EDX spectrum for glass strip in ‘c’. D: clay minerals in matrix. E: diffraction pattern for matrix ‘e’. F: EDX spectrum for matrix ‘f’. G: crystallites in matrix. H: close of crystallite in g showing lattice fringes. I: EDX spectrum of tubule ‘I’ in panel A.

6.4.1.4 Sample B2: Hollow tubules

The matrix is mainly altered clay minerals similar in appearance to sample B1. Clay mineral packets and void spaces are on the order of several hundreds of nanometers (Fig. 6.6A, C, H). Nano-meter scale crystallites are diffusely scattered throughout the matrix (Fig. 6.6A). The electron diffraction patterns of the matrix are indicative of poorly crystalline material (Fig. 6.6B). EDX spectra of the matrix are dominated by Si and O peaks with minor Al, Mg and Fe peaks (Fig. 6.6D, E).

Multiple hollow tubules are present in sample B2 both in longitudinal and horizontal cross section (Fig. 6.7G, H). The tubules have a remarkably consistent diameter of ~500 μm and are round to octagonal in horizontal cross section. They appear to be aggregates of 50 – 80 nm wide ring-like sections aligned along the long axis of the tubules. The margins of the tubules have a blunted 'saw tooth' texture (Fig. 6.7I). Each 'ring' appears to be an aggregate of multiple crystallites similar to those described in sample A2. The interior margins of the tubules are highly irregular and composed of massive poorly resolved fine-grained material (Fig. 6.7G, H, I, K; white arrows). The chemical composition of the tubular features is consistent across 6 EDXS analyses: dominant Si, O; subordinate Fe, Mg, Al and Ca (Fig. 6.6F, G, K). An EDX spectrum was also taken from the material within the centre of the hollow tubules (Fig. 6.6J). The material within the tubules is also dominated by Si and O with Mg, Al, Ca and Fe. The P Kα peak was also detected within the tubules (Fig. 6.6F, G).

X-ray diffraction structural analysis was able to identify the {001}, {110}, and {020} families with corresponding *d*-spacings of 4.9Å, 6.0Å, and 4.4Å respectively (Fig. 6.7J, K). High-resolution TEM images taken from the edge of horizontal cross-sections in figure 6.7k (white arrow) show two sets of lattice fringes: the {110} family with a *d*-value of ~6.2 Å and the {020} family with a *d*-value of ~4.4 Å. Interestingly, despite the obvious multi-crystal appearance to the tubule features, electron diffraction patterns of horizontal cross-sections are indicative of a single crystal (insert Fig. 6.7K). This can be partially explained by the perfect alignment/stacking of the crystal platelets along the *c*-axis.

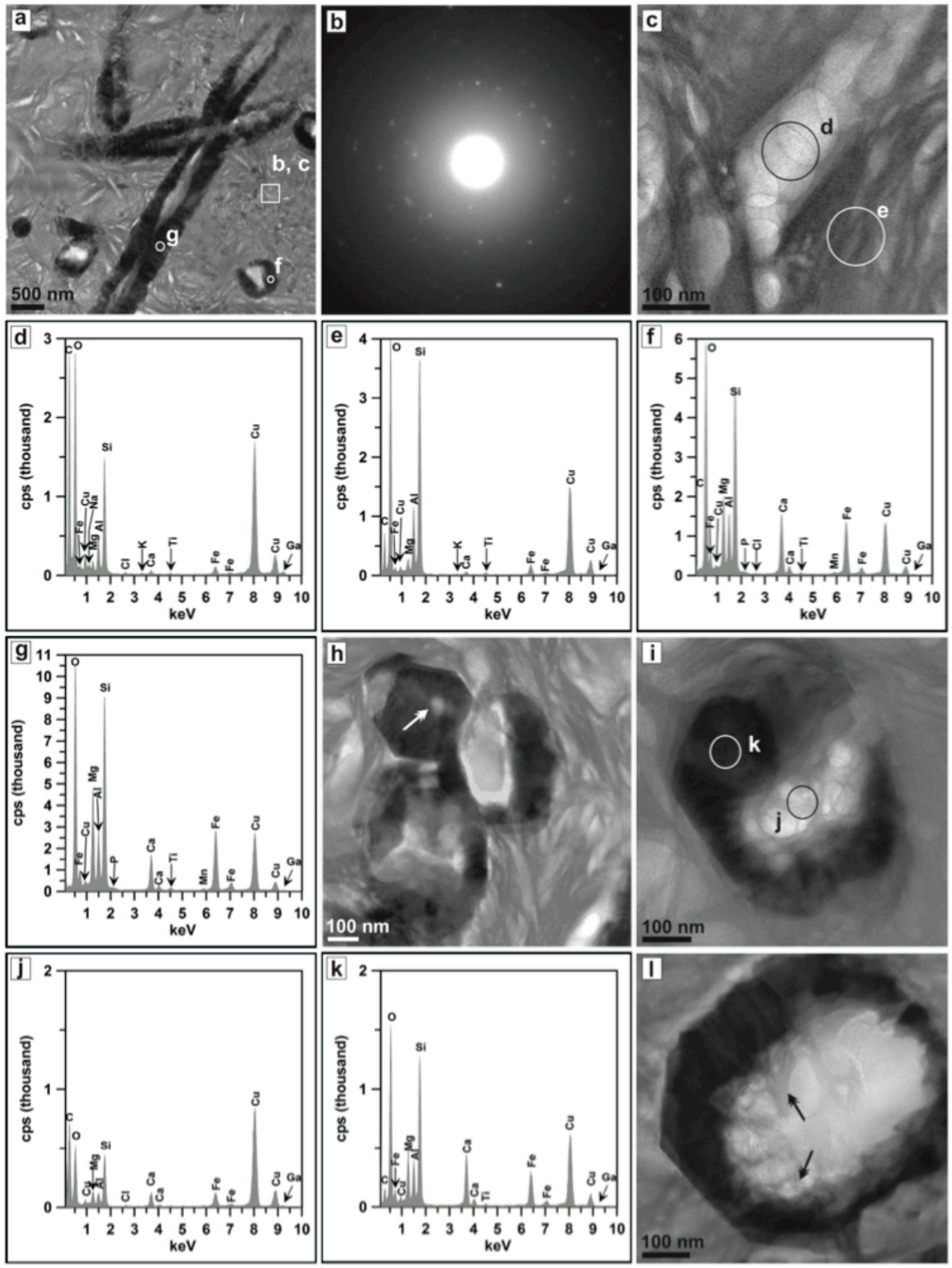

Figure 6.6: Sample B2: hollow tubules.

Transmission electron microscopy images, diffraction patterns and energy dispersive spectroscopy of sample A2. a: overview. b: diffraction of clay matrix. c: close up of clay matrix. d: EDX of C-rich space between clay minerals. e: EDX of clay minerals. f: EDX of tubule. g: EDX of tubule. h: group of tubules with different degree of alteration (see arrow for small hole). i: altered tubule. j: EDX of C-rich tubule filling. k: EDX of tubule. l: altered tubule in which we have a clay mineral (smectite)

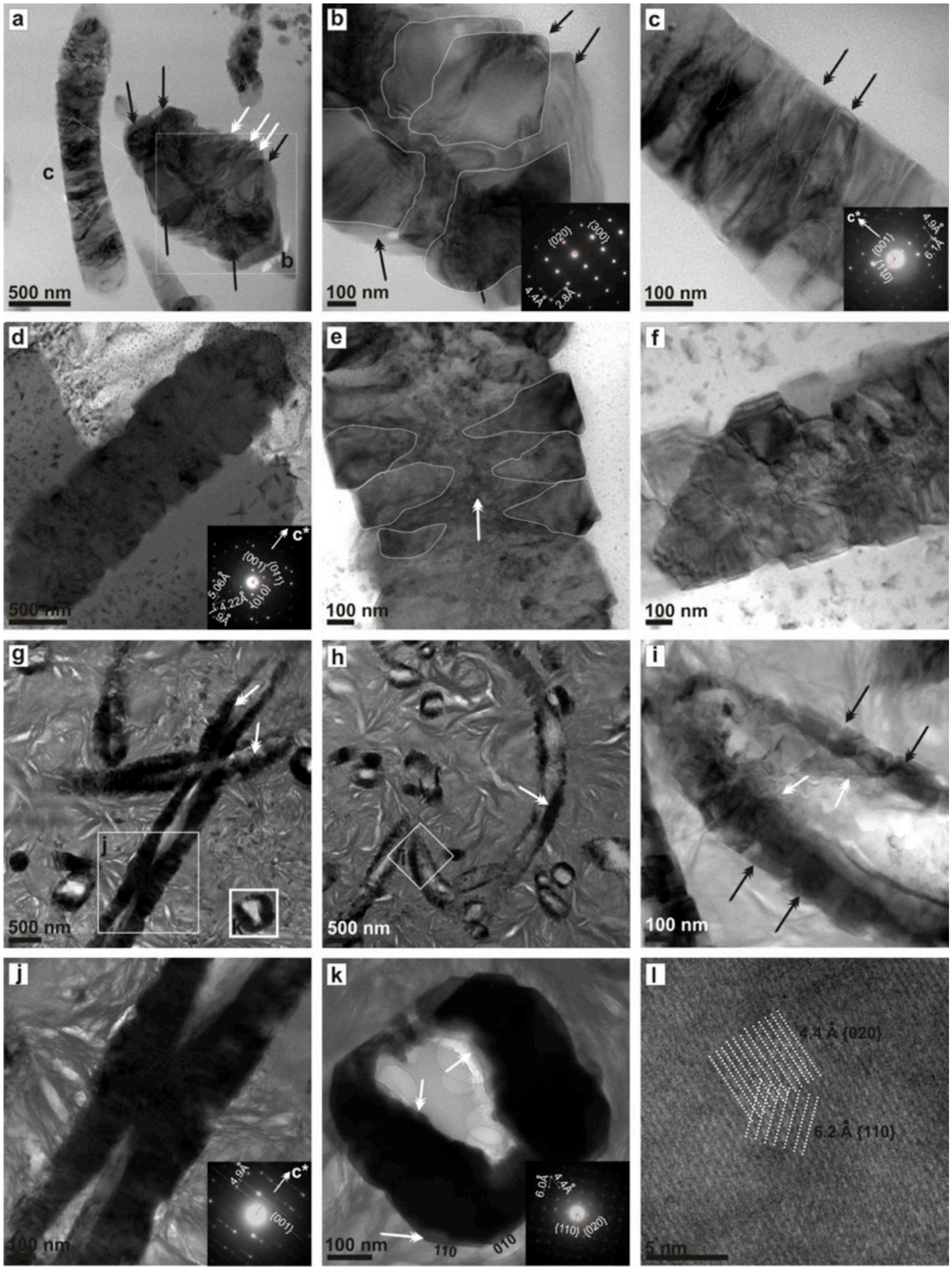

Figure 6.7: Transmission electron microscopy images of tubule features.

Transmission electron microscopy images and diffraction patterns of tubules in samples A2, B1, B2. A – C: sample A2. D – F: sample B1. G – I: sample B2.

Table 6-1: Comparison of *d*-values.

Comparison between *d*-values determined experimentally for tubule features and crystallites (this study) with published values for augite.

PDF#41-1483, Augite, aluminian, Paskapole, Czech Rep.		**A1 crystallites, A2 solid tubules, B1 solid tubules:** values obtained from measurements on electron diffraction patterns		**B2 hollow tubules:** values obtained from lattice fringe measurements on the particle in Fig. 6.7 K		matrix crystals Fig. 6.5 H	
(hkl)	d(Å)	d(Å)	Ø d(Å)	d(Å)	Ø d(Å)	d(Å)	Ø d(Å)
(100)	9.3534						
(200)	4.6767						
(300)	3.1178	2.7826	**2.7826**				
(600)*	1.5589*						
(010)	8.8934	8.7619, 8.3636, 8.0000, 8.0843, 7.8597, 7.6666	**8.1227**			9.1670, 8.9230, 8.8660, 8.8290	**8.9462**
(020)*	4.4467*	4.4356, 4.3495, 4.2199	**4.3350**	4.5500, 4.5496, 4.5289, 4.4712, 4.4441, 4.3907, 4.4359, 4.1680, 4.1300, 4.0886	**4.3757**		
(001)	5.0628	5.0592, 4.9230	**4.9911**				
(002)*	2.5314*						
(110)	6.4446	6.4000, 6.2439, 6.1279, 6.0377, 6.0000, 5.9385, 5.9381, 5.9078	**6.0742**	6.4194, 6.3979, 6.2194, 6.1469, 6.1307, 6.0501, 5.9766, 5.9750, 5.9657, 5.9228, 5.9056, 5.8800, 5.8357, 5.6863	**6.0366**		
(220)*	3.2223*						
(011)	4.3998	4.2197	**4.2197**				
(022)*	2.1999*						

(hkl)* data obtained from PDF#41-1483, aluminian augite; all other (hkl) are calculated from these values

6.4.2 STXM Analysis

Near edge X-ray absorption fine structure (NEXAFS) spectroscopy was completed on all four samples at the Fe L_3 -edges and the C K-edge. NEXAFS spectroscopy provides constraints on the speciation and the molecular configuration of the absorbing atom as the absolute edge energy and near edge fine structure oscillations are sensitive to the oxidation state and the average local bonding geometry respectively (*e.g.*, Myneni 2002).

6.4.2.1 Iron L_3-edge

Spectral composition maps (Fig. 6.9) were calculated for each sample using a combination of forward fitting of internal NEXAFS spectra and iron-chloride reference spectra with the singular value decomposition algorithm available in aXis2000 [Ref]. Three distinct spectral components indicative of differing Fe oxidation are identified based on the ratio of the 707.8 eV and 709.5 eV peaks at the Fe L_3-edge (Crocombetter *et al.* 1995). Based on relative units of optical density, the matrix of all samples has relatively low concentrations of Fe compared to the tubules and crystallites. The matrix of all four samples is the most oxidized component with spectra exhibiting peaks of comparable intensity at both 707.8 eV and 709.5 eV indicative of partial iron oxidation. NEXAFS spectra of the tubules (A2, B1, B2) are dominated by a major peak at 707.8 eV characteristic of reduced iron indicating that $Fe2^{+}$ largely dominates the iron in the tubules. Tubular cores or centres are intermediate in character: oxidized relative to tubular margins, but contain a higher reduced component than the matrix. Tubular margins (hollow tubule wall, B2; edges of solid tubules, A2) have a major 707.8 eV peak and with a minor 709.5 eV component indicating a highly reduced Fe character with a minimal oxidized component. The high resolution mapping of sample B1 shows the presence of a fourth phase rimming the tubules reduced relative to the matrix and tubule centres but oxidized in comparison to the bulk of the tubule. The crystallites in sample A1 did not display any zoning with respect to Fe oxidation state and therefore no patterns of Fe speciation are present. The crystallites are either of reduced Fe- or intermediate Fe character relative to the matrix with no internal zonation.

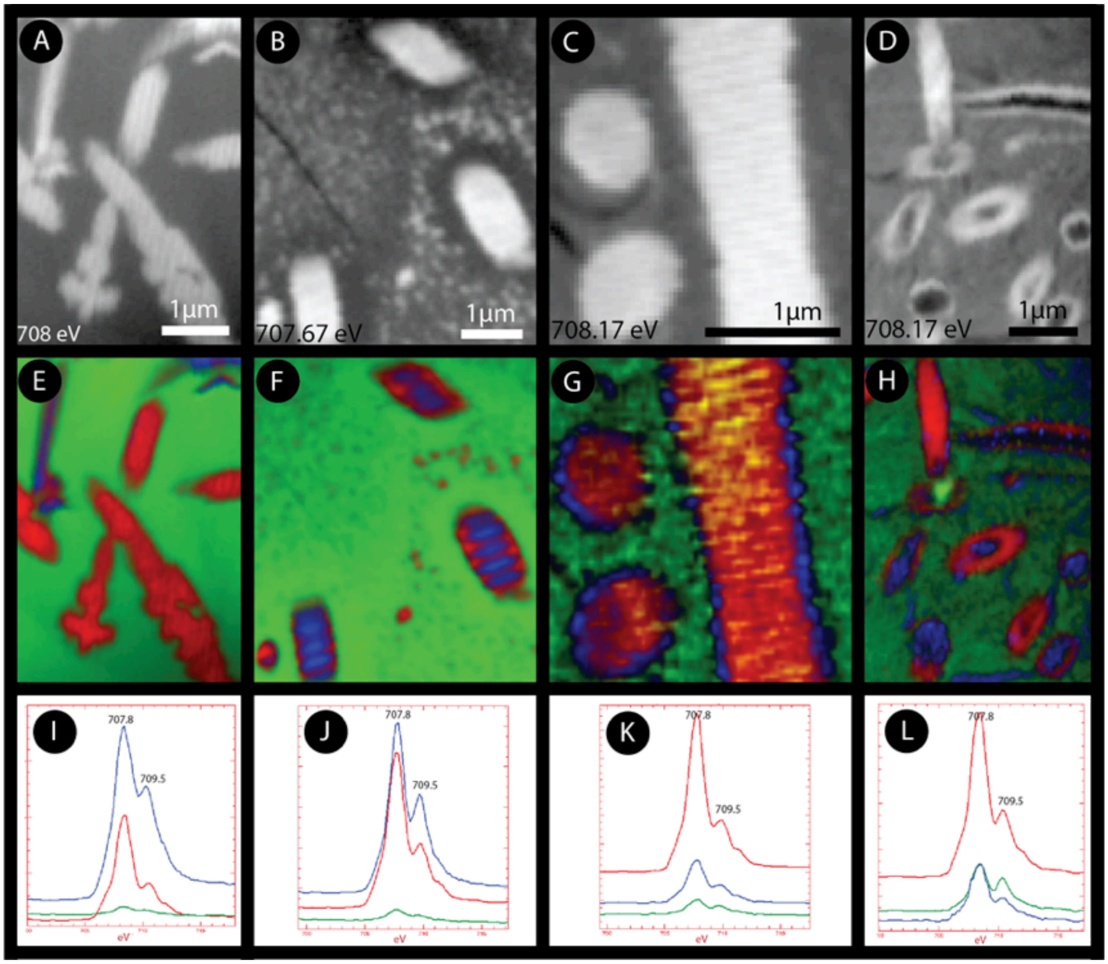

Figure 6.8: STXM Fe L_3-edge analysis.

Scanning transmission microscopy images (A – D) and Fe L_3-edge NEXAFS spectral composition maps (E – H) based on forward fitting of internal spectra (I – L). A, E, I sample A1. B, F, J sample A2. C, G, K sample B1. D, H, L samples B2.

6.4.2.2 Carbon K-edge

Spectral features associated with various organic carbon species are present in all tubule samples (A2, B1, 2) and absent in the sample containing only crystallites (A1). The 285 eV feature consistent with aromatic groups (284.9 eV – 285.5 eV π*C=C; (Myneni 2002) and refs therein) is the most prominent in all three tubule samples. There is also a 288 eV peak interpreted to result from the 1s-π* transition of C=O in carboxylic acids and/or ketones (Myneni 2002 and refs therein). Spectral components were fit to the NEXAFS stacks using the singular value decomposition algorithm in aXis2000 (Hitchcock 2006) based on forward fitting of internal spectra following identification of discrete spectral components (Fig. 6.9).

6.4.2.2.1 Sample A2: solid tubules

Very similar organic components are identified in the matrix and tubules characterized by a dominant peak at 288.7 eV and subordinate peaks at 283.7 eV and 285.4 eV. The tubule spectra are defined by more intense 288.7 eV and 285.4 peaks relative to those peaks in spectra derived from the matrix. Organic carbon spectra derived from a crack is unique and characterized by a dominant 285.4 eV peak and subordinate 288.7 eV peak (Fig. 6.9A, D, G).

6.4.2.2.2 Sample B1: solid tubules

Spectra derived from the tubules in sample B1 are dominated by artefacts due to higher order interference and an organic component cannot be discerned. Two distinct organic components are derived from the matrix with a dominant 285.1 eV peak and subordinate 287.5 eV and 288.6 eV peaks. The spectra are distinguished by their optical density and the relative prominence of the 285.1 eV peak. A 290.6 eV peak, indicative of carbonate, is also identified in the matrix spectra (Fig. 6.9B, E, H).

6.4.2.2.3 Sample B2: hollow tubules

Similar to the features in sample A2, the spectra derived from the tubules are dominated by higher order artefacts. Two distinct organic spectral components are distinguished in the matrix most strongly associated with the interior of the tubules. A peak at 285.2 eV dominates one organic component. The second component also has a dominant peak at 285.2 but also contains peaks of similar intensity at 288.7 eV and 290.1 eV (Fig. 6.9C, F, I).

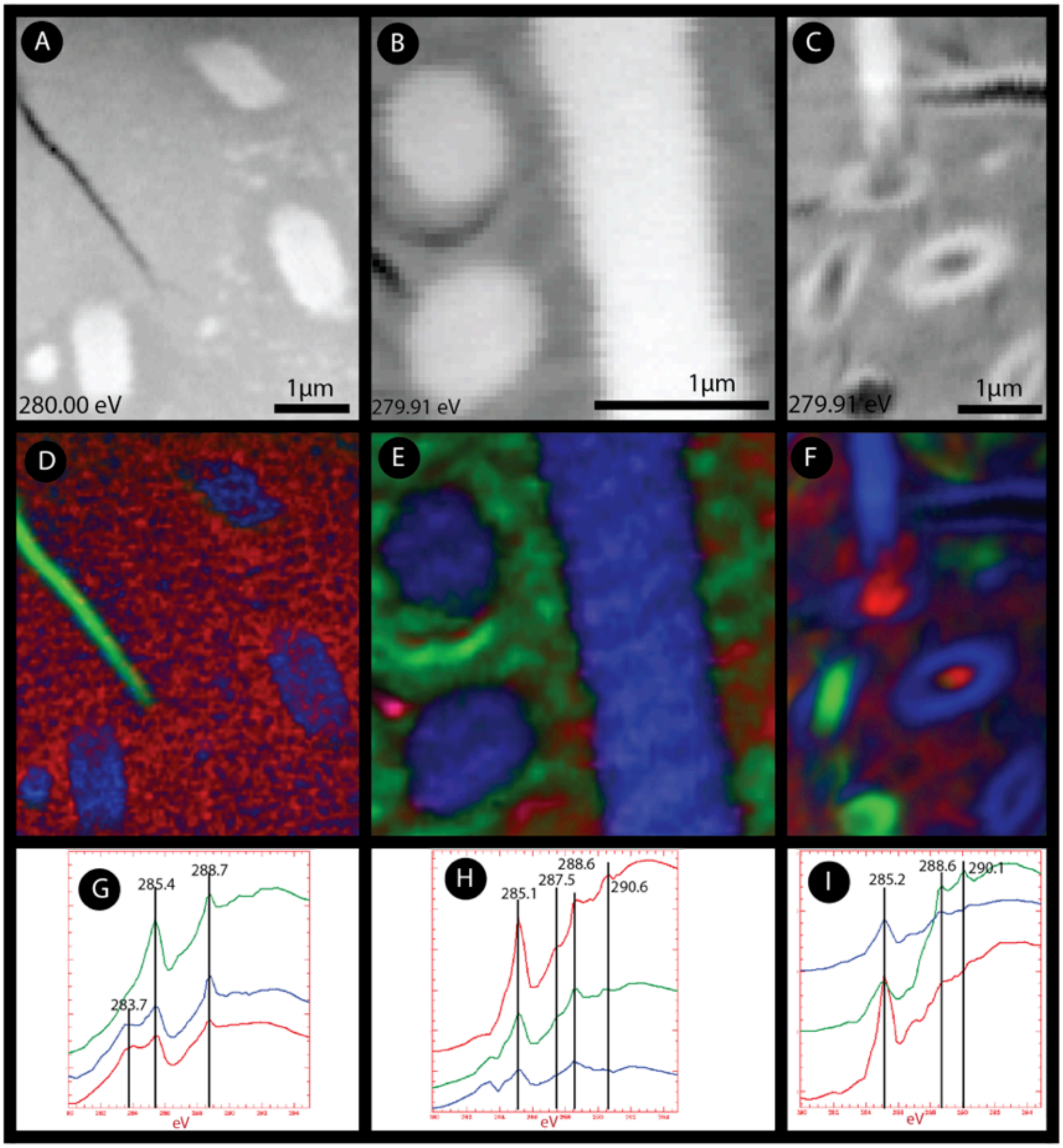

Figure 6.9: STXM C K-edge analysis.

Scanning transmission microscopy images (A – C) and C K-edge NEXAFS spectral composition maps (D – F) based on forward fitting of internal spectra (G – I). A, D, G sample A2. B, E, H sample B1. C, F, I sample B2.

6.5 Discussion

6.5.1 Biogenicity of the Ries tubules

Microbial alteration textures observed in submarine basaltic glasses are interpreted to have formed by microorganisms via local dissolution as they extract bio-essential elements (Staudigel *et al.* 2006, 2008b; McLoughlin *et al.* 2010) from the glass. Many elements present in natural glasses, including the Ries impact glasses, are essential macro and micronutrients (Banerjee & Muehlenbachs 2003; Staudigel *et al.* 2006, 2008a; Benzerara *et al.* 2007; Banerjee *et al.* 2008). The leaching of these bioessential elements from the glass alters the chemistry of the surrounding glass. Furthermore, as elements are actively or passively accumulated, mineral precipitates are commonly formed. These biogenic minerals typically have a mineralogical structure distinct from their abiotic counterparts (McLoughlin *et al.* 2007). The high-resolution techniques implemented in this study have shown the structure of the tubule features to be unlike any known abiotic mineral. In addition, NEXAFS spectroscopy at the C K-edge has found organic matter spatially associated with the tubule features. Both of these findings support a biogenic origin of the tubules.

High-resolution TEM imaging reveals four morphologically distinct features: 1) skeletal quench crystallites (sample A1, Fig. 6.3A, D, G, J); 2) matrix microcrystallites (samples A1, A2, B1, B2; Fig. 6.4A, D, G; Fig. 6.5B, D, G, H); 3) large crystals (sample A2, Fig.6.7A, B); and 4) elongate features comprising the Ries tubules (samples A2, B1, B2; Fig. 6.4G; Fig. 6.5A; Fig. 6.6A, Fig. 6.7A, C, D, E, F, G, H, I, J). As illustrated by high-resolution TEM, the elongate features (tubules) and abiotic crystalline features are morphologically distinct. The matrix microcrystallites are likely formed through quenching mechanisms, incipient re-crystallization of the impact glass, or devitrification mechanisms. Discerning the crystallization mechanism of the matrix microcrystallites is beyond the scope of the current study.

The patterns of Fe speciation as revealed by NEXAFS spectroscopy (Fig. 6.8) are suggestive of biomineralization. Metal-encrusted cell surfaces forming a class of bacterial microfossils through biomineralization are formed through accumulation of metabolic by-products (*e.g.*, Southam and Donald 1999). *Gallionella sp.* and *Leptothrix sp.* both common in marine hydrothermal settings are known to form iron oxide filaments and sheaths encasing the cells (Fortin, 2007 and refs therein). *Shewanella,* and iron reducing bacteria, forms Fe(II) granules during anaerobic respiration that accumulate and adhere to the cell wall eventually encasing the cell in reduced iron (Fortin *et al.* 2008 and references therein). The oxidized tubule centres suggest that the solid tubules were initially hollow with reduced iron walls and subsequently filled with an oxidized authigenic mineral phase during extended hydrothermal alteration. As the A2 tubules and A1 crystallites were subject to the same post-impact conditions, alteration and weathering are discounted as an explanation for the patterns of Fe speciation present in the tubules. Furthermore, the highly reduced character of the tubules discounts oxidation induced during ion beam milling.

NEXAFS carbon spectromicroscopy allows for direct chemical characterization of untreated natural samples at nanometer resolution. Information regarding the local coordination environment of carbon atoms can then be used to infer the presence of specific carbon functional groups in organic molecules (Myneni 2002). Spectral peaks indicative of various organic molecules including alkanes, aromatics, and carboxillic acids/ketones are spatially associated with the tubules. Organic spectra were not derived from areas hosting only crystallites. Samples A1 (crystallites) and A2 (tubules) are from the same sample occurring only microns from each other. The proximity of the features makes contamination and discrepancies in matrix composition highly unlikely. Furthermore, the organic spectra derived from a crack in sample A2 is distinct from all of the organic spectra derived from the samples indicating distinct sources.

The hollow tubules (B2) are associated with the highest concentrations of organic matter while an organic component could not be detected in spectra from the solid tubules in sample A1. The observation that not all of the hollow tubules are associated with organic material suggests that the presence of organic material in the tubule centres is not due to passive accumulation of material. The variation in the concentration of organic matter is likely do to mineralization and preservation. Samples B1 and B2 exhibited higher degrees of hydrothermal alteration suggesting much more extensive and/or longer lived hydrothermal actively. Biogenic tubule formation is constrained by the ability of fluids to remove metabolic waste products (*e.g.*, McLoughlin 2010). Once fluid circulation can no longer support biological activity, tubule formation ceases and the mineralization process begins (*e.g.*, McLoughlin 2010; Staudigel 2008a). Samples B1 and B2 likely experience a longer duration of tubule formation. In samples A1 and A2, the tubules are completely mineralized and very little (A2) or no (A1) organic matter is preserved. The taphonomical continuum from hollow to solid tubules resulting from stages of mineralization and preservation is supported by TEM observations.

6.5.2 Tubule mineralization and preservation

The X-ray diffraction structure analyses of the elongate features in samples A2, B1, and B2 as well as the large crystallite in sample A2 consistently indicate the presence of the following families: {001} *d*-values ranging from 4.9Å – 5.06Å; {110} *d*-values ranging from 6.0Å – 6.2Å; and {0.20} *d*-value of 4.4Å (Table 6.1). Although the morphology of the elongate features is not consistent with any known pyroxene crystal habit, the EDX analyses suggest a chemical composition similar to augite. The *d*-values obtained from the electron diffraction patterns were compared with various *d*-values of pyroxene specimens from XRD databases and the closest match is to an aluminum rich augite from Panska, Czech Republic (PDF#41-1483). While several crystallographic families have been identified, it is clear by the single crystal diffraction patterns indicative of highly crystalline material, that the fine-grained, poorly crystalline phase interstitial to the crystal domains and filling the centre of the tubules is not represented in the XRD data. The complex intergrowth of the two-phase system implies the tubules were not formed through a simple crystallization process. The thickness of the FIB foils was optimized for NEXAFS at the Fe edge and precludes ultra-high resolution imaging of lattice fringes. Without lattice fringe measurements the augite-like mineral cannot be definitively identified.

The post-impact hydrothermal alteration of the Ries impact structure affecting the glass-bearing breccias outside the crater rim was characterized by low-temperatures between <100 – 200^{o}C (Newsom *et al.* 1986; Osinski 2005). Based on the 24 km crater diameter, temperatures of ~ 60^{o}C could have been sustained for several tens of thousands of years

(Osinski *et al.* 2001). These low temperatures are inconsistent with hydrothermal pyroxene growth suggesting that the mineral(s) phase(s) composing the large crystals and tubules are either not a canonical pyroxene or are quench crystallites formed during the initial cooling and quenching of the impact glass at high temperatures. The latter theory is discounted due to the unique and well-characterized morphologies displayed by quench crystallites. Quench crystallites form under out of equilibrium conditions during quenching of a super-cooled melt phase and are typically dendritic and/or skeletal (Bryan, 1972; Lofgren 1974) such as the quench crystallites in sample A1. Neither the tubules nor the large crystallites display morphologies consistent with a quench origin. Furthermore, the presence of both canonical quench crystallites and the elongate features and large crystals within a 100μm^2 area necessitates separate formation mechanisms to account for both types of crystal morphologies in the same matrix glass. X-ray diffraction will produce prominent peaks for only highly crystalline material. TEM images clearly show the presence of an additional, poorly crystalline material complexly associated with the crystal domains in the tubular features (Fig. 6.7).

A detailed study of the hydrothermal system at the Ries constraining the fluid composition has not been completed; however, the composition of the larger crystallites and the tubules (this study) is consistent with hydrothermal mineralization of the host glass-bearing impact breccias. A number of hydrothermal alteration phases consistent with low-temperature (<100 – 200^{o}C) hydrothermal activity including clays, zeolites, quartz, calcite, hematite and goethite have been identified dominated by montmorillonite and Ba-phillipsite (Newsom *et al.* 1986; Osinski 2005). The co-occurrence of the morphologically distinct larger crystals and tubules in the same physical matrix (*e.g.*, Fig. 6.7A) logically implies distinct formation mechanisms despite the mineralogical similarity implied by consistent *d*-values (Table 1). The elongate morphology of the tubular features is not consistent with canonical crystal growth and is reminiscent of minerals templating a pre-existing tubular structure. If the minerals comprising the tubule features were formed through hydrothermal precipitation within a pre-existing structure, then this would explain the chemical and mineralogical similarities with the large crystals (sample A2, Fig. 6.7) also postulated to have formed through hydrothermal precipitation.

The consistency of the *d*-values suggests that the large crystals and solid tubules in sample A2, the solid tubules in samples B1 and the hollow tubules in sample B2 are composed of the same material in various states of alteration. The matrix of sample B2 displays the highest level of alteration while that of sample A2 the lowest degree of alteration. The morphology of the crystal domains comprising the solid tubules is reminiscent of void space with large, euhedral growth dominant crystals at the margins and fine-grained nucleation dominated crystal growth in the interior. The fine-grained, relatively oxidized interior of the tubules is likely a result of hydrothermal mineral precipitation. A three-stage formation mechanism for the tubules is proposed:

> **1) Microbial tunnelling:** Amorphous impact glass in samples A2, B1, and B2 were subject to microbial alteration as proposed by Staudigel *et al.* (2006) and summarized in McLoughlin *et al.* (2010), during the initial post-impact hydrothermal system. If these were iron-reducing micro-organisms as is suggested by the iron speciation patterns and by studies of initial microbial colonizing communities of terrestrial glasses then they likely left concentrations of reduced iron along the wall of the tubules as they tunnelled through the glass. Samples B1 and B2 experience more intense hydrothermal alteration due to the increased surface area exposed to circulating fluids and this initial phase of microbial alteration was of longer duration than in samples A1 and A2.
>
> **2) Tunnel formation cessation**: Eventually either the tubules would reach a length where passive fluid exchange would be insufficient to remove metabolic waste products (samples B1, B2), or the hydrothermal fluid circulation could not longer sustain tubule formation (samples A1, A2) resulting in the death of the micro-organisms and cessation of tubule formation. At this point mineralization of the tubules would begin, initially with deposits of reduced iron acting as nucleation sites along the tubule margins.
>
> **3) Mineralization:** Crystallization continued until space-limited and fine-grained aggregates of material sealed off the tubules. Following the cessation of the post-impact hydrothermal system, surficial weathering and meteoric water circulation

would become the dominant mode of alteration. Glass in samples B1 and B3 would be much more susceptible to surficial weathering due to the increased surface area exposed to the porous matrix of the glass-bearing breccia. Oxidized meteoric water circulation resulting in the observed patterns of iron oxidation at the interface between the tubules and matrix as observed in sample A1 (Fig. 6.7).

6.5.3 The impact structure as a microbial habitat

Recent work has shown that hydrothermal activity is commonplace in the immediate aftermath of an impact event on any H_2O-rich solid planetary surface (Naumov 2005). In an impact crater, impact-melted or -heated materials provide a transient source of heat in an otherwise cold environment. The interaction of water with these hot materials forms a hot rock-water circulatory system that can dissolve, transport, and precipitate various aqueous species (Osinski *et al.*, 2001). The chemical disequilibria characterizing post-impact hydrothermal systems are a source of metabolic energy for microorganisms. The Ries impact structure has an exceptionally well preserved post-impact hydrothermal system (Osinski, 2005).

6.5.4 Impactites as astrobiology targets

Impact events are the only ubiquitous geological process in the Solar System and impact structures represent the dominant geological landform amongst the majority of the terrestrial planets. The habitability of subaerial (Herrera *et al.* 2009) and submarine natural glasses (Mason *et al.* 2007 and references therein) suggests that impact glasses, such as those found at the Ries impact structure, are potential habitats for microorganisms. Given the probable ubiquity of impact glasses in post-impact environments throughout the Solar System, it is important to understand the biological components and potential of such systems. Establishing the biogenicity of the tubular structures observed in the Ries impact glasses has significant astrobiological implications. The high flux rate of meteorite impacts on the early Earth would favour life in endolithic (within rock) environments such as glassy substrates, furthermore, impact events would provide transient energy to terrestrial bodies without endogenous volcanic heat sources to drive hydrothermal activity, such as Mars. The endolithic environments resulting from impact events are important targets for astrobiological investigations of the early Earth and of other terrestrial planets such as Mars.

Understanding the geomicrobiology of impact craters on Earth is critical in furthering the search for life on Mars. The hydrothermal systems associated with impact events may therefore provide an additional setting to study evidence of early life on Earth. Further studies considering the potential hydrothermal habitats of impact craters may not only yield insight into early life and the origin of life on Earth, but furthermore, may comprise a potential habitat for life and past life on other terrestrial planets such as Mars.

The extreme conditions present on Mars, such as intense UV flux, low temperature, and absence of liquid water may encourage the exploitation of endolithic strategies. Banerjee LPSC 2004 McLoughlin *et al.* (2007, 2010) suggest microborings into volcanic glasses as a potential planetary biosignature and lists natural glasses as one of the most promising preservation environments for ichnofossils on early Earth and Mars. By extending this to impact glasses we greatly increase the number of candidate environments.

6.6 Acknowledgements

We gratefully acknowledge Mike Phaneuf, Dave Mayer and Fibics Inc. for the FIB lift-out expertise and FIB foil preparation. We also thank Chithra Karunakaran, Jian Wang, Jay Dynes and all of the beamline staff at the Canadian Light Source. We are thankful to Adam Hitchcock for analytical assistance and discussion and to Martian Obst for technical assistance and reference spectra.

6.7 References Cited

AMES D. E., WATKINSON D. H. and PARRISH R. R. (1998) Dating of a regional hydrothermal system induced by the 1850 Ma Sudbury impact event. *Geology* **26**(5), 447 – 450.

BACH W. and EDWARDS K. J. (2003) Iron and sulfide oxidation within the basaltic ocean crust: implications for chemolithoautotrophic microbial biomass production. *geochimica et Cosmochimica Acta* **67**, 3871 – 3887.

BANERJEE N. R., FURNES H., MUEHLENBACHS K. and STAUDIGEL H. (2004a) Microbial alteration of volcanic glass in modern and ancient oceanic crust as a proxy for studies of extraterrestrial material. In *Lunar and Planetary Science XXXV*.

BANERJEE N. R., FURNES H., MUEHLENBACHS K., STAUDIGEL H. and DE WIT M. (2006a) Preservation of ~3.4 – 3.5 Ga microbial biomarkers in pillow lavas and hyaloclastites from the Barberton Greenstone Belt, South Africa. *Earth and Planetary Science Letters* **241**(3 – 4), 707 – 722.

BANERJEE N. R., FURNES H., MUEHLENBACHS K., STAUDIGEL H., MCLOUGHLIN N. and BEBOUT G. (2008) Biogeochemical tracers of modern and ancient life in seafloor lavas. *Geochimica et Cosmochimica Acta* **72**(12), A51 – A51.

BANERJEE N. R., FURNES H., SIMONETTI A., MUEHLENBACHS K., STAUDIGEL H., DE WIT M. and VAN KRANENDONK M. J. (2006b) Ancient Microbial Alteration of Oceanic Crust on Two Early Archean Cratons and the Search for Extraterrestrial Life. In *37th Annual Lunar and Planetary Science Conference*, League City, TX.

BANERJEE N. R. and MUEHLENBACHS K. (2003) Tuff life: Bioalteration in volcaniclastic rocks from the Ontong Java Plateau. *Geochemistry, Geophysics, Geosystems* **4**(4), 1037 – 1059.

BANERJEE N. R., MUEHLENBACHS K., FURNES H., STAUDIGEL H. and DE WIT M. (2004b) Potential for Early Life Hosted in Basaltic Glass on a Wet Mars. In *Second Conference on Early Mars*.

BANERJEE N. R., SIMONETTI A., FURNES H., MUEHLENBACHS K., STAUDIGEL H., HEAMAN L. and VAN KRANENDONK M. J. (2007) Direct dating of Archean microbial ichnofossils. *Geology* **35**(6), 487 – 490.

BENZERARA K., MENGUY N., BANERJEE N. R., TYLISZCZAK T., BROWN G. E. and GUYOT F. (2007) Alteration of submarine basaltic glass from the Ontong Java Plateau: A STXM and TEM study. *Earth and Planetary Science Letters* **260**(1 – 2), 187 – 200.

BRADY P. V. and GISLASON S. R. (1997) Seafloor weathering controls on atmosphereic CO2 and global climate. *Geochimica et Cosmochimica Acta* **61**, 965 – 973.

BRASIER M. D., GREEN O. R., JEPHCOAT A. P., KLEPPE M. J., VAN KRANENDONK M. J., LINDSAY J. F., STEELE A. and GRASSINEAU N. V. (2002) Questioning the evidence of Earth's oldest fossils. *Nature* **416**, 76 – 81.

BRINGEMEIER D. (1994) Petrofabric examination of the main suevite of the Otting Quarry, Nordlinger Ries, Germany. *Meteoritics & Planetary Science* **29**, 417.

BUCHNER E., SCHWARZ W., SCHMIEDER M. and TRIELOFF M. (2010) Establishing a 14.6 ± 0.2 Ma age for the No¨rdlinger Ries impact (Germany) — A prime example for concordant isotopic ages from various dating materials. *Meteoritics and Planetary Science* **45**(4), 662 – 674.

CADY S., FARMER J. D., GROTZINGER J. P., SCHOPF J. W. and STEELE A. (2003) Biosignatures and the Search for Life on Mars. *Astrobiology* **3**, 351 – 368.

CALDEIRA K. (1995) Long-term control of atmospheric carbon-dioxide - low-termperature sea-floor alteration or terrestrial silicate-rock weathering. *American Journal of Science* **295**, 1077 – 1114.

CHAO E. C. T., H TTNER R. and SCHMIDT-KALER H. (1978) *Principal Exposures of the Ries Meteorite Crater in Southern Germany*. Bayerisches Geologisches Landesamt, Munich. pp. 1.

COCKELL C. S. (2006) The origin and emergence of life under impact bombardment. *Philosophical Transactions of the Royal Society B* **361**, 1845 – 1856.

COCKELL C. S. and HERRERA A. (2008) Why are some microorganisms boring? *Trends Microbiol* **16**(3), 101 – 6.

COCKELL C. S. and LEE P. (2002) The biology of impact craters — a review. *Biological Reviews* **77**, 279 – 310.

COCKELL C. S., LEE P., OSINSKI G., HORNECK G. and BROADY P. (2002) Impact-induced microbial endolithic habitats. *Meteoritics & Planetary Science* **37**(10), 1287 – 1298.

COCKELL C. S., OLSSON-FRANCIS K., HERRERA A. and MEUNIER A. (2009) Alteration textures in terrestrial volcanic glass and the associated bacterial community. *Geobiology* **7**(1), 50 – 65.

COCKELL C. S., OSINSKI G. R. and LEE P. (2003) The impact crater as a habitat: Effects of impact processing of target materials. *Astrobiology* **3**(1), 181 – 191.

CROCOMBETTER J. P., POLLAK M., JOLLET F., THROMAT N. and GAUTIERSOYER M. (1995) X-ray-absorption spectroscopy at the Fe L(2,3) threshold in iron-oxids. *Physical Review B* **52**, 3143 – 3150.

EDWARDS K. J., BACH W. and MCCOLLOM T. M. (2005) Geomicrobiology in oceanography: microbe-mineral interactions at and below the seafloor. *TRENDS in Microbiology* **13**(9), 449 – 456.

FARMER J. D. (2000) Hydrothermal Systems: Doorways to Early Biosphere Evolution. *GSA Today* **10**(7), 1 – 6.

FISK M. R., GIOVANNONI S. J. and THORSETH I. H. (1998) Alteration of oceanic volcanic glass: textural evidence of microbial activity. *Science* **281**, 978 – 980.

FLIEGEL D., MCLOUGHLIN N., KOSLER J., BANERJEE N., SIMONETTI A. and FURNES H. (2008) Direct in situ dating of titanite in biotextures using laser ablation MC-ICP-MS. *Geochimica et Cosmochimica Acta* **72**(12), A274 – A274.

FORTIN D., LANGLEY S. and GLAUSAUER S. (2008) Biominerals. Recorders of the past? *Metal ions in life sciences* **4**, 377 – 411.

FURNES H., BANERJEE N. R., MUEHLENBACHS K., STAUDIGEL H. and DE WIT M. (2004) Early Life Recorded in Archean Pillow Lavas. *Science* **304**(5670), 578 – 581.

FURNES H., BANERJEE N. R., STAUDIGEL H., MUEHLENBACHS K., MCLOUGHLIN N., DE WIT M. and VAN KRANENDONK M. J. (2007) Comparing petrographic signatures of bioalteration in recent to Mesoarchean pillow lavas; tracing subsurface life in oceanic igneous rocks; Earliest evidence of life on Earth. *Precambrian Research* **158**(3 – 4), 156.

FURNES H., MUEHLENBACHS K., TORSVIK V., THORSETH I. H. and TUMYR O. (2001a) Microbial fractionation of carbon isotopes in altered basaltic glass from the Atlantic Ocean, Lau Basin and Costa Rica Rift. *Chemical Geology* **173**(4), 313 – 330.

FURNES H., STAUDIGEL H., THORSETH I. H., TORSVIK T., MUEHLENBACHS K. and TUMYR O. (2001b) Bioalteration of basaltic glass in the oceanic crust. *Geochemistry, Geophysics, Geosystems* **2**(8), 1049 – 1079.

GARCIA-RUIZ J. M., HYDE S. T., CARNERUP A. M., CHRISTY A. G., VAN KRANENDONK M. J. and WELHAM N. J. (2003) Self-assembled silica-carbonate structures and detection of ancient microfossils. *Science* **302**, 1194 – 1197.

HERRERA A., COCKELL C. S., SELF S., BLAXTER M., REITNER J., THORSTEINSSON T., ARP G., DRÖSE W. and TINDLE A. G. (2009) A Cryptoendolithic Community in Volcanic Glass. *Astrobiology* **9**(4), 369 – 381.

HITCHCOCK A. P. H. (2006) aXis2000. aXis2000. Analysis of X-ray Images and Spectra. McMaster University, Hamilton, Ontario, Canada. Available from: http://unicorn.mcmaster.ca/aXis2000.html.

IZAWA M. R. M., BANERJEE N. R., FLEMMING R. L. and BRIDGE N. J. (2010a) Preservation of microbial ichnofossils in basalitc glass by titanite mineralization. *Canadian Mineralogist* **48**, 1233 – 1265.

IZAWA M. R. M., BANERJEE N. R., FLEMMING R. L., BRIDGE N. J. and SCHULTZ C. (2010b) Basaltic glass as a habitat for microbial life: Implications for astrobiology and planetary exploration. *Planetary and Space Science* **58**(4), 583 – 591.

JACOBSEN C., FLYNN G., WIRICK S. and ZIMBA C. (2000) Soft X-ray spectromicroscopy from image sequences with sub-100nm spatial resolution. *Journal of Microscopy* **197**(2), 173 – 184.

KRING D. A. and COHEN B. A. (2002) Cataclysmic bombardment throughout the inner solar system 3.9 – 4.0 Ga. *Journal of Geophysical Research* **107**(E2), 4-1 – 4-6.

MA Y., CHEN C. T., MEIGS G., RANDALL K. and SETTE F. (1991) High-resolution K-shell photoabsorption measurements of simple molecules. *Physical Review A* **44**(3), 1848 – 1858.

MASON O. U., STINGL U., WILHELM L. J., MOESENEDER M. M., DI MEO-SAVOIE C. A., FISK M. R. and GIOVANNONI S. J. (2007) The phylogeny of endolithic microbes associated with marine basalts. *Environmental Microbiology* **9**(10), 2539 – 2550.

MCLOUGHLIN N., BRASIER M., WACEY D., GREEN O. and PERRY R. (2007) On biogenicity criteria for endolithic microborings on early Earth and beyond. *Astrobiology* **7**, 10 – 26.

MCLOUGHLIN N., STAUDIGEL H., FURNES H., EICKMANN B. and IVARSSON M. (2010) Mechanisms of microtunneling in rock substrates: distinguishing endolithic biosignatures from abiotic microtunnels. *Geobiology* **8**, 245 – 255.

MYNENI S. C. (2002) Soft X-ray spectroscopy and spectromicroscopy studies of organic molecules in the environment. In *Applications of Synchrotron Radiation in Low Temperature Geochemistry and Environmental Science: Reviews in Mineralogy and Geochemistry* (ed. P. A. Fenter, Rivers, M. L., Sturchio, N. C., Sutton, S. R.), pp. 485 – 579.

NAUMOV M. V. (2005) Principal features of impact-generated hydrothermal circulation systems: mineralogical and geochemical evidence. *Geofluids* **5**(3), 165 – 184.

NEWSOM H. E., GRAUP G., SEWARDS T. and KEIL K. (1986) Fluidization and Hydrothermal Alteration of the Suevite Deposit at the Ries Crater, West-Germany, and Implications for Mars. *Journal of Geophysical Research-Solid Earth and Planets* **91**(B13), E239 – E251.

OSINSKI G. (2003a) Shocked into life. *New Scientist* **179**(2412), 40 – 43.

OSINSKI G. R. (2003b) Impact glasses in fallout suevites from the Ries impact structure, Germany: An analytical SEM study. *Meteoritics & Planetary Science* **38**(11), 1641 – 1667.

— (2005) Hydrothermal activity associated with the Ries impact event, Germany. *Geofluids* **5**(3), 202 – 220.

OSINSKI G. R., GRIEVE R. A. F. and SPRAY J. G. (2004) The nature of the groundmass of surficial suevite from the Ries impact structure, Germany, and constraints on its origin. *Meteoritics & Planetary Science* **39**(10), 1655 – 1683.

OSINSKI G. R., LEE P., PARNELL J., SPRAY J. G. and BARON M. (2005) A case study of impact-induced hydrothermal activity: The Haughton impact structure, Devon

Island, Canadian High Arctic. *Meteoritics & Planetary Science* **40**(12), 1859 – 1878.

OSINSKI G. R., SPRAY J. G. and LEE P. (2001) Impact-induced hydrothermal activity within the Haughton impact structure, arctic Canada: Generation of a transient, warm, wet oasis. *Meteoritics & Planetary Science* **36**, 731 – 745.

PATTERNSON R. J., MAYER D., WEAVER L. and PHANEUF M. W. (2002) "H-bar lift-out" and "plan-view lift-out" : Robust, Re-thinnable FIB-TEM preparation for ex-situ cross-sectional and plan view FIB specimen preparation. *Microscopy and Microanalysis* **8**(S02), 566 – 567.

PECKMANN J., BACH W., BEHRENS K. and REITNER J. (2008) Putative cryptoendolithic life in Devonian pillow basalt, Rheinisches Schiefergebirge, Germany. *Geobiology* **6**(125 – 135).

POHL J., STÖFFLER D., GALL H. and ERNSTSON K. (1977) The Ries impact crater; Impact and explosion cratering; planetary and terrestrial implications; Proceedings of the Symposium on planetary cratering mechanics. In *Lunar Science Institute topical conference ; Symposium on planetary cratering mechanics, Flagstaff, Ariz* (eds. D. J. Roddy, R. O. Pepin and R. B. Merrill). Pergamon Press New York N.Y. United States (USA), United States (USA).

SAPERS H. M., BANERJEE N. R., PRESTON L. J. and OSINSKI G. R. (in prep-a) Microbial ichnofossils preserved in meteorite impact glass. *Nature*.

SAPERS H. M., OSINSKI G. R., FLEMMING R. L. and BANERJEE N. R. (in prep-b) Enigmatic tubular features in impact glass from the Ries impact structure, Germany. *Geology*.

SOUTHAM G. and DONALD R. (1999) A structual comparison of bacterial microfossils vs. 'nanobacteria' and nanofossils. *Earth-Science Reviews* **48**, 251 – 264.

STAUDIGEL H., FURNES H., BANERJEE N. R., DILEK Y. and MUEHLENBACHS K. (2006) Microbes and volcanoes: A tale from the oceans, ophiolites, and greenstone belts. *GSA Today* **16**(10), 4 – 10.

STAUDIGEL H., FURNES H., MCLOUGHLIN N., BANERJEE N. R., CONNEL L. B. and TEMPLETON A. (2008a) 3.5 billion years of glass bioalteration: Volcanic rocks as a basis for microbial life? *Earth-Science Reviews* **89**(3 – 4), 156 – 176.

STAUDIGEL H., FURNES H., MCLOUGHLIN N., BANERJEE N. R., CONNELL L. B. and TEMPLETON A. (2008b) Microbial glass bioalteration: Inferring mechanisnis of biocorrosion from trace fossil morphology. *Geochimica et Cosmochimica Acta* **72**(12), A893 – A893.

STAUDIGEL H., HART S. R., SCHMINCHKE H. U. and SMITH B. M. (1989) Cretaceous ocean crust at DSDP site-417 and site-418 - carbon uptake from weathering versus loss by magmatic outgassing. *geochimica et Cosmochimica Acta* **53**, 3091 – 3094.

STÖFFLER D. (1984) Glasses formed by hypervelocity impact. *Journal of Non-Crystalline Solids* **67**, 465 – 502.

THORSETH I. H., TORSVIK T., FURNES H. and MUEHLENBACHS K. (1995) Microbes play an important role in the alteration of oceanic crust. *Chemical Geology* **126**, 137 – 146.

TORSVIK T., FURNES H., MUEHLENBACHS K., THORSETH I. H. and TUMYR O. (1998) Evidence for microbial activity at the glass – alteration interface in oceanic basalts. *Earth and Planetary Science Letters* **162**, 165 – 176.

VON ENGELHARDT W. (1990) Distribution, petrography and shock metamorphism of the ejecta of the Ries Crater in Germany; a review; Cryptoexplosions and catastrophes in the geological record, with a special focus on the Vredefort Structure. *Tectonophysics* **171**(1 – 4), 259.

Chapter 7

7 Microbial alteration of impact glass

Sapers, H.M., Banerjee, N. R., Osinski, G. R., Preston, L. J.

7.1 Introduction

Bioalteration of terrestrial basaltic glasses produces characteristic tubular and granular aggregate textures (Banerjee *et al.*, 2007). Such bioalteration textures preserved in Archean greenstone belts constitute one of the oldest records of life on Earth (Banerjee *et al.*, 2007). Examination of impact glasses from the Ries impact structure, Germany, has revealed tubular textures with remarkably similar morphologies to the tubular bioalteration of submarine volcanic glasses (Fig. 7.1). In Chapter 4 the geologic context of the tubules is defined concluding that the tubules were not likely to have been formed through purely abiotic processes. Arguments for biogenicity including morphology consistent with biological behavior and chemical evidence suggestive of biological processing are developed in Chapter 5. Results from the first high-resolution biogeochemical study of impact glass are presented in Chapter 6 supporting a biogenic origin of the Ries tubules. In Chapter 7, the methodology used in Chapters 5 and 6 is discussed in detail and the results presented in the context of other putative ichnofossils preserved in impactites. This chapter will further discuss the astrobiological implications of microbially mediated alteration of meteorite impact glass. The biogeochemical study of the Ries impact glasses comprising this thesis is the first such study to present a robust dataset characterizing putative microbial alteration of impact materials and thus this work presents the first such evidence of ichnofossils in impact glass. Given the probable ubiquity of impact glasses in post-impact environments throughout the Solar System, it is important to understand the biological components and potential of such systems.

The initial catastrophic biological effects of hypervelocity impacts are well established. However, a growing body of evidence suggests that meteorite impact events also have beneficial effects particularly for microbial life. This has led many to suggest that impact craters may have been important habitats for life on early Earth (Cockell and Lee, 2002).

More speculatively, impacts may have acted as ‘cradles’ for prebiotic chemical reactions. Impact-ejected rocks may have provided refuges for microbial life during the ~3.8 Ga late heavy bombardment and may even have allowed the transfer of life between planetary bodies (*e.g.*, Cockell 2006). Although impact craters are uncommon on present day Earth, (~50 000 km^2 globally), they are ubiquitous on rocky and icy bodies within the solar system often comprising the dominant geological features.

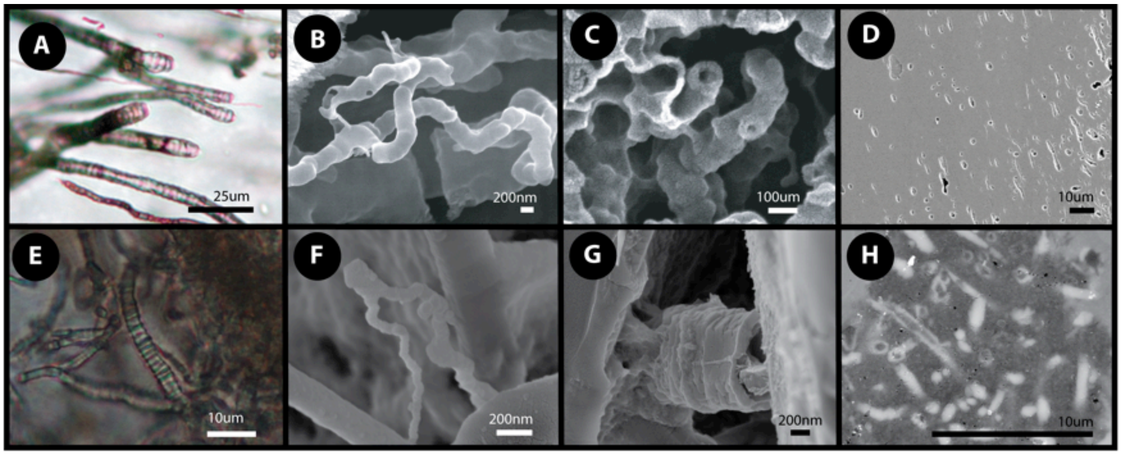

Figure 7.1: Tubular alteration textures in natural glasses.

A – D: Bioalteration in submarine basaltic glass (Banerjee, 2003). E – H: putative bioalteration in impact glass. A, E (RI_00_056): Plane polarized light. Notice the segmentation in the tubular textures and bifurcation in E. B, F (RI_10_006): SEM secondary electron image. Complex, undulating, irregular structures. C, G (RI_10_006): SEM secondary electron image. Hollow tubular textures hosted in glass grains. G: Note the ovoid cross section and lack of continuous longitudinal striae in this hollow tubule. D, H (RI_00_056): SEM secondary electron image (D), back scattered electron image (H). Notice the similarity of the hollow etch structures in D and the mineralized tubular structures in H.

Any hypervelocity impact into a water-rich target on a solid planetary body has the potential to generate hydrothermal system (Naumov, 2005). The hyperthermophilic root of the phylogenic tree of life suggests an essential role for thermophilic environments in the origin or the early evolutionary history of life. Previous work has associated primitive life on Earth with submarine volcanic activity: filamentous microfossils as old as ca. 3.2 Ga have been found in volcanogenic massive sulfide deposits (Nisbet, 2000); bioalteration of volcanic glasses back to 3.5 Ga provide the earliest record of life on Earth (Staudigel *et al.*, 2006) suggesting that submarine hydrothermal settings may have played an essential role in the origin of life. Impact-induced hydrothermal systems share many characteristics with submarine volcanic hydrothermal systems including the presence of chemical and thermal energy for microbial metabolism and the precipitation of hydrothermal minerals such as clays and zeolites, which may have catalyzed important prebiotic chemical reactions. An impact event results in local sterilization; a biological resetting event followed by distinct ecological successional stages (Cockell & Lee 2002c). Impact events create novel microbial niches such as the endolithic habitat created by the shock-induced increased porosity of crystalline target rock. For example, photosynthetic cyanobacteria have been documented and studied growing within the near-surface layers of highly shocked gneisses from the Haughton impact structure, Canada (Cockell *et al.* 2002). Impact glass is another potential impact-induced microbial habitat for life on Earth as well as a potential preservation environment for microbial trace fossils on Earth and possibly other planets such as Mars.

The Ries crater in southern Germany is one of the best characterized terrestrial impact structures (*e.g.*, Pohl *et al.*, 1977). Furthermore, detailed studies have characterized the post-impact hydrothermal system of the Ries crater. In addition, the Ries crater has exceptionally preserved proximal impact ejecta deposits including a glass-bearing breccia unit. The rapid quenching of molten material following a hypervelocity impact results in the formation of impact glasses. Impact glasses share many similarities with volcanic glasses, however, fundamental differences impact glasses unique geochemical systems. The bulk compositions of impact melts are diverse, reflecting heterogeneities in the target lithologies. Furthermore, impact melts often display heterogeneity on multiple scales. In addition, the presence of lechatelierite (a silica glass phase) is indicative of high temperatures (>1713°C; Stöffler, 1984) reflecting formation conditions distinct from normal igneous processes. Meteoritic contamination may result in siderophile element anomalies or isotopic anomalies (Osinski 2003).

7.2 The Ries Impact Structure: Geological Setting

The mid – Miocene Ries impact structure located in southern Germany is arguably one of the best-characterized and best-preserved terrestrial impact structures (see Pohl *et al.*, 1977 and von Engelhardt 1990 for reviews). Shoemaker and Chao (1961) first recognized the impact origin of the Ries structure in by documenting coesite and lechatelierite within the lithic components of glass-bearing breccias. $^{40}Ar/^{39}Ar$ laser-probe dating of tektites constrains the age of the Ries impact structure to 14.6 $\pm$ 0.2 Ma (Buchner *et al.* 2010). Ries is a complex crater with a diameter of ~24 km (Pohl *et al.*, 1977; Fig. 7.2). The approximately circular inner basin has a diameter of 12 km interpreted to represent the maximum extent of the transient cavity (Wünnemann *et al.* 2005; Bader & Schmidt-Kaler 1979). A crystalline inner ring of uplifted basement surrounds the inner basin. The megablock zone, a tectonic ridge comprised of a system of concentric normal faults, extends from the inner ring to the crater rim with a maximum extent of ~24 km (Pohl *et al.* 1977). The two-layer target is comprised of dominantly Mesozoic flat lying sediments that unconformably overlie crystalline Hercynian basement (Pohl *et al.*, 1977; Graup 1978). At the time of impact the thickness of the sedimentary package varied from ~470 m in the north to ~820 m in the south. The lower sedimentary unit consists of sandstone, siltstone and marl overlain by an upper limestone unit (Schmidt-Kaler 1978). The Hercynian basement consists of steeply dipping gneisses, amphibolites, and ultrabasic rocks that are cut by later granitic intrusions (Graup 1978).

Impactites are well preserved (*e.g.*, Chao *et al.* 1978); surficial "suevite" comprises one of four main proximal ejecta deposits (von Engelhardt 1990). The surficial "suevites" (impact melt-bearing breccias) are divided into two distinct lithological units: 1) the dominant main suevite that represents a clast-rich particulate impact melt rock or impact melt-bearing breccia (von Engelhardt 1990; Osinski *et al.* 2004); 2) subordinate basal suevite (Bringemeier 1994). Four main glass types occur within the main suevite both as groundmass phases and as discrete glass clasts (Osinski 2003). Glass clasts are typically vesiculated, schlieren-rich mixtures containing abundant mineral and lithic fragments (von Engelhardt 1990). The glass clasts hosted within the suevite have been classified based on composition and microtextures (Osinski 2003).

Type I glasses are the most abundant in the Ries suevites. These glasses contain Al-rich pyroxene quench crystallites and have SiO_2 contents ~63%. Type II glasses have a similar SiO_2 content as type I; however, they contain only plagioclase crystallites as well as a generation of dense, micron-scale vesicles. Type III glasses have low SiO_2 contents, are hydrated relative to the other glasses, and contain relatively little FeO, MgO, and K_2O, while having high Al_2O_3, CaO, and Na_2O contents. Type IV glasses have very high SiO_2 contents commonly >90%. Type I glasses have the highest concentrations of FeO and MgO of all 4 glass types (Osinski 2003). Type I glasses are the focus of this study as they comprise >90% of the glass clasts hosted within the Ries surficial suevite (Osinski 2003).

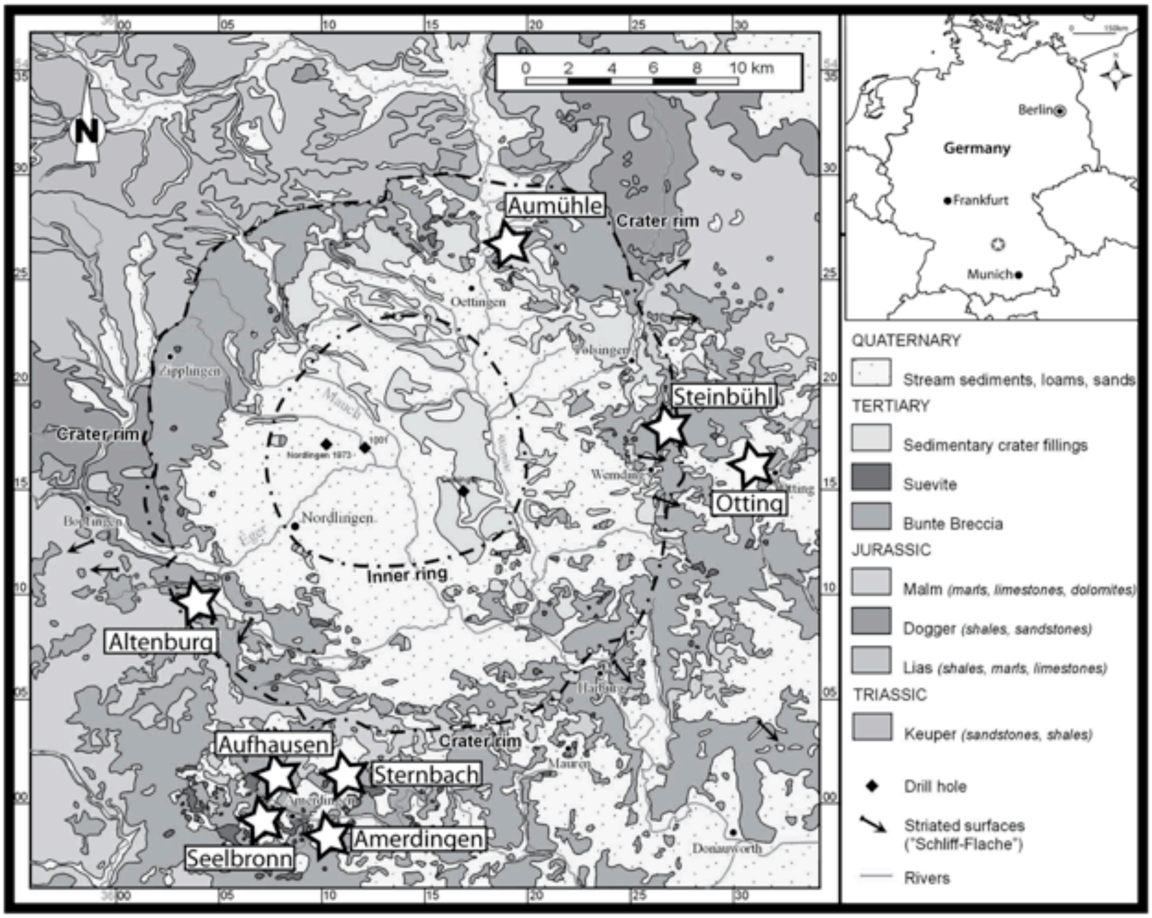

Figure 7.2: Simplified geologic map of the Ries impact structure.

Simplified geologic map of the Ries impact structure. White stars indicate the suevite outcrops with glass clasts hosting tubular features. Modified from Osinski (2003).

7.3 Impact-generated hydrothermal systems

Recent work has shown that hydrothermal activity is commonplace in the immediate aftermath of an impact event on any water-rich solid planetary surface (Naumov 2005; Osinski *et al.* 2005; Osinski *et al.* in press). In an impact crater, the heat source is provided by impact-melted or -heated materials providing a transient source of heat in an otherwise cold environment. The interaction of water with these hot materials forms a hot rock-water circulatory system that can dissolve, transport, and precipitate various mineral species (Osinski *et al.* 2001). This has important astrobiological implications as hydrothermal systems in general may have played a role in the origin and evolution of early life on Earth and possibly other planets such as Mars (Farmer 2000).

The Ries crater is one of the first impact sites where a post-impact hydrothermal system has been proposed (Engelhardt 1972; Salger 1977; Stähle & Ottemann 1977; Osinski 2005). The occurrence of secondary mineralization and hydrothermal alteration of the impact suites has been noted and described (*e.g.*, Förstner 1967; Engelhardt 1972; Stähle 1972; Jankowski 1977; Stöffler *et al.* 1977; Engelhardt & Graup 1984; Engelhardt *et al.* 1995; Graup 1999; Osinski 2003; Osinski *et al.* 2004; see Osinski (2005) for a detailed study of hydrothermal alteration of the Ries impactites). Using a combination of petrographic and analytical SEM techniques, Osinski (2005) has identified a number of hydrothermal alteration phases within the glass-bearing breccias including clays (dominantly montmorillonite), zeolites, quartz, calcite, hematite and goethite. Alteration phases of the crater suevite include: K-feldspar, albite, clays, chlorite, zeolites, calcite, and minor phases including pyrite, goethite, barite and siderite. Alteration occurs in three main settings: 1) open-space cavity and fracture fillings within the groundmass; 2) vesicle linings/fillings within impact glass clasts; and 3) pervasive alteration of groundmass phases and glass clasts (Osinski, 2005). Overall the glass clasts are well preserved in the surficial suevites (Engelhardt & Graup 1984; Engelhardt *et al.* 1995; Graup 1999; Osinski 2003, 2005). The hydrothermal fluids of the Ries post-impact hydrothermal system were likely derived from a combination of meteoric water from the over lying crater lake and ground waters from nearby country rocks. There is no evidence of a magmatic or metamorphic source (Osinski 2005).

Recent work by Muttik *et al.* (2008) suggests that the Ries post-impact hydrothermal system was limited to the intensely altered glass-bearing breccias within the crater and the alteration of the glass-bearing breccia outside the crater rim is due to weathering process. It is argued that the main alteration phase of these glass-bearing breccias identified as montmorillonite and Ba-phillipsite by whole rock powder XRD is chemically homogenous throughout the surficial suevites consistent with low temperature hydrous devitrification of impact glasses. It is significant to note that neither clasts of pre-impact target rocks nor impactite phases were enriched in Ba. Therefore the Ba must have been dissolved by the hydrothermal fluids, transported and precipitated during zeolitization of the surficial suevites (Osinski 2005). However, Osinski (2005) noted that hydrothermal alteration in the surficial suevites was limited to localized zones including fractures and vugs. Bulk XRD is not a sufficient technique to identify trace assemblages in spatially restricted zones. It is likely that alteration assemblages formed by post-impact weathering processes are the predominate assemblages of the surficial suevites considering the limited extent of hydrothermal activity in these units. Furthermore no explanation is offered regarding the Ba-phillipsite phase within the glass-bearing breccias outside the crater rim. A recent study suggests that alteration of glass clasts within these glass-bearing breccias followed a progression from high- to low-temperature alteration with textures consistent with hydrothermal alteration, *sensu stricto*, between the two temperature end members (Sapers et al 2009).

7.4 Analytical Techniques

A representative suite of impact-melt bearing breccias from the Ries impact structure (Fig. 7.2) were examined in hand sample, polished thin section, and analyzed with Fourier Transform Infra-red (FTIR) spectroscopy, scanning electron microscopy (SEM), and energy dispersive X-ray spectroscopy. Approximately 100 thin sections derived from five field campaigns (2000, 2001, 2005, 2009, 2010), were chosen for petrographic study. Reflected and transmitted plane polarized and crossed polarized light was used for imaging using a Nikon Eclipse LV100POL petrographic light microscope equipped with a Nikon DS-Ri1 12 megapixel camera. Extended-depth of focus images (EDF) were obtained using plane-polarized transmission microscopy by aligning multiple images in the z plane using Nikon Elements software. On average 25 – 35 images were collected at ~0.4μm *z*-spacing and merged to created a single EDF image. Reflected light was used to target areas for SEM analysis by identifying regions where tubules intersected the thin section surface. Two glass clasts one from the Amerdingen and Seelbronn localities that contained representative tubular textures were chosen from the optical images for further analysis.

Three glass clasts were chosen for micro-X-ray diffraction (μ-XRD) analysis from a polished thin section of the Amerdingen. Glass clasts were chosen based on size (>50μm) and absence of large vesicles and lithic inclusions. X-ray diffraction data were collected in coupled geometry with θ1=5º and θ2= 17º with a frame width of 30.5º and scanning speed of 1.22º/min using the Bruker D8 Discover micro X-ray diffractometer (μXRD) at the University of Western Ontario (Flemming 2007), operated using CuKα radiation generated at 40 kV and 40 mA with a beam diameter of 50 μm. Diffracted X-rays were detected by a General Area Detector Diffraction System (GADDS). Diffractograms were analyzed using the BrukerAXS EVA software package and the International Center for Diffraction Data (ICDD) PDF-4 database.

High-resolution backscatter electron (BSE) imaging and energy dispersive X-ray (EDX) spectroscopy spot analyses were carried out with a Leo 1540 FIB/SEM CrossBeam field emission SEM equipped with an Oxford Instruments INCA EDX system allowing for elemental analysis, sensitive to ~0.5 wt. % or less for all elements from C – U in the Nanofabrication Laboratory, University of Western Ontario. Samples were Pt sputter coated using the Denton Vacuum Desk 2 for 200 seconds at 15 mA. The sections were analyzed under high vacuum with an accelerating voltage of 15 – 20 kV and a working distance ~10 mm. Energy dispersive X-ray (EDX) spectroscopy mapping and spot analyses of selected samples allowed for the identification of elemental distribution on a micron scale.

Further SEM imaging and EDX mapping was carried out on a Hitachi SU6600 variable pressure field emission SEM (Schottky emitter) equipped with an Oxford Instruments 80mm^2 silicon drift detector at the University of Western Ontario Zircon and Accessory

Phase analysis facility. The spectral resolution of the EDX detector was 129eV at an accelerating voltage of 5.9 keV. Samples were analyzed under vacuum at a working distance between ~10 – 15μm and an accelerating voltage of 10 – 15kV with a probe current of 1 – 2nA. BSE images were captured with a five segment solid-state detector. Samples were coated as above and all data was analyzed with Oxford Instruments INCA software.

A carbon tab was prepared for BSE imaging. Pieces of a large glass clast from the Seelbronn sample were crumbled then crushed with a mortar and pestle to sub-millimeter sized angular fragments. The fragments were then stuck to a 1 cm double-backed conductive adhesive carbon tab, which was then stuck to a titanium stub mount. The full assembly was then Pt coated using the Denton Vacuum Desk 2 for 200 seconds at 15 mA.

Fourier Transform Infra-Red (FTIR) spectroscopy was carried out on both tubule-free and tubule-rich areas of the Amerdingen sample using a Bruker IFS55 FTIR with a Baseline TM Horizontal Attenuated Total Reflection (ATR) attachment equipped with a germanium crystal, under an IRScope II microscope. The infrared microscope is a sampling accessory used to obtain infrared spectra of very small samples. The microscope provided visual assessment of the sample and condensed the infrared beam for spectral acquisition. Analyses of the polished thin section were carried out at Surface Science Western. A spectral resolution of 4 cm^{-1} was used, with a scan and sample background of 100 scans, over a spectral range of 4000 – 700 cm^{-1} (2.5 – 14.2 μm), analysing a spot size between 50 and 60 μm in diameter. All analyses were calibrated to the ATR-equipped germanium crystal and atmospheric H_2O and CO_2 bands were subtracted out. Measurements were carried out on the pure glass thin section surrounding the sample and the mounting media to identify contaminants and to enable the removal of these contaminants from the spectra obtained.

7.5 Results

7.5.1 Transmitted light optical microscopy

Transmitted light optical microscopy allows the tubular structures to be viewed in a three-dimentional context (Fig. 7.3). The fresh glass hosting the tubular alteration textures are isotropic, holohyaline to cryptocrystalline schlieren-rich, characterized by complex flow textures and vary in colour from colourless to brown, yellow, pink or green, yellow-brown being dominant (*cf.* Osinski 2003). The glass typically has a cloudy appearance, which increases with tubule density. Increasing alteration and hydration also darken the glass; highly altered glass clasts may appear dark brown to black. Tubules are concentrated along fractures or clast margins (Fig. 7.4), form radiating aggregates and have complex, convoluted morphologies forming a morphological continuum between loose undulating curves and coiled morphologies (Figs. 7.3B, 7.4A). Curvature appears random, non-oriented and unique to individual tubules (Fig. 7.3B; 7.5A). Coils may be either dextral or sinistral and typically have one complete revolution (Fig. 7.3B) but may display up to five whorls (Fig. 7.4A). Tubules have diameters ~1μm and commonly have length to width ratios >5. Some appear to display bifurcation or asymmetric branching (Fig. 7.3A). Approximately one-third of tubules display annulation reminiscent of distinct segmentation (Fig. 7.3A). These segmented tubules typically display less curvature than their non-segmented counterparts (Fig. 7.3). Individual segments have length to width ratios approximately 1:2 (Fig. 7.3B) and vary in diameter from ~1μm to approaching 3μm. Occasionally segmented tubules with large (~3μm) diameters are observed that have segments with length to width ratios approaching 1:6 (Fig. 7.4B). Tubules are commonly observed to cluster by like-morphology (Fig. 7.3A, C).

In summary, areas displaying evidence of hydrous alteration such as optical darkening have a higher concentration of tubules (Fig. 7.4). The glass often displays flow features that are not associated with tubule distribution. Most importantly, the tubules are not found in areas of fresh glass devoid of alteration features and they are cross-cut by a later series of fractures that are not associated with evidence of alteration (*e.g.*, Fig. 7.4C, D).

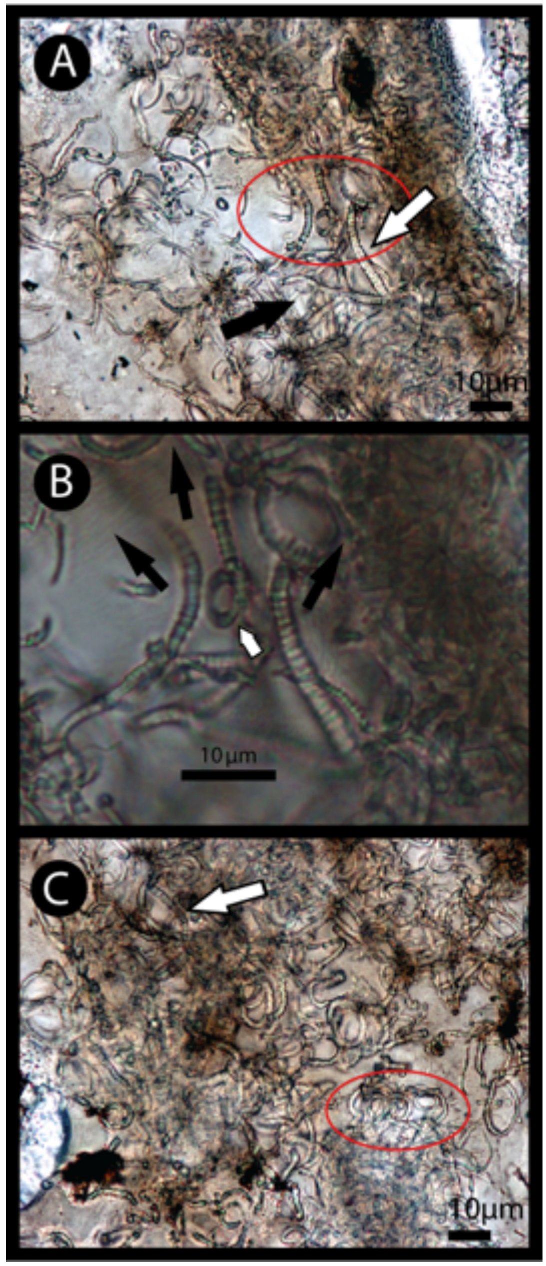

Figure 7.3: Transmitted light EDF photomicrographs of tubular features.

Transmitted light EDF photomicrographs of tubular features in type I impact glass illustrating complex morphologies sample RI_00_056. A and C: dense masses of non-intersecting tubular features. Notice branching, smooth-walled tubules indicated by black arrow; tubules displaying annulations suggestive of segmentation (white arrows); and the tendency for tubules of like morphologies to cluster shown by red ellipses. B: zoom-in of area in the red ellipse of A showing diverging segmented tubules. Directionality indicated by black arrows. Notice the complete coil indicated by the white arrow.

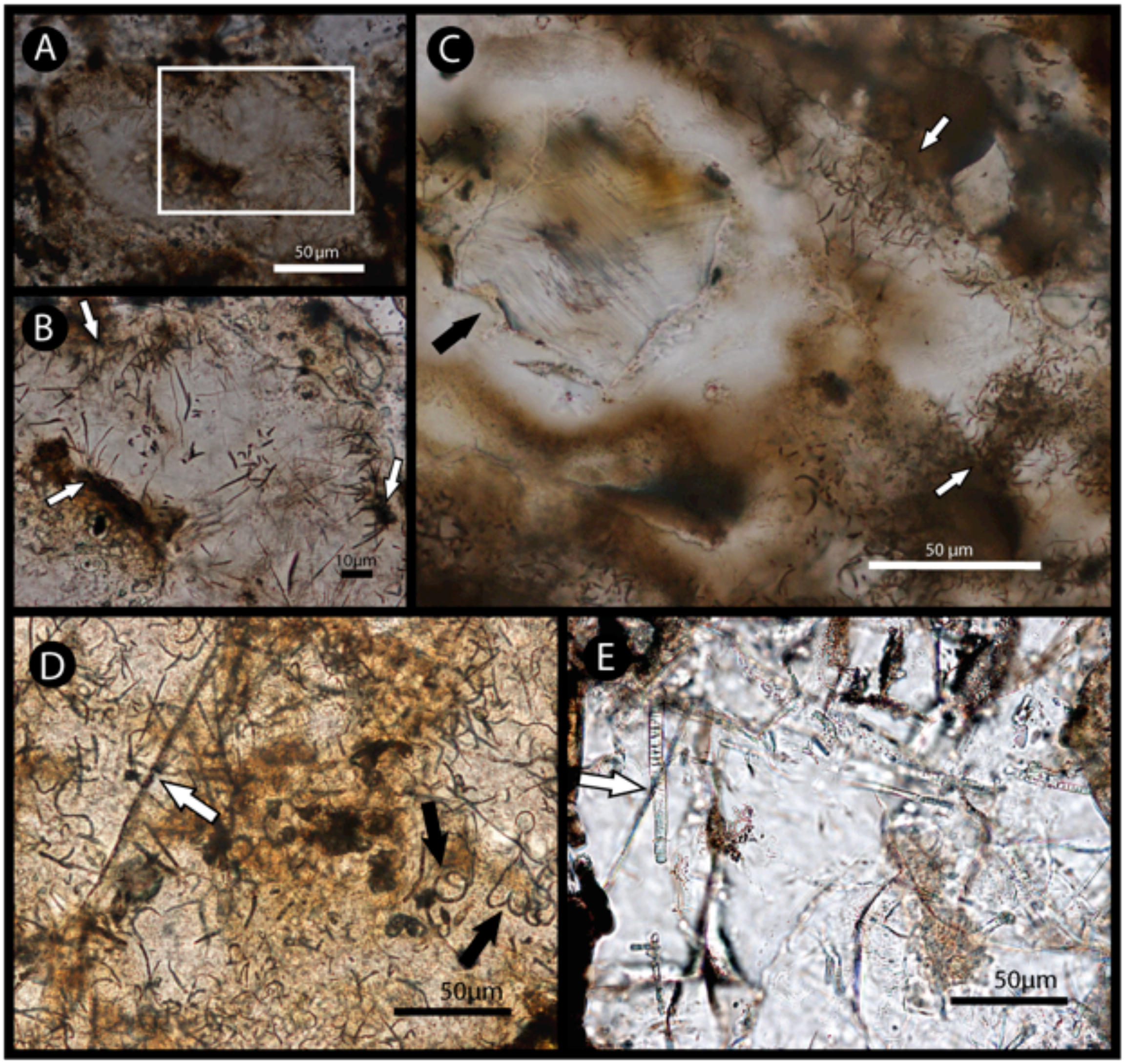

Figure 7.4: Association of tubular features with clast margins and fractures.

A: 0.5mm glass clast hosting tubular alteration. Notice the association of the tubules with the clast margin. A (RI_10_013 5m): EDF image of the area bound by the white box in A. Note the extension of the tubules perpendicular to hydrous alteration phases (white arrows). C (RI_10_013 4m): Tubules concentrated around the hydrothermally altered margins of a glass clast (white arrows). Note the large, partially resorbed, shocked quartz grain (black arrow). The presence of the PDFs in the quartz grain in an unambiguous indicator of impact shock metamorphism. Also note the absence of tubules in the vicinity of the quartz grain. D, E: Late fractures cross-cutting tubular structures. D (RI_10_013 0m): a late fracture not associated with hydrous alteration cross cuts a series of smooth-walled, curvilinear tubular features (white arrow). Also note the spiral tubular features indicated by the black arrows. E (RI_05_040): a large (~ 6μm) segmented tubule is cross cut by a late fracture (white arrow).

7.5.2 Scanning electron microscopy

Scanning electron microscopy was used to image the surface expression of the tubular alteration texture. The tubules appear as irregular, sub-linear to tightly curled, bright objects in the darker grey glassy matrix (Fig. 7.5). The margins of the tubular features are sharp and range from highly irregular (Fig. 7.5D) to smooth (Fig. 7.5B). Fine-scale (sub-micron) textures in both the glass and tubules are absent. Some tubules appear hollow with a circular cross-section, displaying smooth margins, ± annulations, are approximately 0.4 – 1μm in diameter, and up to hundreds of microns in length (Fig. 7.5C, D). Other tubules appear to be filled with an unidentified mineral phase and are either ovoid or rhomboid in cross-section. They have smaller length to width ratios compared to the hollow tubules and vary in diameter from 1 – 3 μm. Margins are either smooth or display highly irregular ornamentation perpendicular to the long axis of the feature (Fig. 7.5C – D).

Tubules and matrix in both of the Amerdingen and Seelbronn samples were analyzed with EDX spectroscopy. Relative to the Si-rich glassy matrix the tubules are depleted by ~5x in Na, ~2x in K, ~1.5x in Al and Si. The tubules are enriched by ~6x in Mg and Fe, and ~1.5x in Ca (Fig. 7.6). These qualitative elemental ratios are based on normalized spectral intensities from linescans produced from EDX elemental maps. In areas where tubules are densely concentrated, they are surrounded by a zone depleted in Mg, Fe, Ca and Na and enriched in K (Fig. 7.7).

Both bright and dark crystallites, relative to the glassy matrix, were observed. Three types are distinguished by morphology and elemental chemistry. Most commonly observed are bright skeletal dendrites of a calcic pyroxene composition (Fig. 7.8), followed by darker tabular laths of feldspar (Fig. 7.8) and rare bright, rounded Ti, Mg, and Fe oxides. Quartz grains with irregular boundaries are scattered throughout the glassy matrix (Figs. 7.4, 7.6). The matrix adjacent to the quartz grains is darker and higher in Si content compared to the surrounding matrix (Fig. 7.6). Tubular features are generally associated with areas containing crystallites chemically consistent with pyroxene. Areas dominated by quartz grains or high-Si, have few to no tubules (Figs. 7.4, 7.6).

Imaging the angular crushed glass fragments adhered to the stub-mount provided a three-dimensional surface of the tubular structures within the glass grain. Tubules were observed as dense masses within fractures and voids (Fig. 7.9), with curved to sub-linear morphologies and diameters ranging from 0.2 μm to 1 μm. The full extent of the tubule length could not be determined, however, visible sections extend >10μm. Two distinct morphologies are recognized: tubules with an ovoid cross section and tubules with a rhomboid cross section. The former are either hollow or solid while all tubules with a rhomboid cross-section appear solid.

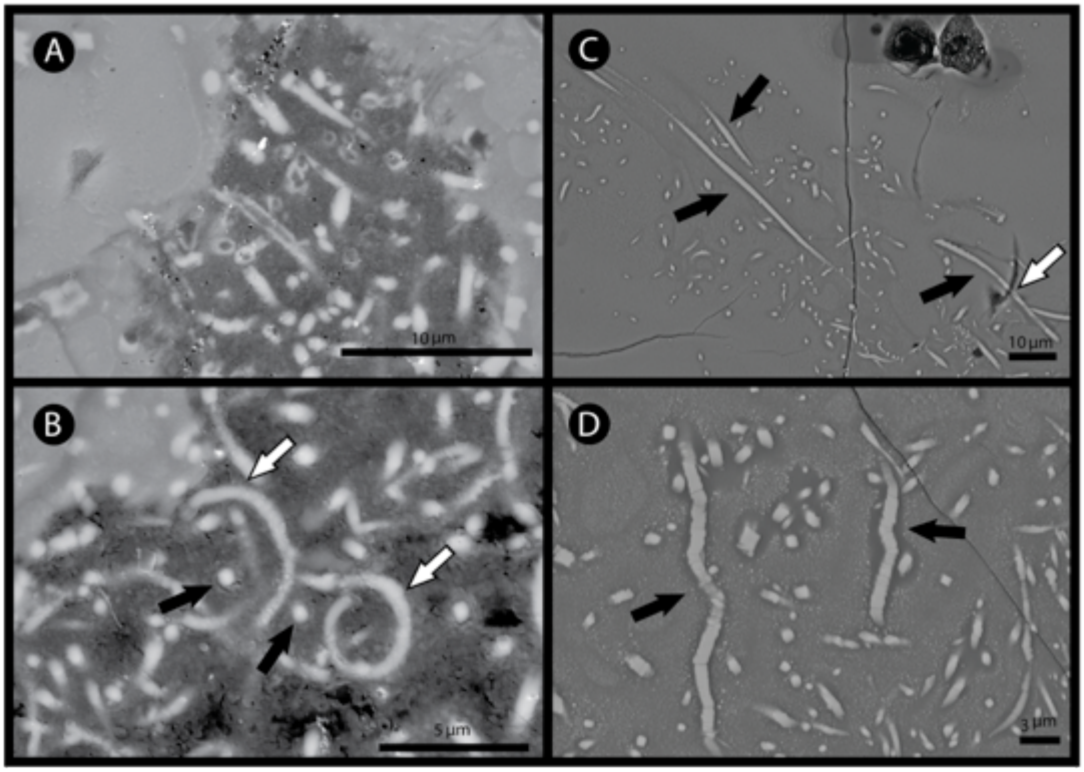

Figure 7.5: BSE SEM images of tubular features.

A (RI_00_056): tubular features appear hollow in cross section. B (RI_00_056): Note the tightly curled morphologies (white arrows) and ovoid solid cross sections (black arrows). C (RI_09_006): The features appear as gently undulating, filaments extending 100s of microns in length (black arrows). Notice the hollow cross section indicated by the white arrow. D (RI_09_006): Undulating features displaying annulations indicated by black arrows.

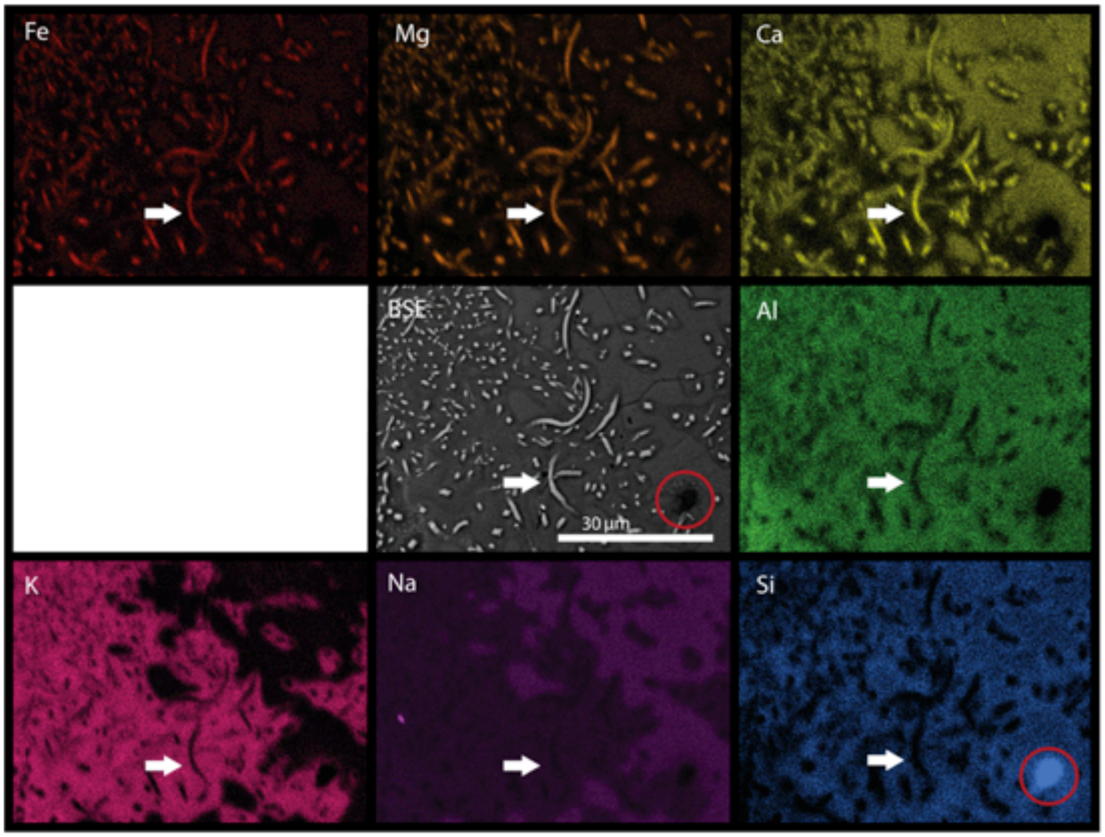

Figure 7.6: Elemental composition of tubular features.

The tubules are enriched in Fe, Mg and Ca while depleted in Al, Si, K, and Na. Note the Si- Al-rich composition of the glassy matrix. The tubules are concentrated in areas of high K and lower Na and Ca compositions. This may represent areas of alteration possibly as a result of biological processing. These areas are visible in the central BSE image as dark gray halos around the tubules. Note the absence of tubules in the vicinity of a relict quartz grain circled in red on the Si and BSE panels. Sample RI_09_006.

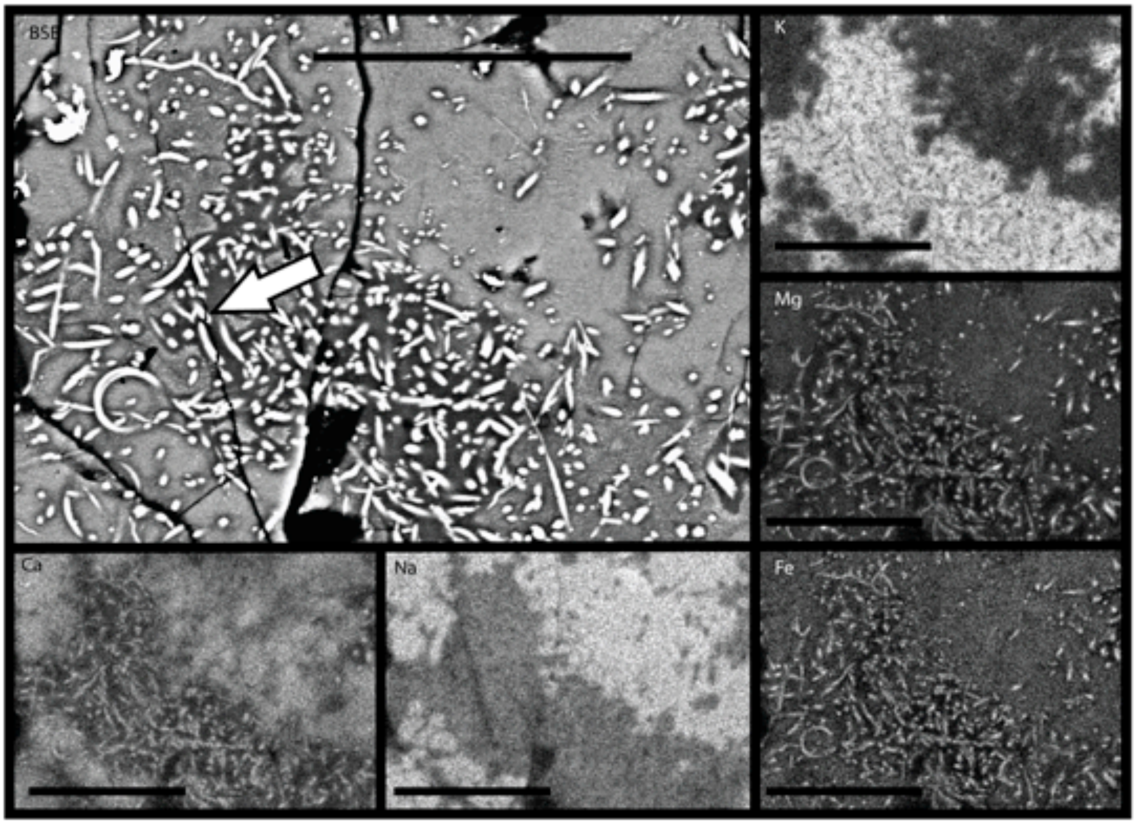

Figure 7.7: matrix composition surrounding tubular features.

EDX mapping illustrating matrix composition surrounding tubular features. Tubules surrounded by zone depleted in Ca, Na, Fe and Mg while enriched in K. Tubules are enriched in Ca, Fe and Mg and depleted in Al, Si, K, and Na. Note the late fracture cross cutting tubule features indicated by the white arrow on the BSE panel. Scale bars 30µm. Sample RI_09_006.

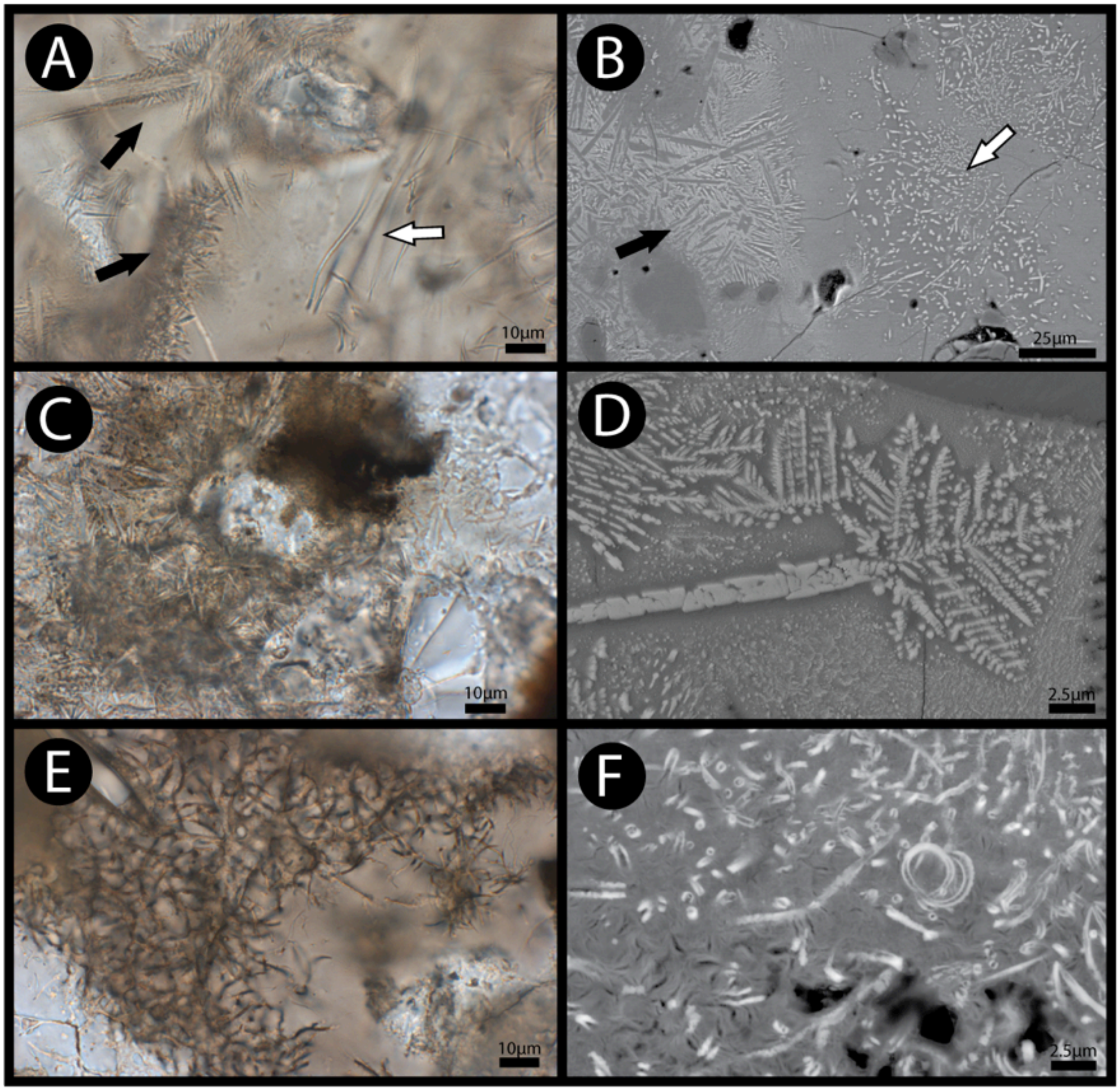

Figure 7.8: Micrographs illustrating the distinct morphologies between quench crystallites and tubules.

A, C, E: transmitted light photomicrographs. B, D, F: Backscatter secondary electron scanning electron micrographs. A – B (RI_10_006): Tubules (white arrows) and quench crystallites (black arrows). Notice the close propinquity and distinct morphologies of the two features. C (RI_10_009A1), D (RI_10_006): Quench crystallites displaying characteristic skeletal and dendritic morphologies. E – F (RI_10_009A1): Tubular features in dense, non-intersecting clusters concentrated around clast margins (E); hollow in cross-section, note the convoluted morphologies

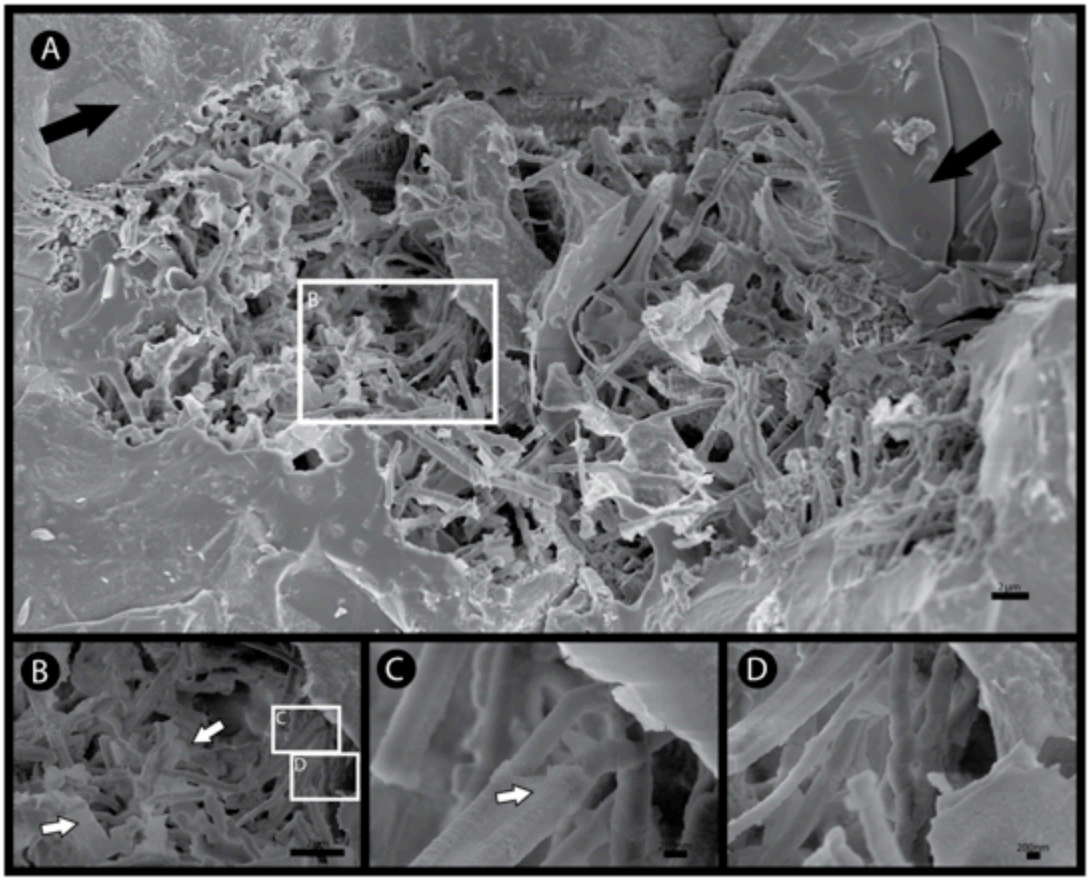

Figure 7.9: Secondary electron SEM images of a dense mass of mineralized tubules.

A: Dense mass of mineralized tubules in altered void of impact-glass sample RI_10_006. Note the smooth appearance of fresh glass (black arrow right) compared to the pitted texture of altered glass (black arrow left). B: close up of boxed area in A. Notice the film of material coating many of the tubules (white arrows). C, D: close up of boxed areas in B.

7.5.3 Micro-XRD

Micro XRD conducted on 3 glassy clasts suggests the presence of a complex suite of micro-crystalline material (Fig. 7.10). Clay minerals include montmorillonite, illite and nontronite. There is also evidence for chlorites, zeolites, carbonates, and iron sulphides. Peaks indicative of quartz, orthoclase and K-feldspar are also present. The large angle between the detector and X-ray gun required to record clay peaks elongated the analysis ellipse. As a result cataclastic matrix material was also analyzed with the intended glass clast target.

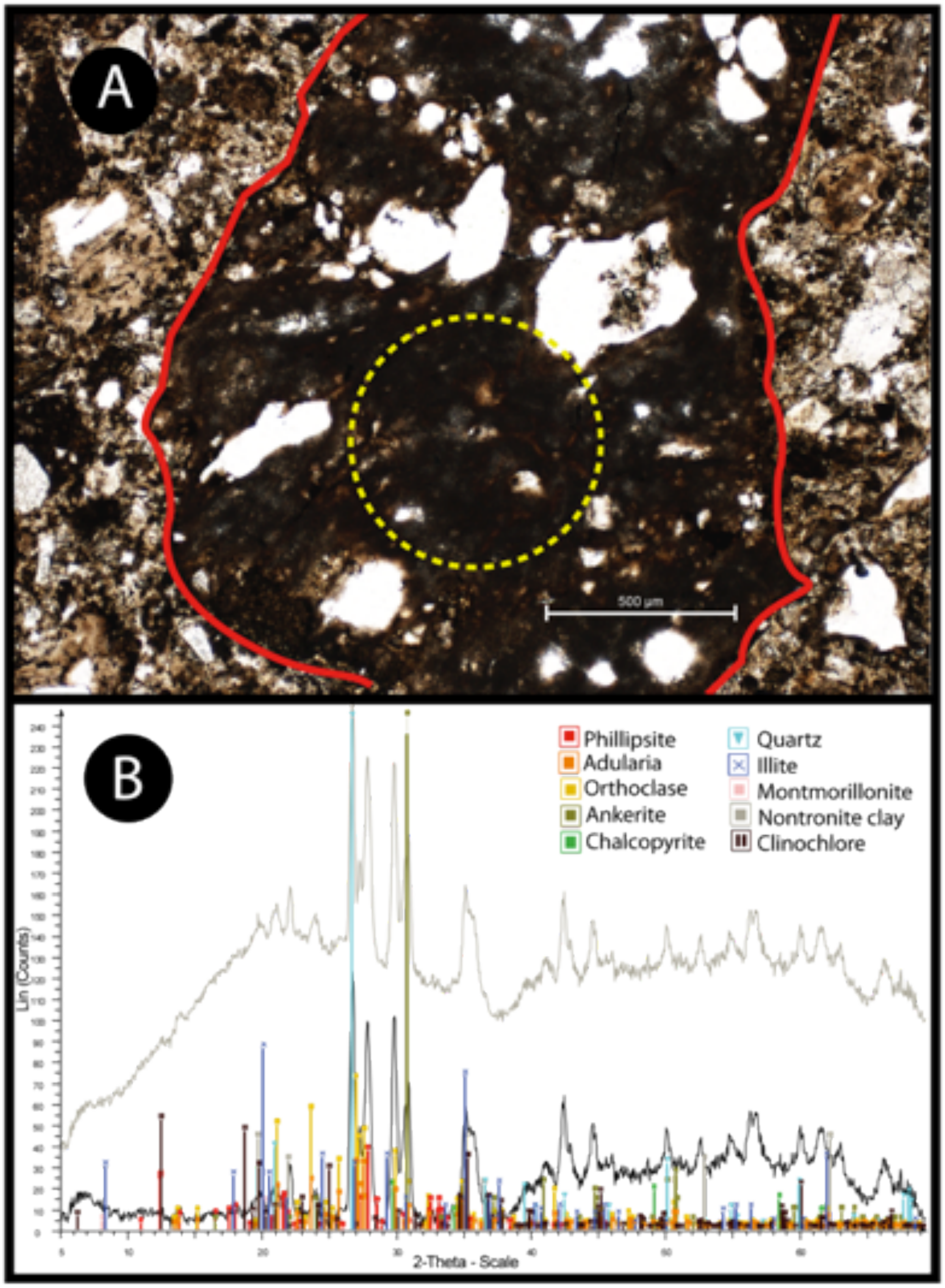

Figure 7.10: Mineralogy of glass clast as determined by µ-XRD.

An example analysis area and corresponding XRD patterns and their respective mineralogical assignments are shown. A: photomicrograph of a glass clast. The margins of the clast are shown in red and the approximate µ-XRD footprint is shown by the dashed yellow ellipse. B: µ-XRD patterns indicating the presence of a complex assemblage of micro-crystalline material. The original spectra is shown in grey; note the large glass hump. Effects of background and glass are subtracted out to produce the black spectra. Sample RI_00_056.

7.5.4 FTIR Spectroscopy

7.5.4.1 Tubular regions

FTIR absorption bands were identified at 3592, 3394 and 3251 cm^{-1} that are due to the OH symmetric stretching vibrational mode of partially hydrogen-bonded water molecules, and the asymmetric and symmetric OH stretch of water molecules fully hydrogen-bonded with surrounding water molecules respectively (Verma *et al.* 2007). This region of OH bands can be contributed through OH stretching vibrational modes relating to the minerals present, or potentially to an organic matrix (Fig. 7.11A).

Absorption bands identified at 1153, 1095, and 977, cm^{-1} are the Si-O asymmetric stretching vibrational modes of SiO_4 tetrahedra, whilst absorption bands at 790 and 732 cm^{-1} are the Si-O-Si and Si-O stretching vibrational modes. An absorption band at 763 cm^{-1} may be that of carbonate ions (CO_3^{2-}) due to carbonate being present within the glasses (Legodi *et al.* 2001; Prencipe *et al.* 2004; Tatzber *et al.* 2007). Finally, the 646 cm^{-1} absorption band can be derived as a Ti-O stretching vibrational mode of TiO_6 octahedra.

Interestingly, absorption bands were observed corresponding to organic functional groups. Aliphatic $C-H_x$ moieties are observed at 2958, 2938, 2875 and 2859 cm^{-1}. The shoulder band absorption at 2958 cm^{-1} and the absorption band at 2938 cm^{-1} are derived from the asymmetric stretching vibrational modes of CH_3 and CH_2, respectively. An absorption band at 2875 cm^{-1} relates to the symmetric stretching vibrational mode of CH_3 whilst the symmetric CH_2 stretching vibrational mode is observed at 2859 cm^{-1}.

An absorption band at 1731 cm^{-1} is due to a C=O stretching vibrational mode (Schmitt and Flemming 1998) and references therein). An absorption band at 1635 cm^{-1} may be derived from the amide I C=O stretching vibrational mode (Krimm & Bandekar 1986), however, it overlaps the positioning of the H_2O bending vibrational mode. An absorption band at 1562 cm^{-1} corresponds to an Amide II vibrational mode (Krimm & Bandekar, 1986). A band at 1509 cm^{-1} may be that of a C-C stretching vibrational mode but is also located where the strongest absorption band corresponding to the epoxy is found. Further absorptions are identified at 1457 and 1382 cm^{-1} of CH_3 asymmetric and symmetric bending vibrational modes respectively. Finally the 1095 cm^{-1} shoulder absorption band may not only correspond to the Si-O asymmetric stretching vibrational mode, but also that of a PO_2^- symmetric stretch (Fig. 7.11A inset).

7.5.4.2 Tubular-free regions

An FTIR absorbance spectrum from the tubular-free glasses indicates an absorption band located at 3259 cm^{-1} on a broad band centred at 3380 cm^{-1}. These are the symmetric and asymmetric OH stretching vibrational modes of water molecules fully hydrogen bonded with surrounding water molecules (Verma *et al.* 2007). An absorption band at 1627 cm^{-1} is that of H_2O. The absorption bands at 1095 and 985 cm^{-1} are the Si-O asymmetric stretching vibrational modes of SiO_4 tetrahedra; and the 779 and 732 cm^{-1} absorption bands are Si-O-Si or Si-O stretching vibrational modes of SiO_4 tetrahedra. The absorption band at 644 cm^{-1} is that of a stretching vibrational mode of Ti-O from TiO_6 octahedra. A shoulder is observed on this absorption at 624 cm^{-1} that is assigned to belong to the mineral component of the sample, however, an exact determination is unavailable at present (Fig. 7.11B). No organic bands as seen in the tubular-rich areas are identified. An absorption band at 1517 cm^{-1} is observed, however this is due to the epoxy as explained above.

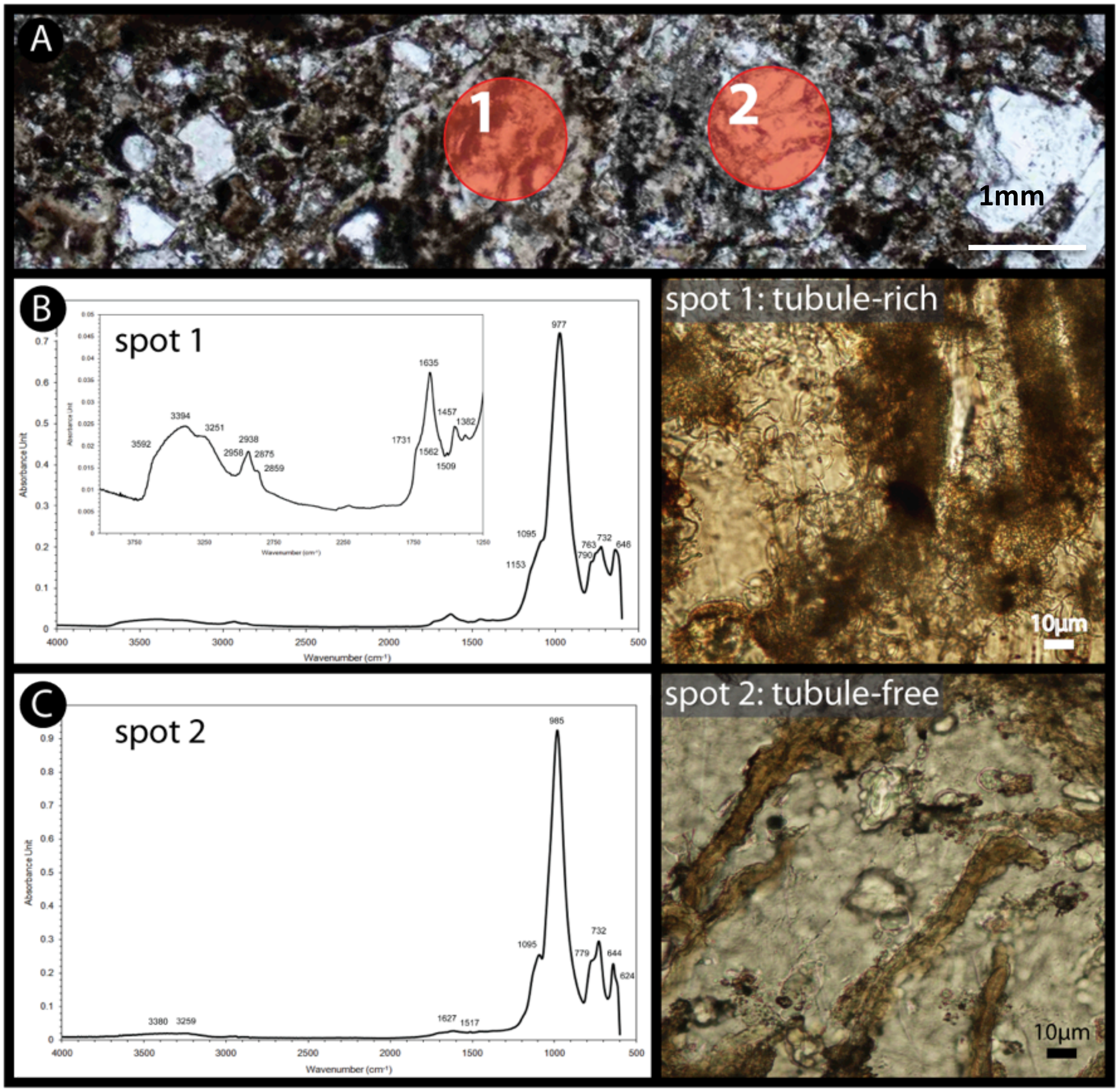

Figure 7.11: Transmitted light images and FTIR absorbance spectra.

Transmitted light images and FTIR absorbance spectra from a tubule-rich area (spot 1) and tubule-free area (spot 2). A: photomicrograph of Amerdingen suevite indicating the approximate locations of FTIR analyses (red circles). B: FTIR absorbance spectra from spot 1, a tubule-rich area. Si-O, Ti-O and OH stretching absorption bands are observed. The main organic vibrational mode frequencies are identified on the inset expanded absorbance spectrum. Peak numbers match those described within the text. The photomicrograph to the right shows the dense clots of tubular features hosted within the glass. C: FTIR absorbance spectra from spot 2, a tubule-free area. Si-O, Ti-O and OH stretching absorption bands are again observed. No organic bands are observed. The photomicrograph to the right shows the absence of tubular features. Sample RI_00_056.

7.6 Discussion

7.6.1 Evidence for biogenicity of the Reis tubules

7.6.1.1 Biogenicity criteria

Systematic criteria for determining the biogenic morphology of tubular glass alteration has been reviewed in detail elsewhere (*e.g.*, Staudigel *et al.* 2006; McLoughlin *et al.* 2007; McLoughlin *et al.* 2008). McLoughlin *et al.* (2007) developed a three-pronged approach to assessing the biogenicity of putative ichnofossils. Tentative bioalteration features must satisfy the following three criteria before a biogenic origin can be determined: "(1) a geological context that demonstrates the syngenicity and antiquity of the putative biological remains; (2) evidence of biogenic morphology and behaviour; and (3) geochemical evidence for biological processing" (McLoughlin 2007). Recently this biogenicity criteria has been applied to a series of tubular alteration textures observed in a Palaeozoic ophiolite and Precambrian greenstone belts: Titanite mineralized tubular textures were observed in ~442 Ma pillow lavas from a Caledonian west Norwegian ophiolite (Fliegel *et al.* 2011); Annulated tubular textures in Proterozoic pillow lavas from the Pechanga greenstone belt (Fliegel *et al.* 2010); and tubular alteration features in Archean pillow lavas from the Wutai greenstone belt (McLoughlin *et al.* 2010). In all three cases, titanite dating and the overprinting of later metamorphic events demonstrated the syngenicity and antiquity of the features. The Caledonian tubules (Fliegel *et al.* 2011) lacked the morphological complexity and large length to width ratios typically associated with tubule bioalteration features (*e.g.*, Furnes *et al.* 2004; Banerjee *et al.* 2006; McLoughlin *et al.* 2009). In contrast, the Pechanga (Fliegel *et al.* 2010) and Wutai (McLoughlin *et al.* 2010) features do display a complexity suggestive of biogenic morphology and behaviour. The Caledonian features did not meet the biogenicity criteria as they did not display complex morphologies suggestive of a biotic origin and geochemical evidence could neither support nor refute biological processing. The origin of these features remains ambiguous although the authors suggest they may represent the initial stages of microbial etching (Fliegel *et al.* 2011). The complex morphology together with geochemical evidence of biological processes allowed the Pechanga tubular features to be classified as ichnofossils preserving microbial tunnelling (Fliegel *et al.* 2010). Geochemical evidence is not discussed with respect to the Wutai features, however their morphological similarity to both *in situ* bioalteration of modern ocean crust and ichnofossils in other Precambrian greenstone belts lead the authors to conclude that the Wutai tubular features are biogenic in origin (McLoughlin *et al.* 2010).

7.6.1.2 Morphological evidence

Staudigel *et al.* (2007) presented a set of characteristics concerning the distribution and morphology of putative bioalteration features. We summarize these criteria in the context of the Ries glasses. The tubule features in the Ries glasses are associated with clast margins, fractures, and vesicles displaying alteration fronts consistent with post-impact hydrothermal alteration (Fig. 7.4). This is consistent with tubule formation only where the impact glass was in contact with circulating fluids. As mentioned above, tubules are cross-cut by later fractures (Fig. 7.4) which do not exhibited alteration fronts, or associated tubules. This distribution of tubules correlated with glass-fluid interfaces is consistent with reports of bioalteration in submarine basaltic glasses (*e.g.*, Furnes *et al.* 2007) and is fundamental to the proposed process of tubule formation discussed below. The tubules themselves are villiform forming straight to complex and highly convoluted vermicular features in the glass (*e.g.*, Fig. 7.4A). They may or may not bifurcate, branch (Fig. 7.3A) and/or exhibit annulations suggestive of segmentation (*e.g.*, Fig. 7.4B). There is no parsimonious abiotic explanation of these morphologies. Ambient inclusion trails (AITs) are discounted as the hollow tubules lack the longitudinal striations diagnostic of AITs. Furthermore, none of the tubular features observed to date contain terminal inclusions (see McLoughlin *et al.*, 2010 for distinguishing AITs from biogenic tunneling). Biogenic behavior is suggested by the distribution of the tubular features. Like morphologies are often clustered together, suggestive of discrete populations. Segmented tubules are clustered together while non-segmented or spiral-shaped tubules cluster in other regions (Fig. 7.3). This distribution of clusters of tubules with like morphologies is suggestive of microbial populations. Consistent with reports of bioalteration in submarine basaltic glasses *e.g.*, (Banerjee and Muehlenbachs 2003; Furnes *et al.* 2004, 2007), the tubules in the Ries glasses do not intersect, in contrast to quench crystallites, and appear to avoid each other as indicated by changes in direction as two tubules approach each other (Fig. 7.3). This is expected in microbial populations sharing a substrate. We further expand on the morphological evidence for biogenicity by following the textual arguments of Staudigel *et al.* (2007) and (McLoughlin *et al.* 2007):

- Tubules do not line up on opposite sides of fracture and therefore do not represent planes of weakness.
- Tubule diameters are on the order of a micron, consistent with the size of microbial cells and microbial borings in terrestrial volcanic glass (Staudigel *et al.* 2008a).
- The tubule diameter remains constant, i.e. there is no narrowing or flaring at the entrance or terminus of the tubule as would be expected from abiotic dissolution or vesicle generation.
- A population of tubules in the Ries glasses display regular segmentation consistent with segmented biotic filaments suggestive of multiple cells within a sheath.
- A sub-population of segmented tubules show clear bifurcation suggestive of cell division.
- The spiral morphology of some tubules in the Ries glasses is extremely hard to reconcile abiotically, but closely resembles bacterial spirochete morphology (McLoughlin *et al.* 2009).

The morphology of putative ichnofossils is a notoriously ambivalent indicator of biogenicity (Brasier *et al.* 2002; Cady *et al.* 2003; Garcia-Ruiz *et al.* 2003 and others), therefore, we also present geochemical evidence of biological processing in addition to the presence of organic compounds associated with morphological evidence.

7.6.1.3 Geochemical evidence

Infrared spectroscopy applied to the study of microorganisms over the last 60 years (*e.g.*, Heber *et al.* 1952; Norris 1959) has identified a number of distinct functional group frequencies belonging to aliphatic hydrocarbons, amides and carbonyl group molecules, which may be assigned to various functional groups in lipids, proteins and carboxylic acids. These groups can also be found as part of the structure of other organic compounds that are non-biological in nature, however in this study their spatial association with the tubule patterns may infer that they reflect biomolecules preserved within the tubules.

FTIR spectroscopy is used to compare the functional groups present within the tubule-free and tubule-rich areas of the glasses. Spectral absorptions are assigned to distinct functional groups or chemical substructures that encompass information about various biomolecules. A recent FTIR investigation of tubule bioalteration in submarine basaltic glass from the Ontong Java Plateau (OJP) found evidence of organic compounds in tubule-rich regions including: aliphatic hydrocarbons, amides, esters and carboxylic group absorption bands (Preston *et al.* in press). These organic molecules were interpreted to represent the fatty acids of cell membranes, proteins and peptides produced by microorganisms inhabiting the glass. In this study, the FTIR spectra are comparable to the spectra of the bioaltered OJP glasses and also indicate the presence of various organic molecules included aliphatic hydrocarbons, esters, amides and carboxylic groups.

Within the Ries glasses, the dominant spectral features observed are those associated with silicate minerals and glasses due to Si-O-Si, Si-O-Al and/or Al-O-Al fundamental vibrational modes (*e.g.*, McMillan 1984; McMillan and Hofmeister 1988). These spectral features are centred on 977 cm^{-1} in the tubule-rich areas, and 985 cm^{-1} in the tubule-free glasses. Absorption bands observed at 644 and 646 cm^{-1} are tentatively assigned to the Ti-O stretching vibrational modes of TiO_6 octahedra based on studies by (Zhang *et al.* 2002). A Ti phase is observed to be present in the Si-rich glass as confirmed by EDX mapping (data not shown). The OH absorption bands observed around 3250 and 3400 cm^{-1} are common to all spectra obtained, indicating the samples are hydrated; likely representing water molecules bound within the glass matrix. The absorption band at ~3590 cm^{-1} (symmetric OH stretching vibrational mode of partially hydrogen bonded water molecules) is identified in all spectra from the tubule-rich areas but is absent in those from the tubule-free glasses. A similar occurrence of partially hydrogen bonded water molecules in bioaltered areas of the OJP glasses was inferred from the FTIR spectra of that study. In the case of the OJP glasses, the presence of the ~3590 cm^{-1} absorption band in areas of dense tubular alteration and its absence in tubule-free areas was interpreted to imply that the partially hydrogen bonded water molecules were bound to an organic matrix (Preston *et al.* 2011). The H_2O absorption band commonly located at ~1640 cm^{-1} overlaps with that of the amide I absorption band described later. This absorption band has a relatively high absorbance within the tubule-rich spectra, but is weaker in the glass spectra. Perhaps indicating greater hydration of the glass containing tubules. Four internal vibration modes of the CO_3^{2-} ions can be observed (V_n), with the 763 cm^{-1} vibrational mode of this study being that of v_4, indicating the presence of minor carbonates. This is the only spectral evidence for carbonates within the samples and is only found within the tubule-rich areas.

The aliphatic C-H_x stretching vibrational bands between 3000 and 2800 cm^{-1} may be derived from groups usually present in fatty acid components of cell membranes (Helm *et al.* 1991). The asymmetric CH_2 stretching vibrational mode in this region has the highest absorbance value, followed by the CH_3 symmetric absorption band in the FTIR spectra. A dominance of CH_2 absorbance bands would indicate that the areas under analysis are highly aliphatic in nature however this is not the case for the Ries tubules. There are two CH_2 absorbance bands identified and four CH_3 indicating the dominance of CH_3 aliphatic groups in the tubule-rich areas despite the higher absorbance of the CH_2 feature. An abundance of CH_2 spectral bands indicates an aliphatic nature, the implications of a dominance of CH_3 functional groups is unclear, however, this combination of CH_2 and CH_3 absorption bands may imply a mix of carbon molecules dominated by branched rather than linear aliphatic molecules (Lin and Ritz 1993). In the tubule-free areas, the C-H_x region has inverted absorption bands, indicating that these areas have less aliphatic hydrocarbons than the standards used for calibrations.

Many of the important vibrational modes associated with lipids (Tamm and Tatulian 1997) are identified in the FTIR spectra from the tubule-rich areas of this study, for example the absorption band at 1731 cm^{-1} is that of a C=O stretching vibrational mode of esters found within fatty acids. The infrared spectra of polypeptides exhibit a number of amide absorption bands, which represent different vibrational modes of the peptide bond. An absorption band at 1635 cm^{-1} may be derived from the Amide I C=O stretching vibrational mode (*e.g.*, Byler & Susi 1986; Arrondo *et al.* 1993; Goormaghtigh *et al.* 1994; Jackson & Mantsch 1995). An amide II absorption band of secondary protein structure is observed at 1562 cm^{-1}. These amide vibrational modes are additional evidence that organics, perhaps of biological origin, are preserved within the tubule-rich areas. The Amide I absorption band overlaps with that of H_2O; however both are expected to be present within the samples. The H_2O absorption band is mirrored by bands around 3300 cm^{-1}, whilst the Amide I assignment is strengthened by the Amide II absorption band. Further deconvolution of these bands caused artefacts to be created in the spectra that hindered more detailed interpretations.

The absorption bands at 1509 and 1517 cm^{-1} are tentatively linked to vibrational modes of various carboxylic groups. These are in fact proposed to be from the epoxy used to embed the samples. This absorption band in the epoxy FTIR spectra has the highest absorbance, so even with the removal of the epoxy from the tubule and glass spectra, this still remains a very minor component. No other effects from the epoxy have been observed within any of the spectra collected. Finally the 1095 cm^{-1} tentative assignment to the PO_2^- symmetric stretching vibrational mode, if not due to the minerals present, could be due to the phosphate stretching vibrations within membrane lipids or nucleic acids of DNA (Benedetti *et al.* 1997; Pevsner & Diem 2003).

Tubules are not present in Si-rich regions of the glass nor are they concentrated in areas dominated by partially resorbed quartz grains (Fig. 7.6). This distribution suggests a preference for a glass substrate enriched in the transition metals and alkali elements. In addition, Mg, Fe, Ca, and Na depletion zones surrounding tubule alteration (Fig. 7.7) has been identified as a biological processing signature (McLoughlin *et al.* 2007). The tubule features themselves are preserved by a mineral phase enriched in Mg, Ca and Fe and depleted in Na, K, Al and Si relative to the glassy matrix (Figs. 7.6, 7.7). Ca-clinopyroxene quench crystallites present in the type I glass clast display similar enrichment and depletion patterns. Pyroxene crystallites are rich in bio-essential elements such as Fe and Ca that are lacking in the glassy matrix. It is conceivable that microbes could preferentially extract these bio-essential elements from crystallites. These elements would therefore become concentrated within the tubules and preserved following decay of organic matter. Therefore, this enrichment would be expected if microbes are accumulating these metabolically relevant elements followed by passive accumulation of authigenic mineral phases and subsequent sealing of the channel and decay of organic matter. A similar preservation mechanism has been suggested for tubules preserved by titanite mineralization in Archaean greenstone belts (Banerjee *et al.* 2006; Vogt *et al.* 2010). In the case of Archaean tubules, Ti is passively accumulated by microbes and concentrated within bioalteration features. It is unclear if the transition from hollow, smooth-walled, circular tubules to solid, decorated, rhomboid features represents a continuum of preservation and taphonomical change, or if the solid, rhomboid, linear features represent a discrete abiotic phenomena such as micro-crystallites. Both the hollow and solid tubules have morphologies distinct from the characteristic skeletal and dendritic forms of quench crystallites.

7.6.1.4 Mechanisms of microbial glass tunnelling

To account for the tubular morphologies observed in the Ries glasses, various models of glass tunnelling by microorganisms can be hypothesized (*e.g.*, Dole 1964). A plausible mechanism of euendolithic tunnelling in volcanic glass has been reported in a series of papers (Thorseth *et al.* 1992; Thorseth *et al.* 1995; Staudigel *et al.* 1998, 2008a) and is summarized below. Microbes introduced by circulating fluids may initially colonize fractures and grain boundaries of the glass substrate. As the microbe continues to dissolve the substrate extracting essential metabolites, a cavity forms. Initially, fluid circulation removes waste products as well as preventing authigenic mineral precipitation from sealing off the tunnel. As the tunnel extends, however, fluid circulating would become minimal and alteration and metabolic waste products will begin to build up. Cellular extensions, such as fungal hyphae, have been suggested as a mechanism to continue localized dissolution and tunnel formation (Staudigel *et al.* 2008b). Many prokaryotes (*e.g.*, the actinomyces) are also capable of forming hypha-like extensions (McLoughlin

2010). Eventually, it can be speculated that tunnel formation would no longer be advantageous as waste products and low-permeability mineral alteration products continue to increase. Once the tunnel is no longer sustained by fluid circulation, or cellular extensions are with drawn, the cavies become preserved by authigenic minerals and their diagenetic products.

Impact systems are understudied from the perspective of biological preservation. To the best of the authors' knowledge there are only four studies reporting *potential* fossil evidence of biological activity in impact systems: microbial etching of hydrothermal minerals at the Ries impact structure (Glamoclija *et al.* 2007), the presence of rod-shaped biomorphs in post-impact hydrothermally altered sediments from the Chesapeake Bay impact structure (Glamoclija 2007), evidence of extracellular polymeric substances in a hydrothermally precipitated calcite vein from the Siljan impact structure (Hode *et al.* 2009) and, most recently, a report of filamentous 'fossils' hosted in hydrothermally precipitated mineral assemblages within fractured impact breccia from the Dellen impact structure (Ivarsson *et al.* 2009; Plainaki *et al.* 2010). In all the above studies there is a systemic failure to recognize both biogenicity criteria as well as a systematic study of the host material: all evidence rests on tenuous morphological evidence.

7.6.2 Implications for astrobiology

Impact events are the only ubiquitous geological process in the Solar System and impact structures represent the dominant geological landform amongst the majority of the terrestrial planets. The habitability of subaerial (Herrera *et al.* 2009) and submarine natural glasses (Mason *et al.* 2007 and references therein) suggests that impact glasses, such as those found at the Ries impact structure, are potential habitats for microorganisms. Given the probable ubiquity of impact glasses in post-impact environments throughout the Solar System, it is important to understand the biological components and potential of such systems. Establishing the biogenicity of the tubular structures observed in the Ries impact glasses has significant astrobiological implications. The high flux rate of meteorite impacts on the early Earth would favour life in endolithic (within rock) environments such as glassy substrates, furthermore, impact events would provide transient energy to terrestrial bodies without endogenous volcanic heat sources to drive hydrothermal activity, such as Mars. The endolithic environments resulting from impact events are important targets for astrobiological investigations of the early Earth and of other terrestrial planets.

The extreme conditions present on Mars, such as intense UV flux, low temperature, and absence of liquid water may encourage the exploitation of endolithic strategies. McLoughlin *et al.* (2007, 2010) suggest microborings into volcanic glasses as a potential planetary biosignature and lists natural glasses as one of the most promising preservation environments for ichnofossils on early Earth and Mars. By extending this to impact glasses we greatly increase the number of candidate environments.

A recent paper by Ivarsson and Lindgren (2010) highlights the significance of impact ejecta as a target for an astrobiology focused Mars sample return mission. Impact events have the potential to excavate deep into the crust of the target body making the subsurface available for study precluding the need for drilling. The subsurface of Mars has been targeted as one of the most promising environments preserving past or present traces of life (Ivarsson and Lindgren 2010 and references therein). A better understanding of the habitability potential of impact glasses may provide insight into the possibility of similar microbial niches on other terrestrial planets, including Mars (Cockell *et al.* 2005). Establishing the biogenicity of the Ries tubules would result in the discovery of a novel habitat for life on Earth within impact ejecta. This can be extrapolated to a potential habitat within impact ejecta on other planets such as Mars.

7.7 References Cited

AMES D. E., WATKINSON D. H. and PARRISH R. R. (1998) Dating of a regional hydrothermal system induced by the 1850 Ma Sudbury impact event. *Geology* **26**(5), 447 – 450.

ARRONDO J. L. R., MUGA A., CASTRESANA J. and GOÑI F. M. (1993) Quantitative studies of the structure of proteins in solution by Fourier transform infrared spectroscopy. *Progress in Biophysics and Molecular Biology* **59**, 23 – 56.

BADER K. and SCHMIDT-KALER H. (1979) Location and structure of the Ries Crater rim north of Oettingen by refraction-seismic measurements. *Meteoritics* **14**(4), 340.

BANERJEE N., FURNES H., MUEHLENBACHS K., STAUDIGEL H. and DE WIT M. (2006) Preservation of ~3.4 – 3.5 Ga microbial biomarkers in pillow lavas and hyaloclastites from the Barberton Greenstone Belt, South Africa. *Earth and Planetary Science Letters* **241**, 707 – 722.

BANERJEE N., SIMONETTI A., FURNES H., MUECHLENBACHS K., STAUDIGEL H., HEAMAN L. and VAN KRANENDONK M. J. (2007) Direct dating of Archean microbial ichnofossils. *Geology* **35**(6), 487 – 490.

BANERJEE N. R. and MUEHLENBACHS K. (2003) Tuff life: Bioalteration in volcaniclastic rocks from the Ontong Java Plateau. *Geochemistry, Geophysics, Geosystems* **4**(4), 1037 – 1059.

BENEDETTI E., BRAMANTI E., PAPINESCHI F., ROSSI I. and BENEDETTI E. (1997) Determination of the Relative Amount of Nucleic Acids and Proteins in Leukemic and Normal Lymphocytes by Means of Fourier Transform Infrared Microspectroscopy. *Applied Spectroscopy* **51**(6), 792 – 797.

BENZERARA K., MENGUY N., BANERJEE N., TYLISZCZAK T., BROWN JR G. E. and GUYOT F. (2007) Alteration of submarine basaltic glass from the Ontong Java Plateau: A STXM and TEM study. *Earth and Planetary Science Letters* **260**, 187 – 200.

BRASIER M. D., GREEN O. R., JEPHCOAT A. P., KLEPPE M. J., VAN KRANENDONK M. J., LINDSAY J. F., STEELE A. and GRASSINEAU N. V. (2002) Questioning the evidence of Earth's oldest fossils. *Nature* **416**, 76 – 81.

BRINGEMEIER D. (1994) Petrofabric examination of the main suevite of the Otting Quarry, Nordlinger Ries, Germany. *Meteoritics & Planetary Science* **29**, 417.

BUCHNER E., SCHWARZ W., SCHMIEDER M. and TRIELOFF M. (2010) Establishing a 14.6 ± 0.2 Ma age for the Nördlinger Ries impact (Germany) — A prime example for concordant isotopic ages from various dating materials. *Meteoritics and Planetary Science* **45**(4), 662 – 674.

BYLER D. M. and SUSI H. (1986) Examination of the secondary structure of proteins by deconvolved FTIR spectra. *Biopolymers* **25**, 469 – 487.

CADY S. L., FARMER J. D., GROTZINGER J. P., SCHOPF J. W. and STEELE A. (2003) Morphological Biosignatures and the Search for Life on Mars. *Astrobiology* **3**(2), 351 – 368.

CHAO E. C. T., HUTTNER R. and SCHMIDT-KALER H. (1978) *Principal Exposures of the Ries Meteorite Crater in Southern Germany*. Bayerisches Geologisches Landesamt, Munich. pp. 1.

COCKELL C. S. (2004) Impact-shocked rocks — insights into Archean and extraterrestrial microbial habitats (and sites for prebiotic chemistry?). *Advances in Space Research* **33**, 1231 – 1235.

— (2006) The origin and emergence of life under impact bombardment. *Philosophical Transactions of the Royal Society B* **361**, 1845 – 1856.

COCKELL C. S. and LEE P. (2002) The biology of impact crater — a review. *Biological Reviews* **77**, 279 – 310.

COCKELL C. S., LEE P., OSINSKI G., HORNECK G. and BROADY P. (2002) Impact-induced microbial endolithic habitats. *Meteoritics & Planetary Science* **37**(10), 1287 – 1298.

COCKELL C. S., OLSSON-FRANCIS K., HERRERA A. and MEUNIER A. (2009) Alteration textures in terrestrial volcanic glass and the associated bacterial community. *Geobiology* **7**(1), 50 – 65.

COCKELL C. S., LEE P., BROADY P., LIM D. S. S., OSINSKI G. R., PARNELL J., KOEBERL C., PESONEN L. and SALMINEN J. (2005) Effects of asteroid and comet impacts on habitats for lithophytic organisms, A synthesis. *Meteoritics and Planetary Science* **40**(12), 1901 – 1914.

DOLE S. H. (1964) *Habitable Planets for Man*. Blaisell, New York.

FISK M. R., GIOVANNONI S. J. and THORSETH I. H. (1998) Alteration of oceanic volcanic glass; textural evidence of microbial activity. *Science* **281**(5379), 978 – 980.

FLEMMING R. L. (2007) Micro X-ray diffraction (mXRD): A versatile technique for characterization of Earth and planetary materials. *Canadian Journal of Earth Sciences* **44**, 1333 – 1346.

FLIEGEL D., KOSLER J., MCLOUGHLIN N., SIMONETTI A., DE WIT M. J., WIRTH R. and FURNES H. (2010a) In-situ dating of the Earth's oldest trace fossil at 3.34Ga. *Earth and Planetary Science Letters* **299**(3 – 4), 290 – 298.

FLIEGEL D., WIRTH R., SIMONETTI A., FURNES H., STAUDIGEL H., HANSKI E. and MUEHLENBACHS K. (2010b) Septate-tubular textures in 2.0-Ga pillow lavas from the Pechenga Greenstone Belt: a nano-spectroscopic approach to investigate their biogenicity. *Geobiology* **8**(5), 372 – 390.

FLIEGEL D., WIRTH R., SIMONETTI A., SCHREIBER A., FURNES H. and MUECHLENBACHS K. (2011) Tubular textures in pillow lavas from a Caledonian west Norwegian ophiolite: A combined TEM, LA–ICP–MS, and STXM study. *Geochemistry, Geophysics, Geosystems* **12**(2).

FURNES H., BANERJEE N. R., MUEHLENBACHS K., STAUDIGEL H. and DE WIT M. (2004) Early Life Recorded in Archean Pillow Lavas. *Science* **304**(5670), 578 – 581.

FURNES H., BANERJEE N. R., STAUDIGEL H., MUEHLENBACHS K., MCLOUGHLIN N., DE WIT M. and VAN KRANENDONK M. J. (2007) Comparing petrographic signatures of bioalteration in recent to Mesoarchean pillow lavas; tracing subsurface life in oceanic igneous rocks; Earliest evidence of life on Earth. *Precambrian Research* **158**(3 – 4), 156.

FURNES H., BANERJEE N. R., STAUDIGEL H., MUEHLENBACHS K., MCLOUGHLIN N., DE WIT M. and VAN KRANENDONK M. J. (2007) Comparing petrographic signatures of bioalteration in recent to Mesoarchean pillow lavas; tracing subsurface life in oceanic igneous rocks; Earliest evidence of life on Earth. *Precambrian Research* **158**(3 – 4), 156.

FURNES H., STAUDIGEL H., THORSETH I. H., TORSVIK T., MUEHLENBACHS K. and TUMYR O. (2001) Bioalteration of basaltic glass in the oceanic crust. *Geochemistry, Geophysics, Geosystems* **2**(8), 1049 – 1079.

GARCIA-RUIZ J. M., HYDE S. T., CARNERUP A. M., CHRISTY A. G., VAN KRANENDONK M. J. and WELHAM N. J. (2003) Self-assembled silica-carbonate structures and detection of ancient microfossils. *Science* **302**, 1194 – 1197.

GLAMOCLIJA M. (2007) Fossil Microbial Signatures from impact induced hydrothermal settings; Preliminary SEM results from the ICDP-USGS Chesapeake Bay impact structures drilling project. In *GSA Denver Annual Meeting*, pp. 1 – 3, Denver.

GLAMOCLIJA M., SCHIEBER J. and REIMOLD U. (2007) Microbial Signatures from Impact-Induced Hydrothermal Setting of the Ries Crater, Germany; A Preliminary SEM Study. In *Lunar and Planetary Science XXXVIII*, pp. 1 – 2.

GOORMAGHTIGH E., CABIAUX V. and RUYSSCHAERT J.-M. (1994) Determination of soluble and membrane protein structure by Fourier transform infrared spectroscopy. I. Assignments and model compounds. II. Experimental aspects, side chain structure, and H/D exchange. III. Secondary structures. In *Subcellular Biochemistry* (eds. H. J. Hilderson and G. B. Ralston), pp. 329 – 450. Plenum Press, New York.

GRAUP G. (1978) *Das Kristallin im Noerdlinger Ries; petrographische Zusammensetzung und Auswurfmechanismus der kristallinen Truemmermassen, Struktur des kristallinen Untergrundes und Beziehungen zum Moldanubikum. The crystallines of the Nordlinger Ries; petrographic composition and ejection mechanisms of crystalline debris, structure of crystalline basement and relationship to the Moldanubicum*. Ferdinand Enke Verlag, Stuttgart, Federal Republic of Germany (DEU), Federal Republic of Germany (DEU).

HEBER J. R., SEVENSON R. and BOLDMAN O. (1952) Infrared spectroscopy as a means for identification of bacteria. *Science* **116**, 111 – 112.

HELM D., LABISCHINSKI H., SCHALLEHN G. and NAUMANN D. (1991) Classification and identification of bacteria by Fourier-transform infrared spectroscopy. *Journal of General Microbiology* **137**, 69 – 79.

HERRERA A., COCKELL C. S., SELF S., BLAXTER M., REITNER J., ARP G., DRÖSE W., THORSTEINSSON T. and TINDLE A. G. (2008) Bacterial Colonization and Weathering of Terrestrial Obsidian in Iceland. *Geomicrobiology Journal* **25**, 25 – 37.

HERRERA A., COCKELL C. S., SELF S., BLAXTER M., REITNER J., THORSTEINSSON T., ARP G., DRÖSE W. and TINDLE A. G. (2009) A Cryptoendolithic Community in Volcanic Glass. *Astrobiology* **9**(4), 369 – 381.

HODE T., CADY S. L., VON DALWIGK I. and KRISTIANSSON P. (2009) Evidence of Ancient Microbial Life in an Impact Structure and Its Implications for Astrobiology, A Case Study, in *From Fossil to Astrobiology* (eds. Seckbach, J., Walsh, M.) Springer Science + Business Media B. V.

IVARSSON M. and LINDGREN P. (2010) The Search for Sustainable Subsurface Habitats on Mars, and the Sampling of Impact Ejecta. *Sustainability* **2**(7), 1969 – 1990.

IVARSSON M., LINDGREN P., NEUBECK A., BROMAN C., HOLM N. and HENKEL H. (2009) Filamentous structures in a hydrothermal system of the Dellen impact structure, Sweden, putative microfossil? *40th Lunar and Planetary Science Conference*, 1 – 2.

IZAWA M., BANERJEE N., FLEMMING R. and BRIDGE N. (2010) Preservation of Microbial Ichnofossils in Basaltic Glass By Titanite Mineralization. *The Canadian Mineralogist* **48**, 1255 – 1265.

JACKSON M. and MANTSCH H. H. (1995) The use and misuse of FTIR spectroscopy in the determination of protein structure. *Critical Reviews in Biochemistry and Molecular Biology* **30**, 95 – 120.

KRIMM S. and BANDEKAR J. (1986) Vibrational spectroscopy and conformation of peptides, polypeptides, and proteins. *Advances in Protein Chemistry* **38**, 181 – 364.

KRING D. A. (2000) Imapct events and their effect on the origin, evolution, and distribution of life. *GSA Today* **10**(8), 1 – 7.

LEGODI M. A., DE WAAL D., POTGIETER J. H. and POTGIETER S. S. (2001) Technical note rapid determination of CaCO3 in mixtures utilising FTIR spectroscopy. *Minerals Engineering* **14**, 1107 – 1111.

LIN R. and RITZ G. P. (1993) Reflectance FTIR Microspectroscopy of Fossil Algae Contained in Organic-Rich Shales. *Applied Spectroscopy* **47**, 265 – 271.

LINDGREN P., IVARSSON M., NEUBECK A., BROMAN C., HENKEL H. and HOLM N. G. (2010) Putative fossil life in a hydrothermal system of the Dellen impact structure, Sweden. *International Journal of Astrobiology* **9**(3), 137 – 146.

MASON O. U., STINGL U., WILHELM L. J., MOESENEDER M. M., DI MEO-SAVOIE C. A., FISK M. R. and GIOVANNONI S. J. (2007) The phylogeny of endolithic microbes associated with marine basalts. *Environmental Microbiology* **9**(10), 2539 – 2550.

MCLOUGHLIN N., BRASIER M., WACEY D., GREEN O. and PERRY R. (2007) On Biogenicity Criteria for Endolithic Microborings on Early Earth And Beyond. *Astrobiology* **7**(1), 10 – 26.

MCLOUGHLIN N., FLIEGEL D. J., FURNES H., STAUDIGEL H., SIMONETTI A., ZHAO G. and ROBINSON P. T. (2010) Assessing the biogenicity and syngenicity of candidate bioalteration textures in pillow lavas of the ~2.52 Ga Wutai greenstone terrane of China. *Chin. Sci. Bull.* **55**(2), 188 – 199.

MCLOUGHLIN N., FURNES H., BANERJEE N., MUEHLENBACHS K. and STAUDIGEL H. (2009) Ichnotaxonomy of microbial trace fossils in volcanic glass. *Journal of the Geological Society* **166**(1), 159 – 169.

MCLOUGHLIN N., FURNES H., BANERJEE N., STAUDIGEL H., MUECHLENBACHS K., DE WIT M. and VAN KRANENDONK M. (2008) Micro-bioerosion in volcanic glass: extending the ichnofossil record to Archaean basaltic crust. In *Current Developments in Bioerosion* (eds. M. Wisshak and L. Tapanila). Springer-Verlag, Berlin Heidelberg.

MCLOUGHLIN N., STAUDIGEL H., FURNES H., EICKMANN B. and IVARSSON M. (2010b) Mechanisms of microtunneling in rock substrates: distinguishing endolithic biosignatures from abiotic microtunnels. *Geobiology* **8**(4), 245 – 255.

MCMILLAN P. (1984) Structural studies of silicate glasses and melts — applications and limitations of Raman spectroscopy. *American Mineralogist* **69**, 622 – 644.

MCMILLAN P. F. and HOFMEISTER A. M. (1988) Infrared and Raman Spectroscopy. In *Spectroscopic Methods in Mineralogy and Geology* (ed. F. C. Hawthorne), pp. 99 – 150. Mineralogical Society of America.

MELOSH H. J. (1989) Impact cratering; a geologic process. *Oxford Monographs on Geology and Geophysics* **11**, 245.

MUTTIK N., KIRSIMÄE K., SOMELAR P. and OSINSKI G. R. (2008) Post-impact alteration of surficial suevites in Ries crater, Germany: Hydrothermal modification or weathering processes? *Meteoritics & Planetary Science* **43**(11), 1827 – 1840.

MUTTIK N., SIMÄE K., SOMELAR P. and VENNEMANN T. (2010) Alteration of suevitic impactites at the Ries crater, Germany: Stable isotope composition of smectite minerals and fluid temperatures. In *41st Lunar and Planetary Science Conference*.

NAUMOV M. V. (2005) Principal features of impact-generated hydrothermal circulation systems: mineralogical and geochemical evidence. *Geofluids* **5**(3), 165 – 184.

NAUMOV M. V., PLADO J. and PESONEN L. J. (2002) Impact-generated hydrothermal systems; data from Popigai, Kara, and Puchezh-Katunki impact structures; Impacts in Precambrian shields. In *4th IMPACT programme workshop on Meteorite impacts in Precambrian shields, Lappajarvi* (ed. C. Koeberl). Springer Berlin Federal Republic of Germany (DEU), Federal Republic of Germany (DEU)\.

NISBET E. (2000) Palaeobiology: The realms of Archaean life. *Nature* **405**(6787), 625 – 626.

NORRIS K. P. (1959) Infrared spectroscopy and its application to micro-biology. *Hygiene* **57**, 326 – 345.

OSINSKI G. R. (2003) Impact glasses in fallout suevites from the Ries impact structure, Germany: An analytical SEM study. *Meteoritics & Planetary Science* **38**(11), 1641 – 1667.

— (2005) Hydrothermal activity associated with the Ries impact event, Germany. *Geofluids* **5**(3), 202 – 220.

OSINSKI G. R., GRIEVE R. A. F. and SPRAY J. G. (2004) The nature of the groundmass of surficial suevite from the Ries impact structure, Germany, and constraints on its origin. *Meteoritics & Planetary Science* **39**(10), 1655 – 1683.

OSINSKI G. R., SPRAY J. G. and LEE P. (2001) Impact-induced hydrothermal activity within the Haughton impact structure, arctic Canada: Generation of a transient, warm, wet oasis. *Meteoritics and Planetary Science* **36**, 731 – 745.

OSINSKI G. R., TORNABENE L. L., BANERJEE N. R., COCKELL C. S., FLEMMING R., IZAWA M. R. M., MCCUTCHEON J., PARNELL J., PRESTON L., PICKERSGILL A. E., PONTEFRACT A., SAPERS H. M., AND SOUTHAM G (2012) Impact-generated hydrothermal systems on Earth and Mars. *Icarus* (in press)

PEVSNER A. and DIEM M. (2003) IR Spectroscopic Studies of Major Cellular Components. III. Hydration of Protein, Nucleic Acid, and Phospholipid Films. *Biopolymers* **72**, 282 – 289.

POHL J., STÖFFLER D., GALL H. and ERNSTSON K. (1977) The Ries impact crater; Impact and explosion cratering; planetary and terrestrial implications; Proceedings of the Symposium on planetary cratering mechanics. In *Lunar Science Institute topical conference ; Symposium on planetary cratering mechanics, Flagstaff, Ariz* (eds. D. J. Roddy, R. O. Pepin and R. B. Merrill). Pergamon Press New York N.Y. United States (USA), United States (USA).

PRENCIPE M., PASCALE F., ZICOVICH-WILSON C. M., SAUNDERS V. R., ORLANDO R. and DOVESI R. (2004) The vibrational spectrum of calcite (CaCO3): an ab initio quantum-mechanical calculation. *Physics and Chemistry of Minerals* **31**, 559 – 564.

PEVSNER A. and DIEM M. (2003) IR Spectroscopic Studies of Major Cellular Components. III. Hydration of Protein, Nucleic Acid, and Phospholipid Films. *Biopolymers* **72**, 282 – 289.

PLAINAKI C., MILILLO A., MURA A., ORSINI S. and CASSIDY T. (2010) Neutral particle release from Europa's surface. *Icarus* **210**(1), 385 – 395.

PRESTON L. J., BANERJEE N. R. AND IZAWA M. R. M. (2011) Infrared spectroscopic characterization of organic matter associated with microbial bioalteration textures in basaltic glass. *Astrobiology Special Edition* **11**, 585 – 599.

RICHARDSON L. J., DEMING D., HORNING K., SEAGER S. and HARRINGTON J. (2007) A spectrum of an extrasolar planet. *Nature* **445**, 892 – 895.

SANTELLI C. M., ORCUTT B. N., BANNING E., BACH W., MOYER C. L., SOGIN M. L., STAUDIGEL H. and EDWARDS K. J. (2008) Abundance and diversity of microbial life in ocean crust. *Nature* **453**, 653 – 657.

SAPERS H. M., OSINSKI G. R. and BANERJEE N. (2009) Differential alteration of glass clasts in the surficial suevites of the Ries Crater, Germany. In *72nd Annual Meteoritical Society Meeting*.

SCHMITT J. and FLEMMING H.-C. (1998) FTIR Spectroscopy in microbial and material analysis. *International Biodeterioration & Biodegradation* **41**, 1 – 11.

SHOEMAKER E. M. and CHAO E. C. T. (1961) New Evidence for the Impact Origin of the Ries Basin, Bavaria, Germany. *Journal of Geophysical Research* **66**(10), 3371 – 3378.

STAUDIGEL H., FURNES H., BANERJEE N., DILEK Y. and MEUHLENBACHS K. (2006) Microbes and volcanoes: A tale from the oceans, ophiolites, and greenstone belts. *GSA Today* **16**(10), 4 – 10.

STAUDIGEL H., FURNES H., MCLOUGHLIN N., BANERJEE N. R., CONNEL L. B. and TEMPLETON A. (2008a) 3.5 billion years of glass bioalteration: Volcanic rocks as a basis for microbial life? *Earth-Science Reviews* **89**(3 – 4), 156 – 176.

STAUDIGEL H., FURNES H., MCLOUGHLIN N., BANERJEE N. R., CONNELL L. B. and TEMPLETON A. (2008b) Microbial glass bioalteration: Inferring mechanisnis of blocorrosion from trace fossil morphology. *Geochimica et Cosmochimica Acta* **72**(12), A893 – A893.

STAUDIGEL H., YAYANOS A., CHASTAIN R., DAVIES G., TH VERDURNMEN E. A., SCHIFFMAN P., BOURCIER R. and DE BAAR H. (1998) Biologically mediated dissolution of volcanic glass in seawater. *Earth and Planetary Science Letters* **164**(1 – 2), 233 – 244.

TAMM L. K. and TATULIAN S. A. (1997) Infrared spectroscopy of proteins and peptides in lipid bilayers. *Quarterly Reviews of Biopysics* **30**, 365 – 429.

TATZBER M., STEMMER M., SPIEGEL H., KATZLBERGER C., HABERHAUER G. and GERZABEK M. H. (2007) An alternative method to measure carbonate in soils by FTIR spectroscopy. *Environmental Chemistry Letters* **5**, 9 – 12.

TEMPLETON A. and KNOWLES E. (2009) Microbial Transformations of Minerals and Metals: Recent Advances in Geomicrobiology Derived from Synchrotron-Based X-Ray Spectroscopy and X-Ray Microscopy. *Annual Review of Earth and Planetary Sciences* **37**(1), 367 – 391.

THORSETH I. H., FURNES H. and HELDAL M. (1992) The importance of microbiological activity in the alteration of natural basaltic glass. *Geochimica et Cosmochimica Acta* **56**(2), 845 – 850.

THORSETH I. H., FURNES H. and TUMYR O. (1995) Textural and chemical effects of bacterial activity on basaltic glass; an experimental approach. *Chemical Geology* **119**(1 – 4), 139 – 160.

VERMA D., KATTI K. and KATTI D. (2007) Nature of water in nacre: A 2D Fourier transform infrared spectroscopic study. *Spectrochimica Acta A* **67**, 784 – 788.

VON ENGELHARDT W. (1990) Distribution, petrography and shock metamorphism of the ejecta of the Ries Crater in Germany; a review; Cryptoexplosions and catastrophes in the geological record, with a special focus on the Vredefort Structure. *Tectonophysics* **171**(1 – 4), 259.

VOGT S. S., BUTLER R. P., RIVERA E. J., HAGHIGHIPOUR N., HENRY G. W. and WILLIAMSON M. H. (2010) The Lick-Carnegie exoplanet survey: A 3.1M planet in the habitable zone of the nearby M3V star Gliese 581. *The Astrophysical Journal* **723**, 954 – 998.

WESTALL F. and FOLK R. L. (2003) Exogenous carbonaceous microstructures in Early Archaean cherts and BIFs from the Isua Greenstone Belt: implications for the search for life in ancient rocks. *Precambrian Research* **126**(313 – 330).

WIERZCHOS J., ASCASO C., SANCHO L. G. and GREEN A. (2003) Iron-rich diagenetic minerals are biomarkers of microbial activity in antarctic rocks. *Geomicrobiology Journal* **20**, 15 – 24.

WÜNNEMANN K., MORGAN J. V. and JÖDICKE H. (2005) Is Ries crater typical for its size? An analysis based upon old and new geophysical data and numerical modelling. In *Large Meteorite Impacts III* (eds. T. Kenkmann, F. Hörz and A. Deutsch), pp. 67 – 83. Geological Society of America, Boulder, CO.

ZHANG M., SALJE E. K. H., BISMAYER U., GROAT L. A. and MALCHEREK T. (2002) Metamictization and recrystallization of titanite: An infrared spectroscopic study. *American Mineralogist* **87**, 882 – 890.

Chapter 8

8 Conclusions

The reclassification of the Rochechouart impactites and implications for the Rochechouart impact structure presented in Chapter 3 illustrate the value of looking at previously studied rocks with higher resolution micro analytical techniques. The first detailed scanning electron microscopy observations of the Rochechouart impactites resulted in the classification of the impactites based on observable intrinsic characteristics. Not only do these results have implications for the crater size and formation as discussed in Chapter 3, but furthermore, this study sets a precedent for the classification of indeterminate lithologies that do not fit the end-member nomenclature proposed by the most recent recommendations of the IUGS Subcommission on the Systematics of Metamorphic Rocks (SCMR; Stöffler and Grieve, 2007) as well as in situations where field context is unavailable.

Classical classification schemes do not account for intermediate lithologies and as a result, transitional lithologies are inadequately described by end-member nomenclature. Further to the issue of transitional lithologies, the currently accepted IUGS impactite classification scheme is based on the location of the impactite with respect to the transient cavity. Such classification requires interpretation of field context and absolute knowledge of the location of the crater rim. Both of these perquisites are currently debated in the literature leading to ambiguous and inconsistent use of nomenclature. Interpretive bias aside, the majority of terrestrial impact structures are not preserved well enough to consistently and accurately delineate the extent of the transient cavity. Furthermore, in cases where there is no field context classification based on provenance is purely speculative. The petrographic evaluation of the Rochechouart impactites presented in Chapter 3 allows for a systematic classification integrating the most recent recommendations of the IUGS SCMR with descriptive nomenclature allowing for indeterminate and transitional units. Such a classification system based on observable, intrinsic characteristics can be extrapolated to collections where there is an extremely limited sample size or complete lack of field context such as deeply eroded impact structures, drill cores, Apollo samples, meteorites, and future planetary sample returns. Being able to correlate these samples and compare them to samples with a field context is invaluable and fundamental to understanding impact cratering as a geological process occurring not just on Earth but also on other terrestrial bodies. The detailed high-resolution petrographic study of the Rochechouart impactites provides the context with which to approach the Ries samples. An important step in establishing biogenicity, often absent in other studies assessing putative biogenic features, is a careful and thorough evaluation of the geologic context to demonstrate the integrity, syngenicity, and antiquity of the features in question.

The work contained in this thesis has illustrated the presence of enigmatic tubular features hosted within impact glass clasts from impact melt-bearing breccias from the Ries impact structure, Germany. The host glasses at the Ries contain crystallites dominated by Ca- and Al-rich pyroxene (Osinski, 2003; this study). These pyroxene crystallites are typically skeletal to dendritic, which are well-understood quench crystal morphologies (*e.g.*, Marshall 1961; Iddings 1899; Lofgren 1977). Previous studies also describe tubular and complexly curved, non-canonical pyroxene crystallites (Osinski, 2003; Engelhardt *et al.* 1995). Our work suggests these features are not purely mineralogical in origin and display morphological and geochemical evidence consistent with biological activity (Chapters 4 – 7). Furthermore, the scale of these features preclude traditional X-ray diffraction studies and nanoscale analyses such as TEM based techniques have not yet been used to investigate the nature of these anomalous 'crystallites.' The complex morphologies and convoluted structures characterizing these features combined with organic functional group identification imply that these features represent biological trace fossils within impact glass.

Previous studies by have shown similar tubular features to exist within oceanic basaltic glasses from the Ontong Java Plateau that are widely accepted to represent bioalteration textures (*e.g.*, Banerjee & Muehlenbachs 2003; Benzerara *et al.* 2007). Bioalteration of natural volcanic glasses is a well-documented phenomenon in modern oceanic crust, Phanerozoic ophiolites and Archaean greenstone belts. In addition, it has been shown that endolithic microbial communities thrive in terrestrial and submarine volcanic glasses with a range of SiO_2 contents (Richardson *et al.* 2007; Santelli *et al.* 2008; Cockell *et al.* 2009; Herrera *et al.* 2009). It has been shown that microbes colonize glasses while extracting metabolically relevant elements leaving traces, such as tubular features, (Banerjee & Muehlenbachs 2003; Herrera *et al.* 2008; McLoughlin *et al.* 2008 and refs therein) of this activity.

Volcanic glasses have been shown to comprise an important and significant microbial habitat on Earth requiring the re-evaluation of the limits of the biosphere. It is conceivable that impact glass also comprises a microbial habit. Furthermore, the micro-habitats created by meteorite impacts have been shown to be conducive to microbial colonization (Cockell & Lee 2002a). In particular, impact-induced hydrothermal systems (as documented to have occurred at Ries, Osinski 2005; Muttik *et al.* 2008) have been postulated to facilitate microbial colonization following an impact event. Meteorite impact events interacted significantly with the terrestrial biosphere throughout Earth's history. In the Hadean and Early Archaean during the Late Heavy Bombardment period 3.8 – 4.2 Ga (Kring & Cohen 2002) a cataclysmic spike in large impact events coincided with the origin of life on Earth suggesting a role for impact events in the early evolution, if not origin, of life on Earth. Impacts during the Phanerozoic would have acted as primary biological succession events irreversibly altering the habitat of the affected area.

Several theories suggest a hot, aqueous environment for the origin of life; submarine hydrothermal systems comprise one of the predominant candidate environments for prebiotic chemistry (*e.g.,* Martin *et al.* 2008; Nisbet & Sleep 2001). Although there is wide spread speculation on the geological setting for the origin of life, there is some consensus regarding the requisite conditions. Liquid water, organic polymers including the bioessential elements fundamental to organic compounds (C, H, O, N, P, and S), an excess of Gibbs free energy and a thermodynamic regime capable of supporting disequilibrium, chemical or otherwise, a mechanism to concentrate the prebiotic constitutes and a proto-membrane in which they can be contained, and energy to facilitate or initiate prebiotic reactions. Phylogenetic and metabolic research into the last universal common ancestor suggests a high temperature setting (*e.g.,* Schwartzman & Lineweaver

2004). Submarine hydrothermal systems, black smokers, satisfy all of these requirements. However, such systems have a limited geological context and the extent of such plate-tectonic dependent phenomena during the Hadean and early Archean is not well established. Post-impact hydrothermal systems extend the possible environments for the origin of life on Earth. High impact flux during the Late Heavy Bombardment would have established such system in a variety of geologic settings increasing the chemical complexity of candidate environments. Post-impact hydrothermal systems were likely more common than submarine hydrothermal systems on the primitive Earth and would therefore constitute a statistically more probably environment for the origin of life. The vesicular nature of impact glass and pore-space created in shocked target rocks may have acted as proto-membranes to concentrate prebiotic constituents. Furthermore, clays are a common weathering product of subaerial glasses and a phyllosilicates substrate has been suggested as an initial template for the earliest self-replicating molecules (Ponnamperuma *et al.* 1982). It has been postulated that meteorites during the Late Heavy Bombardment have delivered the initial organic molecules to Earth (Chyba & Sagan 1992). The high flux rate of meteorite impacts on the early Earth would favor life in chasmoendolithic environments suggesting that meteorite impacts played a pivotal role in the early evolution, if not origin of, life on Earth and possibly life on other planets.

If impact-induced environments were not the initial geological setting for the origin of life, impact events during the Late Heavy Bombardment almost certainly influenced early life (*e.g.,* Maher & Stevenson 1988; Abramov & Mojzsis 2009). Periodic global heating may account for the thermophillic root of life preserved in 16s rRNA sequences (Pace 1994; Schwartzman & Lineweaver 2004). In this sense meteorite impacts could not only have generated the putative bottleneck resulting in a perceived thermophilic last universal common ancestor, but would also select for thermo-tolerant life surviving previous impacts (Cockell & Lee 2002). The endolithic habitats produced by increasing the porosity of crystalline targets during shock metamorphism would provide a refuge from frequent meteorite bombardment and intense UV radiation. Impact glass, an amorphous substrate relatively easily attacked by microbially produced acids, can thermodynamically support autotrophic metabolisms.

Large impact events occurring once life has been firmly established on Earth have undoubtedly influenced evolution. Although often cited a catastrophic events (Sleep *et al.* 1989) such as the Chicxulub impact ultimately leading to the mass extinction as the Cretaceous-Palaeogene (K – Pg) boundary 65 Myr ago (Alvarez *et al.* 1980), impact events can be viewed as biological resetting events generating unique habitats and novel microbial niches (Cockell & Lee 2002). The endolithic habitats created by through the impact process have been shown to harbour a diverse microbial community (Cockell 2004; Parnell *et al.* 2004). Furthermore, shock metamorphism has been shown to mobilize bioessential elements (Pontefract *et al.* 2012) and based on the elemental and mineralogical characterization presented in this thesis impact glasses would provide a suitable nutrient source. Establishing the tubules in the Ries glass as biogenic features extends the known environments on Earth for the microbial colonization of natural glasses. Impact glass would have been much more prevalent on the Archaean Earth during the Late Heavy Bombardment and likely comprises a significant component of natural glass on other rocky bodies in our Solar System such as Mars.

The search for evidence of life on Mars has driven space exploration. Most recently, Curiosity, the Mars Science Laboratory, landed in Gale Crater on Mars August 5, 2012 to begin a multi-year mission to assess habitability potential and search for life on Mars (Grotzinger *et al.* 2012). Although a detailed multi-analytical study to assess the biogenicity of suggestive features requires sample return, remote instruments such as those onboard Curiosity could potentially be used to identify impact glass associated with hydrothermal alteration. Previous missions have not specifically identified impact glass as a high-priority target, however, the ubiquity of impact glasses on the terrestrial planets and the preservation potential of natural glasses on Earth suggest that impact glass on Mars may be of significant astrobiological interest. Using the X-ray diffraction capabilities of CheMin (Blake *et al.* 2012), the broad spectral features indicative of amorphous material could potentially distinguish impact glass from crystalline material. Using laser ablation and the ChemCam (Wiens *et al.* 2012) suite, chemical information can be combined with the mineralogical information acquired from CheMin to identify potential hydrothermal mineral assemblages. By using non-contact instruments, samples can be prioritized by the presence amorphous material occurring in association with minerals typical of hydrothermal alteration for collection and further analysis by on board instruments such as SAM. The mass spectrometer, gas chromatograph, and tunable laser spectrometer comprising the SAM instrument suite can then be used on high-priority samples to identify the presence of light elements (H, O, N) associated with organic molecules (Mahaffy *et al.* 2012). Samples containing amorphous material, hydrothermal mineralogical assemblages and evidence of organics could then be targeted for future sample return missions. Given the density of tubular features in the Ries glasses, a minimum of 1 cm^3 of material would be required for a similar, multi-analytical, robust geological and biological characterization of the sample.

In summary a biogenic origin for the Ries tubules is concluded. Given the probable ubiquity of impact glasses in post-impact environments throughout the Solar System, it is important to understand the biological components and potential of such systems. Establishing the biogenicity of the alteration structures observed in impact glasses has significant and far-reaching astrobiological implications, as impact cratering is a ubiquitous geological process throughout the solar system. Thus, post-impact hydrothermal systems expand the potential environments for the origin of life and for later microbial colonization to environments without endogenous volcanic heat sources to drive hydrothermal activity. Understanding the geomicrobiology of impact craters on Earth is critical in furthering the search for life on Mars. The hydrothermal systems associated with impact events may therefore provide an additional setting to study evidence of early life on Earth. Further studies considering the potential hydrothermal habitats of impact craters may not only yield insight into early life and the origin of life on Earth, but furthermore, may comprise a potential habitat for life and past life on other terrestrial planets such as Mars.

8.1 References Cited

ABRAMOV, O., and MOJZSIS, S. J. (2009) Microbial habitability of the Hadean Earth during the late heavy bombardment. *Nature* **459**, 419 – 422.

ALVAREZ, L.W., ALVAREZ, W., ASARO, F. AND MICHEL, H.V. (1980) Extraterrestrial cause for the Cretaceous/Tertiary extinction. *Science* **208**, 1095 – 1108.

AMES D. E., WATKINSON D. H. and PARRISH R. R. (1998) Dating of a regional hydrothermal system induced by the 1850 Ma Sudbury impact event. *Geology* **26**(5), 447 – 450.

BANERJEE N. R. and MUEHLENBACHS K. (2003) Tuff life: Bioalteration in volcaniclastic rocks from the Ontong Java Plateau. *Geochemistry, Geophysics, Geosystems* **4**(4), 1.

BENZERARA K., MENGUY N., BANERJEE N., TYLISZCZAK T., BROWN JR G. E. and GUYOT F. (2007) Alteration of submarine basaltic glass from the Ontong Java Plateau: A STXM and TEM study. *Earth and Planetary Science Letters* **260**, 187 – 200.

BLAKE, D., VANIMAN, D., ACHILLES, C., ANDERSON, R., BISH, D., BRISOW, T., CHEN, C., CHIPERA, S., CRISP, J., DES MARAIS, D., DOWNS, R. T., FARMER, J., FELDMAN, S., FONDA, M., GAILHANOU, M., MA, H., MING, D. W., MORRIS, R. V., SARRAZIN, P., STOLPER, E., TREIMANN, A., and YEN, A. (2012) Characterization and calibration of the CheMin mineralogical instruments on Mars Science Laboratory. *Space Science Reviews* **170**(1 – 4), 341 – 399.

CHYBA, C. and SAGAN, C. (1992) Endogenous production, exogenous delivery and impact-shock synthesis of organic molecultes: an inventory for the origins of life. *Nature* **355**, 125 – 132.

COCKELL C. S. (2004) Impact-shocked rocks - insights into Archean and extraterrestrial microbial habitats (and sites for prebiotic chemistry?). *Advances in Space Research* **33**, 1231 – 1235.

— (2006) The origin and emergence of life under impact bombardment. *Philosophical Transactions of the Royal Society B* **361**, 1845 – 1856.

COCKELL C. S. and LEE P. (2002) The biology of impact crater — a review. *Biological Reviews* **77**, 279 – 310.

COCKELL C. S., OLSSON-FRANCIS K., HERRERA A. and MEUNIER A. (2009) Alteration textures in terrestrial volcanic glass and the associated bacterial community. *Geobiology* **7**(1), 50 – 65.

GROTZINGER, J. P., CRISP, J., VASAVADA, A. R., ANDERSON, R. C., BAKER, C. J., BARRY, R., BLAKE, D. F., CONRAD, P., EDGETT, K. S., FERDOWSKI, B., GELLERT, R., GILBERT, J. B., GOLOMBEK, M., GÓMEZ-ELVIRA, J., HASSLER, D. M., JANDURA, L., LITVAK, M., MAHAFFY, P., MAKI, J., MEYER, M., MALIN, M. C., MITROFANOV, I., SIMMONDS, J. J., VANIMAN, D., WELCH, R. V., and WIENS, R. C. (2012) Mars Science Laboratory Mission and Science Investigation. *Space Science Reviews* **140**(1 – 4), 5 – 56.

HERRERA A., COCKELL C. S., SELF S., BLAXTER M., REITNER J., ARP G., DRÖSE W., THORSTEINSSON T. and TINDLE A. G. (2008) Bacterial Colonization and

Weathering of Terrestrial Obsidian in Iceland. *Geomicrobiology Journal* **25**, 25 – 37.

HERRERA A., COCKELL C. S., SELF S., BLAXTER M., REITNER J., THORSTEINSSON T., ARP G., DRÖSE W. and TINDLE A. G. (2009) A Cryptoendolithic Community in Volcanic Glass. *Astrobiology* **9**(4), 369 – 381.

IDDINGS, J., 1899, Geology of Yellowstone National Park: U.S. Geological Survey Monograph 32, Pt. 2, 893 p.

KRING D. A. and COHEN B. A. (2002) Cataclysmic bombardment throughout the inner solar system 3.9 – 4.0 Ga. *Journal of Geophysical Research* **107**(E2), 4-1 – 4-6.

LOFGREN, G., 1974, An experimental study of plagioclase crystal morphology: Isothermal crystallization. *American Journal of Science* **274**, 243 – 273.

MAHAFFY, P. M., WEBSTER, C. R., CABANE, M., CONRAD, P. C., COLL, P., and the SAM TEAM. (2012) The Sample Analysis as Mars Investigation and instrument suite. *Space Science Reviews* **170**(1 – 4), 401 – 478.

MAHER, K. A., and STEVENSON, D. J. (1988) Impact frustration of the origin of life. *Nature* **331**, 612 – 614.

MARSHALL, R. R., 1961, Devitrification of Natural Glass. *Geological Society of America Bulletin* **72**, 1493 – 1520.

MCLOUGHLIN N., FURNES H., BANERJEE N., STAUDIGEL H., MUECHLENBACHS K., DE WIT M. and VAN KRANENDONK M. (2008) Micro-bioerosion in volcanic glass: extending the ichnofossil record to Archaean basaltic crust. In *Current Developments in Bioerosion* (eds. M. Wisshak and L. Tapanila). Springer-Verlag, Berlin Heidelberg.

MUTTIK N., KIRSIMÄE K., SOMELAR P. and OSINSKI G. R. (2008) Post-impact alteration of surficial suevites in Ries crater, Germany: Hydrothermal modification or weathering processes? *Meteoritics & Planetary Science* **43**(11), 1827 – 1840.

NISBET, E. G. and SLEEP, N. H. (2001) The habitat and nature of early life. *Nature* **409**, 1083 – 1091.

OSINSKI G. R. (2005) Hydrothermal activity associated with the Ries impact event, Germany. *Geofluids* **5**(3), 202 – 220.

OSINSKI G. R., LEE P., PARNELL J., SPRAY J. G. and BARON M. (2005) A case study of impact-induced hydrothermal activity: The Haughton impact structure, Devon Island, Canadian High Arctic. *Meteoritics & Planetary Science* **40**(12), 1859 – 1878.

PACE, N. R. (1997) A Molecular View of Microbial Dirversity and the Biosphere. *Science* **276**, 634 – 740.

PARNELL, J., LEE, P., COCKELL, C. S., and OSINSKI, G. R. (2004) Microbial colonization in impact-generated hydrothermal sulphate deposits, Haughton impact structure, and implications for sulphates on Mars. *International Journal of Astrobiology* **3**(3), 247 – 256.

PONNAMPERUMA, C. SHIMOYAMA, A. and FRIEBELE, E. (1982) Clay and the origin of life. *Origins of Life* **12**, 9 – 40.

PONTEFRACT, A., OSINSKI, G. R., LINDGREN, P., PARNELL, J., COCKELL, C. S., and SOUTHAM, G. (2012) The effects of meteorite impacts on the availability of bioessential elements for endolithic organsims. *Meteoritics & Planetary Science* **47**(10), 1681 – 1691

RICHARDSON L. J., DEMING D., HORNING K., SEAGER S. and HARRINGTON J. (2007) A spectrum of an extrasolar planet. *Nature* **445**, 892 – 895.

SANTELLI C. M., ORCUTT B. N., BANNING E., BACH W., MOYER C. L., SOGIN M. L., STAUDIGEL H. and EDWARDS K. J. (2008) Abundance and diversity of microbial life in ocean crust. *Nature* **453**, 653 – 657.

SCHWARTZMAN, D. W. and LINEWEAVER, C. H. (2004) The hyperthermophilic origin of life revisited. *Biochemical Society Transactions* **32**(2), 168 – 171.

SLEEP, N. H., ZAHNLE, K. J., KASTING, J. F., and MOROWITZ, H. J. (1989) Annihilation of ecosystmes by large asteroid impacts on the early Earth. *Nature* **342**, 139 – 142.

STÖFFLER D. AND GRIEVE R. (2007) Classification and nomenclature scheme; impactites. In *Metamorphic rocks, a classification and glossary of terms; recommendations of the International Union of Geological Sciences Subcommission on the Systematics of Metamorphic Rocks* edited by Fettes D. and Desmons J. Cambridge: University Press Cambridge. pp. 82 – 92.

WESTALL F. and FOLK R. L. (2003) Exogenous carbonaceous microstructures in Early Archaean cherts and BIFs from the Isua Greenstone Belt: implications for the search for life in ancient rocks. *Precambrian Research* **126,** 313 – 330.

WIENS, R. C., MAURICE, S., BARRACLOUGH, B., SACCOCCIO, M. and the CHEMCAM TEAM. (2012) The ChemCam Instruments Suite on the Mars Science Laboratory (MSL) rover: Body unit and combined systems tests. *Space Science Reviews* **170,** 1 – 4, 167 – 227.

WIERZCHOS J., ASCASO C., SANCHO L. G. and GREEN A. (2003) Iron-rich diagenetic minerals are biomarkers of microbial activity in antarctic rocks. *Geomicrobiology Journal* **20**, 15 – 24.

Appendices

Appendix A: Samples locations

		Geographic coordinates§		
Sample #	**Locality:**	**Easting:**	**Northing:**	**Sample / location description:**
00-001	Otting	3631339	5416222	Suevite - rich in glass clasts
00-002	Otting	3631342	5416193	Suevite - weathered
00-003	Otting	3631371	5416110	Suevite - rich in glass clasts
00-004	Otting	3631371	5416110	Diorite clast from suevite
00-005	Otting	3631293	5416075	Suevite - rich in glass clasts
00-006	Otting	3631293	5416075	Glass clast from suevite
00-007	Otting	3631260	5416071	Suevite - rich in glass clasts
00-008	Otting	3631082	5416171	Glass clast from suevite
00-009	Otting	3631082	5416171	Suevite - rich in glass clasts
00-010	Otting	3631082	5416171	Vesiculated gneiss clast from suevite
00-011	Gundelsheim	3634110	5419521	Monomict limestone (Bunte) breccia
00-012	Aumühle	3619410	5426780	Suevite - fine grained from contact zone
00-013	Aumühle	3619410	5426780	Suevite - fine grained from contact zone
00-014	Aumühle	3619410	5426780	Suevite - fine grained from contact zone
00-015	Aumühle	3619410	5426780	Polymict (Bunte) breccia
00-016	Aumühle	3619410	5426780	Polymict (Bunte) breccia
00-017	Aumühle	3619410	5426780	Polymict (Bunte) breccia
00-018	Aumühle	3619410	5426780	Suevite
00-019	Aumühle	3619409	5426784	Gneiss clast from suevite
00-020	Aumühle	3619409	5426784	Glass clast from suevite
00-021	Aumühle	3619409	5426784	Polymict breccia underlying suevite (Bunte)
00-022	Aumühle	3619409	5426784	Polymict breccia underlying suevite (Bunte)
00-023	Aumühle	3619423	5426786	Monomict limestone (Bunte) breccia
00-024	Aumühle	3619423	5426786	Suevite - fine grained
00-025	Aumühle	3619407	5426792	Suevite
00-026	Aumühle	3619407	5426792	Glass clast from suevite

00-027	Aumühle	3619407	5426792	Gneiss clast from suevite
00-028	Zipplingen	3603351	5421959	Suevite
00-029	Zipplingen	3603351	5421959	Suevite
00-030	Zipplingen	3603351	5421959	Suevite - glass clasts weathered out
00-031	Zipplingen	3603351	5421959	Suevite - glass clasts weathered out
00-032	Zipplingen	3603351	5421959	Suevite - reddish groundmass colour
00-033	Unterwilfingen	3606010	5420799	Clast from polymict breccia
00-034	Unterwilfingen	3606010	5420799	Monomict limestone (Bunte) breccia
00-035	Unterwilfingen	3605995	5420796	Clast from polymict breccia
00-036	Unterwilfingen	3605995	5420796	Clast from polymict breccia
00-037	Unterwilfingen	3605995	5420796	Clast from polymict breccia
00-038	Unterwilfingen	3605995	5420796	Clast from polymict breccia
00-039	Unterwilfingen	3605995	5420796	Clast from polymict breccia
00-040	Unterwilfingen	3605993	5420794	Clast from polymict breccia
00-041	Unterwilfingen	3605993	5420794	Clast from polymict breccia
00-042	Unterwilfingen	3605993	5420794	Clast from polymict breccia
00-043	Unterwilfingen	3605993	5420794	Clast from polymict breccia
00-044	Unterwilfingen	3605993	5420794	Clast from polymict breccia
00-045	Unterwilfingen	3605993	5420794	Clast from polymict breccia
00-046	Unterwilfingen	3605989	5420798	Parautchthonous gneiss ('inner ring')
00-047	Unterwilfingen	3605989	5420798	Parautchthonous granite ('inner ring')
00-048	Altenburg	3605170	5409482	Suevite
00-049	Seelbronn	3608291	5400422	Suevite
00-050	Seelbronn	3608291	5400422	Suevite
00-051	Seelbronn	3608291	5400422	Suevite
00-052	Seelbronn	3608291	5400422	Suevite
00-053	Seelbronn	3608291	5400422	Vesiculated gneiss clast from suevite
00-054	Seelbronn	3608291	5400422	Monomict limestone (Bunte) breccia
00-055	Amerdingen	3609761	5398912	Suevite
00-056	Amerdingen	3609761	5398912	Suevite
00-057	Amerdingen	3609761	5398912	Suevite
00-058	Sternbach	3609762	5410033	Sedimentary clast from suevite
00-059	Sternbach	3609762	5410033	Suevite
00-060	Sternbach	3609762	5410033	Suevite
00-061	Mauren	3622091	5401147	Suevite

01-001	Hoppingen	3621295	5407851	Limestone 'megablock'
01-002	Ronheim	3623451	5407340	Polymict (Bunte) breccia
01-003	Aumühle	3619422	5426788	Suevite with pipe structure
01-004	Aumühle	3619410	5426780	Suevite - contact zone
01-005	Aumühle	3619410	5426780	Marl clast from suevite
01-006	Aumühle	3619410	5426780	Suevite with pipe structure

01-007	Aumühle	3619410	5426780	Suevite
01-008	Aumühle	3619406	5426791	Suevite - black with purple glass clasts
01-009	Aumühle	3619406	5426791	Suevite - black with purple glass clasts
01-010	Aumühle	3619406	5426791	Suevite - black with purple glass clasts
01-011	Steinbühl	3627752	5417801	Suevite - heavily weathered/altered
01-012	Steinbühl	3626951	5418011	Faulted limestones from crater rim
01-013	Steinbühl	3626951	5418011	Faulted limestones from crater rim
01-014	Polsingen	3624372	5420803	Impact melt rock
01-015	Polsingen	3624372	5420803	Impact melt rock
01-016	Herkheim	3610556	5410729	Polymict crystalline breccia
01-017	Holheim	3607307	5410051	Faulted limestones from crater rim
01-018	Holheim	3607307	5410051	Faulted limestones from crater rim
01-019	Langenmuhle	3608910	5423049	Crystalline breccia?
01-020	Langenmuhle	3608910	5423049	Crystalline breccia?
01-021	Langenmuhle	3608910	5423049	Crystalline breccia?
01-022	Langenmuhle	3608910	5423049	Crystalline breccia?
01-023	Unterwilfingen	3606002	5420807	Polymict breccia
01-024	Zipplingen	3603350	5421959	Suevite
01-025	Zipplingen	3603350	5421959	Suevite
01-026	Schmühingen	3611382	5408121	Polymict crystalline breccia
01-027	Aufhausen	3609262	5401757	Suevite
01-028	Aufhausen	3609262	5401757	Suevite
01-029	Aufhausen	3609262	5401757	Glass clast from suevite
01-030	Anhausen	3608291	5406271	Glass clast from suevite
01-031	Anhausen	3608291	5406271	Suevite - heavily altered and weathered
01-032	Holheim	3606863	5410052	Faulted limestones from crater rim
01-033	Holheim	3606863	5410052	Faulted limestones from crater rim
05-001	Iggenhausen	3601599	5399529	Malm limest. Megablock; gries structure
05-002	Iggenhausen	3601599	5399529	Malm limest. Megablock; gries structure
	Guldesmuhle	3599940	5395020	Sand pit
	Hainsfarth	4400000	5425000	Sedimentary crater-fill deposits
05-003	Megasheim	4401719	5424517	Sedimentary crater-fill deposits
05-004	Polsingen	4405213	5420863	Impact melt rock
05-005	Polsingen	4405213	5420863	Impact melt rock; altered
05-006	Amerbach	4404745	5417630	Impact melt rock
05-007	Otting	4411482	5416117	Suevite
05-008	Otting	4411482	5416117	Suevite
	Otting			House next to quarry
	Gundelsheim	4414422	5419412	Quarry in Malm limestone
	Harburg	4404206	5407633	Quarry in Bunte Breccia
05-009	Wennenberg	4399490	5413647	Polymict crystalline breccia

05-010	Wennenberg	4399490	5413647	Polymict crystalline breccia
05-011	Aumühle	4399752	5426819	Soft, green transitional lithology
05-012	Aumühle	4399752	5426819	Impact breccia; hard, red, from transitional zone
05-013	Aumühle	4399752	5426819	Suevite-like breccia
05-014	Aumühle	4399752	5426819	Impact breccia; hard, red, from transitional zone
05-015	Aumühle	4399752	5426819	Suevite; contact with Bunte Breccia
05-016	Aumühle	4399752	5426819	Suevite; contact with Bunte Breccia
05-017	Aumühle	4399752	5426819	Breccia vein from within Bunte Breccia
05-018	Aumühle	4399752	5426819	Suevite; degassing pipe
05-019	Aumühle	4399752	5426819	Suevite; degassing pipe
05-020	Aumühle	4399752	5426819	Glass stringer in unusual facies of suevite
05-021	Aumühle	4399752	5426819	Melt-rich suevite/impact melt breccia
05-022	Aumühle	4399752	5426819	Melt-rich suevite/impact melt breccia
05-023	Hohenaltheim			Suevite; sedimentary-rich
05-024	Sternbach	4390282	5401387	Shale clast from suevite
05-025	Sternbach	4390282	5401387	Suevite with calcite vug
05-026	Sternbach	4390282	5401387	Shale clast from Bunte Breccia
	Seelbronn	3608166	5400843	Suevite quarry
	Altenburh	3605177	5409458	Suevite quarry
	Holheim			Quarry in Malm limestone
05-027	Wengenhousen	3607282	5420353	Clast from polymict crystalline breccia
05-028	Wengenhousen	3607282	5420353	Clast from polymict crystalline breccia
05-029	Wengenhousen	3607282	5420353	Clast from polymict crystalline breccia
05-030	Wengenhousen	3607282	5420353	Clast from polymict crystalline breccia
05-031	Wengenhousen	3607282	5420353	Clast from polymict crystalline breccia
05-032	Wengenhousen	3607282	5420353	Clast-rich sedimentary crater-fill
05-033	Unterwilfingen	3606058	5420731	Gneiss-cored glass clast
05-034	Unterwilfingen	3606058	5420731	Soft breccia
05-035	Unterwilfingen	3606058	5420731	Gneiss-cored glass clast
05-036	Zipplingen	3603300	5421933	Suevite

§Coordinate system: DHDN/3-degree Gauss Zone 2.

09-001	Wengenhousen	010,28.080	48,54.613	v. altered Fe-rich clast from polymict crystalline breccia
09-002	Wengenhousen	010,28.080	48,54.613	v. altered chalky clast and matrix polymict crystalline breccia
09-003	Wengenhousen	010,28.080	48,54.613	altered Fe-rich polymict breccia - dark zone
09-004	Unterwilfingen	010,26.784	48,54.917	highly altered suevite
09-005	Zipplingen	010,24.539	48,55,580	glass rich suevite (some blue glass)
09-006	Seelbron	010,28.189	48,44.114	skinny glass clast
09-007	Seelbron	010,28.189	48,44.114	glass clast with in filled vesicles

09-008a	Seelbron	010,28.189	48,44.114	v. altered white vesicular glass
09-008b	Seelbron	010,28.189	48,44.114	altered blue and purple glass
09-009	Seelbron	010,28.189	48,44.114	unusual blue vesicular glass
09-010a	Seelbron	010,28.189	48,44.114	5 glass clasts
09-010b	Seelbron	010,28.189	48,44.114	rusty glass clast
09-011	Seelbron	010,28.189	48,44.114	glass clast with white mineralization/alteration
09-012	Seelbron	010,28.189	48,44.114	v. shocked clast - altered glass?
09-013	Seelbron	010,28.189	48,44.114	altered multi-coloured glass - with layer of alteration
09-014	Altenburg	010,25.863	48,48.790	altered glass clasts with vesicles filled with white material
09-015	Altenburg	010,25.863	48,48.790	glass clasts
09-016	Altenburg	010,25.863	48,48.790	dark matrix
09-017	Altenburg	010,25.863	48,48.790	light matrix
09-018	Sternbach	010,30.466	48,30,466	large piece of white chalky vein material
09-019	Sternbach	010,30.466	48,30,466	small pieces of white chalky vein material
09-020	Sternbach	010,30.466	48,30,466	altered glass clasts
09-021	Sternbach	010,30.466	48,30,466	2 glass clasts with infilling of calcite?
09-022	Sternbach	010,30.466	48,30,466	suevite with altered glass clasts and fresh glass
09-023	Sternbach	010,30.466	48,30,466	3 pieces of suevite with altered glass clasts
09-024	Sternbach	010,30.466	48,30,466	suevite with large glass clast
09-025	Polsingen	010,42.331	48,55.069	dark red melt, sandy lithic clasts
09-026	Polsingen	010,42.331	48,55.069	red melt various alteration colours
09-027	Polsingen	010,42.331	48,55.069	altered melt- white chalky crust
09-028	Polsingen	010,42.331	48,55.069	large piece of melt with angular lithic clasts
09-029	Polsingen	010,42.331	48,55.069	moderately altered melt
09-030	Altenburg	010,25.863	48,48.790	white chalky material from vein 'B'
09-031	Altenburg	010,25.863	48,48.790	white chalky material from vein 'C'
09-032	Altenburg	010,25.863	48,48.790	left margin of vein stained and coarse material
09-033	Altenburg	010,25.863	48,48.790	40cm above 032, R margin, fine grained carbonate material
09-034	Altenburg	010,25.863	48,48.790	limestone block from W side
09-035	Altenburg	010,25.863	48,48.790	limestone block from E side
09-036	Altenburg	010,25.863	48,48.790	suevite near limestone contact
09-037	Altenburg	010,25.863	48,48.790	glass clasts near sample 36
09-038	Altenburg	010,25.863	48,48.790	suevite glass near base of hill under W limestone block
09-039	Aumühle	010,37.703	48,58.266	suevite from 1m above contact
09-040	Aumühle	010,37.703	48,58.266	glass clasts 50cm above contact
09-041	Aumühle	010,37.703	48,58.266	lisegene banding 'concretions' on quarry floor
09-042	Aumühle	010,37.703	48,58.266	dark red-brown muddy vein fill
09-043	Aumühle	010,37.703	48,58.266	subvertical fractures 'suevite matrix'
09-044	Aumühle	010,37.703	48,58.266	transitional layer flat side is top
09-045	Aumühle	010,37.703	48,58.266	bunte breccia below transitional layer
09-046	Aumühle	010,37.293	48,58.293	suevite glass
09-047	Aumühle	010,37.293	48,58.293	suevite alteration in sub-vertical yellow-brown 'pipes'

09-048	Aumühle	010,37.293	48,58.293	alteration zone proximal to pipes, reddish, irregular, globular
09-049	Aumühle	010,37.293	48,58.293	grey suevite close to pipe material 047 glasses purple
09-050	Aumühle	010,37.293	48,58.293	yellow-brown muddy filling from central hole in 'pipe'
09-051	Aumühle	010,37.293	48,58.293	purple glass clasts
09-052	Otting	010,47.462	48,52.635	grey massive suevite
10-001a	Otting	010,47.468	48,52.651	surface alteration of suevite
10-00b	Otting	010,47.468	48,52.651	fresh surface of suevite
10-002	Otting	010,47.468	48,52.651	altered suevite from pipe-like structure
10-003	Otting	010,47.468	48,52.651	coarse-grained vein fill material
10-004	Otting	010,47.468	48,52.651	chiselled out coarse-grained vein fill material
10-005 0cm	Aumühle			Aumühle suevite transect on W face
10-005 50cm	Aumühle			Aumühle suevite transect on W face
10-005 60cm	Aumühle			Aumühle suevite transect on W face
10-005 70cm	Aumühle			Aumühle suevite transect on W face
10-005 90cm	Aumühle			Aumühle suevite transect on W face
10-005 1m	Aumühle			Aumühle suevite transect on W face
10-005 1.5m	Aumühle			Aumühle suevite transect on W face
10-005 2m	Aumühle			Aumühle suevite transect on W face
10-005 2.5m	Aumühle			Aumühle suevite transect on W face
10-005 3m	Aumühle			Aumühle suevite transect on W face
10-005 3.5m	Aumühle			Aumühle suevite transect on W face
10-005 4m	Aumühle			Aumühle suevite transect on W face
10-005 4.5m	Aumühle			Aumühle suevite transect on W face
10-005 5m	Aumühle			Aumühle suevite transect on W face
10-006	Aumühle			breccia pipe on N face, material scraped from inside 'pipe'
10-007	Aumühle			transistional zone between suevite and Bunte breccia
10-008	Amerdingen	3609761	5398912	suevite - old quarry blocks - altered
10-009	Amerdingen	3609761	5398912	suevite - old quarry blocks - appears altered, but coherent c fresh glass
10-010	Seelbronn	010,28.189	48,44.114	lime stone Bunte breccia
10-011	Polsingen	010,42.331	48,55.069	impact melt - collected as display sample
10-012 0m	Aumühle			Aumühle suevite transect part 1 (upper face) on N face
10-012 1m	Aumühle			Aumühle suevite transect part 1 (upper face) on N face
10-012 2m	Aumühle			Aumühle suevite transect part 1 (upper face) on N face
10-012 3m	Aumühle			Aumühle suevite transect part 1 (upper face) on N face
10-012 4m	Aumühle			Aumühle suevite transect part 1 (upper face) on N face
10-012 5m	Aumühle			Aumühle suevite transect part 1 (upper face) on N face
10-012 6m	Aumühle			Aumühle suevite transect part 1 (upper face) on N face
10-012 7m	Aumühle			Aumühle suevite transect part 1 (upper face) on N face
10-012 8m	Aumühle			Aumühle suevite transect part 1 (upper face) on N face
10-013 0m	Aumühle			Aumühle suevite transect part 2 (lower face) on N face
10-013 1m	Aumühle			Aumühle suevite transect part 2 (lower face) on N face

10-013 2m	Aumühle			Aumühle suevite transect part 2 (lower face) on N face
10-013 3m	Aumühle			Aumühle suevite transect part 2 (lower face) on N face
10-013 4m	Aumühle			Aumühle suevite transect part 2 (lower face) on N face
10-013 5m	Aumühle			Aumühle suevite transect part 2 (lower face) on N face
10-013 6m	Aumühle			Aumühle suevite transect part 2 (lower face) on N face
10-014	Aumühle			fine-grained suevite - bunte breccia transitional zone on E wall
10-015	Aumühle			very fine grained grey unite btw suevite and breccia E wall
10-016	Aumühle			white crud at base of transition zone E wall
10-017	Aumühle			pink crud in transition zone E wall
10-018	Aumühle			yellow flakes below pink crud E wall
10-019	Aumühle			yellow-red-orange banded alteration of breccia E wall
10-020 0cm	Aumühle			transect through transitional zone on E wall
10-020 50cm	Aumühle			transect through transitional zone on E wall
10-020 1m	Aumühle			transect through transitional zone on E wall
10-020 1.5m	Aumühle			transect through transitional zone on E wall
10-020 2m	Aumühle			transect through transitional zone on E wall
10-021	Aumühle			suevite 3.5m tangent to transect,10-020, ~50cm above contact
10-022	Erbisberg	010,30.720	48,49.873	limestone with 'stromatelite' texture
10-023	Erbisberg	010,30.720	48,49.873	loose limestone block with 'tubular' texture
10-024	Hainsfarth			sediments with stromatelites with reported preserved 'tubular' textures
10-025	Unterwilfingen	010,26.784	48,54.917	powder-like chalky highly altered glass clast in suevite dyke
10-026	Unterwilfingen	010,26.784	48,54.917	matrix of altered suevite dyke to the right of 10-025

Appendix B: Field photographs

Otting


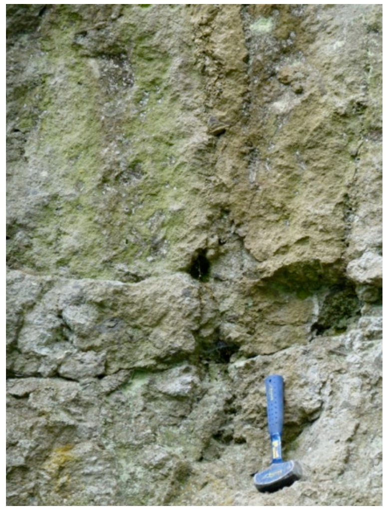




Aumühle

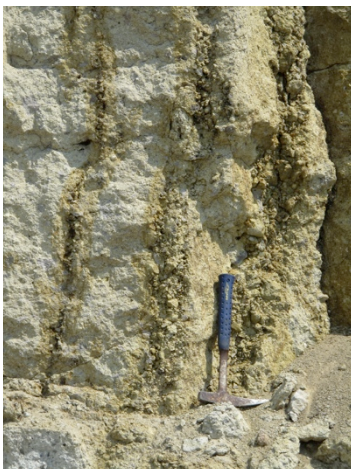

Gundelsheimer

Erbisberg

Seelbron

Amerdingen




Appendix C: Photomicrographs

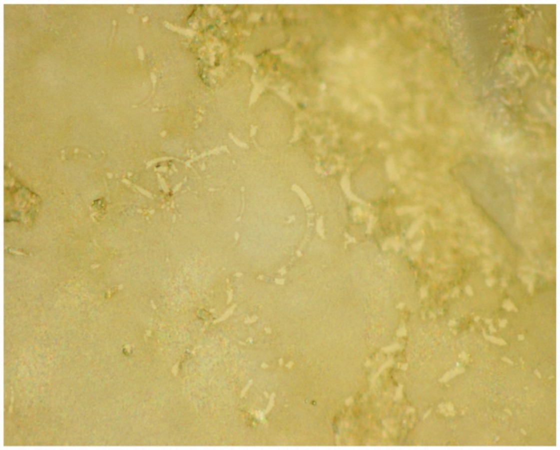

003 reflected copy

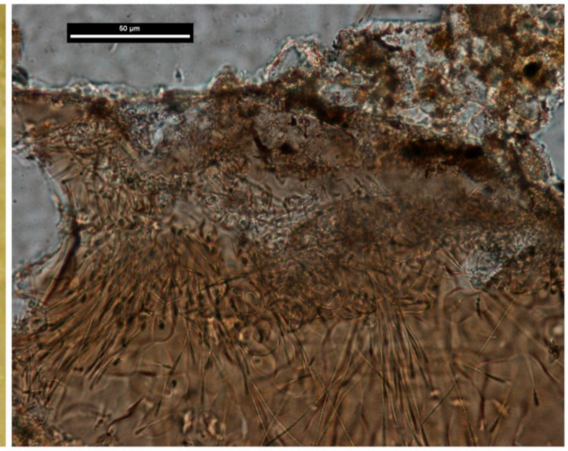

RI 00_056 003 50X copy

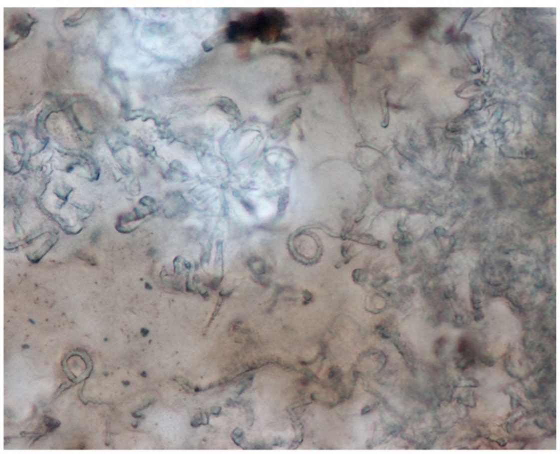

RI-056 Z-Series-Focused_001 copy

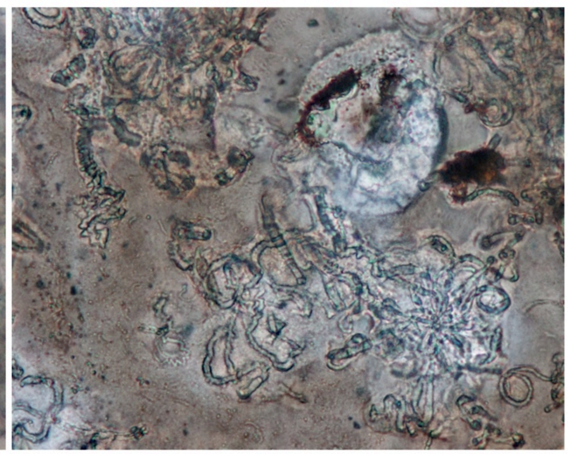

RI-056 Z-Series-Focused_002 copy

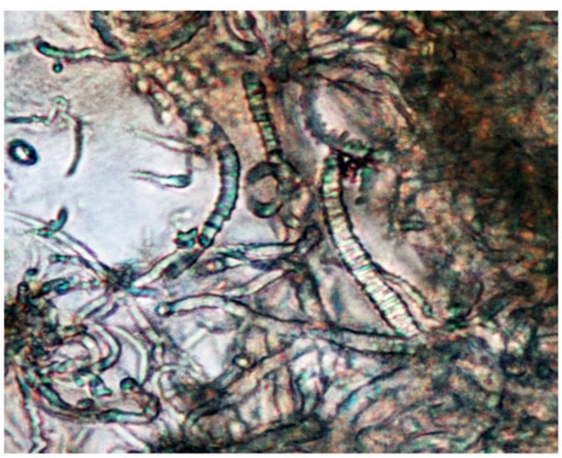

RI-056 Z-Series-Focused_003 copy

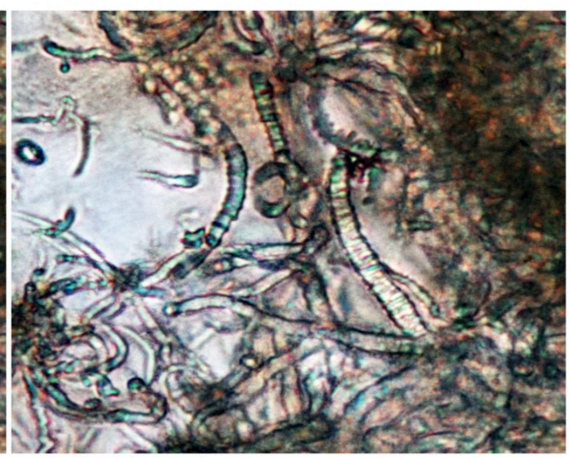

RI-056 Z-Series-Focused_003-adjusted

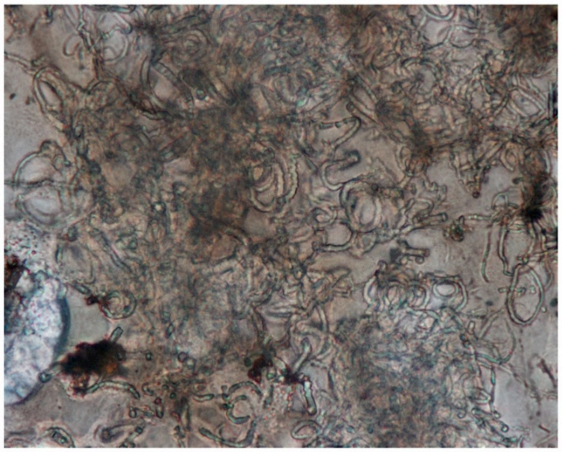
RI-056 Z-Series-Focused_004 copy

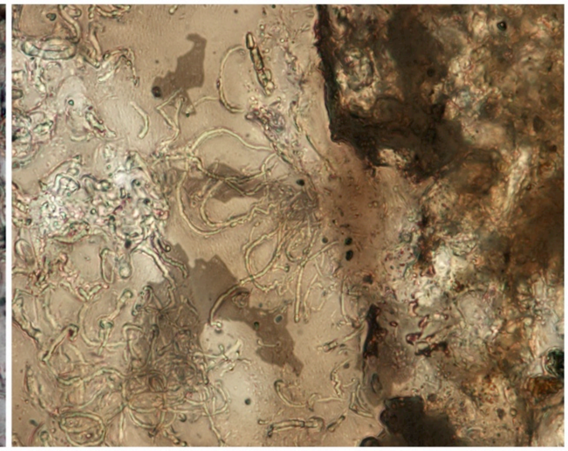
RI_056 z stack 1

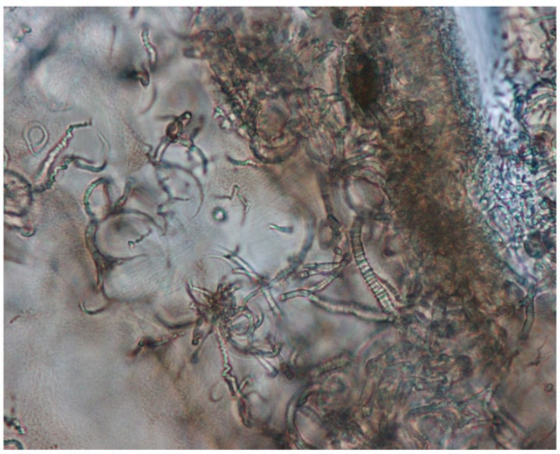
RI_056_003 x100 copy

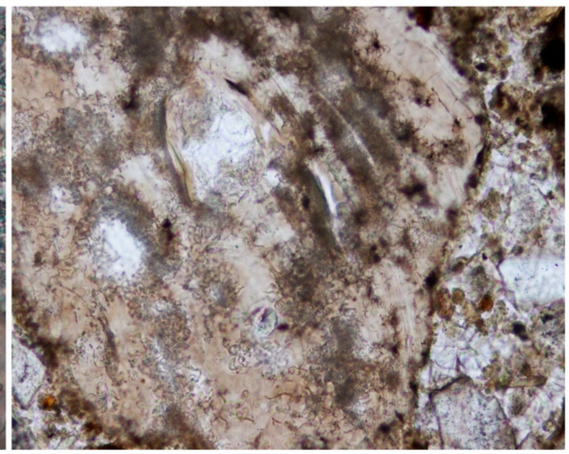
RI_056_003 x20 copy

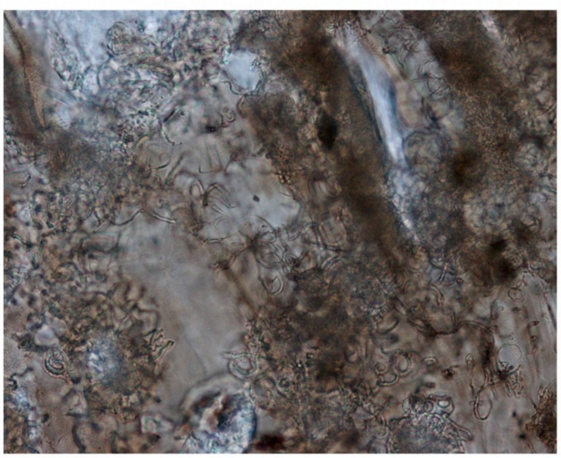
RI_056_003 x50 copy

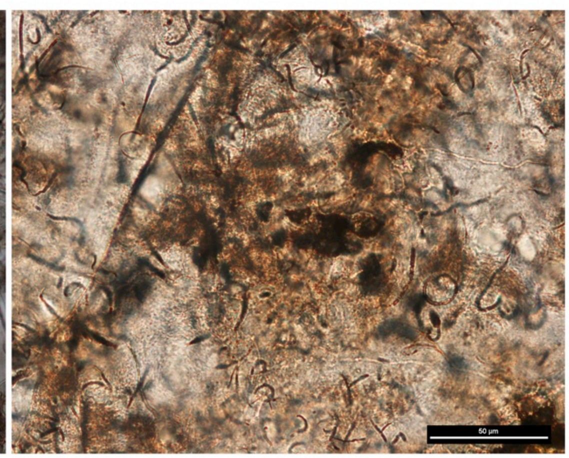

RI_10_013 0m_008

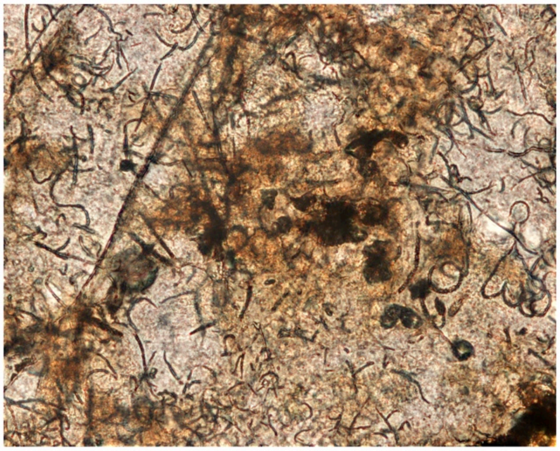
RI_10_013 0m_009 (z-stack) 50X

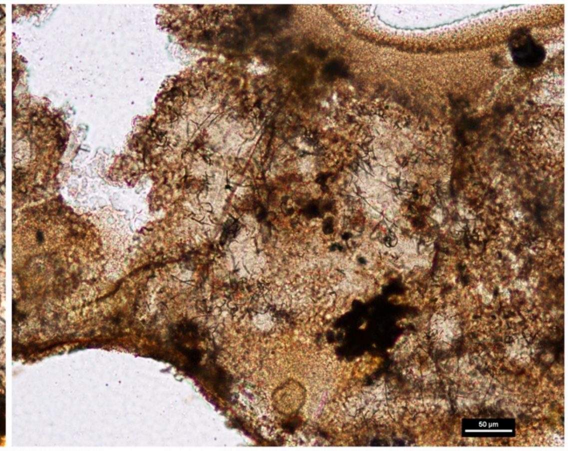

RI_10_013 0m_010

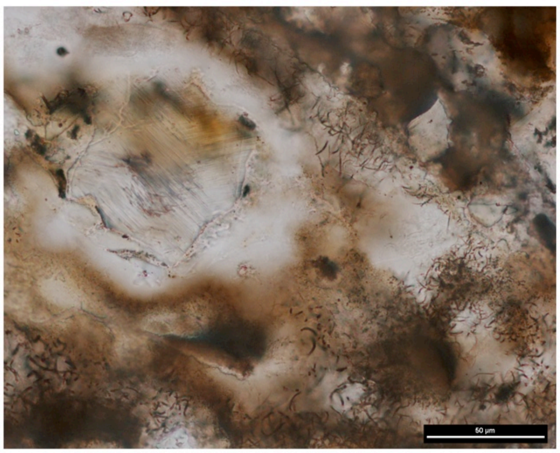

RI_10_013 4m_001

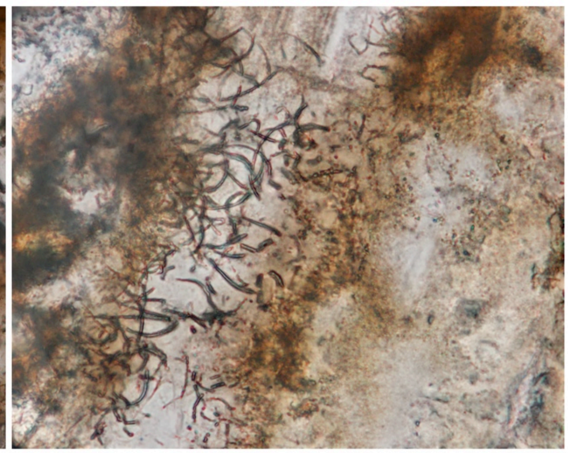
RI_10_013 4m_005 (z-stack)

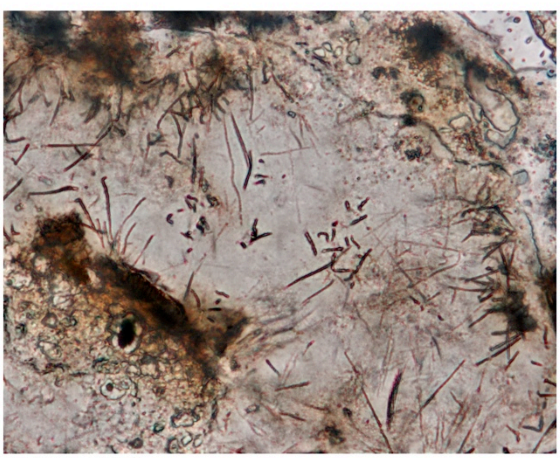
RI_10_013 5m_006 (z-stack)

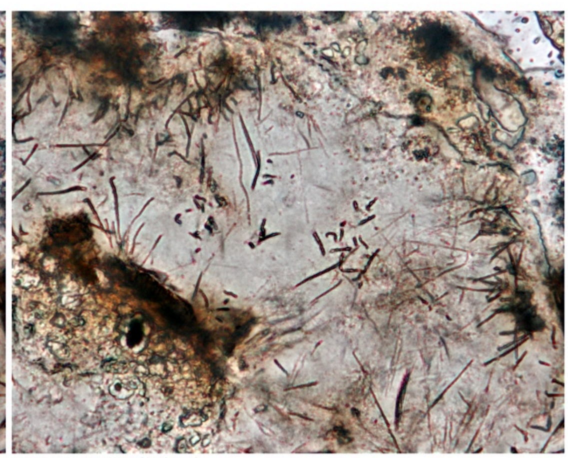
RI_10_013 5m_006 (z-stack)-adjusted

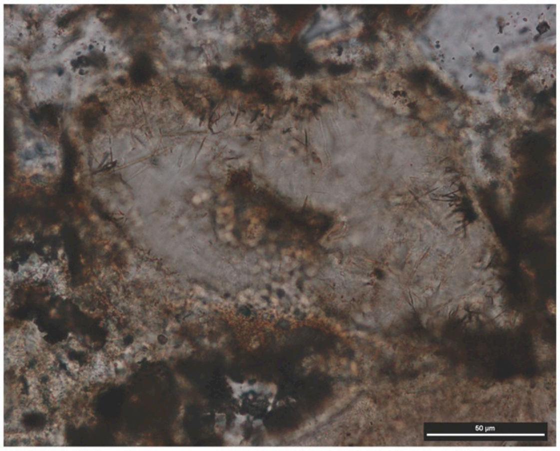

RI_10_013 5m_007

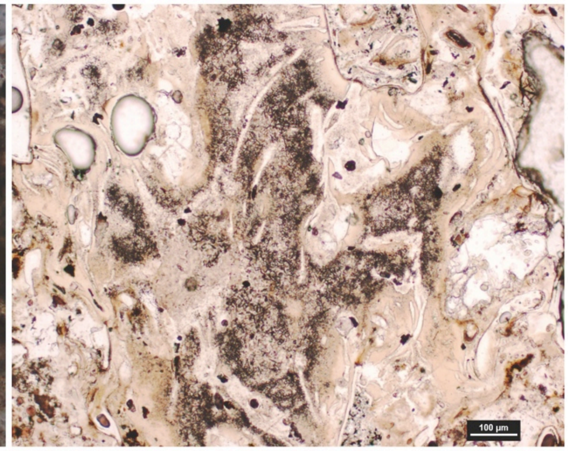

RI_10_013 5m_012

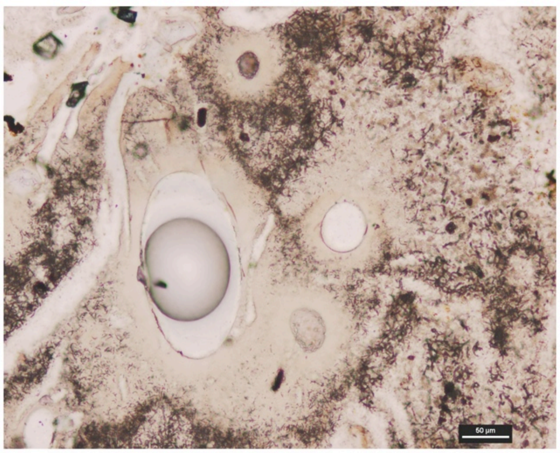

RI_10_013 5m_014

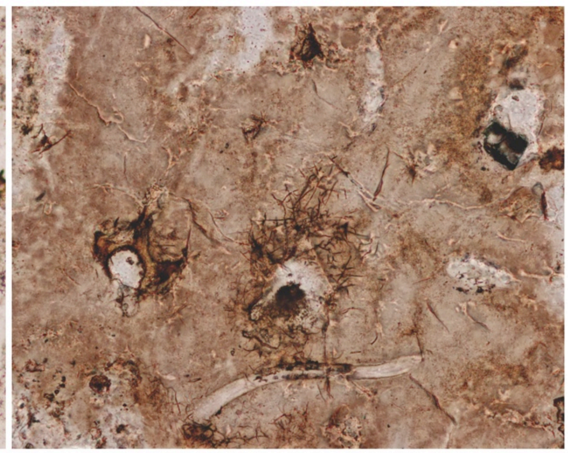
RI_10_013 5m_016 (z-stack)

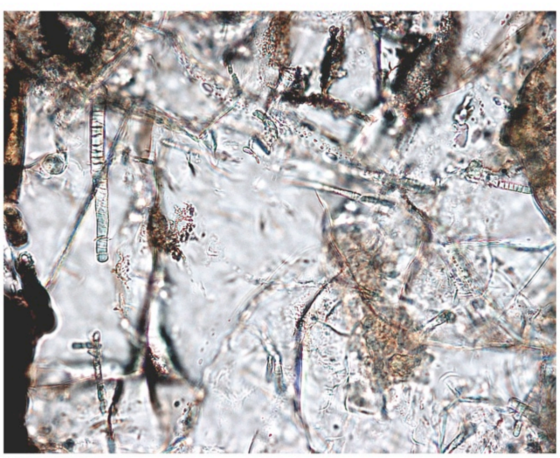
Ri 05 040_001 50x copy

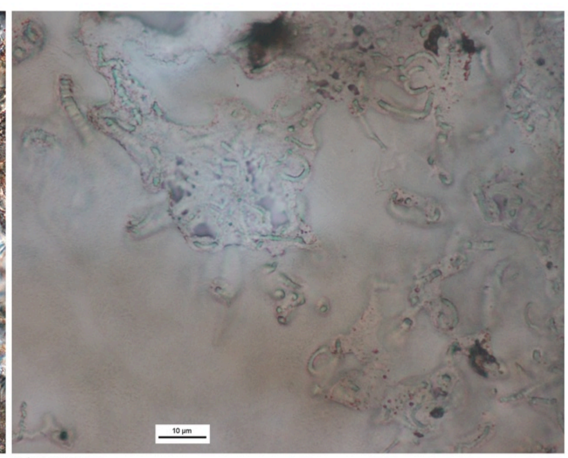

scale 001 copy

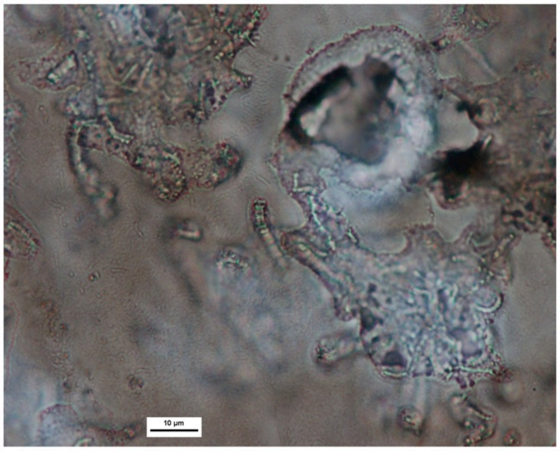
scale 002 copy

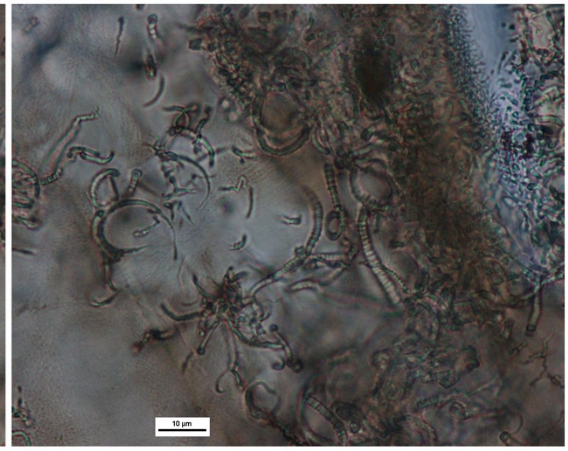
scale 003 copy

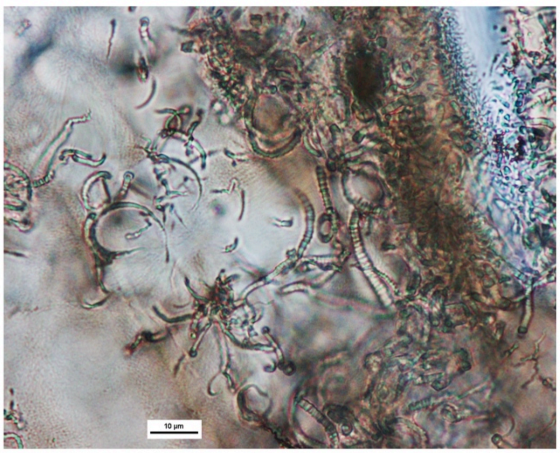
scale 003-adjusted

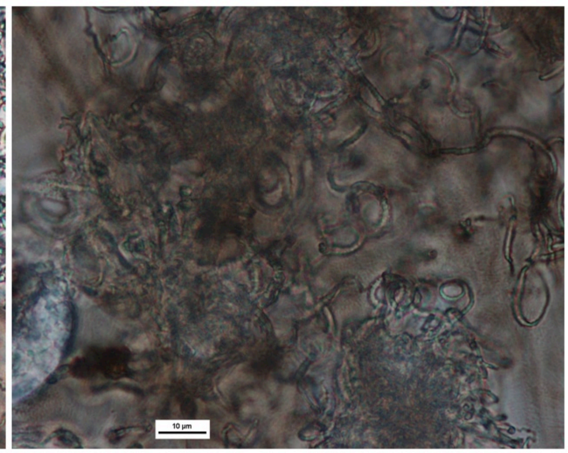
scale 004 copy

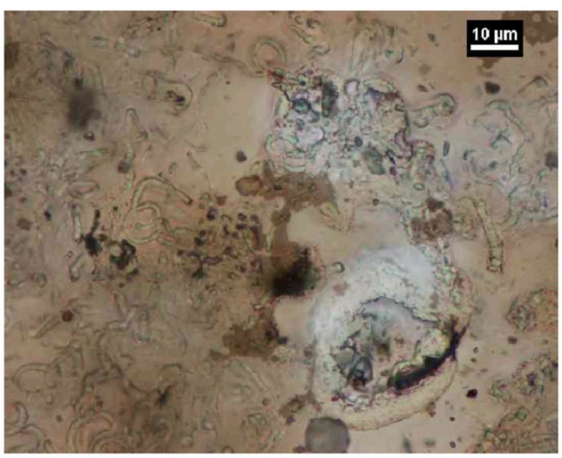

stack 1 composite copy

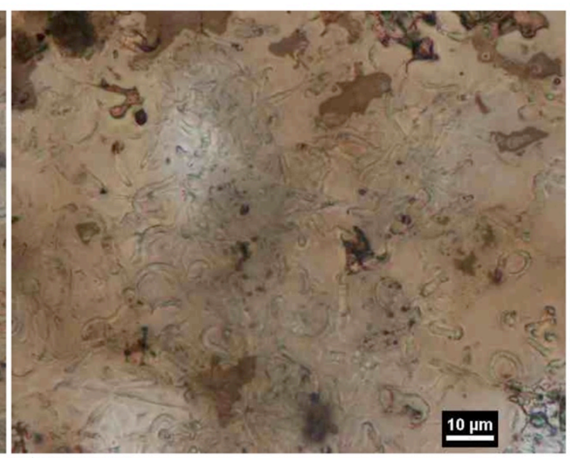

stack 2 composite copy

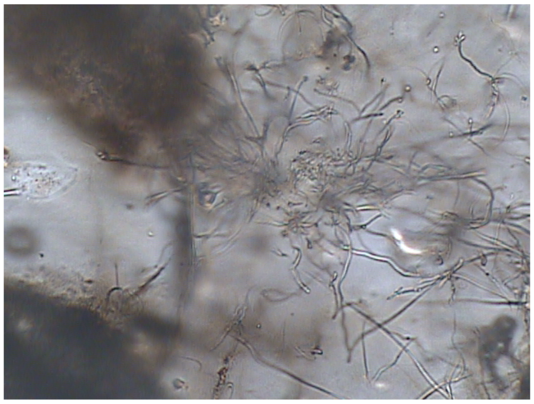
RI_10_006b_10


RI_10_006b_11

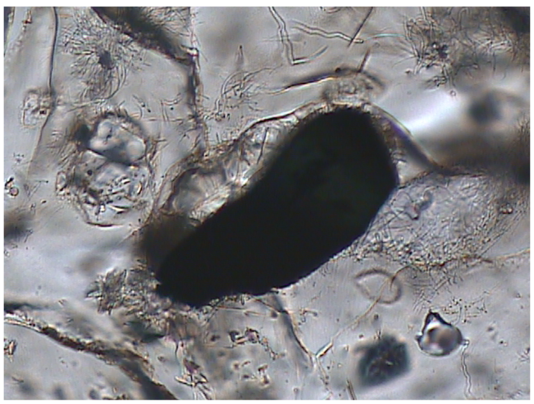
RI_10_006b_11

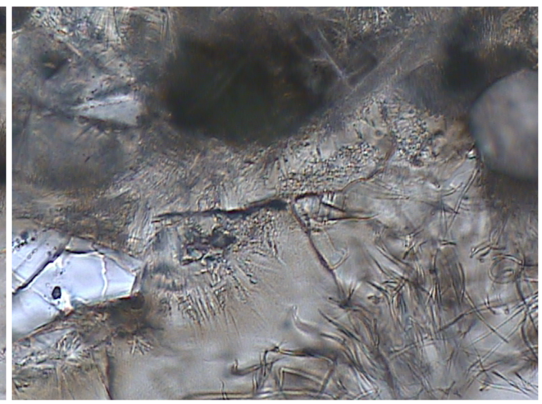
RI_10_006b_13

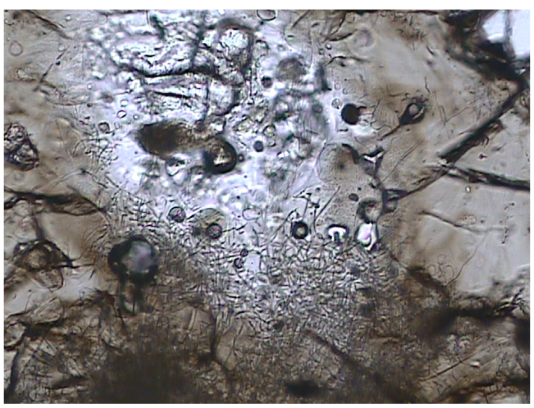
RI_10_006b_13


RI_10_006b_15

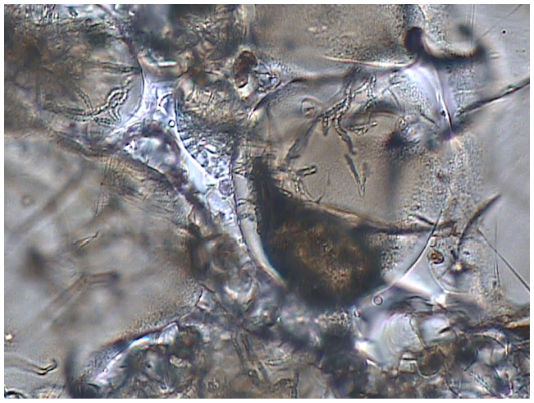

RI_10_006b_03

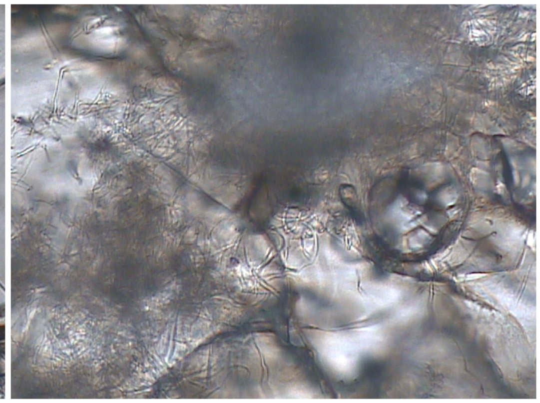

RI_10_006b_03

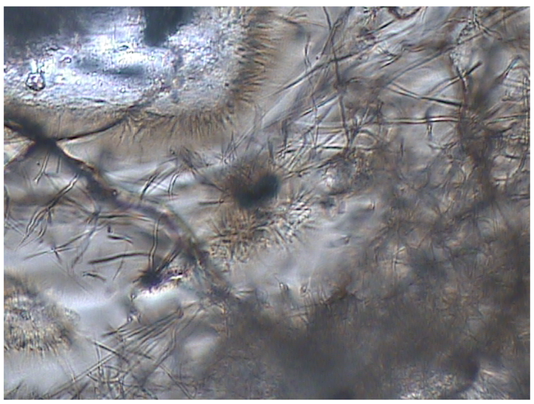

RI_10_006b_05

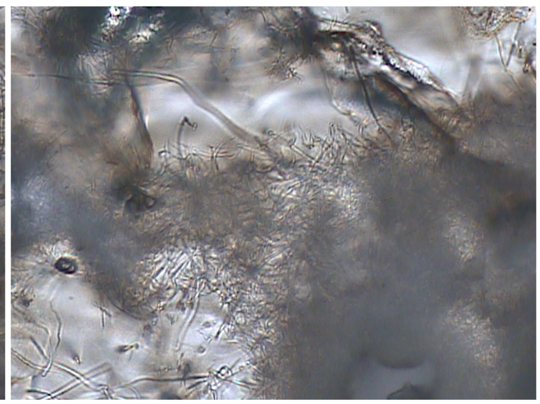

RI_10_006b_05

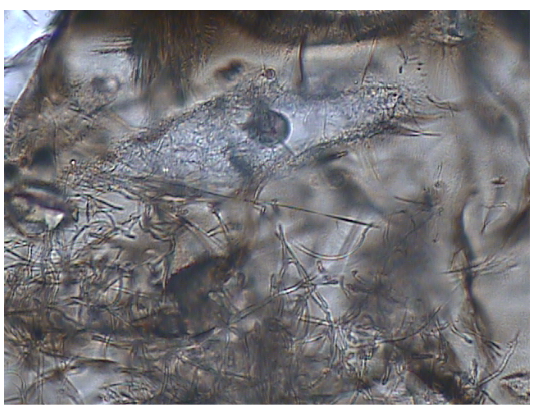

RI_10_006b_07

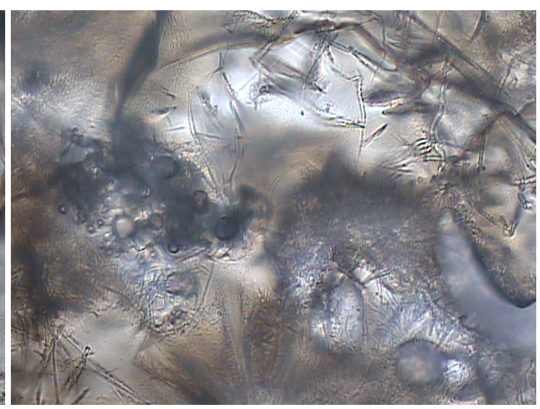

RI_10_006b_08

Appendix D: Scanning electron microscopy images

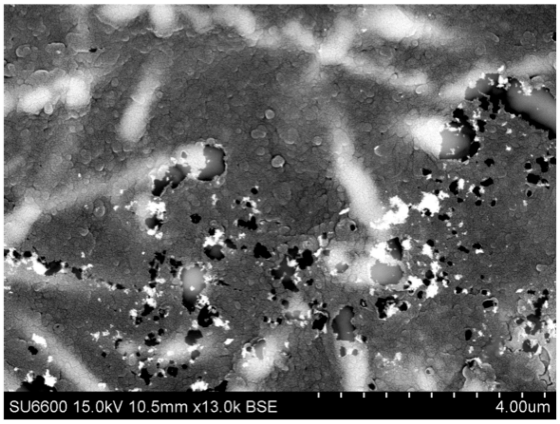

001_BSE copy

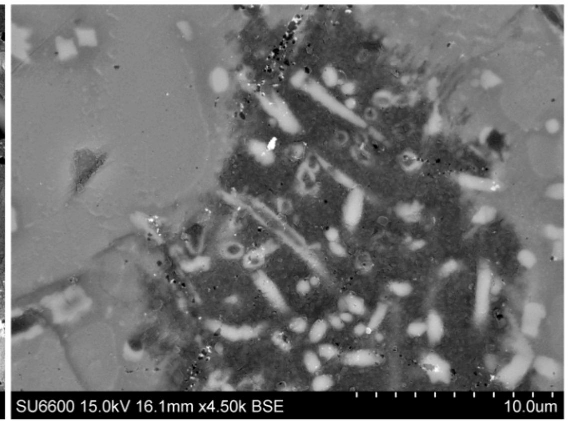

002_BSE copy

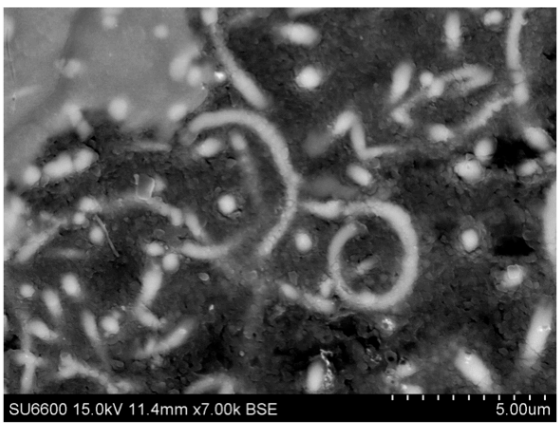

003 BSE copy

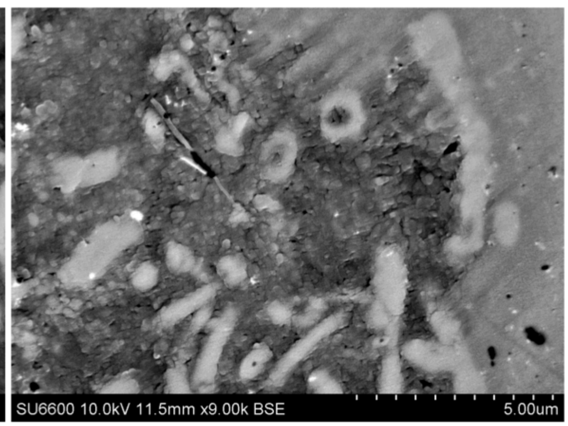

004 BSE copy

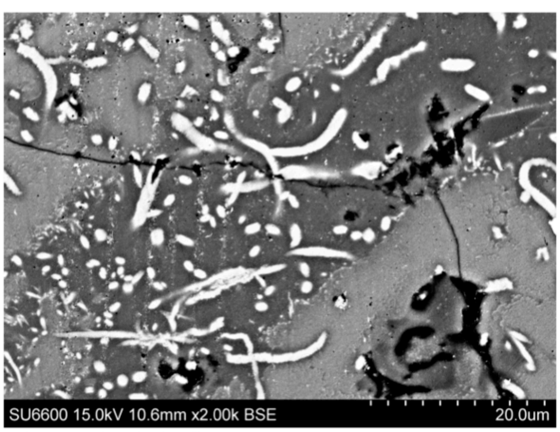

005 bse ivan test 15kv 8.5 deg tilt smallhr1 copy

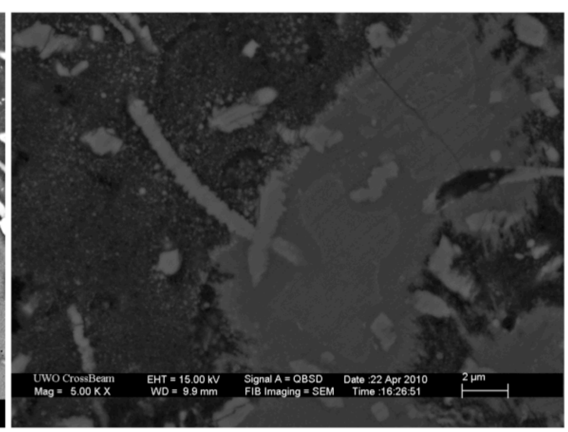

RI_056_00204 copy

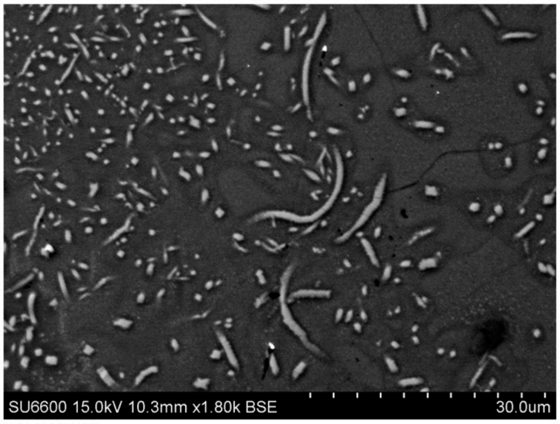

RI_09_006 0010BSE copy

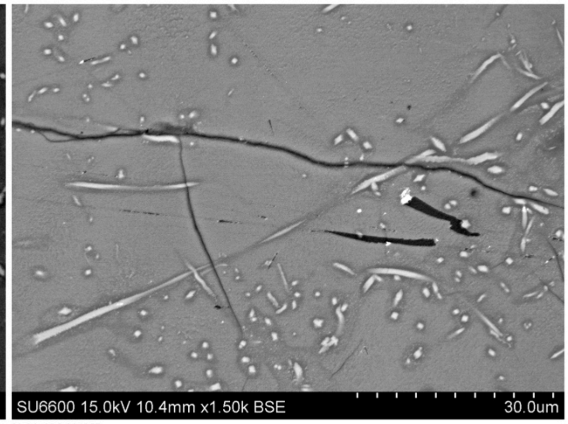

RI_09_006 0018SE copy

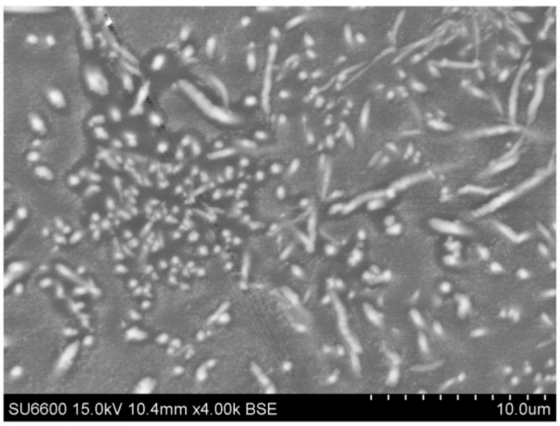

RI_09_006 0028SE copy

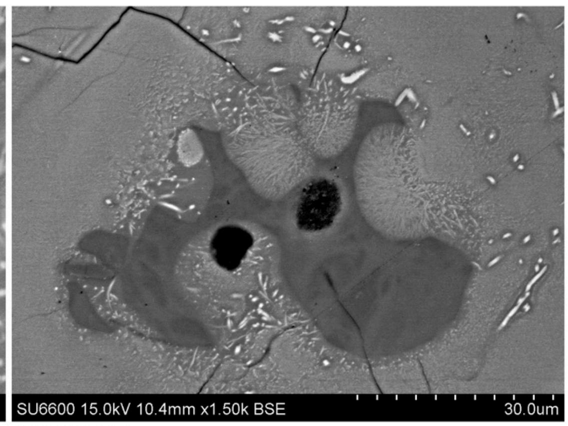

RI_09_006 003BSE copy

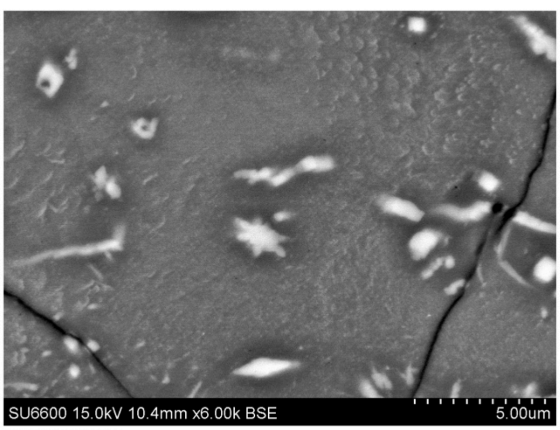

RI_09_006 004BSE copy

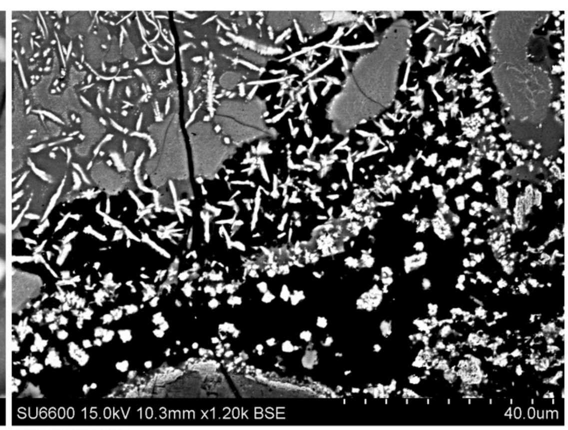

RI_09_006 005BSE copy

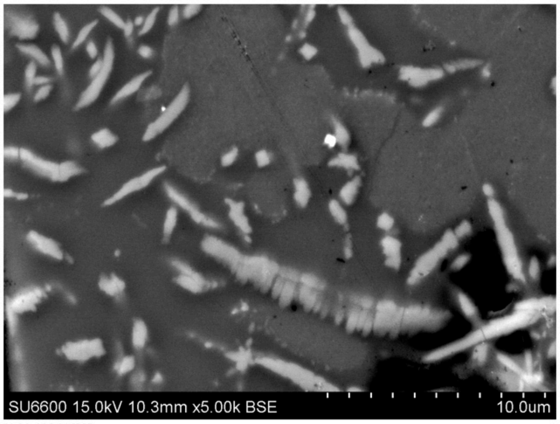

RI_09_006 006BSE copy

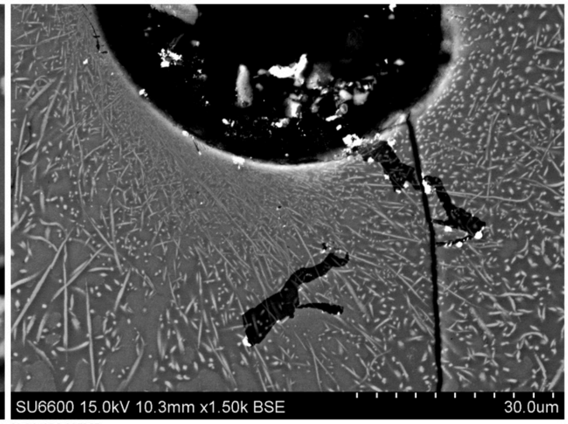

RI_09_006 007BSE copy

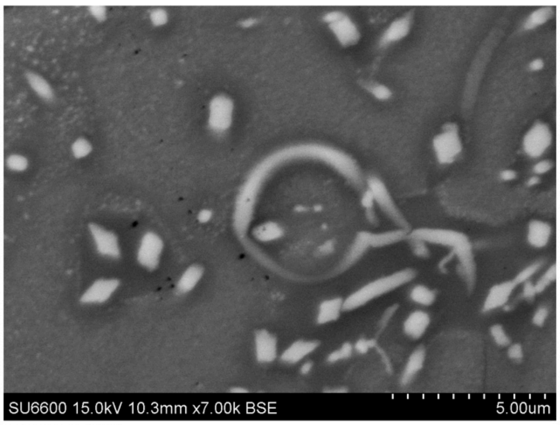

RI_09_006 008BSE copy

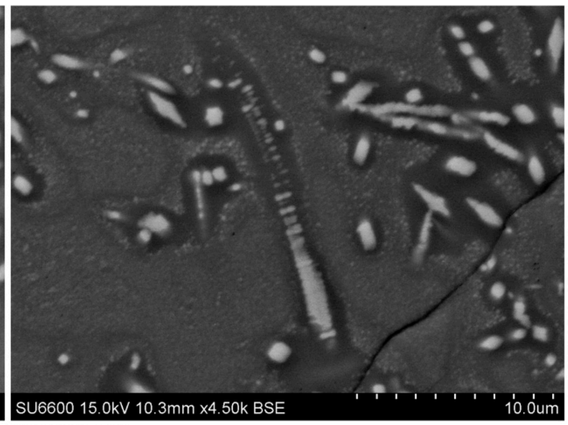

RI_09_006 009BSE copy

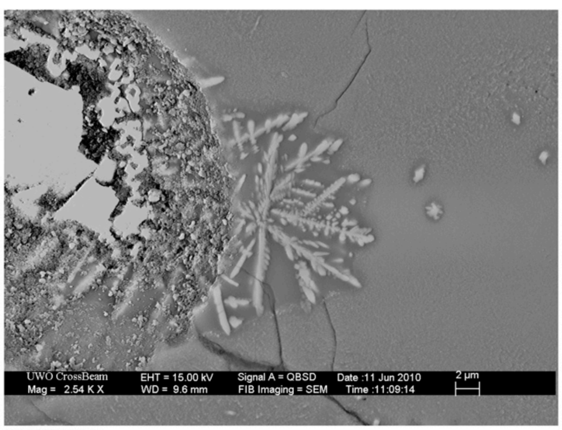

RI_09_006_11 copy

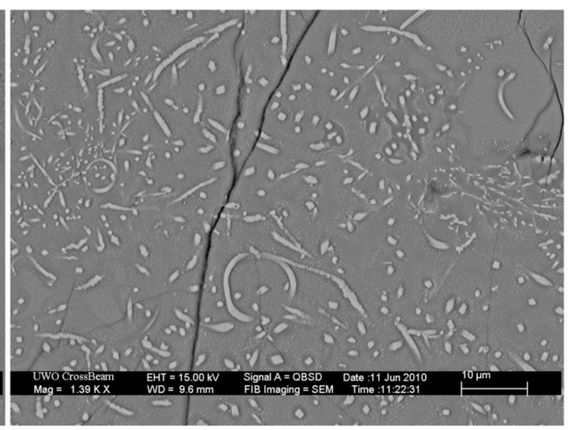

RI_09_006_14 copy

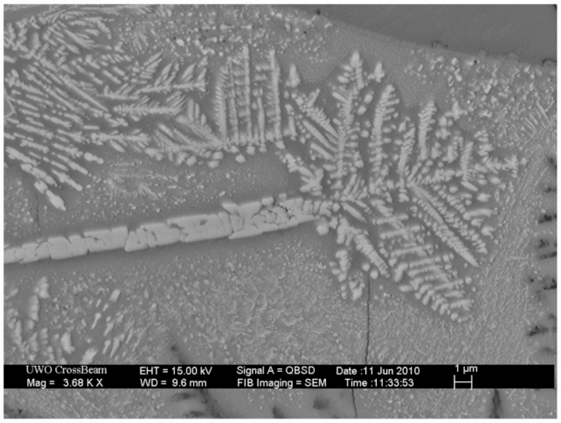

RI_09_006_17 copy

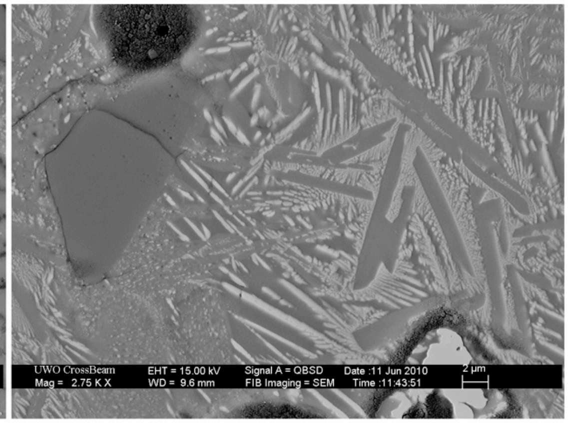

RI_09_006_18 copy

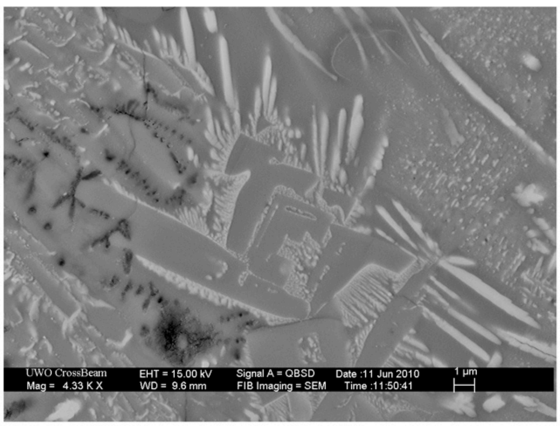

RI_09_006_20 copy

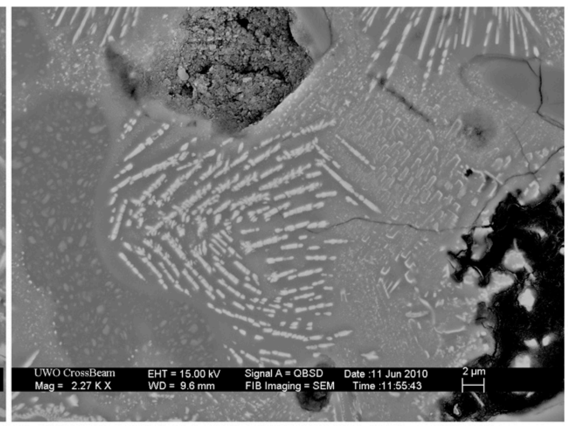

RI_09_006_21 copy

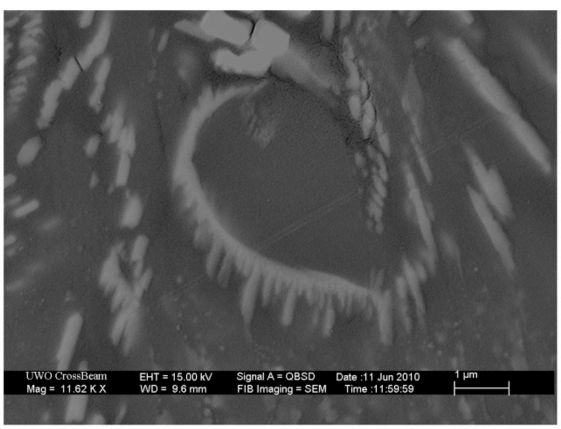

RI_09_006_22 copy

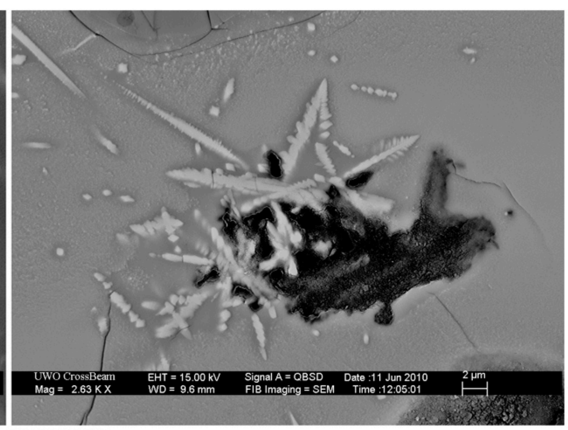

RI_09_006_23 copy

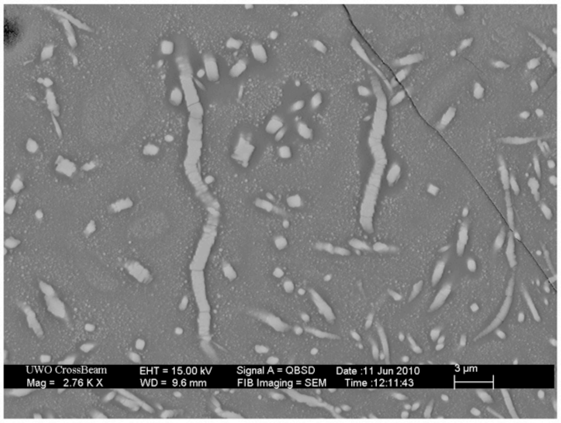

RI_09_006_25 copy

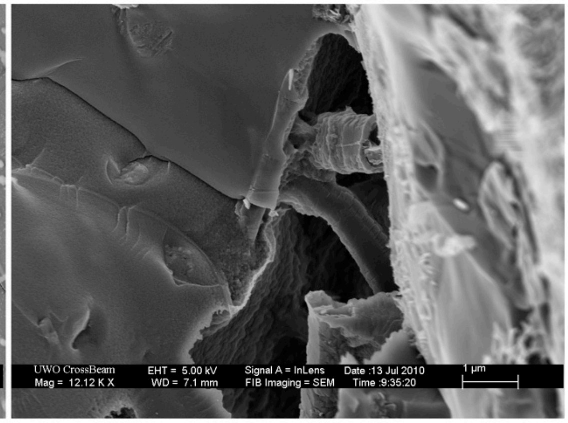

RI_10_006 glass grain 0204 copy

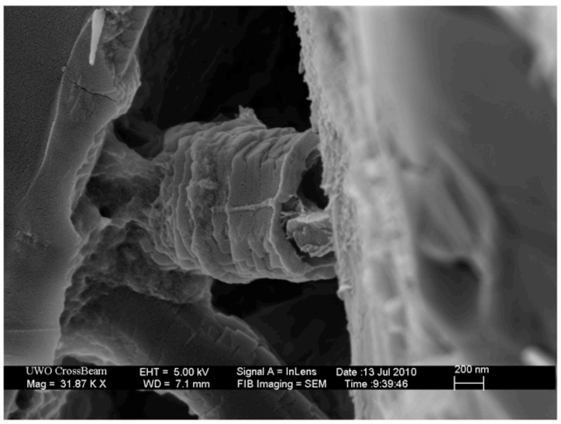

RI_10_006 glass grain 0305 copy

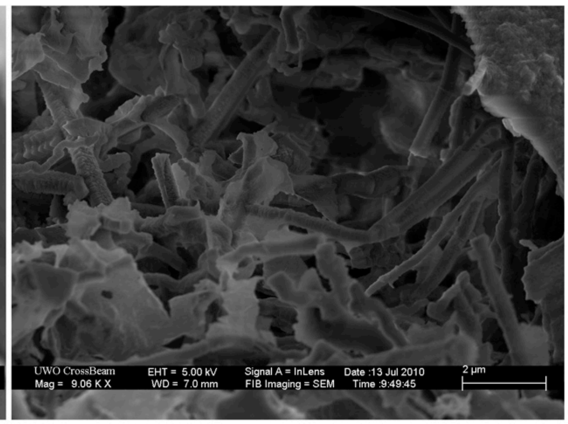

RI_10_006 glass grain 0406 copy

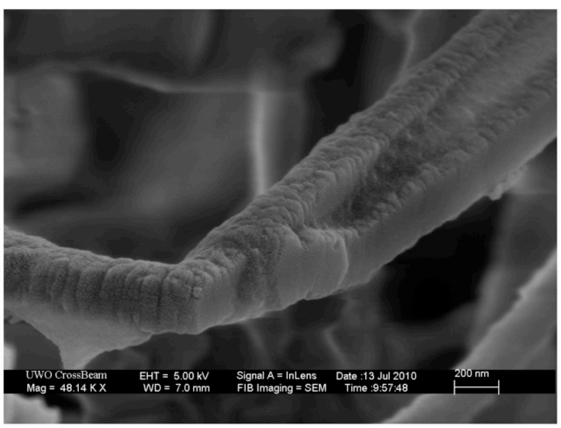

RI_10_006 glass grain 0507 copy

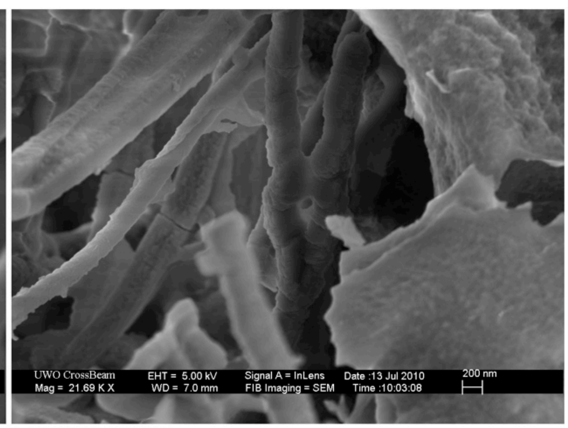

RI_10_006 glass grain 0609 copy

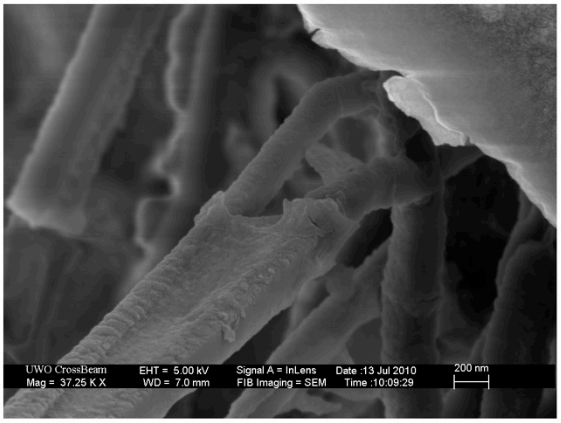

RI_10_006 glass grain 0710 copy

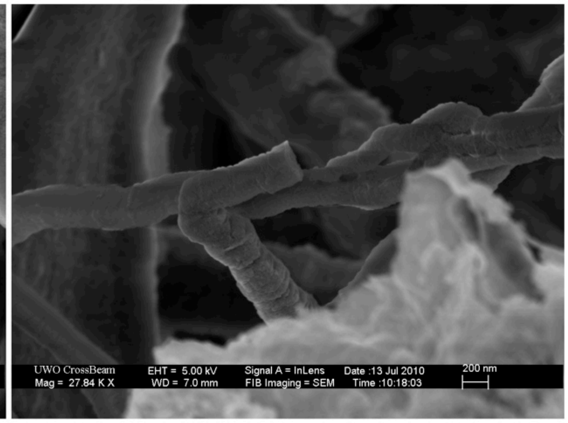

RI_10_006 glass grain 0811 copy

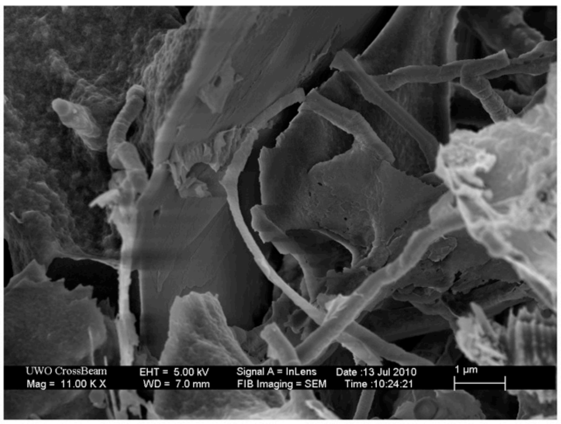

RI_10_006 glass grain 0912 copy

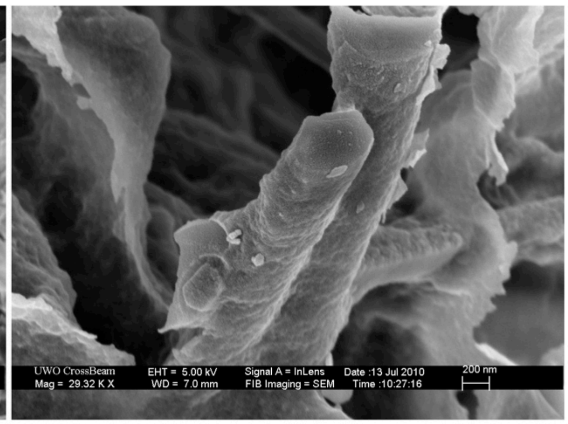

RI_10_006 glass grain 1013 copy

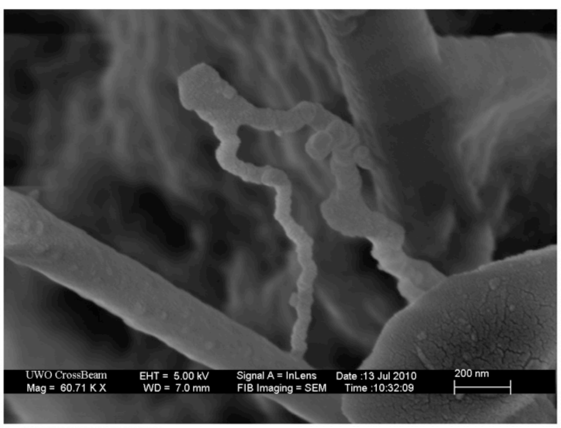

RI_10_006 glass grain 1114 copy

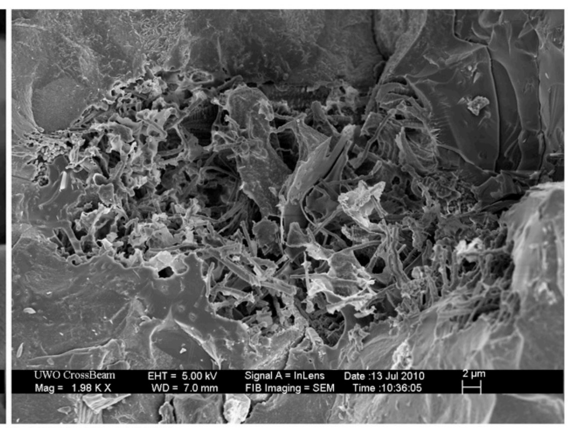

RI_10_006 glass grain 1215 copy

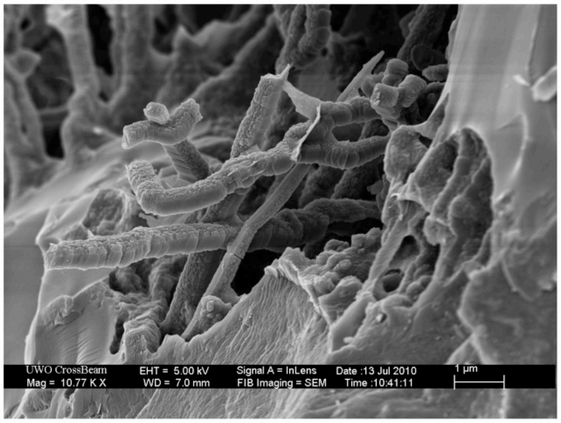

RI_10_006 glass grain 1316 copy

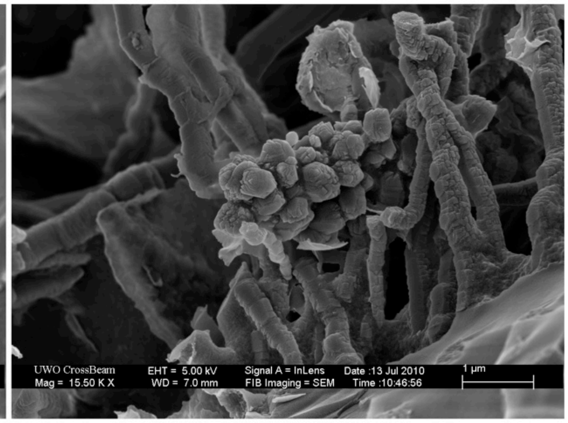

RI_10_006 glass grain 1417 copy

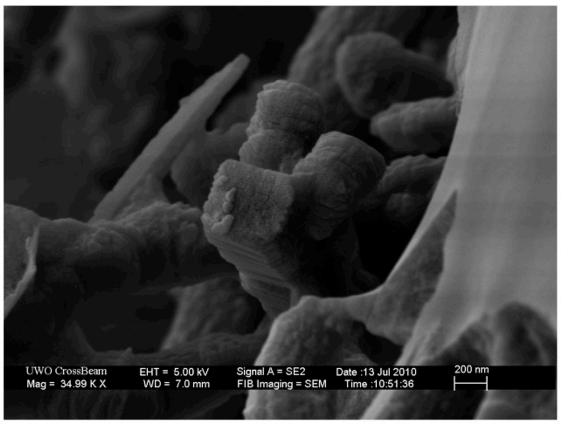

RI_10_006 glass grain 1518 copy

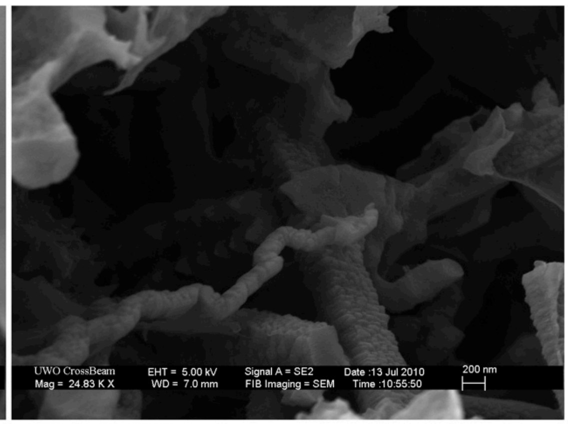

RI_10_006 glass grain 1619 copy

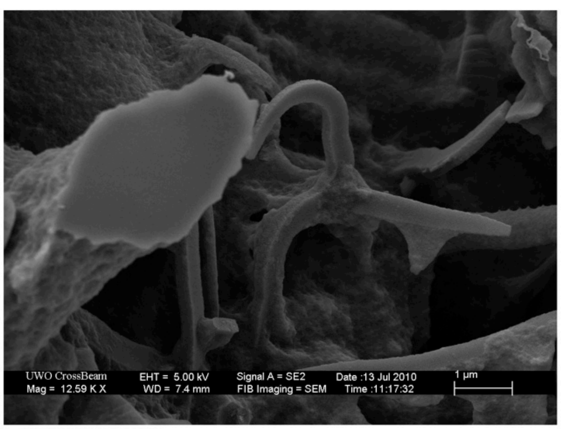

RI_10_006 glass grain 1821 copy

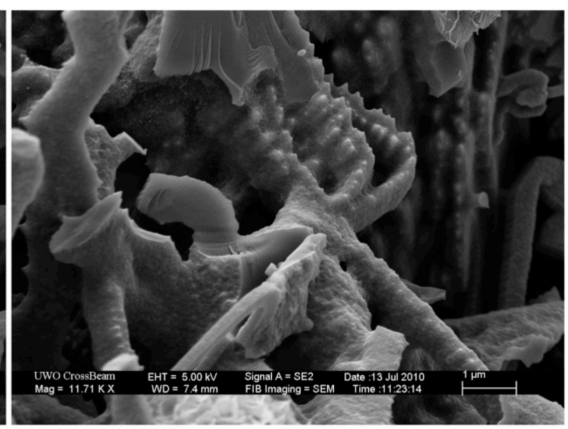

RI_10_006 glass grain 2023 copy

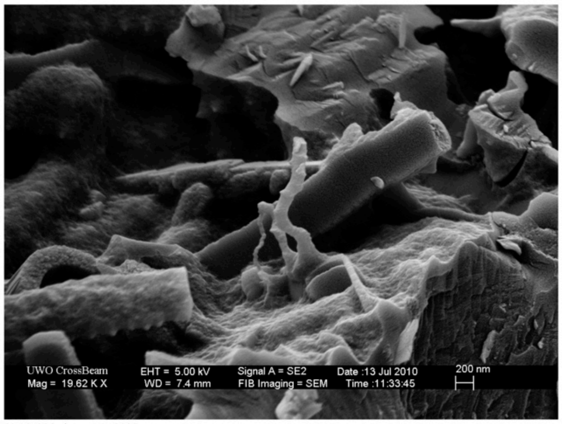

RI_10_006 glass grain 2225 copy

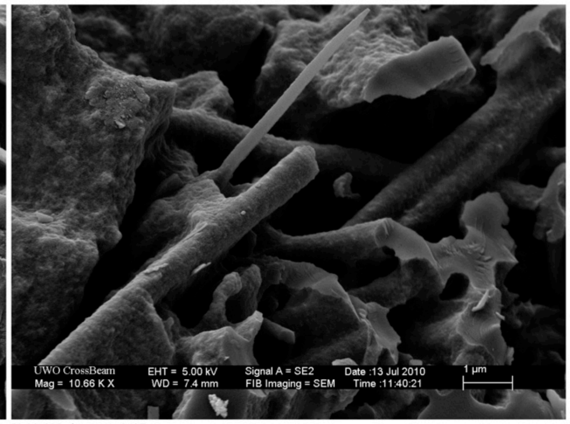

RI_10_006 glass grain 2427 copy

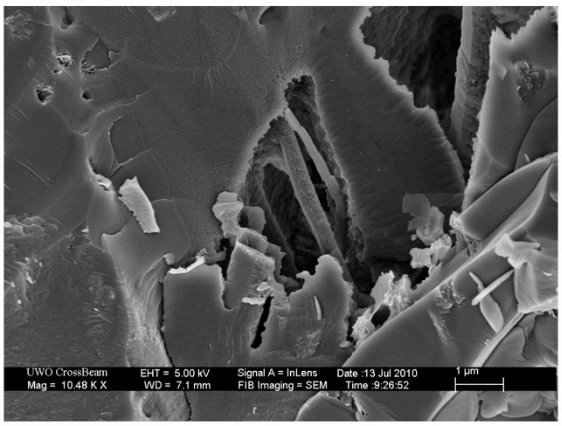

RI_10_006 glass grain02 copy

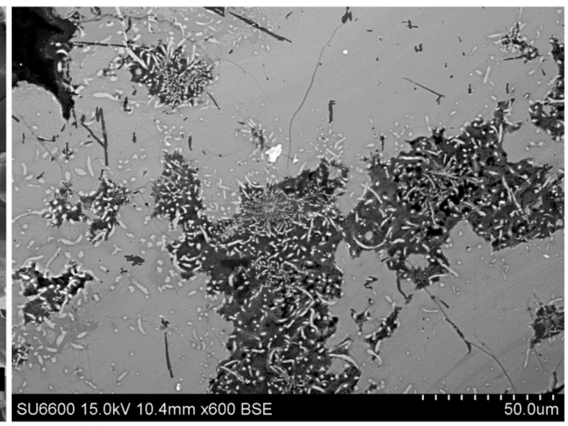

context 2 BSE for 001 copy

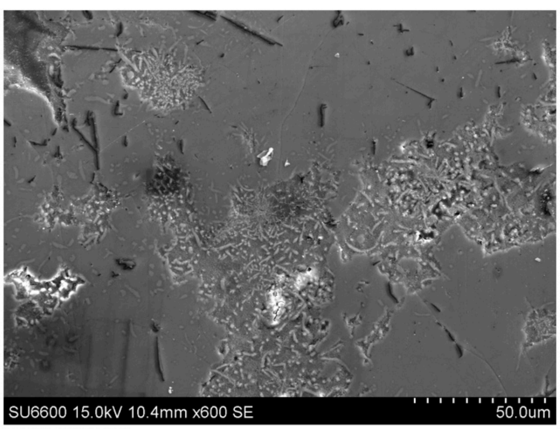

context 2 SE for 001 copy

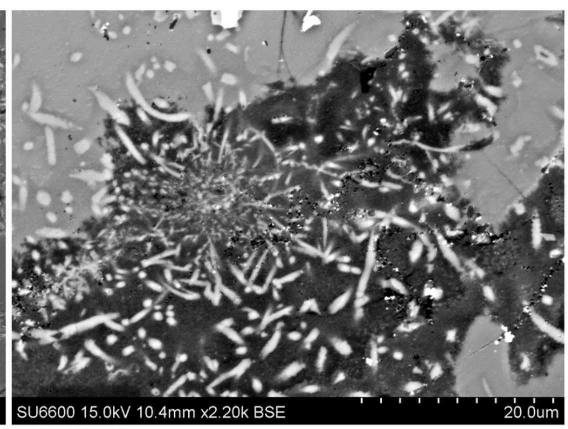

context BSE for 001 copy

Appendix E: Electron microprobe data

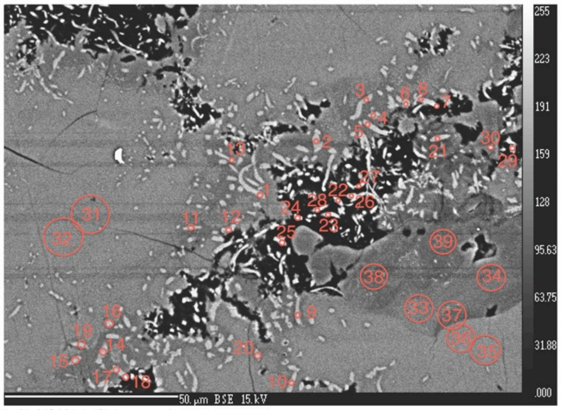

RI_01_056 001_1_BSE_1 annotated

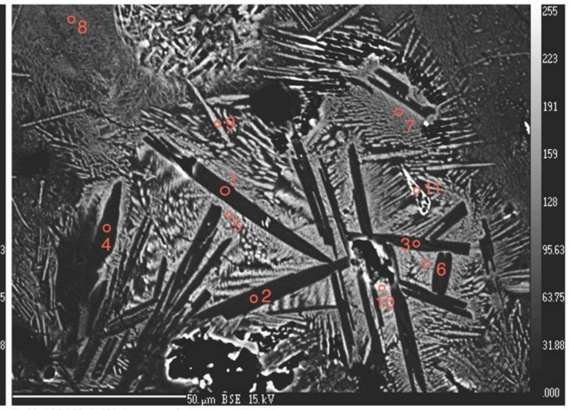

RI_09_086 003_1_BSE_1 annotated

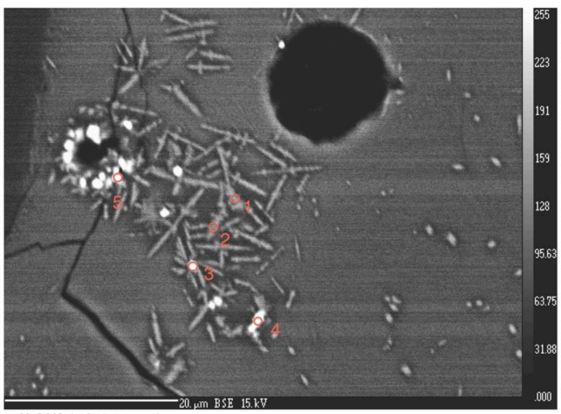

RI_09_6 003_1_BSE_1 annotated

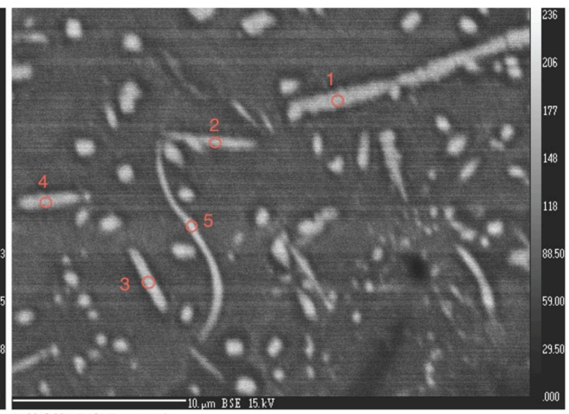

RI_09_6 005_1_BSE_1 annotated

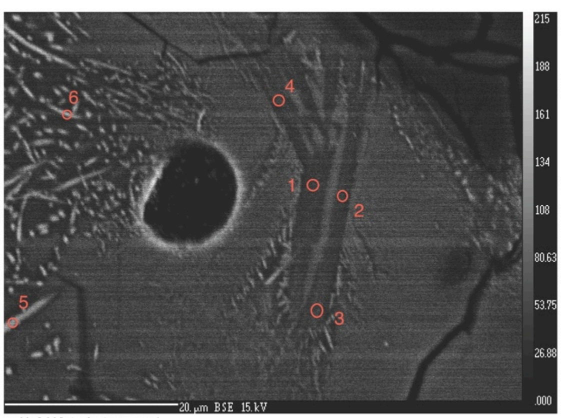

RI_09_6 006_1_BSE_1 annotated

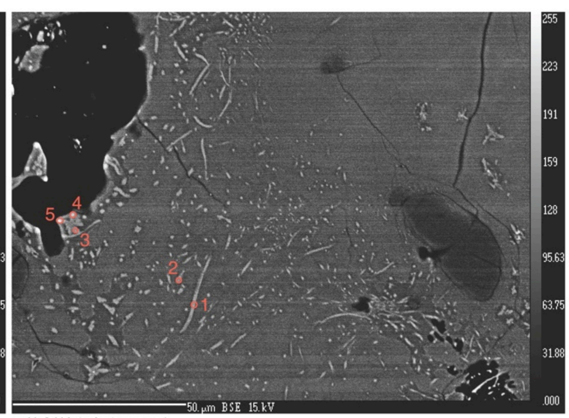

RI_09_6 008_1_BSE_1 annotated

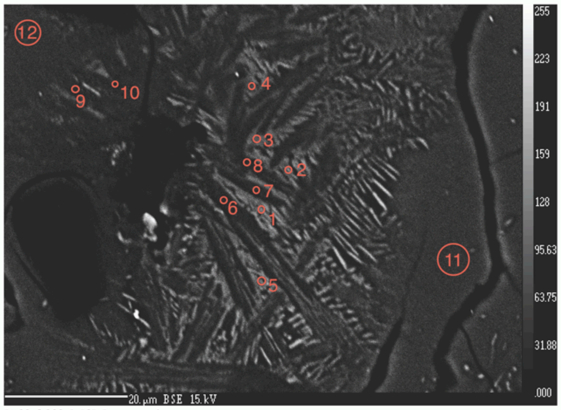

RI_09_6 009_1_BSE_1 annotated

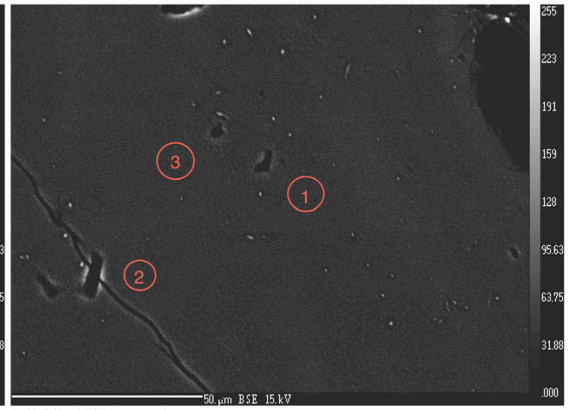

RI_09_6 011_1_BSE_1 annotated

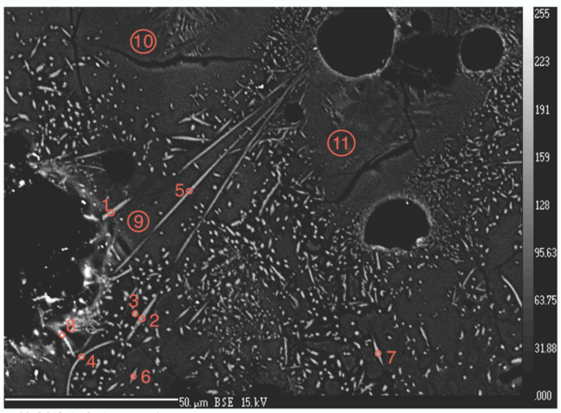

RI_09_6 013_1_BSE_1 annotated

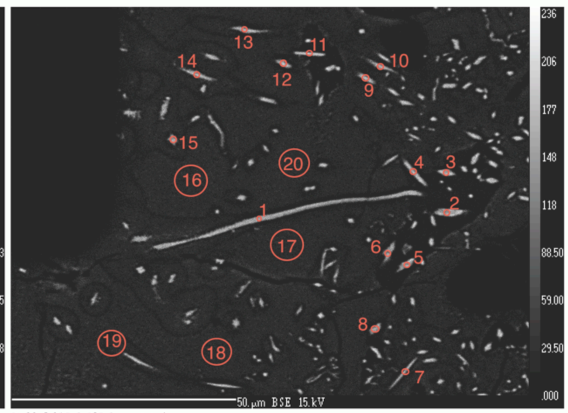

RI_09_6 015_1_BSE_1 annotated

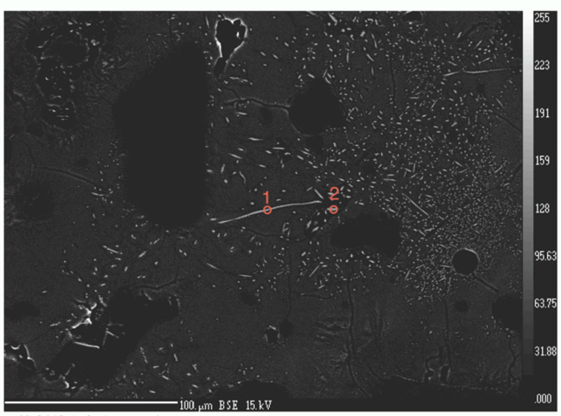

RI_09_6 016_1_BSE_1 annotated

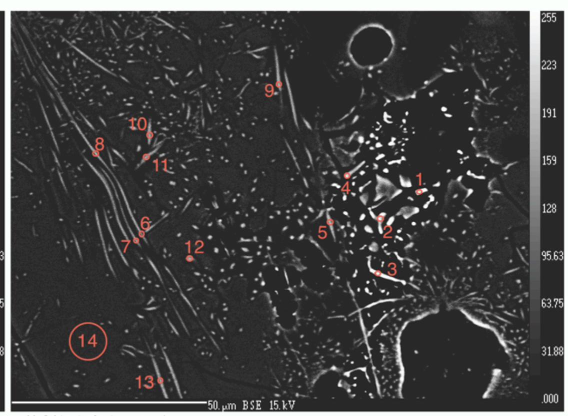

RI_09_6 017_1_BSE_1 annotated

Focused phase (5µm)

Comment	SiO2	Na2O	MgO	K2O	CaO	FeO	MnO	TiO2	Cl	Al2O3	Cr2O3	NiO	Total
RI_01_6 017.0012	13.4859	0.564	3.358	2.3161	2.291	4.6242	0.0855	0.1928	0.0072	4.7635	0.0165	0.0212	31.726
RI_00_056 001.0025	25.2612	0.0948	3.327	0.2764	6.1806	6.8207	0.1076	0.631	0.1869	7.3036	0.0782	0.0294	50.2974
RI_01_6 017.003	26.6925	0.0817	6.8677	0.1323	5.7161	14.2151	0.315	0.6551	0.1513	13.7249	0.1828	0.0119	68.7462
RI_09_6 003.003	29.22	0.5969	3.9394	1.4631	3.0154	54.2702	0.1743	1.8946	0.0058	10.9253	0.5169	-0.0284	105.9933
RI_09_6 003.005	30.9173	0.7596	1.4154	2.4544	0.8081	46.1045	0.1029	1.5261	0.015	11.5318	0.7322	0.0268	96.394
RI_00_056 001.0026	31.3622	0.1146	5.7982	0.2713	9.2715	9.5025	0.1948	0.8927	0.1692	9.7504	0.0905	-0.0192	67.3988
RI_00_056 001.0028	32.5814	0.1936	5.8979	0.2236	8.3617	10.4522	0.2296	0.9115	0.1279	10.4812	-0.046	-0.0269	69.3877
RI_09_86 003 0012	33.3145	0.9807	1.1866	1.754	1.381	29.6414	0.0696	2.2806	0.0563	13.7714	4.0617	0.0454	88.543
RI_00_056 001.0029	34.3503	0.221	5.3775	0.3449	7.0173	9.4971	0.1594	0.8567	0.2903	10.6802	0.0953	0.0522	68.9422
RI_00_056 001.0027	34.6311	0.2536	7.4222	0.1091	12.4115	11.2423	0.2763	0.6392	0.0887	10.741	0.1543	-0.0007	77.9686
RI_00_056 001.0022	35.6623	0.1135	7.4216	0.1894	10.7013	10.9284	0.2419	0.7311	0.0877	10.7586	0.1883	0.0424	77.0664
RI_00_056 001.0024	36.0341	0.1717	6.3872	0.3535	7.0701	11.48	0.2972	0.8897	0.1157	11.6059	0.1636	-0.0117	74.5569
RI_01_6 017.009	37.1701	0.5932	6.6117	2.1376	4.8574	12.6266	0.3543	0.4398	-0.002	12.2674	0.0131	0.0569	77.126
RI_00_056 001.0018	37.2723	0.8929	8.1681	0.6155	10.3449	12.0538	0.3224	0.7021	0.0507	12.1693	0.0706	-0.0076	82.6549
RI_01_6 017.004	37.6247	0.1573	9.0532	0.2486	4.37	14.1251	0.3337	0.4311	0.0571	9.5499	0.0785	0.0055	76.0346
RI_00_056 001.0023	37.6409	0.1159	8.3395	0.1733	10.7287	12.4133	0.2842	0.6842	0.0772	11.5797	0.1369	0.0256	82.1994
RI_01_6 017.005	38.1875	0.8408	5.7596	2.5623	5.4713	12.2415	0.2775	0.3853	0.0196	13.7544	0.0169	0.0128	79.5294
RI_01_6 017.0011	38.4212	0.5459	4.032	2.4909	6.2412	9.1917	0.185	0.5643	0.0075	12.0287	0.0407	0.0271	73.7764
RI_01_6 017.007	39.3717	0.5047	4.4169	2.9353	5.8337	8.6698	0.2157	0.5732	0.0017	11.6699	0.1173	0.0379	74.3478
RI_00_056 001.007	39.5867	1.8149	4.5302	0.6566	8.3309	7.4713	0.1408	0.266	0.1213	10.6614	0.1447	0.0107	73.7355
RI_01_6 017.0010	39.5988	0.7507	4.143	3.7256	6.212	5.9486	0.1865	0.5619	0.0076	11.8983	0.0226	0.0038	73.0594
RI_00_056 001.008	40.572	1.6217	7.0384	0.387	12.4464	10.8608	0.2576	0.5257	0.0261	12.2577	0.1026	0.0197	86.1158
RI_01_6 017.008	40.9312	0.6732	3.9984	3.4141	5.4775	7.0878	0.1922	0.556	0.014	11.8549	0.1008	0.0163	74.3163
RI_01_6 017.006	41.6339	0.9191	3.214	4.0282	4.0129	5.5331	0.1842	0.5771	0.0012	12.1733	0.079	-0.0062	72.3497
RI_00_056 001.0017	43.0994	0.8543	8.4458	0.2573	9.5663	14.3	0.34	0.6698	-0.0046	13.4063	0.0652	0.017	91.0168
RI_00_056 001.0016	43.6794	1.4004	7.8484	0.3647	9.6927	13.4722	0.3059	0.632	0.0013	13.9253	0.0537	-0.0099	91.3663
RI_00_056 001.005	44.1479	0.9642	7.1791	0.3713	12.4278	12.1598	0.2634	0.5594	0.0003	13.8615	0.046	0.0327	92.0133
RI_00_056 001.006	44.427	1.9221	7.6371	0.4941	10.8603	11.8402	0.2987	0.5585	0.0111	13.2472	0.0635	0.0548	91.4148
RI_00_056 001.002	44.7692	1.1824	7.8695	0.4951	11.0586	11.4614	0.2727	0.6109	0.0079	12.9906	0.1373	0.0278	90.8832
RI_00_056 001.0020	44.9731	1.0751	8.6729	0.3379	8.7898	12.8091	0.3842	0.7204	0.0066	13.7425	0.1746	0.0244	91.7104
RI_00_056 001.004	45.8285	1.7555	7.1919	0.4602	10.0925	11.4614	0.2364	0.64	0.0054	13.6126	0.1541	-0.0647	91.3737
RI_01_6 016.002	46.4298	0.3999	11.3899	1.0797	7.3798	14.3197	0.3975	0.352	0.0026	13.2103	0.0491	0.0307	95.041
RI_09_6 008.006	46.5136	0.6443	4.9242	2.3312	2.6829	8.3992	0.2251	0.598	0.1559	18.0369	0.1046	0.0083	84.6242
RI_09_6 008.005	47.3135	0.5389	8.8683	1.6454	3.4687	13.7359	0.3406	0.7171	0.0327	15.6974	0.1508	0.0365	92.5459
RI_00_056 001.0019	47.4276	2.4549	4.3626	0.6187	5.9136	9.5105	0.201	0.6268	0.0038	15.2447	0.1541	0.0236	86.542
RI_09_86 003 007	47.4301	0.5173	5.1219	2.1983	4.5516	14.9547	0.1813	1.0397	0.0205	8.8419	0.1119	0.0684	85.0377
RI_00_056 001.0014	47.5247	2.1331	6.5118	0.5254	7.1753	11.7248	0.3177	0.5859	0.0127	15.2218	0.0674	-0.0005	91.7999
RI_09_86 003 006	47.9439	1.097	4.5907	2.5969	3.4385	16.7617	0.2064	0.7846	0.0232	9.6723	0.0323	-0.0017	87.1459
RI_00_056 001.009	48.4509	1.8925	5.297	0.7279	6.9388	10.7585	0.2888	0.7719	0.0245	15.6236	0.0304	-0.0263	90.7786
RI_09_86 003 0010	48.6668	1.855	5.0693	1.0698	3.994	16.6417	0.1953	0.5669	0.018	12.5004	0.0684	0.0533	90.6988
RI_09_86 003 008	48.6671	1.5099	4.8129	1.7931	4.6194	13.0412	0.1551	0.6647	0.0274	11.3972	0.137	-0.008	86.8168
RI_00_056 001.0010	48.9035	2.1145	6.4094	0.9402	7.1979	9.3799	0.245	0.7674	0.0169	14.2581	0.1073	-0.0022	90.338
RI_00_056 001.0015	48.9578	2.5038	5.8952	0.5582	6.3711	11.4861	0.2707	0.6479	0.0144	15.8896	0.1415	0.0058	92.7421
RI_09_86 003 0011	49.1551	0.4445	5.5929	1.7029	4.3351	18.3776	0.2212	0.9646	0.0234	9.0474	0.1683	0.0489	90.0819

RI_09_86 003 004	49.3876	4.513	0.2024	0.4771	8.3241	1.572	-0.0081	0.0615	0.0184	22.6295	-0.0147	-0.0239	87.1389
RI_01_6 016.001	49.8228	0.6177	8.4905	1.4907	7.413	10.9699	0.3215	0.5921	0.0146	12.5119	0.0507	0.018	92.3134
RI_00_056 001.0013	49.8978	1.9428	5.0989	0.9149	8.635	8.9165	0.2521	0.5565	0.0194	14.4588	0.1446	-0.0026	90.8346
RI_09_6 013 001	50.3392	0.7876	6.4783	2.6796	6.0721	8.8826	0.2346	0.6919	0.0104	13.0258	0.0217	-0.0058	89.2179
RI_01_6 016.006	50.3436	0.596	8.5982	1.6749	6.0958	11.9694	0.3288	0.5368	0.0085	13.4057	0.0132	0.0384	93.6094
RI_09_86 003 002	50.4896	4.935	0.2477	0.5643	8.1509	1.533	-0.0295	0.082	0.0092	22.5929	-0.0316	0.0416	88.585
RI_01_6 016.0013	50.5119	0.7032	9.6284	1.6812	6.9181	11.8504	0.3298	0.578	0.0071	12.289	0.0355	0.0178	94.5505
RI_09_86 003 003	50.9428	5.0328	0.1205	0.6228	7.7129	1.4175	-0.0164	0.0504	0.0136	23.0218	-0.0069	-0.037	88.8748
RI_01_6 016.0012	50.9782	0.9462	8.349	1.3861	6.4634	12.6922	0.3175	0.6259	0.0065	13.8592	0.1208	0.0515	95.7966
RI_01_6 016.008	51.2038	0.7242	9.1891	1.7289	5.5497	12.5143	0.319	0.5598	0.0026	13.7449	0.0454	0.0125	95.5943
RI_01_6 016.003	51.3246	0.7082	8.1585	2.0763	5.5501	12.4397	0.2563	0.4843	0.0108	14.9786	0.1301	0.0051	96.1226
RI_00_056 001.0021	51.4601	0.217	3.5919	1.202	9.271	7.5144	0.1497	0.244	0.078	14.2899	0.0014	0.0573	88.0766
RI_01_6 016.005	51.6487	0.5195	8.045	2.3712	6.9392	10.8094	0.3381	0.5339	0.0104	13.3149	-0.0202	0.0084	94.5183
RI_01_6 016.0010	51.7205	0.5867	7.8584	2.3236	7.464	10.313	0.3409	0.5893	0.0135	12.5703	0.0717	-0.0113	93.8407
RI_09_6 006.001	51.828	4.0414	0.3922	0.4926	10.8858	0.9365	0.0107	0.1014	0.0119	25.8107	-0.0297	-0.073	94.4085
RI_09_6 013 004	52.0186	0.6939	7.7775	2.4173	5.3139	11.0408	0.3386	0.8877	0.0202	14.2	0.0893	0.0079	94.8056
RI_00_056 001.0012	52.0462	3.8291	3.6723	1.4757	4.8008	7.633	0.1822	0.7356	0.0222	15.483	0.1392	-0.0038	90.0155
RI_01_6 016.0011	52.1168	0.9696	7.5698	2.749	3.7238	11.587	0.2922	0.4544	0.0201	15.6449	0.0897	-0.0004	95.2169
RI_09_6 013 003	52.22	0.5703	6.9164	2.5042	5.4931	9.9968	0.3181	0.7719	0.0109	13.8855	0.0989	-0.0044	92.7816
RI_09_86 003 009	52.2291	3.4394	2.9394	1.2101	4.5859	10.1758	0.1145	0.6092	0.0135	14.0847	0.2003	-0.0371	89.5648
RI_01_6 016.009	52.5906	0.7377	7.9636	2.6384	6.1945	10.5158	0.2405	0.5997	0.0123	13.099	0.0681	0.0495	94.7099
RI_09_6 003.004	52.6427	1.7754	3.0521	3.5145	3.6588	15.2011	0.1278	0.7995	0.0022	13.1982	0.3358	-0.0097	94.2984
RI_09_6 008.003	52.7477	0.7816	8.3057	2.7367	3.8727	12.027	0.2769	0.7535	0.0101	14.1111	-0.0237	0.0018	95.6012
RI_00_056 001.0011	52.979	2.735	3.7128	1.0681	7.0366	7.8515	0.2342	0.4589	0.0027	16.2811	0.1754	-0.03	92.5054
RI_09_6 003.002	52.9895	0.8913	4.8099	2.934	6.861	10.3157	0.2467	0.5128	0.005	13.2259	0.0375	-0.0009	92.8284
RI_09_6 013 007	53.0937	0.9053	6.2714	1.9225	7.4327	9.8539	0.1991	0.6125	-0.0007	13.7301	0.029	0.0214	94.0708
RI_09_6 013 002	53.1124	0.6642	5.9918	2.7871	6.812	8.5091	0.2961	0.7723	0.0098	13.8908	0.0433	0.0265	92.9154
RI_01_6 016.0014	53.2337	0.5621	6.5073	2.3625	6.8185	10.5776	0.2478	0.6092	0.0104	13.6412	0.2002	-0.0039	94.7666
RI_00_056 001.003	53.4115	1.8274	3.1764	0.6825	7.3194	8.174	0.1694	0.5629	0.004	17.1873	0.1634	-0.026	92.652
RI_09_6 009 001	53.4761	1.0539	5.2429	2.7915	3.8802	9.6361	0.1797	1.1201	0.0069	14.0336	0.1494	-0.0087	91.5617
RI_09_6 009 005	53.487	1.095	4.661	3.2668	4.1	8.8624	0.2086	1.1308	0.0217	14.3875	0.0394	-0.0439	91.2163
RI_09_6 005.001	53.661	0.286	6.7006	1.6872	7.5294	10.5249	0.2644	0.5682	0.0098	13.4716	0.0383	0.0021	94.7436
RI_09_6 013 008	53.8748	0.2938	3.1727	3.4501	4.3655	6.2144	0.206	0.7595	0.0221	15.669	-0.0705	0.0174	87.975
RI_01_6 016.004	53.8753	1.129	7.9746	2.3307	5.7778	9.9419	0.2992	0.5749	0.0009	13.7488	0.1361	0.0514	95.8405
RI_09_6 009 006	53.9049	5.0197	1.0329	0.6862	8.06	1.8714	0.0673	0.2305	-0.0032	21.936	0.0036	-0.0264	92.7828
RI_09_6 006.005	53.9503	1.0644	5.8607	3.1937	6.963	8.5823	0.2474	0.6401	0.0014	13.11	0.093	0.0559	93.7621
RI_09_6 005.004	54.2984	0.6584	6.5204	2.6319	6.9829	9.4077	0.2286	0.5891	0.0039	13.3939	0.089	0.0587	94.863
RI_09_6 009 007	54.4454	4.9649	1.6275	0.8764	6.7679	2.3682	0.0416	0.3195	0.0057	20.2243	0.0065	-0.0034	91.6446
RI_09_6 009 002	54.5363	0.9462	4.9278	3.4648	4.2401	7.6662	0.1956	1.1327	0.0113	13.2113	0.0795	-0.0201	90.3916
RI_09_86 003 005	54.5966	6.1255	0.2303	1.05	5.2205	1.5183	0.0237	0.1185	0.0165	20.461	-0.0476	-0.008	89.3053
RI_00_056 001.001	54.7862	2.5777	2.3304	1.9002	4.0496	6.9329	0.1077	0.6961	0.014	17.0619	0.0082	0.0352	90.5001
RI_00_056 001.0030	54.8132	0.3151	0.5033	0.7021	0.578	35.0908	0.0811	0.147	0.012	2.2392	0.0189	0.513	95.0136
RI_09_6 009 003	54.8242	2.0315	5.9203	2.2807	3.6361	8.4758	0.2083	0.8327	0.0066	14.2642	0.0486	-0.0061	92.5231
RI_09_6 006.002	55.1554	4.1709	0.9425	1.0796	7.8272	1.727	0.0371	0.2995	0.0016	20.7638	0.088	0.0055	92.0981
RI_09_6 013 006	55.4809	1.2768	5.2853	2.8226	4.8373	8.3937	0.2268	0.6611	0.0073	14.4356	0.0232	-0.0016	93.449
RI_09_6 008.004	55.4911	1.1961	4.6807	3.3913	3.1791	7.8769	0.1741	0.8696	0.0162	17.2887	0.0617	0.0029	94.2283

RI_09_6 009 008	55.6937	4.3948	1.6827	1.5575	6.0678	2.3374	0.0545	0.5034	0.0153	18.8058	0.0054	-0.0033	91.1151
RI_09_6 005.007	55.797	0.6802	4.0268	3.2994	6.6218	5.7624	0.137	0.5527	0.0053	13.6	0.0908	0.042	90.6155
RI_09_6 009 004	55.955	2.2499	5.5112	1.9416	4.2665	7.9646	0.2043	0.8018	0.003	14.3776	0.1257	0.0231	93.4243
RI_09_6 006.004	56.1685	4.5239	1.2221	1.0797	7.7139	2.0306	0.0449	0.3451	0.0016	20.3262	-0.0184	0.0351	93.4732
RI_09_6 009 009	57.1347	4.2921	2.3202	1.1129	5.9781	3.4086	0.0536	0.5382	0.0085	17.2596	0.1033	0.021	92.2307
RI_01_6 016.0015	57.378	0.951	3.3083	4.4423	3.2302	4.647	0.1244	0.6872	0.0029	13.7704	0.0209	-0.0114	88.5513
RI_09_6 013 005	57.4897	1.0398	4.1877	2.6086	5.2618	6.0636	0.2169	0.5631	0.0069	13.9641	-0.0592	0.0613	91.4045
RI_09_6 006.003	57.7267	3.838	2.0432	1.5875	6.9721	3.5791	0.0841	0.6041	0.0171	17.9308	0.1202	0.0296	94.5325
RI_09_6 005.002	57.8905	0.8062	4.2998	3.3816	4.2867	7.926	0.1481	0.6119	-0.0013	14.1734	0.046	-0.0291	93.5398
RI_09_6 009 0010	58.305	3.3707	1.8092	1.5709	5.9643	3.2298	0.0789	0.5285	0.0101	17.9122	0.0855	0.0589	92.924
RI_09_6 008.002	58.8867	1.8587	3.5233	2.1062	3.9012	6.7166	0.1353	0.7542	0.0078	15.4477	0.075	-0.037	93.3755
RI_09_6 003.001	58.9998	1.0806	1.8248	4.4331	3.9007	3.5316	0.0877	0.6537	0.0022	14.74	0.0063	0.0444	89.3048
RI_01_6 017.0013	59.7295	0.9864	2.6774	4.5668	2.8997	4.2852	0.1409	0.682	0.002	14.2178	-0.0016	-0.0506	90.1354
RI_09_6 005.003	59.839	0.8246	2.9085	3.6611	3.6892	4.679	0.1913	0.6449	-0.0004	14.0823	0.0487	-0.0005	90.5676
RI_01_6 016.007	60.3403	1.7349	2.4264	3.4494	3.012	4.21	0.098	0.73	0.0103	14.5504	-0.0356	-0.0137	90.5125
RI_09_6 005.005	60.7271	0.8012	2.7359	3.7147	3.3557	5.3608	0.1095	0.6454	0.0114	14.6564	-0.0475	-0.0112	92.0595
RI_09_6 005.006	61.0529	0.9111	2.1464	4.0462	4.2422	4.5338	0.1065	0.53	0.0042	14.1593	0.0284	0.0204	91.7813
RI_09_6 006.006	61.9603	2.37	1.6903	3.3417	4.0188	3.3937	0.0474	0.6618	0.0022	15.5229	-0.0439	0.0059	92.9711
RI_01_6 017.002	73.712	0.038	0.1194	0.0224	0.1047	1.7933	-0.0219	-0.0029	0.0762	5.1037	0.0075	0.0048	80.9572
RI_01_6 017.001	81.9429	0.0815	0.1719	0.1526	0.4108	0.9272	-0.0169	0.212	0.039	2.5415	0.0617	-0.0219	86.5022
Hematite	0.0296	-0.0014	-0.0145	0.0017	0.0202	90.9408	-0.0061	0.0029		0.028	0.003	-0.012	91.0263
Diopside	54.7489	0.0177	18.3551	0.004	25.2942	0.033	0.0419	0.0442		0.0691	0.0024	-0.0038	98.6104
Rut	54.8206	-0.0041	18.2696	0.0008	25.5152	0.0411	0.0515	0.0753		0.0778	0.0022	-0.0051	98.8541
Sanidine	0.0173	0.0029	0.0117	0.0014	0.0207	0.0284	-0.0019	117.9903		0.0282	0.0069	0.0085	118.1163
Chromite	0.0101	0.0034	7.8077	0.0103	0.0133	35.3236	0.2329	0.8548		13.1814	41.2066	0.1209	98.765

Defocused phase (10µm)

Comment	SiO2	Na2O	MgO	K2O	CaO	FeO	Al2O3	Total
RI_00_056 036	53.014	4.824	2.7478	0.7089	5.3947	5.5702	16.2634	89.4589
RI_00_056 032	53.114	5.0538	2.6805	0.6645	5.1128	5.3772	16.1933	89.1768
RI_00_056 035	53.6677	4.8166	2.4665	0.9954	4.7815	4.8847	15.8234	88.4422
RI_00_056 031	53.6878	5.138	2.4483	0.7508	4.6983	5.263	16.0615	88.8492
RI_09_6 013 009	56.8381	3.4852	2.2942	1.3237	6.3022	4.0276	14.8448	90.0704
RI_09_6 009 012	57.1645	3.9866	2.5352	1.9417	4.2823	4.7587	14.5627	90.2083
RI_09_6 013 0010	57.5087	4.025	2.1831	1.7351	5.0055	4.1873	14.7492	90.2103
RI_09_6 013 0011	57.8591	3.7821	2.3351	1.8545	5.8108	4.3085	13.9428	90.7915
RI_09_6 009 011	58.108	3.938	2.44	2.0827	4.078	4.8313	14.6079	90.9632
RI_09_6 011 002	58.665	3.7744	2.4213	2.6611	3.4113	4.6821	14.498	90.9546
RI_09_6 011 001	58.7268	3.6897	2.1471	2.0726	4.6159	4.2522	14.4185	90.5556
RI_09_6 015 016	58.9942	3.6981	2.4541	2.4365	4.0426	4.7721	14.6689	91.9235
RI_09_6 011 003	59.0076	3.8496	2.2954	2.1866	4.248	4.6803	14.5201	91.6532
RI_09_6 017 014	60.2138	4.1985	2.0276	2.0938	4.056	4.1082	14.773	92.1729
RI_00_056 033	63.9208	3.9826	0.8904	2.1612	2.7056	2.4196	12.5044	89.1409
RI_00_056 034	67.4762	1.449	0.9564	4.3159	0.8937	3.0199	9.04	88.1046
RI_00_056 037	79.7949	0.8405	0.2527	2.1957	0.278	0.8137	4.3328	88.5125
RI_00_056 038	82.1829	0.881	0.117	1.5145	0.2733	0.9264	3.675	89.5828
RI_00_056 039	82.6846	0.6394	0.2369	1.114	1.0905	1.9583	2.8794	90.8142

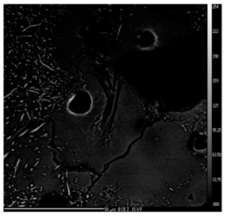
Aug3-2010_10_BSE Z_1

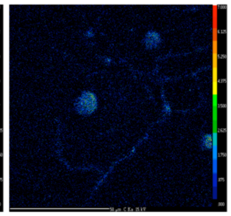
Aug3-2010_10_C Ka_6

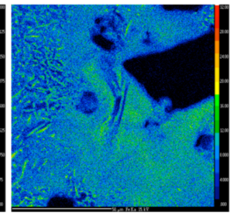
Aug3-2010_10_Fe Ka_5

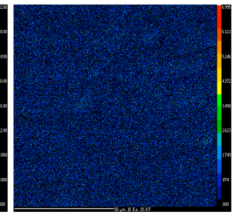
Aug3-2010_10_N Ka_3

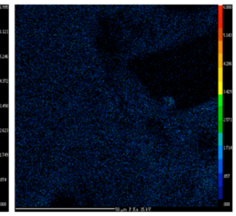
Aug3-2010_10_P Ka_7

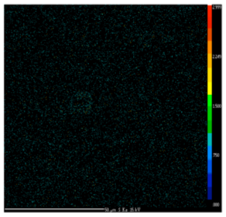
Aug3-2010_10_S Ka_4

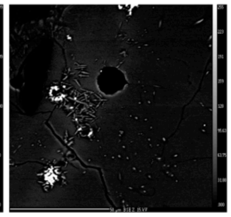
Aug3-2010_11_BSE Z_1

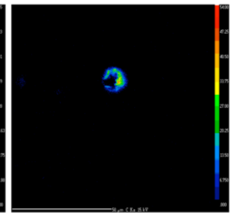
Aug3-2010_11_C Ka_6

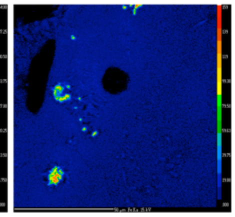
Aug3-2010_11_Fe Ka_5

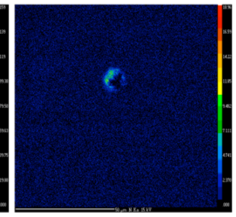
Aug3-2010_11_N Ka_3

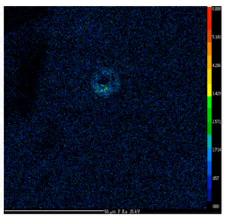
Aug3-2010_11_P Ka_7

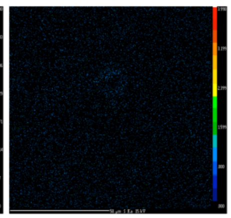
Aug3-2010_11_S Ka_4

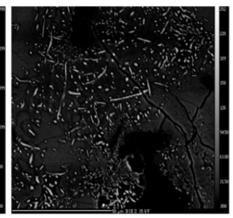
Aug3-2010_12_BSE Z_1

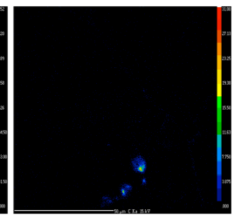
Aug3-2010_12_C Ka_6

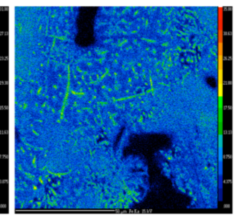
Aug3-2010_12_Fe Ka_5

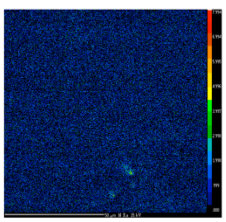
Aug3-2010_12_N Ka_3

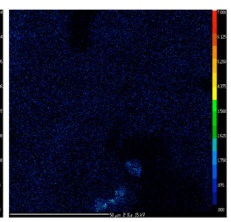
Aug3-2010_12_P Ka_7

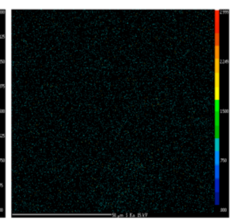
Aug3-2010_12_S Ka_4

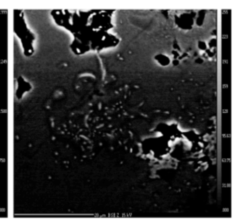
Aug3-2010_1_BSE Z_1

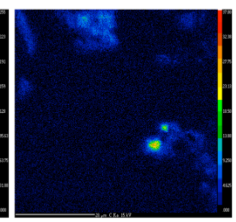
Aug3-2010_1_C Ka_6

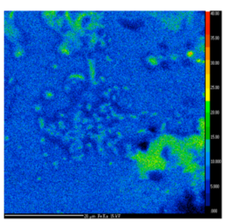
Aug3-2010_1_Fe Ka_5

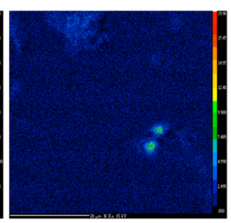
Aug3-2010_1_N Ka_3

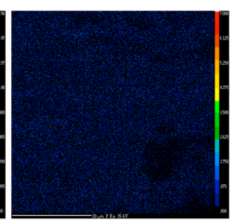
Aug3-2010_1_P Ka_7

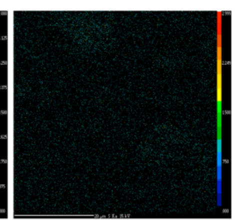
Aug3-2010_1_S Ka_4

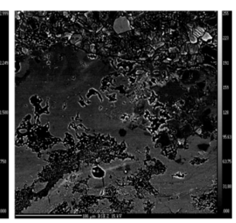
Aug3-2010_2_BSE Z_1

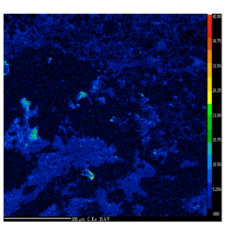
Aug3-2010_2_C Ka_6

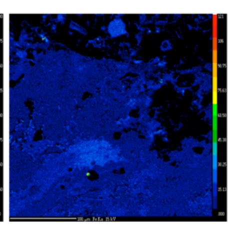
Aug3-2010_2_Fe Ka_5

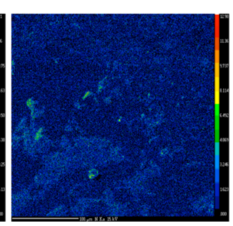
Aug3-2010_2_N Ka_3

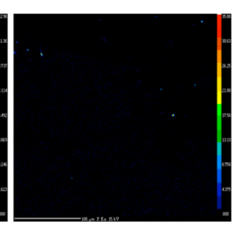
Aug3-2010_2_P Ka_7

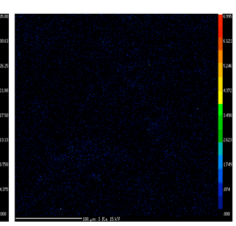
Aug3-2010_2_S Ka_4

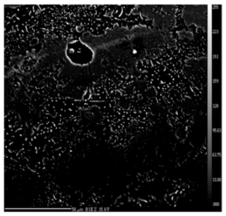
Aug3-2010_4_BSE Z_1

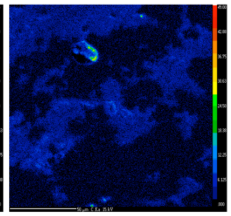
Aug3-2010_4_C Ka_6

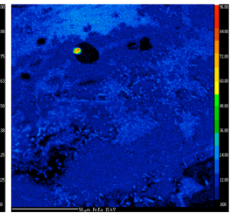
Aug3-2010_4_Fe Ka_5

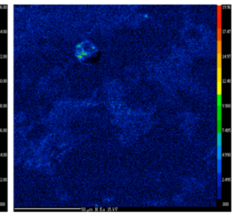
Aug3-2010_4_N Ka_3

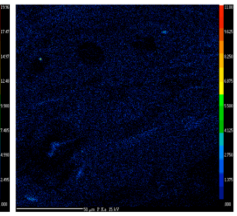
Aug3-2010_4_P Ka_7

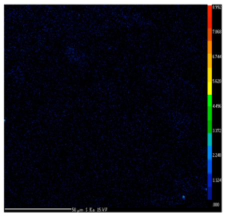
Aug3-2010_4_S Ka_4

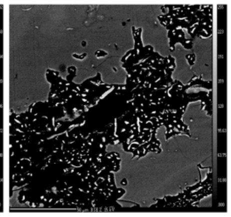
Aug3-2010_5_BSE Z_1

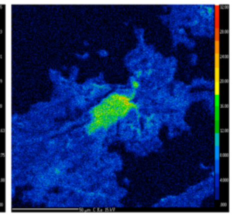
Aug3-2010_5_C Ka_6

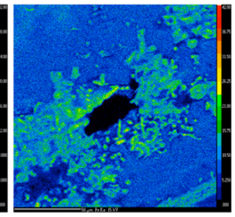
Aug3-2010_5_Fe Ka_5

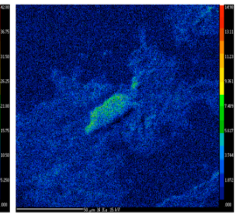
Aug3-2010_5_N Ka_3

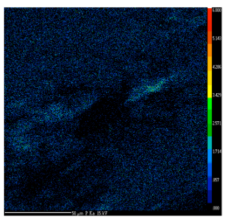
Aug3-2010_5_P Ka_7

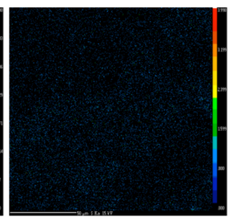
Aug3-2010_5_S Ka_4

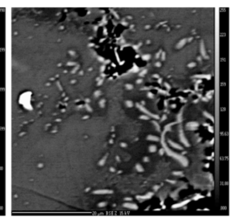
Aug3-2010_6_BSE Z_1

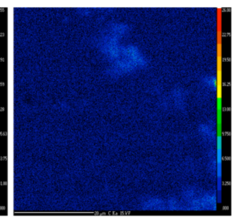
Aug3-2010_6_C Ka_6

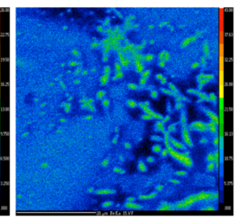
Aug3-2010_6_Fe Ka_5

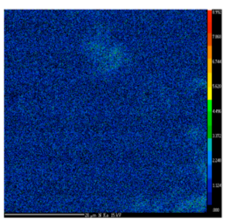
Aug3-2010_6_N Ka_3

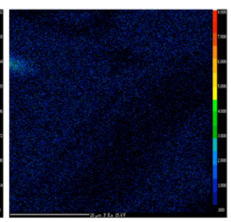
Aug3-2010_6_P Ka_7

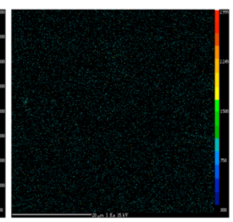
Aug3-2010_6_S Ka_4

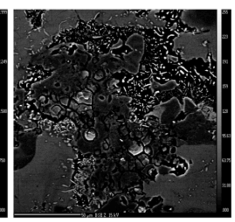
Aug3-2010_7_BSE Z_1

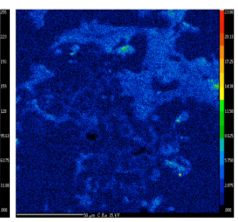
Aug3-2010_7_C Ka_6

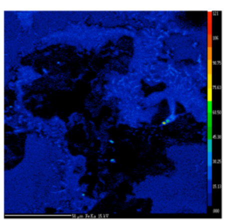
Aug3-2010_7_Fe Ka_5

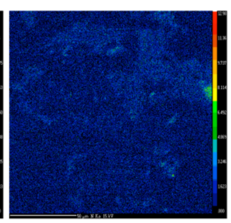
Aug3-2010_7_N Ka_3

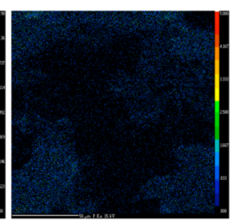
Aug3-2010_7_P Ka_7

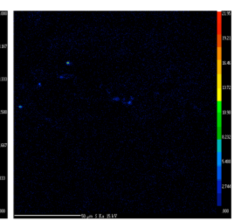
Aug3-2010_7_S Ka_4

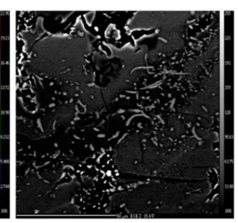
Aug3-2010_8_BSE Z_1

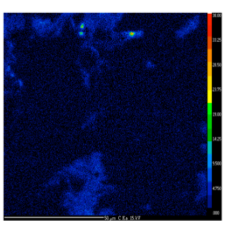
Aug3-2010_8_C Ka_6

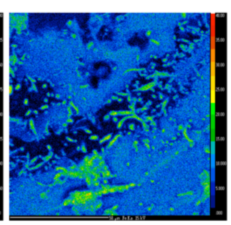
Aug3-2010_8_Fe Ka_5

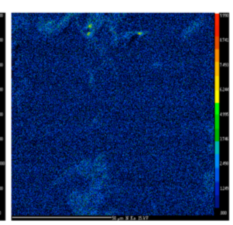
Aug3-2010_8_N Ka_3

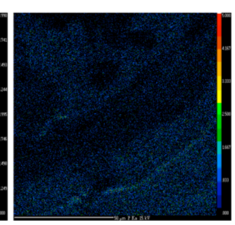
Aug3-2010_8_P Ka_7

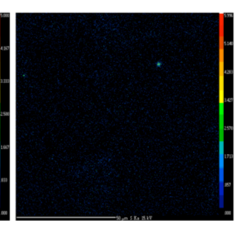
Aug3-2010_8_S Ka_4

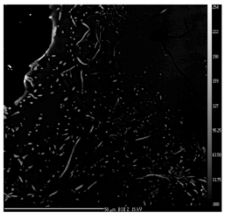
Aug3-2010_9_BSE Z_1

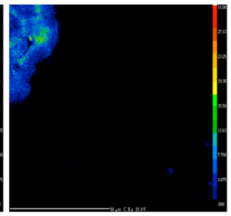
Aug3-2010_9_C Ka_6

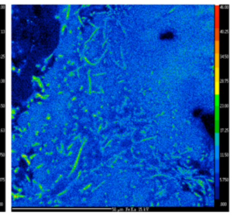
Aug3-2010_9_Fe Ka_5

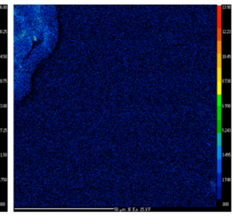
Aug3-2010_9_N Ka_3

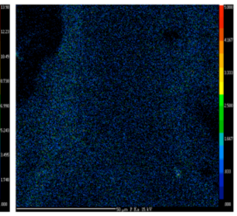
Aug3-2010_9_P Ka_7

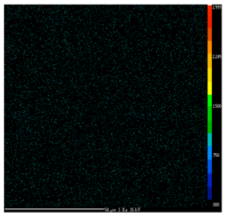
Aug3-2010_9_S Ka_4

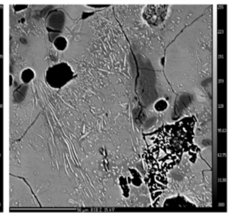
maps Aug 5_1_BSE Z_1

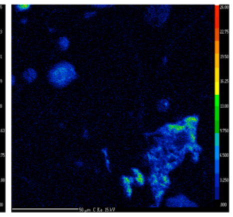
maps Aug 5_1_C Ka_6

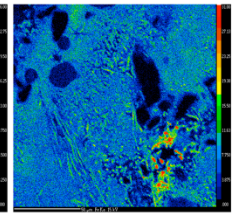
maps Aug 5_1_Fe Ka_5

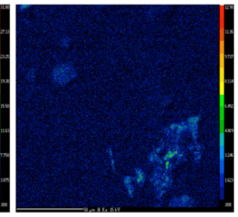
maps Aug 5_1_N Ka_3

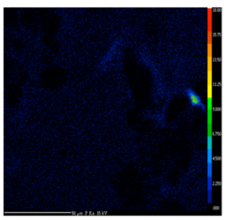
maps Aug 5_1_P Ka_7

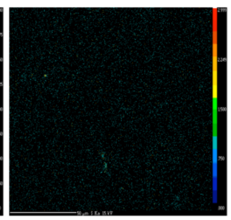
maps Aug 5_1_S Ka_4

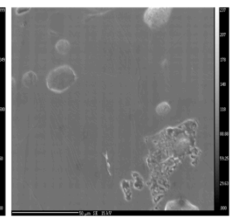
maps Aug 5_1_SE_2

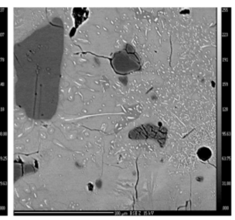
maps Aug 5_2_BSE Z_1

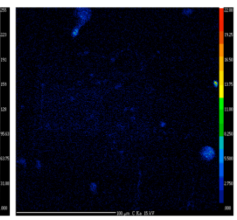
maps Aug 5_2_C Ka_6

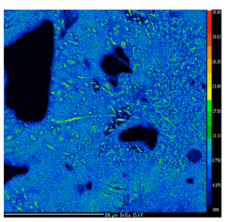
maps Aug 5_2_Fe Ka_5

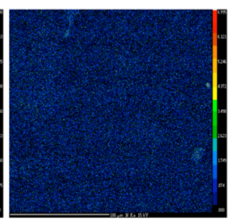
maps Aug 5_2_N Ka_3

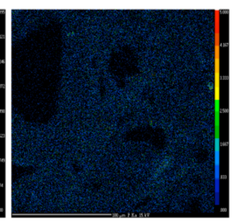
maps Aug 5_2_P Ka_7

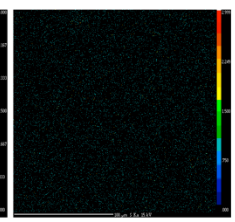
maps Aug 5_2_S Ka_4

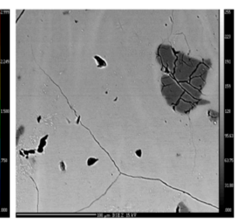
maps Aug 5_3_BSE Z_1

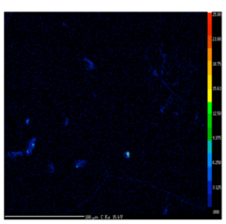
maps Aug 5_3_C Ka_6

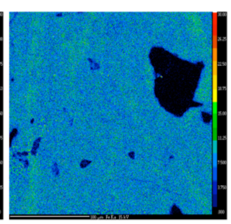
maps Aug 5_3_Fe Ka_5

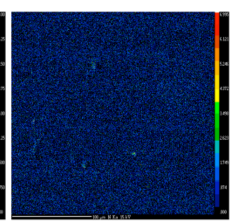
maps Aug 5_3_N Ka_3

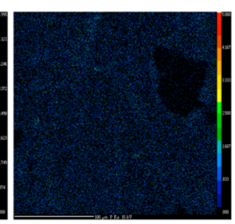
maps Aug 5_3_P Ka_7

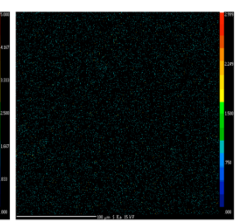
maps Aug 5_3_S Ka_4

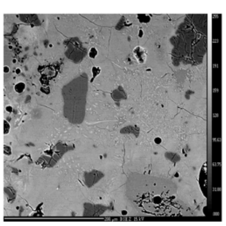
maps Aug 5_4_BSE Z_1

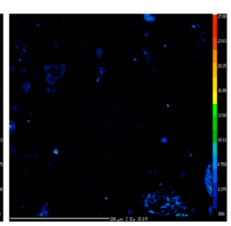
maps Aug 5_4_C Ka_6

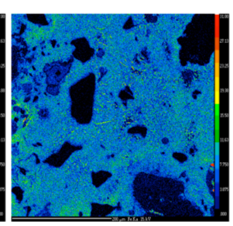
maps Aug 5_4_Fe Ka_5

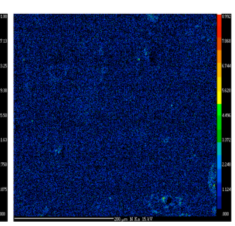
maps Aug 5_4_N Ka_3

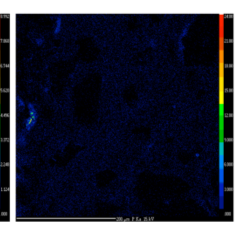
maps Aug 5_4_P Ka_7

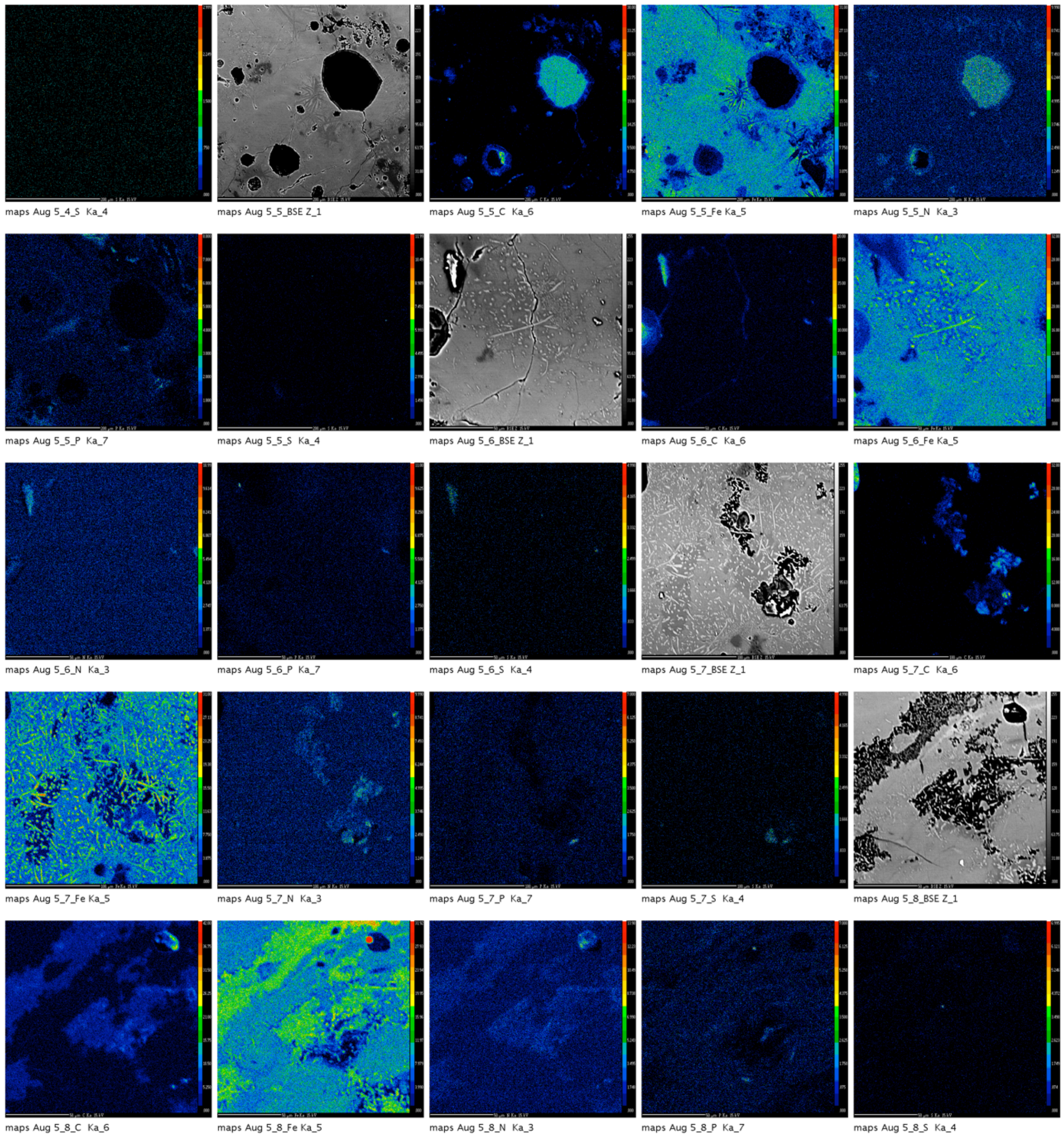
maps Aug 5_4_S Ka_4
maps Aug 5_5_BSE Z_1
maps Aug 5_5_C Ka_6
maps Aug 5_5_Fe Ka_5
maps Aug 5_5_N Ka_3
maps Aug 5_5_P Ka_7
maps Aug 5_5_S Ka_4
maps Aug 5_6_BSE Z_1
maps Aug 5_6_C Ka_6
maps Aug 5_6_Fe Ka_5
maps Aug 5_6_N Ka_3
maps Aug 5_6_P Ka_7
maps Aug 5_6_S Ka_4
maps Aug 5_7_BSE Z_1
maps Aug 5_7_C Ka_6
maps Aug 5_7_Fe Ka_5
maps Aug 5_7_N Ka_3
maps Aug 5_7_P Ka_7
maps Aug 5_7_S Ka_4
maps Aug 5_8_BSE Z_1
maps Aug 5_8_C Ka_6
maps Aug 5_8_Fe Ka_5
maps Aug 5_8_N Ka_3
maps Aug 5_8_P Ka_7
maps Aug 5_8_S Ka_4

Appendix F: μ-XRD data

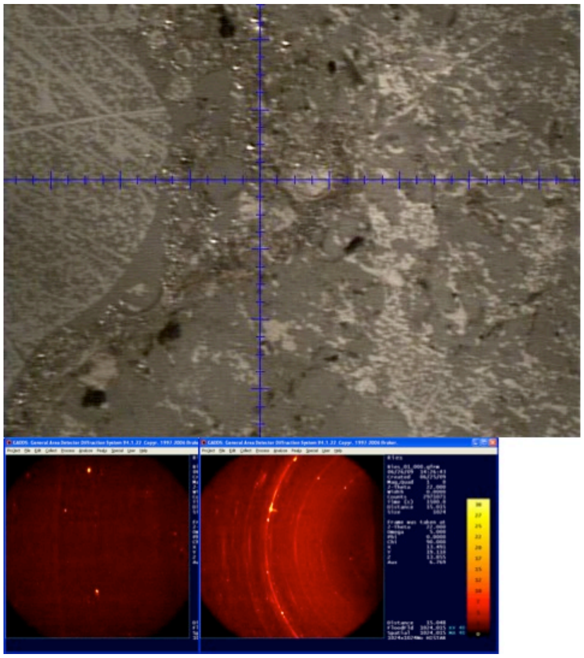

Ri 384 spot 1

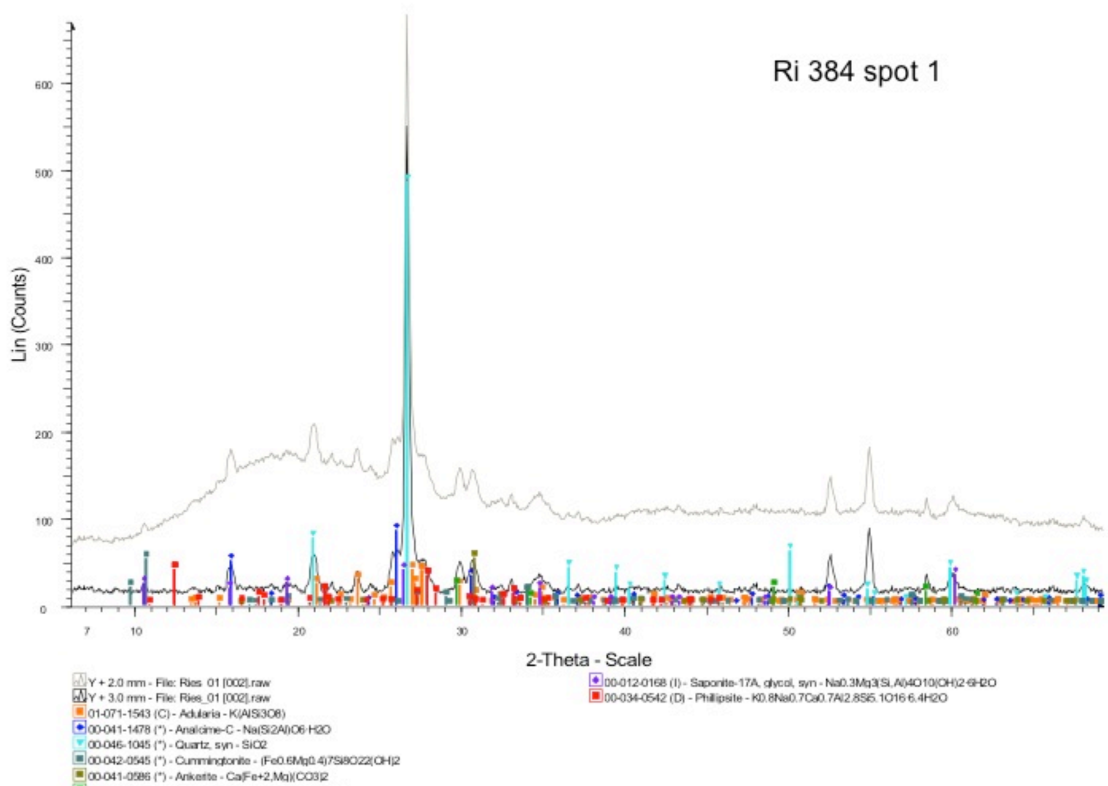

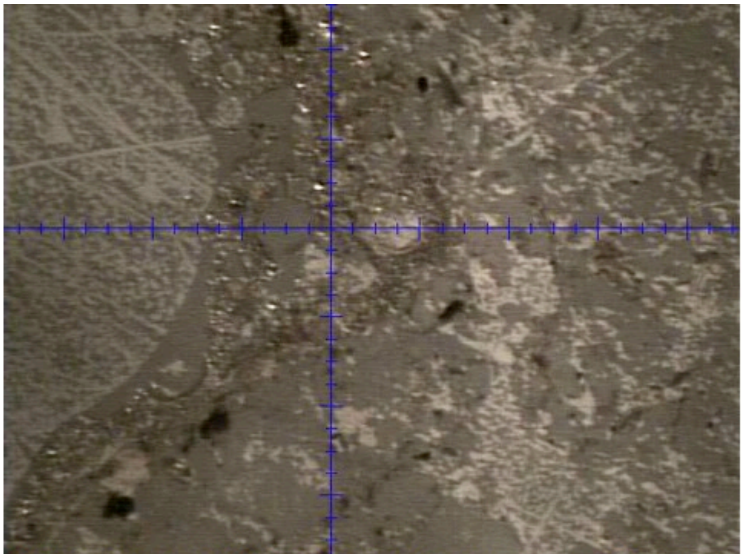

Ri 384 spot 2

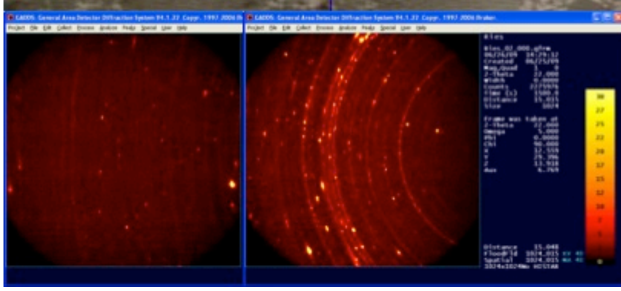

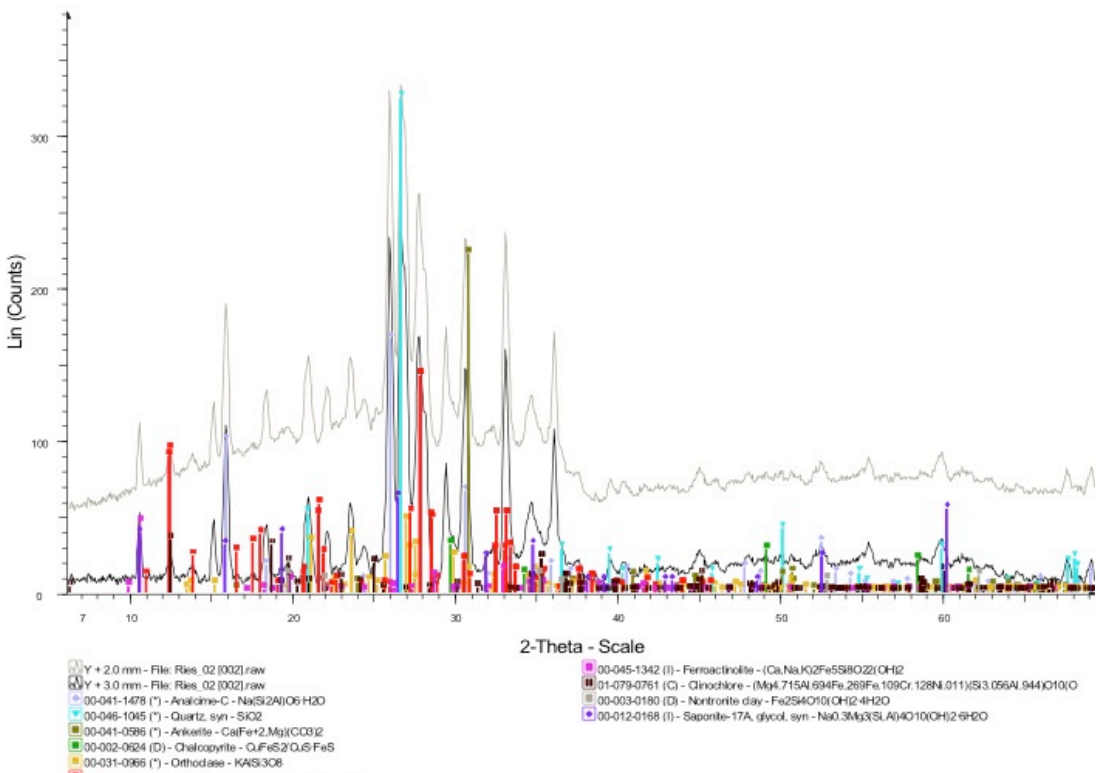
Lin (Counts)
300
200
100
0
7
10
20
30
40
50
60
2-Theta - Scale
Y + 2.0 mm - File: Ries_02 [002].raw
Y + 3.0 mm - File: Ries_02 [002].raw
00-041-1478 (*) - Analcime-C - Na(Si2Al)O6·H2O
00-046-1045 (*) - Quartz, syn - SiO2
00-041-0586 (*) - Ankerite - Ca(Fe+2,Mg)(CO3)2
00-002-0624 (D) - Chalcopyrite - CuFeS2/CuS·FeS
00-031-0966 (*) - Orthoclase - KAlSi3O8
00-039-1375 (I) - Phillipsite-Ca - KCa(Si5Al3)O16·6H2O
00-045-1342 (I) - Ferroactinolite - (Ca,Na,K)2Fe5Si8O22(OH)2
01-079-0761 (C) - Clinochlore - (Mg4.715Al.694Fe.269Fe.109Cr.128Ni.011)(Si3.056Al.944)O10(O
00-003-0180 (D) - Nontronite clay - Fe2Si4O10(OH)2·4H2O
00-012-0168 (I) - Saponite-17A, glycol, syn - Na0.3Mg3(Si,Al)4O10(OH)2·6H2O

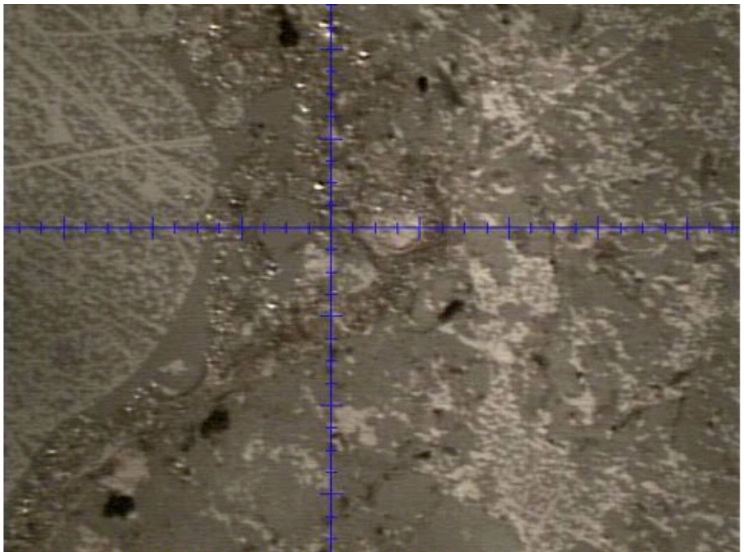

Ri 384 spot 3

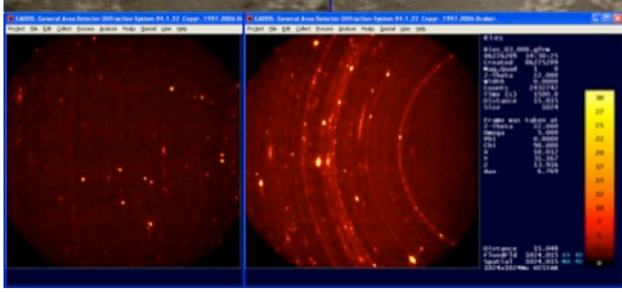

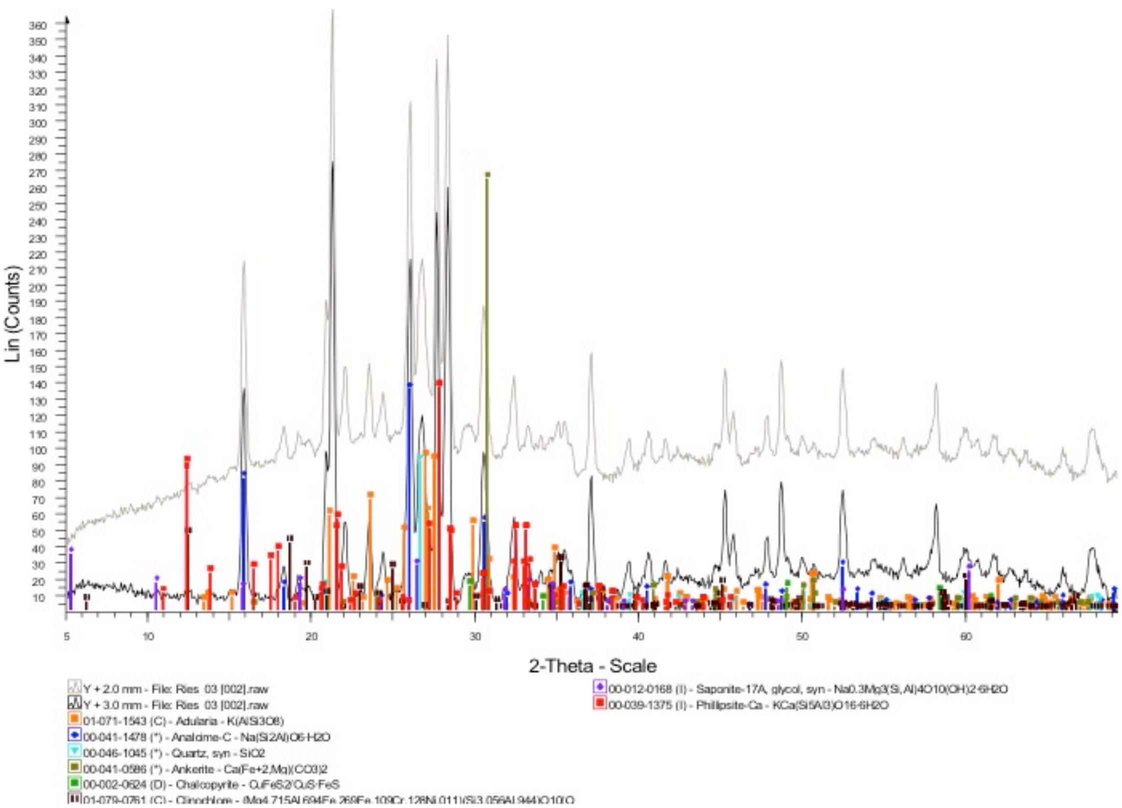

Lin (Counts)
2-Theta - Scale
Y + 2.0 mm - File: Ries 03 [002].raw
Y + 3.0 mm - File: Ries 03 [002].raw
01-071-1543 (C) - Adularia - K(AlSi3O8)
00-041-1478 (*) - Analcime-C - Na(Si2Al)O6·H2O
00-046-1045 (*) - Quartz, syn - SiO2
00-041-0586 (*) - Ankerite - Ca(Fe+2,Mg)(CO3)2
00-002-0624 (D) - Chalcopyrite - CuFeS2/CuS·FeS
00-012-0168 (I) - Saponite-17A, glycol, syn - Na0.3Mg3(Si,Al)4O10(OH)2·6H2O
00-039-1375 (I) - Phillipsite-Ca - KCa(Si5Al3)O16·6H2O

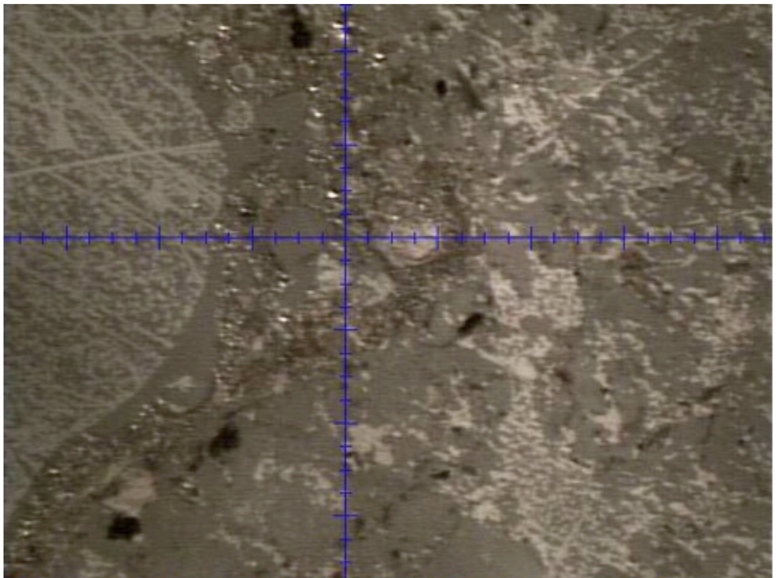

Ri 384 spot 4

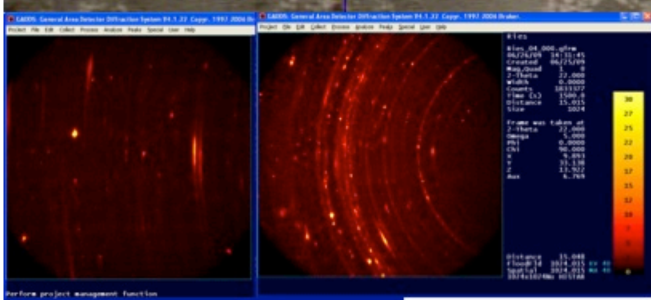

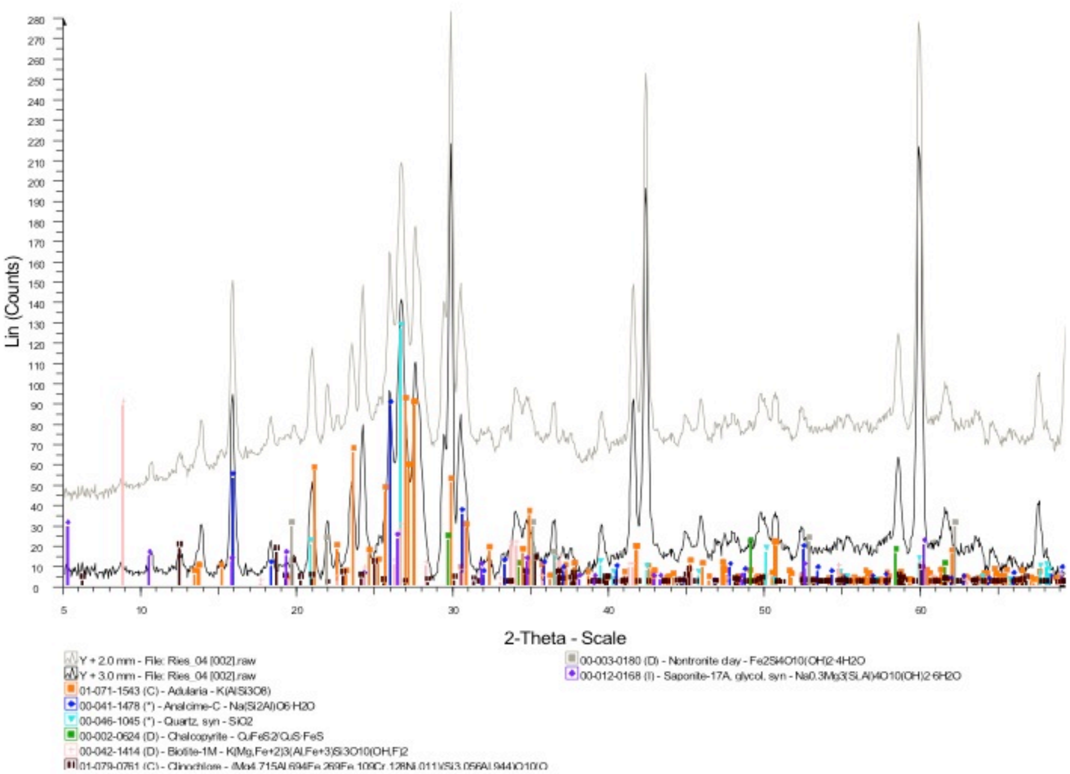

Lin (Counts)
2-Theta - Scale
Y + 2.0 mm - File: Ries_04 [002].raw
Y + 3.0 mm - File: Ries_04 [002].raw
01-071-1543 (C) - Adularia - K(AlSi3O8)
00-041-1478 (*) - Analcime-C - Na(Si2Al)O6·H2O
00-046-1045 (*) - Quartz, syn - SiO2
00-002-0624 (D) - Chalcopyrite - CuFeS2/CuS·FeS
00-042-1414 (D) - Biotite-1M - K(Mg,Fe+2)3(Al,Fe+3)Si3O10(OH,F)2
01-079-0761 (C) - Clinochlore - (Mg4.715Al.694Fe.269Fe.109Cr.128Ni.011)(Si3.056Al.944)O10(O
00-003-0180 (D) - Nontronite clay - Fe2Si4O10(OH)2·4H2O
00-012-0168 (I) - Saponite-17A, glycol, syn - Na0.3Mg3(Si,Al)4O10(OH)2·6H2O

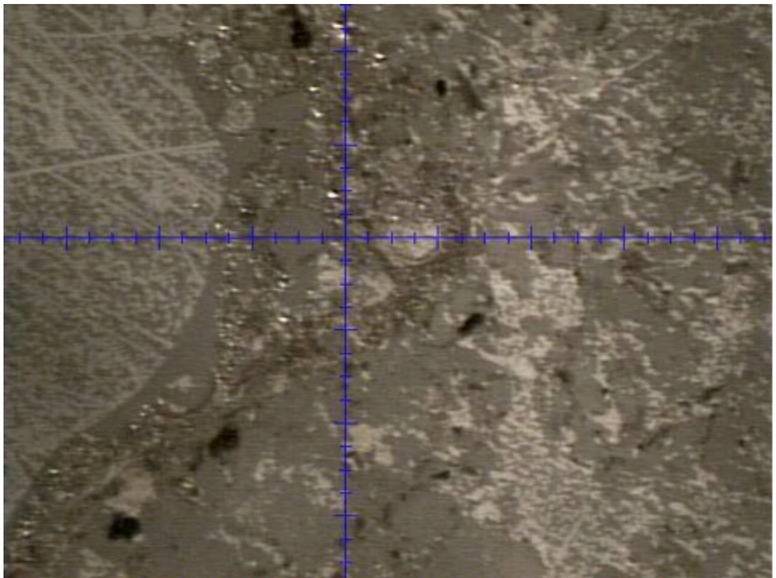

Ri00 056 spot 1

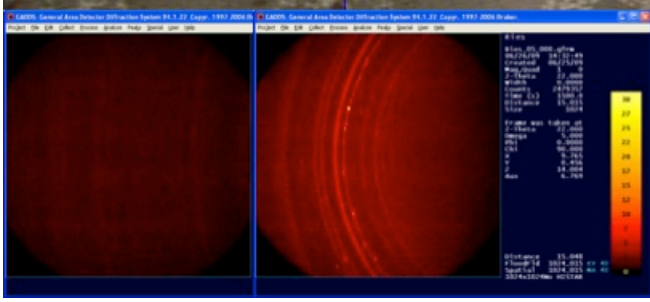

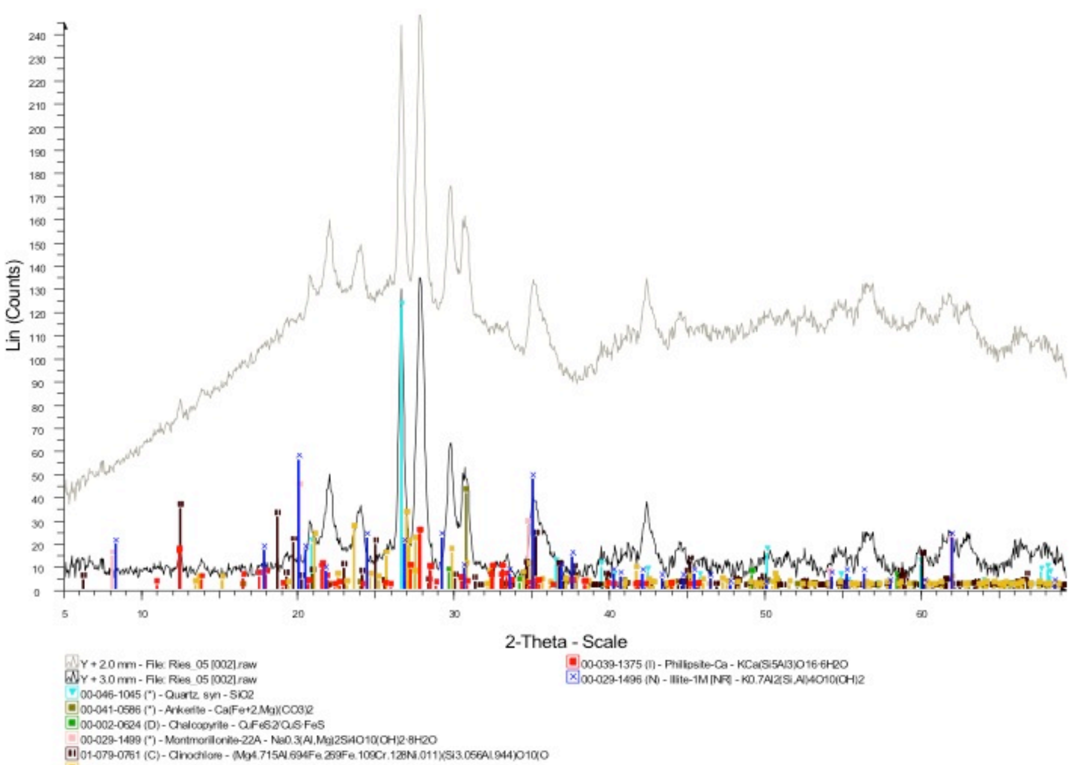

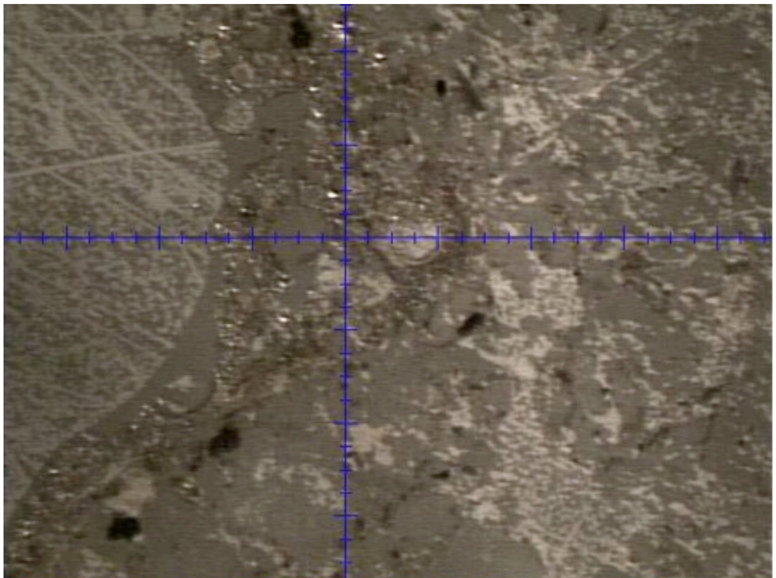

Ri00 056 spot 2

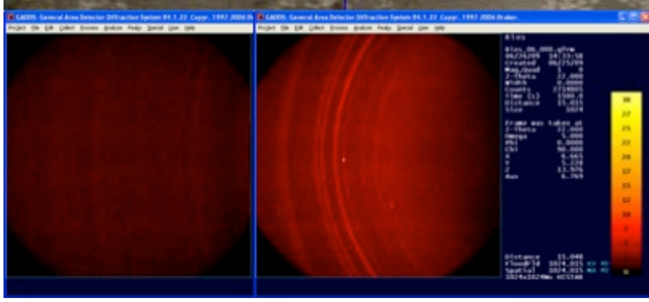

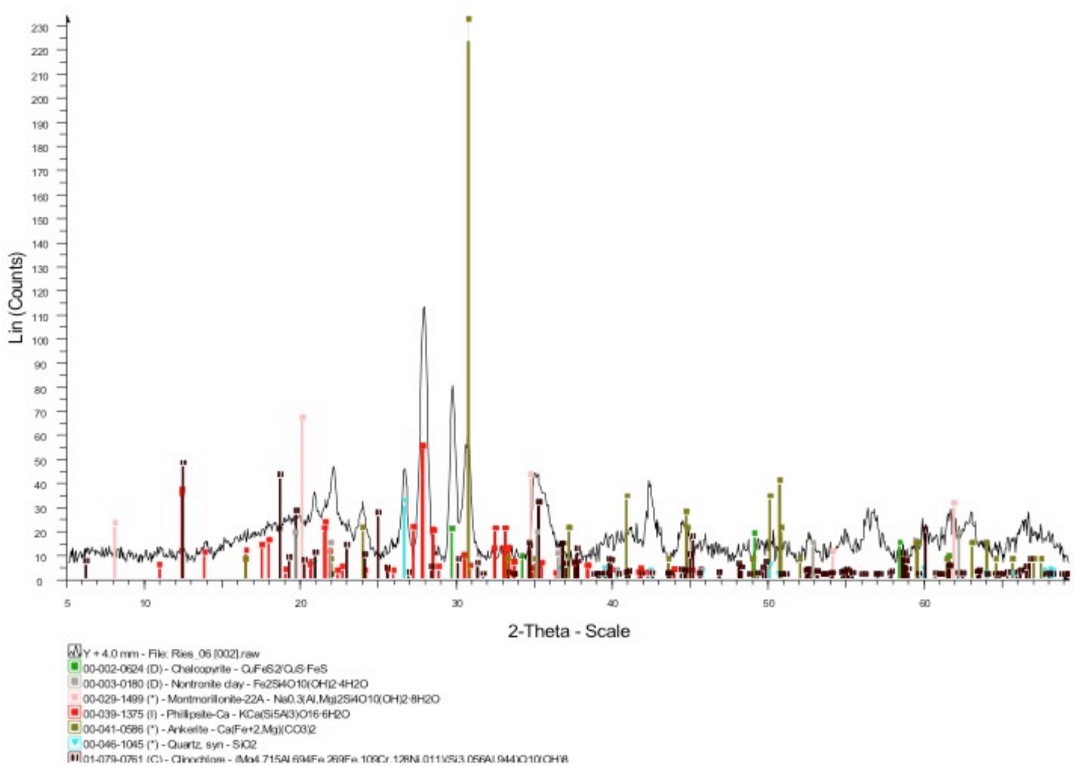

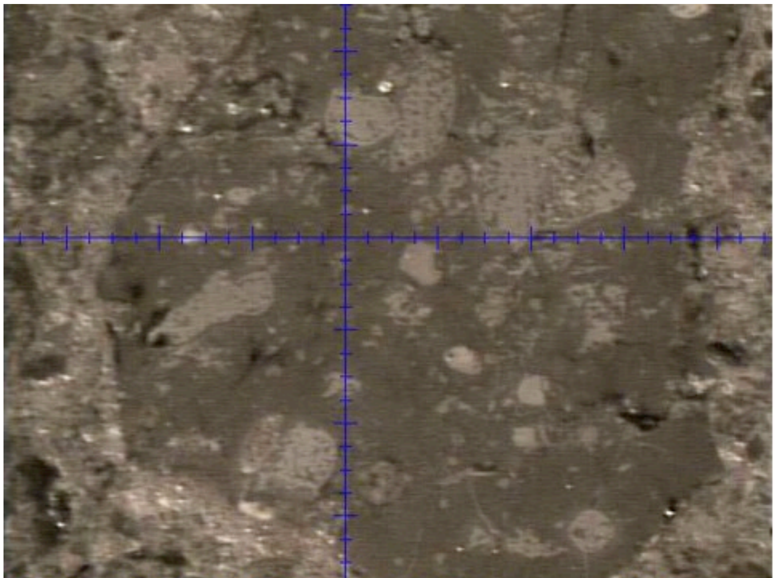

Ri00 056 spot 3

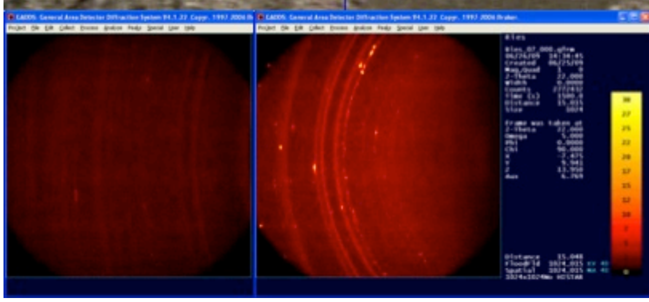

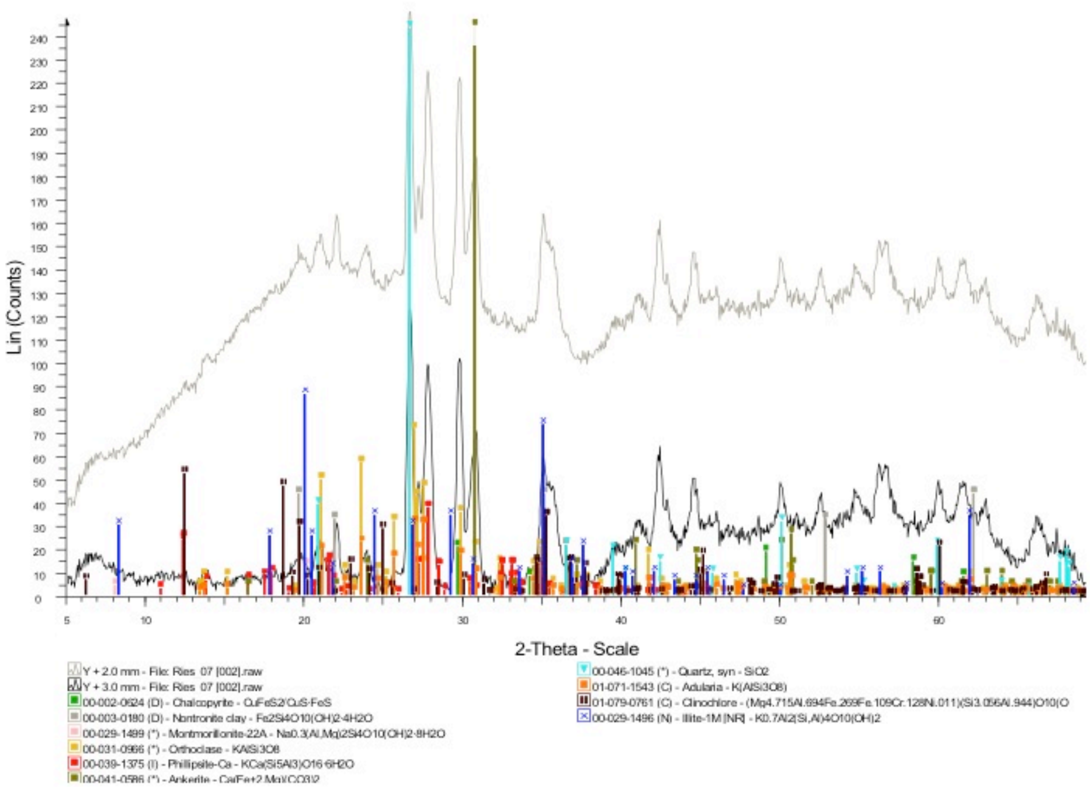

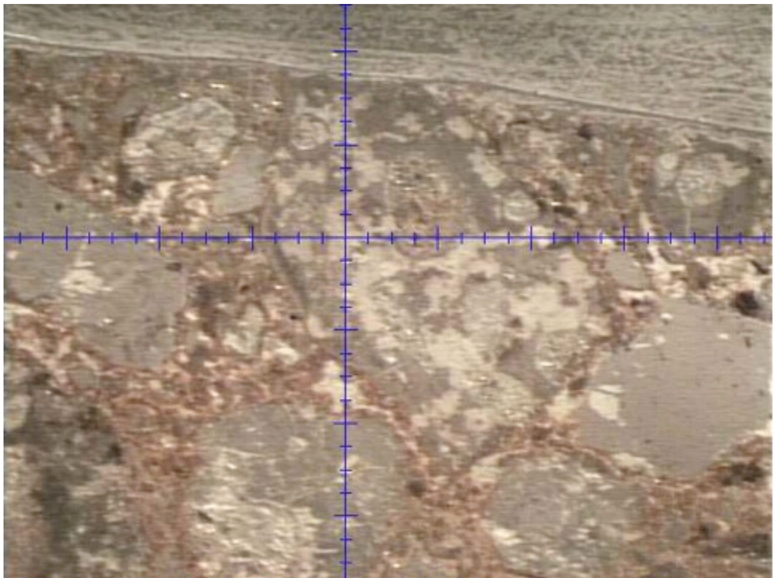

Ri01 011 spot 1a

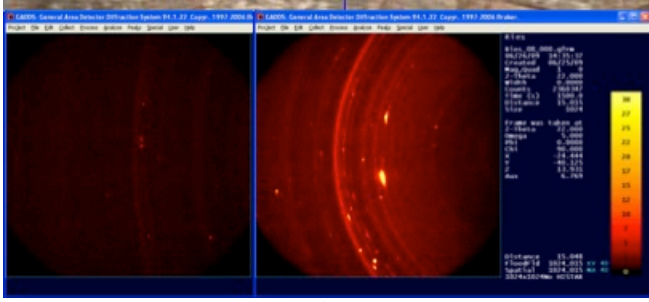

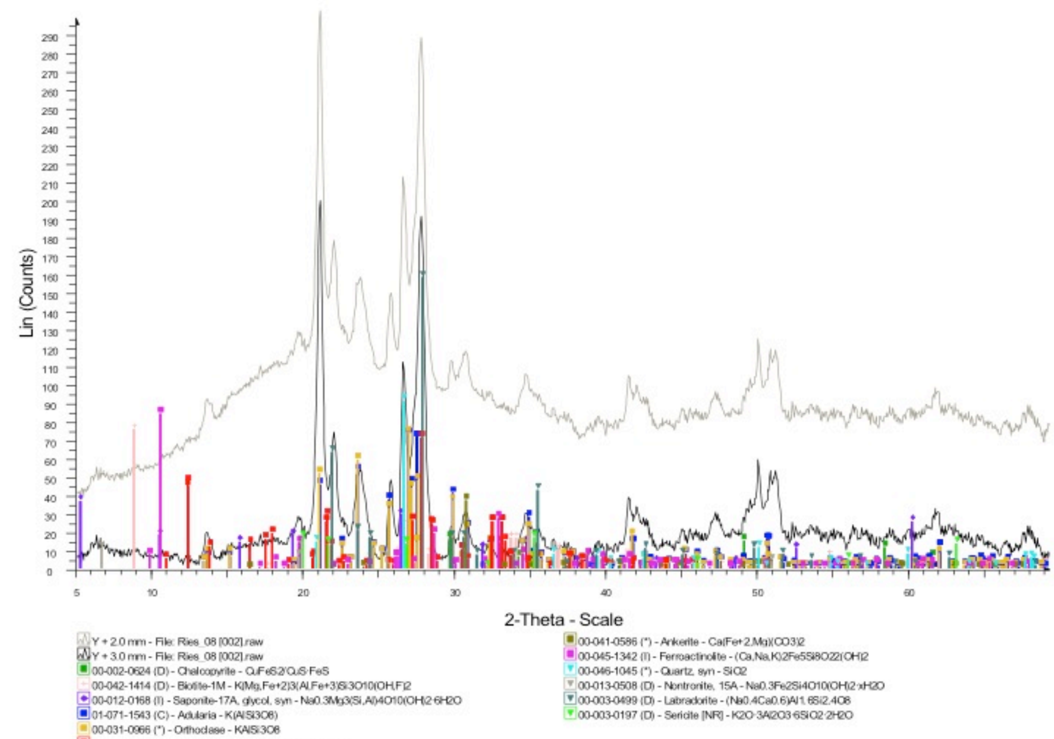

Ri01 011 spot 1b

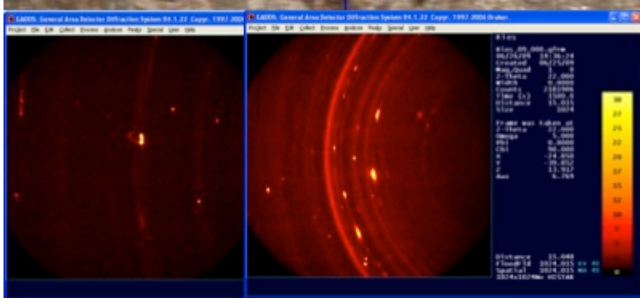

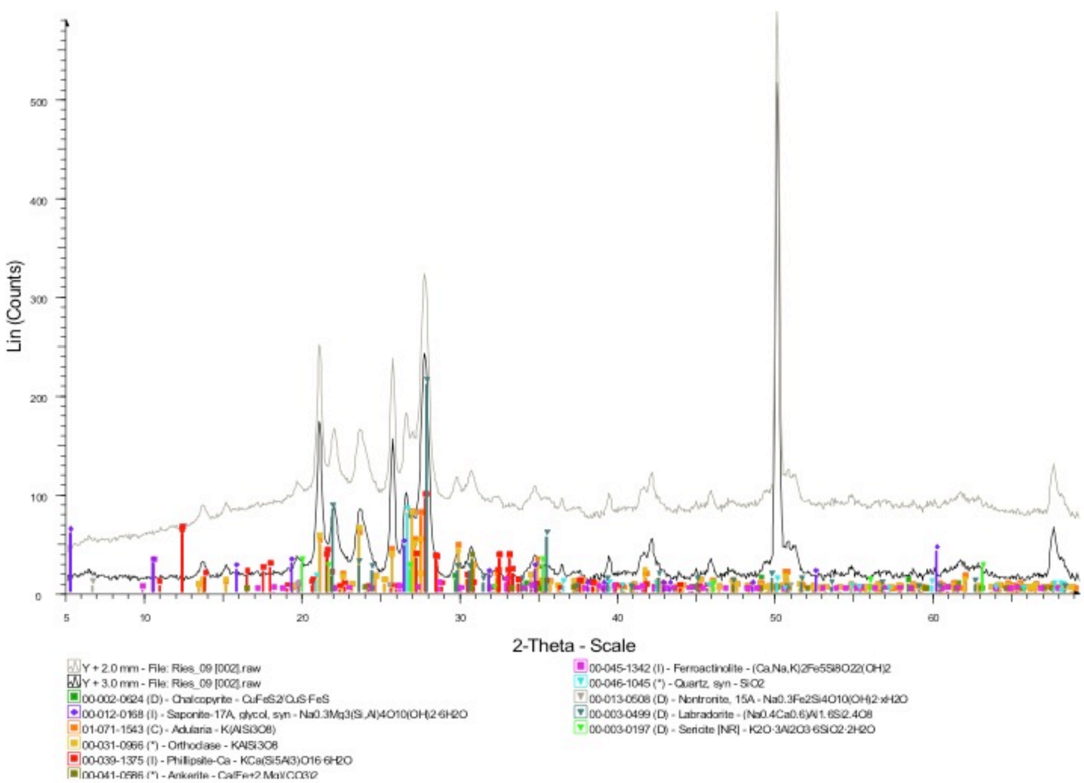

Ri01 011 spot 2

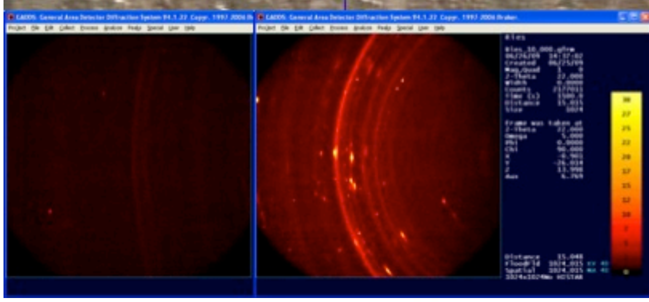

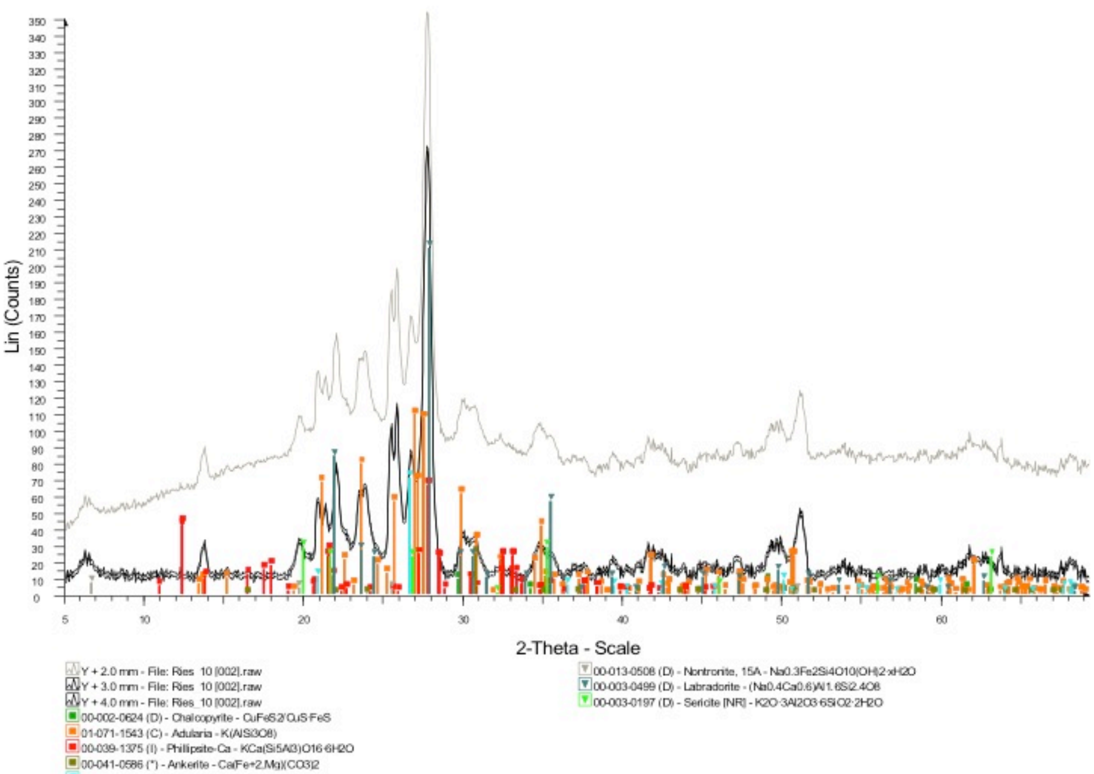

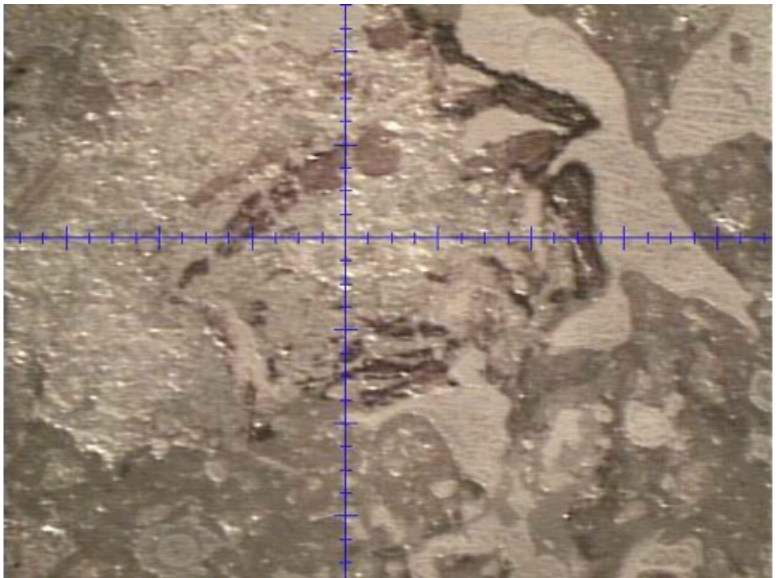

Ri01 011 spot 3a

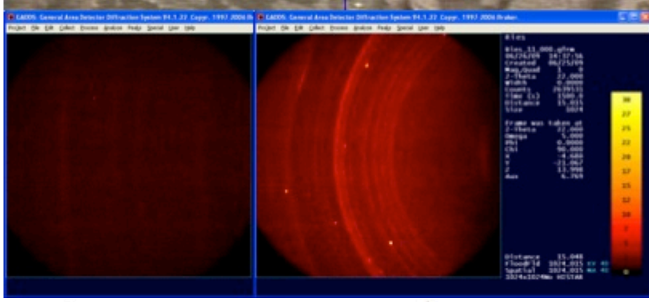

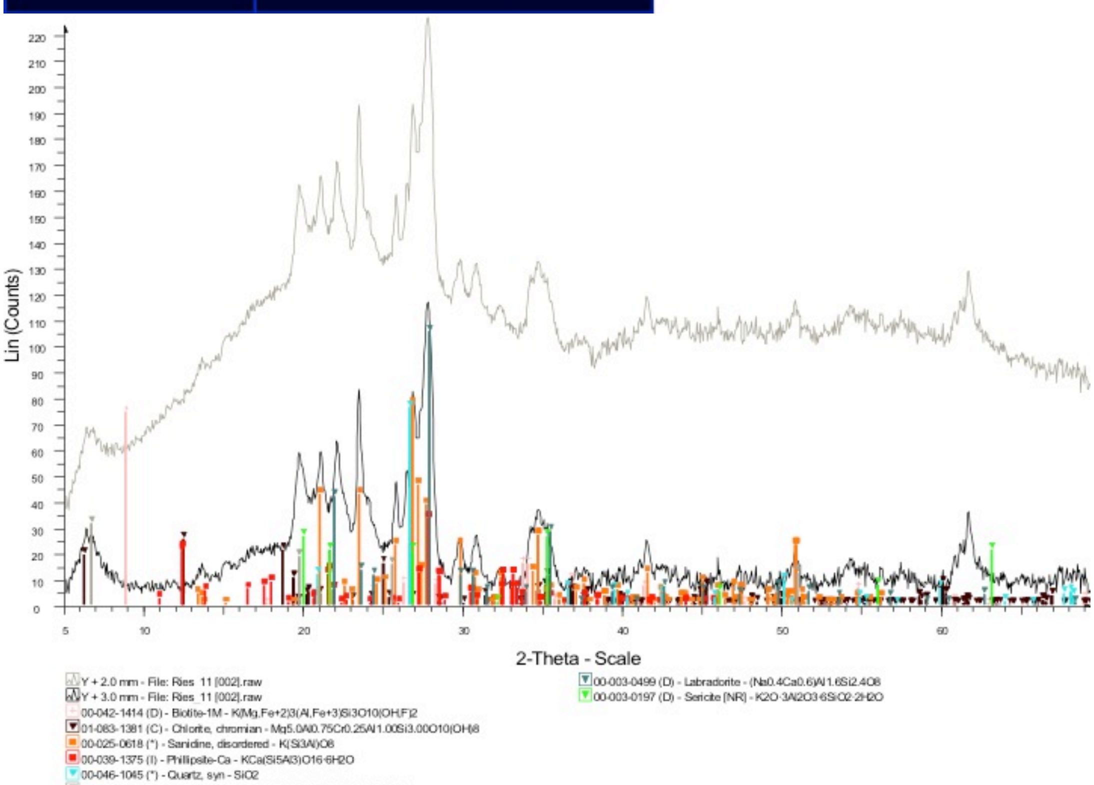

Ri01 011 spot 3d

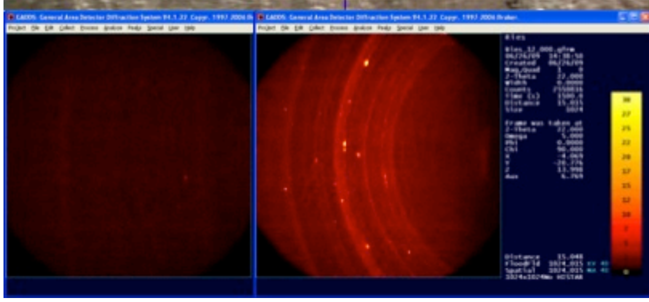

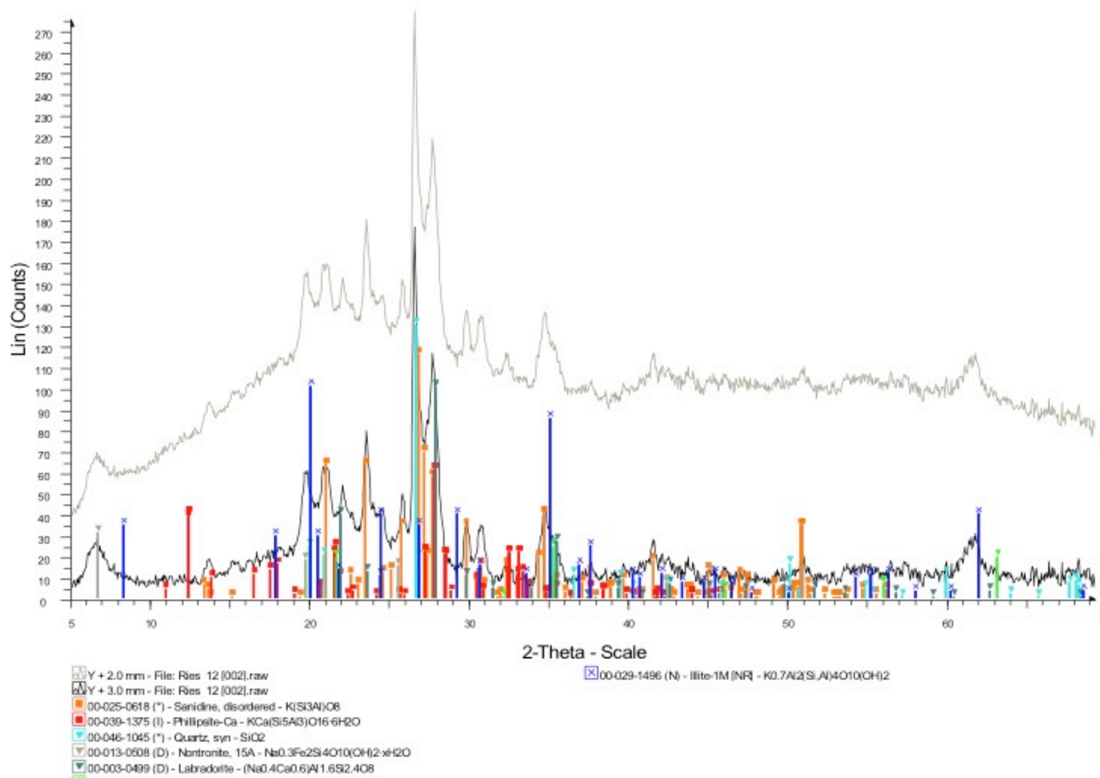

Curriculum Vitae

Name:	Haley M. Sapers
Post-secondary Education and Degrees:	Carleton University Ottawa, Ontario, Canada 2004-2008 B.Sc. Highest Honours Western University London, Ontario, Canada 2008-2012 Ph.D.

Education

2008 – present	*PhD Geology (Planetary Science)* [University of Western Ontario] Thesis title: Multi-analytical characterization of novel ichnofossils in meteorite impact glass. Supervisors: Dr. Gordon Osinski & Dr. Neil Banerjee. Estimated graduation October 2012.
2011	*Sao Paulo Advanced School of Astrobiology* [Universidade de São Paulo] 2nd place student poster prize; 2nd place focus group proposal writing competition
2009	*Canadian Synchrotron Summer School IV* [Canadian Light Source] Winner of the most promising student synchrotron research project and 1st place student poster prize
2004 – 2008	*BSc highest honours combined honours Biology & Geology* [[1]Carleton University and [2]The Geological Survey of Canada] Thesis title: Constraints on the Proterozoic assembly of the western Churchill Province provided by a detrital zircon U-Pb SHRIMP geochronology study: Barbour Bay, Chesterfield domain, Nunavut. Supervisors: Dr. Sharon Carr[1] & Dr. Rob Berman[2]

Research experience

2012	*Japan Society for the Promotion of Science Summer Program* [Institute for study of the Earth's Interior, Misasa, Tottori Prefecture, Japan]: Chemical variation in impact glass hosting microbally mediated alteration. Research supervised by Dr. Eizo Nakamura

2011 – 2012	*Principle Investigator* [Canadian Light Source, Saskatoon, SK, Canada]: Characterization of Putative Bioalteration in Impact Glass by STXM. Canadian Light Source top proposal submission for cycle 14
2010	*NASA Planetary Biology Internship* [NASA Ames, Moffett Field, CA, USA]: Development of fluorescent hydrogen peroxide single cell biosensors. Research supervised by Dr. Lynn Rothschild
2008	*Research project* [University of Western Ontario, London, ON, Canada]: Optical and scanning electron microscopy based characterization of the Rochechouart impactite suite
2008	*Ontario Universities Field Program in Biology* [Punta France, Cuba]: *In situ* effects of interspecific competition within the damselfish guild as observed on spatially isolated patch reefs, Punta Frances, Cuba.
2008	*BSc Honours project* [Carleton University, Ottawa, ON, Canada]: techniques in sensitive high resolution microprobe (SHRIMP) analysis; optical microscopy; scanning electron microscopy (SEM)
2007	*Internship* [Australian Centre for Astrobiology, Macquarie University, NSW, Australia]: Analysis of prokaryotes in the Paralana Hot Spring by fluorescent *in situ* hybridization (FISH); research supervised by Dr. Roberto Anitori,
2006	*NSERC Undergraduate Student Research Award:* Optical petrography morphological diversity survey of foraminiferal fauna from Port Stephens, Australia. Research supervised by Dr. Claudia Schrörder-Adams
2005	*NSERC Undergraduate Student Research Award:* Development of metagenomic DNA isolation protocols from soil samples contaminated with TNT. Research supervised by Dr. Iain Lambert

Field experience

2012	*São Francisco Craton, Brazil.* Graduate Student: International Geoscience Field Experience. Examination of regional geology, tectonics, magmatism, and metallogenic belts emphasizing exploration techniques and tools for finding mineralization
2010; 2009	*Ries Impact structure, Germany.* Team lead: planning and leading fieldwork including logistics, site analysis, detailed transects, detailed sampling, sub-sampling, core logging, descriptions and sampling
2008	*Punta Frances, Cuba.* Participant: SCUBA based observation marine studies, fish censes, remote location training

2007	*Paralana Hot Spring, Flinders Ranges, Australia.* Field assistant: biological aseptic sampling, radiation and remote location training, site journaling, photography
2006	*Ontario, Canada.* Student: 3rd year geology field camp, Carleton University supervised by Dr. Sharon Carr. Mapping techniques in metamorphic and igneous structural geology
2005	*Ontario, Canada.* Student: 2nd year geology field camp, Carleton University supervised by Dr. Claudia Schröder-Adams and Dr. Paul Gammon. Introduction to geological mapping and field techniques

Articles in refereed journals

Sapers, H. M., Preston, L. J., Banerjee, N. R., Osinski, G. R. Tubular alteration features in impact glass: A novel microbial habitat and astrobiology target. *Nature.* In Prep.

Sapers, H. M., Osinski, G. R., Flemming, R. L., Banerjee, N. R. (in review) Enigmatic tubular features in impact glass from the Ries impact structure, Germany. *Geology.*

Sapers, H. M., Banerjee, N. R., Osinski, G. R., Schumann, D. STXM and TEM analysis of putative ichnofossils in meteorite impact glass. *PNAS*. In Prep.

Sapers, H. M., Banerjee, N. R., Osinski, G. R., Preston, L. J., Flemming, R. L., Schumann, D. Microbial alteration of meteorite impact glass: characterization and implications. *Astrobiology*. In Prep.

Sapers, H. M., Osinski, G. R., Buitenhuis, E., Banerjee, N. R., Flemming, R. L., Hainge, J., Blain, S. Mineralogical variation at the Ries hydrothermal system. *Meteoritics and Planetary Science.* In Prep.

Sapers, H. M., Osinski, G. R., Banerjee, N. R., Ferrière, L., Lambert, P., Izawa, M. R. M. Impactites from the Rochechouart impact structure, France: A case study in the continuum nature of impact products. *Earth and Planetary Science Letters.* In Prep.

Sapers, H. M., Osinski, G. R., Banerjee, N. R. (2009) Differential alteration of glass clasts in the surficial suevites of the Ries Crater, Germany. *Meteoritics and Planetary Science Supplement*. **44**: 5175.

Banerjee, N. R., Izawa, M. R. M., **Sapers, H. M**., Whitehouse, M. (2011) Geochemical biosignatues preserved in microbially altered glass. *Surface and Interface Analysis* **43:** 1 – 2 pp 452 – 457.

Osinski, G. R., Tornabene, L., Banerjee, N. R., Cockell, C., Flemming, R. L., Izawa, M. R. M., McCutcheon, J., Parnell, J., Preston, L., Pickersgill, A., Pontefract, A., **Sapers, H. M**., Southam, G. (2012) Impact-generated hydrothermal systems on Earth and Mars. *Icarus*. In press.

Osinski, G. R., Barfoot, T., Ghafoor, N., Izawa, M. R. M., Banerjee, N. R., P. Jasiobedzki, Tripp, J., Richards, R., Haltigin, T., Auclair, S. A., **Sapers, H. A.,** Thomson, L., Flemming, R. L. (2010) Lidar and mSM as scientific tools for planetary exploration. *Planetary and Space Science* **58:** 4 pp 691 – 700.

Angerhausen, D., **Sapers, H. M.**, Citron, R., Bergantini, A., Lutz, S., Lopes Queiroz, L., da Rosa Alexandre, M., Araujo, A. C. V.. (2012) HABEBEE: Habitability of Eyeball-Exoearths. *Astrobiology*. In review

5. Conference Abstracts

Sapers, H. M., Banerjee, N. R., Osinski, G. R., Preston, L. J. A multi-analytical approach to assess the biogenicity of putative microbial ichnofossils in impact glass. Misasa IV (2012), Misasa, Japan (International meeting, Poster)

Sapers, H. M., Banerjee, N. R., Osinski, G. R., Preston, L. J., Schumann, D. Microbial Alteration of Impact Glass. Joint Annual Meeting GAC-MAC (2012), St. John's, Newfoundland, Canada (National conference, Oral)

Sapers, H. M., Osinski, G. R., Buitenhuis, E., Banerjee, N. R., Flemming, R. L., Hainge, J., Blain, S. The Ries post-impact hydrothermal system: Spatial and temporal mineralogical variation. Lunar and Planetary Science Conference, 43rd. (2012), The Woodlands, TX, USA (International conference, Oral)

Sapers, H. M., Banerjee, N. R., Osinski, G. R., Schumann, D. Characterization of putative ichnofossils in impact glass using STXM. Astrobiology Science Conference (2012), Atlanta, GA, USA (International conference, Oral)

Sapers, H. M., Banerjee, N. R., Osinski, G. R. Investigating putative bioalteration of impact glass. Canadian Light Source Annual Users Meeting, Saskatoon, SK (2011). (National meeting, Poster)

Sapers H. M., Osinski G. R. and Banerjee N. R. 2011. Putative bioalteration textures hosted within impact melt glasses from the Ries crater, Germany. Joint Annual Meeting GAC-MAC-SEG-SGA. Ottawa, Ontario, May 2011 (National conference, Oral).

Sapers H. M., Pontefract A., Izawa M. R. M., Preston L. J., Banerjee N. R., Osinski G. R., Southam G. and Cockell C. S. 2011. Impacts, Volcanoes, and Astrobiology. Gordon Research Conference on Geobiology. Ventura Beach, CA, January 30, 2011 (International conference, Poster).

Sapers H. M., Osinski G. R., and Banerjee N. R. 2010. Enigmatic tubular textures hosted in impact glasses from the Ries impact structure, Germany. Astrobiology Science Conference. League City, Texas, April 28, 2010 (International conference, Oral).

Sapers, H. M., Osinski, G. R., Banerjee, N. R. (2009) Re-evaluating the Rochechouart impactites: Petrographic classification, hydrothermal alteration, and evidence for carbonate bearing target rocks. Lunar and Planetary Science Conference, 40th, p. 848 – 850 (International conference proceedings, Oral)

Sapers, H. M., Osinski, G. R., Izawa, M. R. M., Banerjee, N. R., Reclassification of the Rochechouart Impactites. Planetary Science Research Symposium, Toronto, ON. (2009). (National conference, Oral)

Sapers, H. M., Izawa, M. R. M., Whitehouse, M. J., Banerjee, N R. Geochemical Biosignatures Preserved in Microbially Altered Basaltic Glass. International Conference on Secondary Ion Mass Spectrometry Toronto, ON (2009). (International conference, Poster)

Sapers, H. M., Banerjee, N. R., Osinski, G. R., Characterization of Putative Bioalteration of Suevitic Glass from the Ries Impact Crater, Germany. Canadian Light Source Annual Users Meeting, Saskatoon, SK (2009). (National meeting, Poster)

Sapers, H. M., Osinski, G. R., Banerjee, N. R. Putative Bioalteration textures hosted within impact melt glasses from the Ries Crater, Germany. AGU 2009 Joint Assembly Toronto, ON (2009). (International conference, Poster)

Izawa, M. R. M., **Sapers, H. M**., Osinski, G. R., Banerjee, N. R., Flemming, R., Singleton, A. C., Thompson, L., Auclair, S, Laliberty, D. M., Ngo, H. Q. Mineralogy of post-impact hydrothermal deposits at the Haughton impact structure and implications for microbial colonization. AGU 2009 Joint Assembly Toronto, ON (2009). (International conference Poster)

Sapers, H. M., Osinski, G. R., Izawa, M. R. M., Auclair, S., Banerjee, N. R., Cockell, C. S. Impact craters as hydrothermal habitats for life on Early Earth and Mars. Canadian Space Exploration Workshop Montreal, QB (2008). (National meeting, Poster)

Sapers, H. M., Anitori, R. A. Analysis of prokaryotes in the Paralana Hot Spring by fluorescent in situ hybridization (FISH). Advances in Earth Science Research Ottawa, ON (2007). (Regional conference, Poster).

Major scholarships

2012 – 2014	*NSERC CREATE Canadian Astrobiology Training Program Post Doctoral Fellowship,* The Natural Science and Engineering Research Council of Canada [$80 000]
2010 – 2013	*Canada Vanier Scholarship*, The Natural Science and Engineering Research Council of Canada [$150 000]

2012	*Summer Programs in Japan NSERC Supplement*, Japan Society for the Promotion of Science/ The Natural Science and Engineering Research Council of Canada [$8000]
2011	*André Hammer Prize,* The Natural Science and Engineering Research Council of Canada [$10 000]
2010	*NASA Planetary Biology Internship,* Marine Biological Laboratory [$3500]
2009 – 2012	*Canadian Astrobiology Training Program Fellowship,* The Natural Science and Engineering Research Council of Canada [$8400]
2009	*Barringer Family Meteorite Impact Research Grant,* The Barringer Crater Company [$4000]
2008 – 2012	*Western Graduate Research Award,* University of Western Ontario [$21 000]
2008 – 2010	*Alexander Graham Bell Canadian Graduate Scholarship (NSERC CGS M),* The Natural Science and Engineering Research Council of Canada [$35 000]
2008 – 2009	*Entrance scholarship Faculty of Science,* The University of Western Ontario [$5000]
2008 – 2009	*Entrance scholarship Department of Geology,* The University of Western Ontario [$8000]

Other scholarships & awards

2011	*SPASA 2nd place student poster prize,* Sao Paulo Advanced School of Astrobiology
2011	*SPASA 2nd place focus group proposal,* Sao Paulo Advanced School of Astrobiology
2009	*Student poster prize Canadian Light Source,* Canadian Light Source
2008	*AESRC student poster award*
2008	*GAC student prize winner,* Geological Association of Canada
2008	*Chancellor's Medal,* Carleton University
2008; 2010	*Space Awareness and Learning Student Grant,* Canadian Space Agency
2006 – 2007	*Bickell Foundation Scholarship,* Carleton University [$2500]
2006 – 2007	*C. C. Gibson Scholarship,* Carleton University [$1000]
2005; 2006	*NSERC Undergraduate Student Research Award (USRA),* Carleton University [$5000/yr]

2005 – 2006 2007 – 2008	*Collins Continuation Scholarship,* Carleton University [$2000/yr]
2005 – 2006 2007 – 2008	*Morley E. Wilson Scholarship,* Carleton University [$2750/yr]
2005 – 2007	*Ruth Lifeso Scholarship,* Carleton University [$2750]
2005 – 2006	*General in-course Scholarship,* Carleton University [$1000]
2004 – 2008	*Dean's List,* Carleton University
2003 – 2004	*Academic Excellence Award,* University of Alberta [$700]
declined	*Rutherford Scholarship,* University of Alberta
declined	*Rotary Youth Leadership Award,* Rotary International

Work experience

2009	*Teaching Assistant* [The University of Western Ontario, Dept. of Earth and Planetary Sciences]: exam proctor; origin and geology of the Solar System
2008	*Teaching Assistant* [Carleton University, Dept. of Geology]: exam and essay correction; academic help for vertebrate palaeontology course
2008	*Research Assistant* [Carleton University, Dept. of Geology]: research and lecture preparation for plate tectonics fourth-year undergraduate course
2007	*Research Assistant* [Australian Centre for Astrobiology, EDGE laboratory]: microbial ecology, astrobiology

Mentorship & leadership

2010 – 2012	Mentor to a group of undergraduate students cumulating in an international conference presentation and a manuscript in preparation: Mineralogical variation at the Ries hydrothermal system.
2011	Volunteer and mentor for The University of Western Ontario's SGPS Development Series: 'Consult the Experts' external scholarship sessions
2008 – 2011	Speaker and mentor to grade school students at McBride Elementary School and Thomas Haney High School in Vancouver, BC, Canada
2008 – 2011	Regular volunteer for The University of Western Ontario's Fall Preview Day for high school students
2008	Co-president of the Algonquin-Carleton Rotaract club

2004 – 2008 Treasurer and co-excursion leader of the Carleton Geology Undergraduate Society

Media interactions & public lectures

Let's Talk Science, High School Symposium. Invited keynote speaker May 28, 2012. *So what is astrobiology anyway?*

Royal Astronomical Society of Canada, London, ON chapter. Invited talk March 18, 2011. *Deep Impact: Investigating signs of life in terrestrial impact glass*

CBC: All in a Day show: February 15, 2011. Interview on bioalteration in Ries glasses

Metro News: February 15, 2011. Article on bioalteration in Ries glasses

London Ontario's 109.6 The X: February 18, 2011. Interview on bioalteration in Ries glasses

Thesis research highlighted on the Natural Science and Engineering Research Council of Canada's webpage:
(http://www.nserc-crsng.gc.ca/Media-Media/ForMedia-PourMedias/Hamer-Hamer/Sapers-Sapers_eng.asp)

Thesis research featured in a Natural Science and Engineering Research Council of Canada YouTube production: *Two minutes with Haley Sapers*